5-2008

Investigating the Petrogenesis of the Basaltic Crust of Asteroid 4 Vesta: A Combined Petrologic-Spectral Study of the Unbrecciated Eucrites

Rhiannon Gwenllian Mayne
University of Tennessee - Knoxville

To the Graduate Council:

I am submitting herewith a dissertation written by Rhiannon Gwenllian Mayne entitled "Investigating the Petrogenesis of the Basaltic Crust of Asteroid 4 Vesta: A Combined Petrologic-Spectral Study of the Unbrecciated Eucrites." I have examined the final electronic copy of this dissertation for form and content and recommend that it be accepted in partial fulfillment of the requirements for the degree of Doctor of Philosophy, with a major in Geology.

Harry Y. McSween, Major Professor

We have read this dissertation and recommend its acceptance:

Jeffrey E. Moersch, Jeffrey Kovac, Larry A. Taylor, Jessica M. Sunshine, Timothy J. McCoy

Accepted for the Council:

Carolyn R. Hodges

Vice Provost and Dean of the Graduate School

(Original signatures are on file with official student records.)

To the Graduate Council:

I am submitting herewith a dissertation written by Rhiannon Gwenllian Mayne entitled "Investigating the Petrogenesis of the Basaltic Crust of Asteroid 4 Vesta: A Combined Petrologic-Spectral Study of the Unbrecciated Eucrites." I have examined the final electronic copy of the dissertation for form and content and recommend that it be accepted in partial fulfillment of the requirements for the degree of Doctor of Philosophy, with a major in Geology.

_Harry Y. McSween_____
Major Professor

We have read this dissertation
and recommend its acceptance:

__Jeffrey E. Moersch_____

__Jeffrey Kovac_____

__Larry A. Taylor_____

__Jessica M. Sunshine_____

__Timothy J. McCoy_____

Acceptance for the council:

_Carolyn R. Hodges_____
Vice Provost and
Dean of the Graduate School

(Original signatures are on file with official student records.)

INVESTIGATING THE PETROGENESIS OF THE BASALTIC CRUST OF ASTEROID 4 VESTA: A COMBINED PETROLOGIC-SPECTRAL STUDY OF THE UNBRECCIATED EUCRITES

A Dissertation
Presented for the
Doctor of Philosophy Degree
The University of Tennessee, Knoxville

Rhiannon Gwenllian Mayne
May 2008

Dedication

This dissertation is dedicated to my parents, who have been there for me every limp, hobble, and crutch-assisted step of the way. When I have felt like falling apart, they have always been the glue holding me together.

Acknowledgements

This dissertation would not have been possible without all the support, both financially and academically, of my advisor, Harry Y. McSween Jr., whose amazing organizational skills I shall always aspire to, but never quite attain. I would like to thank my committee members Larry A. Taylor, Jeffrey E. Moersch, and Jeffrey Kovac for all the help and comments that helped to improve the chapters within. Jessica M. Sunshine and Timothy J. McCoy, my committee members from afar, both offered invaluable insight, support, guidance, and seemingly inexhaustible patience, for which I am truly grateful.

There have been so many people within the UT Department of Earth and Planetary Sciences that have cheered me on from the sidelines, been a shoulder to cry on, and helped me over the seemingly insurmountable hurdles: Bill Deane, Linda Kah, and Colin Sumrall - it would never have been finished without you! Of course, special thanks go to Alan Patchen, the czar of all things microprobe, who offered sage advice, and always resuscitated the microprobe for me when the 'slave died' in the heat.

The work within these covers would never have been achieved without: a graduate student fellowship at the Smithsonian Institution; collaborations with Schelte J. 'Bobby' Bus and Catherine M. Corrigan; the work of Takahiro Hiroi and other at the RELAB facility; much hard work and time spent at the SEM by Allison Gale.

LaDawn, Teresa, Rod, Amy, John, Debbie, and all the others at Foothills Physical Therapy made sure that my body stayed together for the duration, despite my many attempts to the contrary.

This whole graduate school expedition would have never left base camp if it were not for my friends. Sarah and Liz, you may be thousand of miles away but somehow you always manage to be there when I need you and, for that, I can never thank you enough. Kate, Katie, and Amy, you always prove that the oldies are the 'goodies' when it comes to friends. To the Tennessee crew of the past (Jen Piatek, Rachel Lentz, Karen Stockstill, Keith Milam, Jessica Dunaway, Ben Norton and Kathleen Johnson) and the present (Steven Jaret, Tasha Dunn, Mike DeAngelis, Whitney Kocis, Melissa Hage, and René Lewis), it would never have been the same without you. Additionally, thanks must go to the Scheevel and Reese families for offering me a home away from home and for always keeping me in your prayers and letting me know it. Your laughter, support, help, and, most importantly, friendship has made it all worthwhile.

Finally, my family, those here and those who have gone on, I thank you for shaping me into the person I am today and for never saying I couldn't and always making me believe I could. I love you all.

Abstract

The Dawn mission, which launched in September 2007, will orbit and analyze two of the largest asteroids, 4 Vesta and 1 Ceres. These small, proto-planetary bodies retain a record of the conditions and processes that occurred in the early history of the Solar System, and, as such, provide us with a tool to understand its formation and evolution. Additional information can also be gleaned from the meteorite samples derived from such objects. This dissertation aims to increase understanding of the formation of the basaltic crust of the asteroid Vesta, and the lithologic variety that exists within it, by studying the eucrite meteorites, believed to originate from it.

In order for us to be able to identify different units on the surface of Vesta, we must first understand the relationship that exists between the petrology of the samples and their spectral characteristics, which will be measured by the VIR (Visible Infrared) instrument aboard Dawn. The first part of this dissertation details an in-depth study into the petrology of the unbrecciated eucrites, focusing on those characteristics that impact the spectra, e.g. mineral chemistries and modal abundances.

Select well-characterized unbrecciated eucrites from the petrologic study were then chosen for spectral work. Visible near-infrared (0.3 – 2.5 μm) spectra were collected and the amount of petrologic information that could be extracted from the spectra alone was assessed. We were able to distinguish the spectra of basaltic versus cumulate eucrites, as well as those samples that underwent slow- versus fast cooling and early- versus late-crystallization. This indicates that we may be able to map petrologic units using Dawn and determine the processes that occurred to form them.

Dawn is scheduled to reach Vesta in 2011; however, the Vestoids, a group of asteroids believed to be from Vesta, offer us the opportunity to utilize the combined petrologic-spectral data set now. The spectra of 15 Vestoids were examined and compared to spectra for the howardite, eucrite, and diogenite meteorites, of which Vesta is believed to be the parent body. The Vestoids indicate that both large-scale (>7 km) homogeneous and small-scale (<1 km) heterogeneous units exist on the surface of Vesta.

Table of Contents

List of Tables

List of Figures

I. Introduction

1. Overview

1.1 The Dawn Mission

Spacecraft missions are one of the major ways that we can explore the Solar System; however, most missions have targeted large bodies (e.g. planets and moons), leaving asteroids mostly untouched. The two most notable exceptions to this are the NASA NEAR mission and the Japanese Hayabusa spacecraft. The NEAR mission not only observed asteroid 253 Mathilde, but also orbited and landed on the surface of asteroid 433 Eros, reshaping ideas on the space weathering of asteroidal surfaces (McCoy et al., 2002). Hayabusa is the first sample return mission to an asteroid and is expected to return material from the surface of Itokawa to Earth in the summer of 2010 (Yano et al., 2006). The next step in asteroid exploration is the Dawn mission, which launched September 2007. Dawn will orbit and analyze two of the largest objects, 4 Vesta and 1 Ceres, in the asteroid belt between Mars and Jupiter (Russell et al., 2002; 2004; 2006).

The asteroids represent material that was not accreted into large bodies during the formation of the terrestrial planets. Although some asteroids are known to have differentiated, they have not been subject to the significant reprocessing that occurred due to planetary formation after that time. Instead, the asteroids record the conditions and processes that were taking place in the earliest history of the Solar System, providing us with a tool to understand its formation and evolution. The majority of meteorites in current collections originated from the asteroid belt, and they encompass samples from both primitive (undifferentiated) and evolved (differentiated) bodies.

Vesta and Ceres were chosen as the targets for the Dawn mission because during early solar system history they evolved into very different bodies (Russell et al., 2002; Russell et al., 2006): Ceres is relatively primitive and icy (e.g. Gaffey and McCord, 1978; Larson et al., 1979); Vesta is magmatically differentiated and dry (e.g. McCord et al., 1970). The launch of the Dawn mission has come at a particularly opportune time in light of recent meteorite research, which implies that differentiation of planetary bodies occurred much earlier than previously thought. Undifferentiated meteorites, or chondrites, which represent primitive asteroid material, were, until recently, believed to be the earliest formed materials in the Solar System. However, recent chronological studies of the iron meteorites, which are presumed to represent samples from the cores of disrupted differentiated asteroids, suggest that they formed within ~10 million years of the formation of the solar system (Kleine et al., 2005; Wadhwa et al., 2006). If these new relative ages are correct then the iron meteorites measured are oldest material dated to this point, making them representatives of first-generation planetesimals (Kleine et al., 2005). This may mean that the chondritic asteroids were actually accreted later in solar system history than those that underwent differentiation (Kleine et al., 2005), requiring us to rethink our ideas about the formation of both primitive and differentiated material in the early Solar System, which is the primary science goal of Dawn.

Ceres was the first asteroid to be discovered, in 1801 by Giuseppe Piazzi, who was working on the compilation of a new star catalog (Piazzi, 1801). It is the largest object in the asteroid belt, with a mean radius of ~470km (Millis et al., 1987). Ceres is speculated to be composed of carbonaceous chondrite-like material with water ice. Evidence to substantiate this conclusion comes from its low mean density (McCord and

Sotin, 2003), albedo (Bowell and Zellner, 1973), and relatively featureless visible reflectance spectrum (Chapman et al., 1973). However, recent Hubble Space Telescope observations and modeling of the shape of Ceres suggest that some differentiation may have occurred (Thomas et al., 2005; McCord and Sotin, 2005). Ceres may actually be composed of a rocky core overlain by a water-ice rich mantle (Thomas et al., 2005; McCord and Sotin, 2005), which would make it a far more complicated body than first thought. Dawn carries four main instruments (a framing camera, a visible-infrared mapping spectrometer, a gamma ray and neutron spectrometer, and a magnetometer) as well as radio science experiments to determine gravity fields (Russell et al., 2004). The combination of the measurements taken by this instrumentation will help refine physical models, as well as allowing observation of any surface processes that may be occurring. This may help us decipher the complex history of Ceres.

Vesta was discovered in 1807 by Wilhelm Olbers (e.g. Pilcher, 1979; Foderá Serio et al, 2002), and is usually considered as the second largest asteroid with a mean radius of 258km (Thomas et al., 1997a), although its size is within error of the asteroid 2 Pallas (Drake, 2001). In contrast to Ceres, Vesta is believed to have a basaltic surface, because remote sensing observations (McCord et al., 1970; Binzel et al., 1997; Gaffey, 1997) and models indicate that this asteroid differentiated to form a core, mantle and crust (Hewins and Newsom, 1988; Righter and Drake, 1997). Vesta is commonly regarded as the largest differentiated body in the main-belt (Keil, 2002).

1.2 The Vesta-HED connection

One of the reasons for continued scientific interest in Vesta is its uniqueness, not only as a large differentiated body in the asteroid belt, but also because it is believed that

the howardite, eucrite, diogenite (HED) meteorite family originated from it. The HED family consists of cumulate orthopyroxenites (diogenites), and basalts/gabbros (eucrites) as well as regolith breccias, which contain clasts of both materials (howardites), suggesting formation on a common surface (e.g. Drake, 2001). More support for this theory is given by their common cosmic ray exposure ages, implying they were ejected at the same time, and, therefore, likely from the same body (Eugster and Michel, 1995). They also all lie on the same oxygen isotopic fractionation line, indicating a common origin (Clayton and Mayeda, 1996).

McCord et al. (1970) were first to note the similarity between the spectra of Vesta and the HED meteorites, and Consolmagno and Drake (1977) then later proposed that the HEDs might have originated from Vesta. They noted that the HED group represented crust and upper mantle material only, with no representatives from the lower mantle and core, suggesting that the parent body must still be intact. However, at that time it was not believed dynamically possible to deliver fragments from Vesta to Earth (Wasson and Wetherill, 1979). In 1993 Binzel and Xu (1993) discovered a group of asteroids, known as the "Vestoids" that lie between Vesta and the 3:1 orbital resonance with Jupiter. They were able to establish a dynamic pathway, from the Vestoids, along which the HEDs could travel to Earth. Since then, work on the Vestoids has shown that many of them exhibit spectra consistent with Vesta, and with the mineral compositions observed in the HEDs (Binzel and Xu, 1993; Vilas et al., 2000; Burbine et al., 2001)

The proposed link between Vesta, the HEDs and the Vestoids was strengthened by the work of Thomas et al. (1997b). They examined the surface of Vesta for signs of significant impact excavation using Hubble Space Telescope images and were able to

identify a 460km -wide crater in the southern hemisphere. This basin penetrated through the basaltic crust, and may have exposed upper mantle, olivine-rich material (Gaffey, 1997; Binzel, 1997). Calculations indicate that this single event alone could have ejected 10^6 km^3 of material, of which all the Vestoids together would only make up a few percent (Thomas et al., 1997b). The combined evidence for mechanisms ejecting material from the surface of Vesta, and viable pathways by which to deliver them to Earth has led most planetary scientists to accept that it is the parent body for the HED family. This relationship allows us to link detailed geochemical data collected on the HED meteorites to the surface measurements taken by Dawn.

My Ph.D. dissertation aims to address this ground-truthing opportunity by quantifying the relationship between the petrology and visible near-infrared (VIS-NIR; 0.3 - 2.5 μm) spectra of the unbrecciated eucrites, in order to better understand the petrogenesis of the basaltic crust of Vesta. It is divided into parts (II through IV), representing individual research papers, which will all be submitted to peer reviewed journals.

1.3 The Petrology of Unbrecciated Eucrites – Part II

In order to draw conclusions about the petrology and formation of the surface of Vesta from the spectral data to be returned by Dawn, we must first understand the relationship that exists between the petrology and spectra of the HED meteorites. Part II of my dissertation aims to petrologically characterize the eucrites, particularly in terms of the features that are known to influence the VIS-NIR spectra, such as grain-size, texture, mineral chemistries, and modal mineral proportions. However, the majority of the eucrites are polymict samples, that is, they are breccias and contain mixtures of different

eucrite lithologies. If we were to analyze the spectra of a brecciated sample then it would be hard to know which lithology controlled which spectral features. For this reason, only unbrecciated eucrites were selected for the petrologic part of this study.

The eucrite group is most commonly divided into basaltic and cumulate members. However, the basaltic eucrites (also known as the non-cumulates) can be further subdivided in terms of the geochemistry of its members. The Main Group–Nuevo Laredo trend contains the most abundant type of eucrite, and they are characterized by an anticorrelation between incompatible element contents and Mg# (Stolper, 1977; Mittelfehldt and Lindstrom, 2003). The Stannern trend eucrites show weaker anticorrelation between incompatible element compositions and Mg# (BVSP, 1981; Stolper, 1977). Whilst this section aims to thoroughly characterize the full petrologic range seen within the unbrecciated eucrites, it is important to note that incompatible element concentrations, or trace element geochemistry, will not have a great impact on the spectra of these samples. Therefore, only major-element mineral chemistry was taken into account here. The textural and mineralogical differences that exist amongst the unbrecciated eucrites, and the processes with caused them are explored in this chapter. Most of the eucrites have undergone thermal metamorphism, the degree of which is commonly measured by examining the amount of re-equilibration in the major elements of pyroxene (Fe, Mg, Ca)(Takeda and Graham, 1991). A new method for determining the relative amount of metamorphic equilibration of the eucrites is suggested, which uses both the major and minor elements (Al, Ti, Cr) in pyroxene, as well as the amount of chemical zonation in plagioclase.

1.4 The Spectra of the Unbrecciated Eucrites –Part III

The vast majority of the meteorites studied in Part II were 'finds'. This means that the meteorites were recovered sometime after they fell, as opposed to being recovered as observed falls. Finds, therefore, have been subject to terrestrial weathering processes since they landed, which may have been tens of thousands of years ago. Weathering affects meteorites in the same way as terrestrial rocks, and rust around iron-rich minerals is common. However, the formation of weathering products has been shown to have an influence on the spectrum of a sample. As a result, any sample from Part II that was observed to have signs of terrestrial weathering in either thin section or hand sample was not considered for spectral work.

Eleven unbrecciated eucrites, covering the whole range of properties of the group, were selected from the initial 29, and their VIS-NIR spectra (0.3 – 2.5 μm) were collected using the NASA/Keck Reflectance Experiment Laboratory (RELAB) at Brown University (Pieters, 1983). This wavelength range was chosen because it overlaps with that of the visible-infrared (VIR) spectrometer aboard Dawn, which has ranges in both the visible (0.25-1.0 μm) and infrared (0.95-5.0 μm)(Russell et al., 2006). The relationship between the spectra and mineralogy of the unbrecciated eucrites is addressed, and the implications for the petrogenesis of Vesta are discussed.

1.5 The Spectra of Vestoids– Part IV

Dawn is scheduled to arrive at Vesta in 2010 (Russell et al., 2002); however, the identification of the Vestoids, a group of asteroids that appear dynamically and compositionally related to Vesta (Binzel and Xu, 1993), presents us with the opportunity to utilize the combined petrologic-spectral dataset now.

The Vestoids are thought to represent kilometer-plus-size fragments of the crust of Vesta (Binzel and Xu, 1993) and, hence, can provide a constraint on the approximate size of lithologic provinces that may occur on their parent body. Comparisons between eucrite spectra and individual Vestoids should allow us to constrain the minimum size of individual igneous terrains on the surface of Vesta. If the spectra suggest that more than one type of material is present on the Vestoids, i.e., if the spectral signature of different eucrites, or both eucrites and diogenites, have been averaged over the hemisphere being measured, then it implies that the size of the igneous provinces on Vesta is smaller than the Vestoids. It should be noted that the lithologies on the surface of the Vestoids reflect not only those present on the surface of Vesta, but also those at depth. Therefore, they demonstrate both the lateral and vertical heterogeneity on their parent body. The processes that form large-scale igneous units are different from those that create small-scale ones. If we are able to quantify the scale of the units, or provinces, that exist on and within Vesta then we may also draw conclusions about how they formed.

The final chapter of this dissertation discusses the application of the data gathered in Parts II and III to Vestoid spectra. All spectra were collected by SpeX, a spectrograph at the NASA Infrared Telescope Facility (IRTF) on Mauna Kea. The unbrecciated eucrite spectra from Part III are used in conjunction with available howardite and diogenite spectra (from samples characterized petrologically in the literature) to assess the lithologic variability amongst the Vestoids and, therefore, on the surface of Vesta itself.

1.6 Collaborations

This dissertation has been made possible by numerous collaborations. Allison Gale, while working at the Smithsonian Institution collected much of the SEM data for the unbrecciated eucrites presented in part II, and was responsible for the preparation of the pyroxene-plagioclase mixtures in part III. All laboratory spectra were collected by Takahiro Hiroi at the RELAB facility, Brown University. Schelte Bus, at the University of Hawaii, Hilo, was responsible for the collection of all Vestoid spectra, using SpeX at the NASA IRTF facility on Mauna Kea. Work on the pyroxene-plagioclase mixtures was part of an ongoing collaboration with Jessica Sunshine, Timothy McCoy, Catherine Corrigan, and Schelte Bus. Mössbauer analyses given in Part III were collected at Mount Holyoake University by M. Darby Dyar. However, all the data analysis was performed by Rhiannon Mayne, who was also responsible for the write-up of all results related to those collaborations presented here.

References Cited

Adams J.B. 1974. Visible and near-infrared diffuse reflectance spectra of pyroxene as applied to remote sensing of solid objects in the solar system. *Journal of Geophysical Research* 79: 4829-4836.

Basaltic Volcanism Study Project. 1981. *Basaltic volcanism of the terrestrial planets*. Pergamon Press, Inc., New York. 1286pp.

Binzel R.P. and Xu S. 1993. Chips off asteroid 4 Vesta: Evidence for the parent body of basaltic achondrite meteorites. *Science* 260:186-191.

Binzel R.P., Gaffey M.J., Thomas P.T., Zellner B.H., Storrs A.D., and Wells E.N. 1997 Geologic mapping of Vesta from 1994 Hubble Space Telescope images. *Icarus* 128:95-103.

Bowell E. and Zellner B. 1974. Polarizations of asteroids and satellites. In *Planets, stars, and nebulae studied with photopolarimetry*, edited by Gehrels T. Tucson: University of Arizona Press pp381-404

Burbine T.H., Buchanan P.C., Binzel R.P., Bus S.J., Hiroi T., Heinrichs J.L., Meibom A., and McCoy T.J. 2001. Vesta, vestoids, and the howardite, eucrite, diogenite group: Relationships and the origin of spectral differences. *Meteoritics and Planetary Science* 36:761-781.

Chapman C.R., McCord T.B., and Johnson T.V. 1973. Asteroid spectral reflectivites. *The Astronomical Journal* 78:126-140.

Clayton R.N. and Mayeda T.K. 1996. Oxygen isotope studies of achondrites. *Geochimica et Cosmochimica Acta* 60:1999-2017.

Cloutis E.A. and Gaffey M.J. 1991. Pyroxene spectroscopy revisited: Spectral-compositional correlations and relationships to geothermometry. *Journal of Geophysical Research* 96: 22,809-22,826.

Cochran A.L. and Vilas F. 1998. The changing spectrum of Vesta: Rotationally resolved spectroscopy of pyroxene on the surface. *Icarus* 134:207-212.

Consolmagno G.Y. and Drake M.J. 1977. Composition and evolution of the eucrite parent body: Evidence from rare earth elements. *Geochimica et Cosmochimica Acta* 41:1271-1282. Drake M.J. 2001. The eucrite/Vesta story. *Meteoritics and Planetary Science* 36:501-513.

Drake M.J. 2001. The eucrite/Vesta story. *Meteoritics and Planetary Science* 36:501-513

Eugster O. and Michel Th. 1995. Common asteroid break up events of eucrites, diogenites, and howardites, and the cosmic ray production rates for noble gases in achondrites. *Geochimica et Cosmochimica Acta* 59:177-199.

Feierberg M.A. and Drake M.J. 1980. The meteorite-asteroid connection: the infrared spectra of eucrites, shergottites and Vesta. *Science* 209: 805-807.

Feierberg M.A., Larson H.P., Fink U., and Smith H.A. 1980. Spectroscopic evidence for two achondrite parent bodies: Asteroid 349 Dembowska and 4 Vesta. *Geochimica et Cosmochimica Acta* 59:177-200.

Foderà Serio G., Manara A., and Sicoli P. Giuseppe Piazzi and the discovery of Ceres. In *Asteroids III*, edited by Bottke Jr. W.F., Cellino A., Paolicchi P., and Binzel R.P. Tucson: University of Arizona Press. pp. 3-16.

Gaffey M.J. 1997. Surface lithologic heterogeneity of asteroid 4 Vesta. *Icarus* 107:267-283.

Gaffey M.J. and McCord T.B. 1978. Asteroid surface materials: Mineralogical characterizations from reflectance spectra. *Space Science Reviews* 21:555-628.

Hewins R.H. and Newsom H.E. 1988. Igneous activity in the early solar system. In *Meteorites and the early Solar System*, edited by Kerridge J.F., and Matthews M.S. Tucson: University of Arizona Press. pp. 73-101.

Hsu G. and Crozaz H. 1997. Mineral chemistry and the petrogenesis of eucrites: II cumulate eucrites. *Geochimica et Cosmochimica Acta* 61:1293-1302.

Keil K. 2002. Geological History of Asteroid 4 Vesta: The "Smallest Terrestrial Planet". In *Asteroids III*, edited by Bottke Jr. W.F., Cellino A., Paolicchi P., and Binzel R.P. Tucson: University of Arizona Press. pp. 573-584.

Kleine T., Mezger K., Palme H., Scherer E., and Muenker C. 2005. Early core formation in asteroids and late accretion of chondrite parent bodies: Evidences from ^{182}Hf-^{182}W in CAIs, metal-rich chondrites, and iron meteorites. *Geochimica et Cosmochimica Acta* 69:5805-5818.

Larson H.P., Feierberg M.A., Fink U., and Smith H.A. 1979. Remote spectroscopic identification of carbonaceous chondrite mineralogies: Applications to Ceres and Pallas. *Icarus* 39:257-271.

McCord T.B., Adams J.B., and Johnson T.V. 1970. Asteroid Vesta: Spectral reflectivity and compositional implications. *Science* 168: 1445-144.

McCord T.B. and Sotin C. 2003. Ceres: Evolution and current state. *Journal of Geophysical Research* 110:E05009, doi:10.1029/2004JE002244.

McCord T.B. and Sotin C. 2005. Ceres: Evolution and current state. *Journal of Geophysical Research* 110: E05009, doi:10.1029/2004JE002244.

McCoy T.J., Robinson M.S., Nittler L.R., and Burbine T.H. 2002.The Near Earth Asteroid Rendezvous mission to asteroid 433 Eros: A milestone in the study of asteroids and their relationship to meteorites. *Chemie de Erde* 62:89-121

Millis R.L. et al. 1987. The size, shape, density, and albedo of Ceres from its occultation of BD+8 deg 471. *Icarus* 72: 507-518.

Mittlefehldt D.W. and Lindstrom M.M. 2003. Geochemistry of basaltic eucrites; and Hf and Ta as petrogenetic indicators for altered Antarctic eucrites. *Geochimica et Cosmochimica Acta* 67: 1911-1935.

Piazzi G. 1801. *Risultati delle Osservazioni della Nuova Stella scoperta il dí 1. Gennajo all'Observatorio relae di Palmero.* Palmero: Nella Reale. 25p.

Pieters C.M. 1983. Strength of mineral absorption features in the transmitted component of near infrared reflected light: First results from RELAB. *Journal of Geophysical Research* 88:9534-9544.

Pilcher F. 1979. Circumstances of minor planet discovery. In *Asteroids*, edited by Gehrels T. Tucson: University of Arizona Press. pp. 1130-1154.

Russell C.T., Coradini A., Feldman W.C., Jaumann R., Konopliv A.S., McCord T.B., McFadden L.A., McSween Jr. H.Y., Mottola S., Neukum G., Pieters C.M., Raymond C.A., Smith D.E., Sykes M.V., Williams B.G., and Zuber M.T. 2002. Dawn: A journey to the beginning of the solar system. *Proceedings of the ACM 2002 Conference*. pp. 63-66.

Russell C.T., Coradini A., Christensen U., De Sanctis M.C., Feldman W.C., Jaumann R., Keller H.U., Konopliv A., McCord T.B., McFadden L.A., McSween H.Y., Mottola S., Neukum G., Pieters C.M., Prettyman T.H., Raymond C.A., Smith D.E., Sykes M.V., Williams B., Wise J., Zuber M.T. 2004. Dawn: A journey in space and time. *Planetary Space Science* 52:465-489.

Russell C.T., Capaccioni F., Coradini A., Christensen U., De Sanctis M.C., Feldman W.C., Jaumann R., Keller H.U., Konopliv A., McCord T.B., McFadden L.A., McSween H.Y., Mottola S., Neukum G., Pieters C.M., Prettyman T.H., Raymond C.A., Smith D.E., Sykes M.V., Williams B., and Zuber M.T. 2006. Dawn discovery mission to Vesta and Ceres: Present status. *Advances in Space Research* 38:2043-2048.

Stopler E. 1977. Experimental petrology of eucritic meteorites. *Geochimica et Cosmochimica Acta* 41: 587-611.

Sunshine J.M., Pieters C.M., and Pratt S.F. 1990. Deconvolution of mineral absorption bands: An improved approach. *Journal of Geophysical Research* 95: 6955-6966.

Sunshine J.M. and Pieters C.M. 1993. Estimating modal abundances from the spectra of natural and laboratory pyroxene mixtures using the modified Gaussian model. *Journal of Geophysical Research* 98: 9075-9087.

Takeda H. and Graham A.L. (1991) Degree of equilibration of eucritic pyroxenes and thermal metamorphism of the earliest planetary crust. *Meteoritics* 26, 129-134.

Thomas P.C., Parker J.Wm., McFadden L.A., Russell C.T., Stern S.A., Sykes M.V., and Young E.F. 2005. Differentiation of the asteroid Ceres as revealed by its shape. *Nature* 437:224-226.

Thomas P.C., Binzel R.P., Gaffey M.J., Zellner B.H., Storrs A.D., and Wells E. 1997a. Vesta: Spin pole, size, and shape from HST images. *Icarus* 128: 88-94.

Thomas P.C., Binzel R.P., Gaffey M.J., Storrs A.R., Wells E.N., and Zellner B.H. 1997b. Impact excavation on asteroid 4 Vesta: Hubble Space Telescope results. *Science* 277:1492-1495.

Vilas F., Cochran A.L., and Jarvis K.S. 2000. Vesta and the Vestoids: A new rock group? *Icarus* 147:119-128.

Wadhwa M., Srinivasan G., and Carlson R.W. (2006) Timescales of planetary differentiation in the early solar system. In: *Meteorites and the Early Solar System II* (eds. D.S. Lauretta and H.Y. McSween Jr.) University of Arizona Press, pp. 715-733.

Wassen J.T. and Wetherill G.W. 1979. Dynamical, chemical, and isotopic evidence regarding the formation locations of asteroids and meteorites. In *Asteroids*, edited by Gehrels T. Tucson: University of Arizona Press pp. 926-974.

Yano H., Kubota T., Miyamoto H., Okada T., Scheeres D., Takagi Y., Yoshida K., Abe M., Abe S., Barnouin-Jha O., Fujiwara A., Hasegawa S., Hashimoto T., Ishiguro M., Kato M., Kawaguchi J., Mukai T., Saito J., Sasaki S., and Yoshikawa M. 2006. Touchdown of the Hayabusa Spacecraft at the Muses Sea on Itokawa. *Science* 312:1350-1353.

II. The Petrology of the Unbrecciated Eucrites

This chapter is a reformatted version of a paper, by the same name, submitted to Geochimica et Cosmochimica Acta by Rhiannon G. Mayne, Harry Y. McSween Jr., Timothy.J. McCoy, and Alison Gale.

Mayne R.G., McSween H.Y. Jr., McCoy T.J., and Gale A. 2008. The petrology of the unbrecciated eucrites. *Submitted*.

Abstract

Twenty-nine unbrecciated eucrites have been thoroughly characterized in terms of the petrologic factors that affect their spectra, such as mineral chemistry, proportions, grain sizes, and textures. We have conducted a combined petrologic and spectral study designed to provide insight into the petrogenesis of the basaltic crust of Vesta and the variety of rock-types that exist within it, as well as aid in the petrologic interpretation of spectra to be collected by the Dawn orbiting spacecraft. This paper details the petrologic part of the study. Unbrecciated eucrite samples were selected to avoid the complications of lithologic mixing in the accompanying spectral study. A wide variety of textural types are seen within the basaltic eucrites, they encompass quenched, coarse-grained, and granoblastic samples. Zoned eucrites and those that preserve a history of initial rapid cooling are rare. Nearly all of the eucrite samples have been metamorphosed and would commonly be classified as equilibrated; however, this term reflects only the pyroxene quadrilateral (Mg, Fe, Ca) compositions, and considerable variation is seen within the minor elements (Al, Ti, and Cr) in pyroxenes as well as plagioclase compositions. Using these three components together with pyroxene geothermometry provides a better estimate for the relative degree of thermal metamorphism a eucrite has experienced.

1. Introduction

The HED meteorites are comprised of basaltic and cumulate eucrites (basalts and gabbros, respectively), diogenites (orthopyroxenites), and howardites (regolith breccias composed primarily of eucrites and diogenites), which together constitute the largest group of achondrites. These meteorites are linked by oxygen isotope compositions that lie along a common mass fractionation line (Clayton and Mayeda, 1996), and their radiometric ages indicate asteroid differentiation and magmatism within ~10 million years of the formation of the solar system (Wadhwa et al., 2006). They are commonly believed to have originated on 4 Vesta (McCord, 1970; Consolmagno and Drake, 1977; Drake, 2001; Keil, 2002), a large differentiated asteroid in the main belt. Vesta itself is of great interest, as it appears to represent one of the few protoplanets that have survived intact since their formation early in solar system history (e.g. Drake, 2001). To date, no one model proposed has been able to explain the general geologic evolution of Vesta and reproduce the complex geochemical relationships seen within the entire suite of HED rocks (Mittlefehldt and Lindstrom, 2003); a successful petrogenetic model must be able to explain both.

The Dawn mission, which launched September 2007, will carry, among other instruments, a mapping spectrometer, VIR (Visible Infrared), which will provide measurements in the visible near-infrared (VIS-NIR) range: 0.25μm – 5μm (Russell et al., 2006). This instrument will analyze the surface of Vesta from orbit and enable surface spectral maps to be produced (Russell et al., 2002). In order to interpret such maps it is important that the HEDs themselves are well characterized petrologically, and

that the mineralogical and textural factors that affect their spectra are well understood and quantified. This may then allow us to establish a geologic context for the HEDs, the properties of which suggest formation as surface flows, plutons within the crust, and regolith materials.

Gaffey (1997) observed sub-hemispheric color and spectral variations across the surface of Vesta as it rotated, corresponding to regions with differing mineralogies. He produced a generalized lithologic map of Vesta, describing surface units as eucrite-rich or diogenite-rich. Binzel et al. (1997) utilized Hubble Space Telescope images to compile their own geologic map of Vesta. They observed contrasts in albedo and composition between the western and eastern hemispheres, which suggests a difference in rock types. A predominantly basaltic mineralogy, analogous to eucrites, was suggested for the western hemisphere, whereas the east appears to show a plutonic (diogenetic) component. They suggested that a major impact event might have preferentially excavated plutonic material in the eastern hemisphere. With a resolution of 170-615 m/pixel, depending on the planetocentric radius of the orbit (Russell et al., 2006), Dawn's VIR will vastly improve our knowledge of the spectral variability on the surface of Vesta, and therefore allow the lithologic differences and distributions of units to be investigated.

This paper focuses on the petrology of the unbrecciated eucrites, and is part of a larger study exploring the link between the petrologic and spectral characteristics of these samples. Approximately 85% of the eucrites are polymict or monomict breccias, and most of the eucrite literature has focused on breccias (e.g. Delaney et al., 1984; Hsu and Crozaz, 1996; Kitts and Lodders, 1998; Mittlefehldt and Lindstrom, 2003) rather than the less common unbrecciated meteorites. If we are to understand exactly what factors

influence the spectra of the eucrites, the unbrecciated samples are the key as they avoid the complications of lithologic mixing. Unbrecciated eucrites also provide valuable insight into a variety of eucrite rock-types, reflecting the lithologic heterogeneity that exists within the basaltic crust of Vesta, both at the surface and with depth. If we better understand the relationships between these samples and how they form, we can critically analyze models proposed for their formation and suggest what lithologies may be observed on the surface of Vesta with Dawn.

2. Background

2.1 Eucrite Spectra

In the VIS-NIR wavelength range spectra of the eucrites are dominated by the pyroxenes they contain. They produce two dominant absorptions at around 1 and 2 μm (Gaffey, 1976). The positions of these two absorption bands are directly proportional to the cations in the octahedral sites, primarily Ca^{2+}, Mg^{2+}, and Fe^{2+} (Adams, 1974; Burns, 1993). The 1 and 2-μm band centers both shift to longer wavelengths as the calcium content of the pyroxene is increased (Adams, 1974; Cloutis and Gaffey, 1991). However, it is the presence of iron (Fe^{2+}) in the pyroxene structure that actually causes the major absorptions. Therefore, in order for us to be able to predict the mineral chemistry of the surface of Vesta with remotely sensed data, we must have not only a knowledge of the mineral chemistries of the rocks it may consist of, but also an understanding of the influence of these compositions upon the spectra,

The eucrites contain ilmenite, chromite, troilite, and native iron-nickel metal. The low albedo in some meteorite spectra is associated with the presence of such opaque

phases (Johnson and Fanale, 1973), as they are often dark and spectrally featureless (Cloutis et al, 1990a;1990b), and act to suppress to the major Fe^{2+} silicate absorption bands (Miyamoto et al., 1981). This characteristic will depend on the type and abundance of the phase present and therefore we must attempt to quantify all these factors in order to assess its effect upon the spectra.

2.2 Eucrite Classification

There are several existing schemes that are used to subdivide the eucrites. Eucrites have been distinguished petrographically and chemically as cumulate and non-cumulate/basaltic rocks (e.g. Consolmagno and Drake, 1977; Stolper, 1977, BVSP, 1981). The basaltic eucrites are then commonly split into two main groups, Stannern and Main-Group-Nuevo Laredo, based on their geochemistry. The difference between these two groups lies primarily in their incompatible element concentrations, with the Stannern trend containing higher abundances (Stolper, 1977). However, in this study the aim is to petrologically characterize the unbrecciated eucrites and, later, apply this knowledge to better understand their spectra. The geochemical classification into the Stannern and Main Group-Nuevo Laredo trends is not likely to be spectrally significant when compared to factors such as pyroxene mineral chemistry, which is far more likely to affect the resulting reflectance spectrum. Therefore, the prevalent cumulate and non-cumulate/basaltic classification was used here, because they differ texturally and in terms of mineral chemistry, with cumulates having pyroxenes with higher-Mg contents (Consolmagno and Drake, 1977, Stolper, 1977). However, it should be noted that the unbrecciated basaltic eucrites exhibit a much wider range of textures than the cumulates.

3. Analytical Techniques

3.1 Sample Selection

All previously identified unbrecciated eucrites in the meteorite collection at the U.S. National Museum of Natural History (Smithsonian Institution) were examined in thin section, as well as those samples that were not classified in terms of their brecciation state. In general, the non-Antarctic eucrites have been studied in greater detail than the majority of those in the Antarctic collection. However, we observed that most of the textural variety within the unbrecciated eucrites is seen among meteorites of the Antarctic collection (Mayne et al., 2006). Although we were able to examine more unbrecciated eucrites from the Antarctic collection than the non-Antarctic (approximately 3:1), this cannot be the sole reason attributed to the difference in textural diversity. Non-Antarctic unbrecciated eucrites are dominated by coarse-grained cumulate samples, whereas Antarctic specimens cover a wide spectrum of textural types. Hand samples of the lesser-studied Antarctic meteorites were also examined at NASA Johnson Space Center, to ensure that thin sections were representative of the samples and to check for brecciation on a larger-scale.

It was not possible within the confines of this study to survey all known eucrites; however, we do believe the eucrites chosen here encompass the range of properties seen in this meteorite group. Initially, 29 unbrecciated eucrites (Table 1) were chosen by eliminating meteorite pairs and meteorites known to be breccias. ALH A81001 is an extremely fine-grained, quenched sample and was initially described as polymict (Grossman, 1994); ALH A81313, the only unbrecciated eucrite examined that contains maskelynite, was also classified as a polymict eucrite (Grossman, 1994). Subsequent

studies have suggested that ALH A81001 should be reclassified as unbrecciated (e.g. Warren et al, 1996; Mittlefehldt and Lindstrom, 2003). These two eucrites were included because no evidence for brecciation was observed in hand sample or thin section in this study.

Ibitira has been suggested to originate from a different parent body from the majority of the eucrites (Mittlefehldt, 2005), due to its unique oxygen isotope characteristics (Wiechert et al., 2004) and different pyroxene Fe/Mn ratio (Mittelfehldt, 2005). Because of its prominence in the literature it was decided to include Ibitira in this study. We investigate if the mineralogic differences between it and the other eucrites are overstated.

3.2 SEM Mapping

Elemental X-ray maps were collected on one thin-section of each of the 29 unbrecciated eucrites using the JEOL JSM-840 scanning electron microscope (SEM) in the Mineral Sciences Department of the Smithsonian Institution. A range of magnifications were used for the samples (Table 1), as it is important to be able to resolve the features within each section while still maintaining a reasonable data collection time. Factors such as grain size and exsolution were taken into account in determining resolution; coarser-grained samples were mapped using magnifications as low as 30X, whereas Ibitira, with its fine-scale exsolution, was mapped at 100X. The elemental X-ray maps of Fe, Si, and Al were combined to create mineral maps of each eucrite thin section studied. The maps distinguish pyroxene, plagioclase, silica, and the opaque minerals (oxides, sulfides, and metal) and allow the modal abundances for each of these groups to be measured. Modes were calculated three times for each sample map

using digital pixel counting and Table 2 shows the average mode for each sample and the standard deviation calculated for each mineral group.

3.3 Electron Microprobe

Chemical analyses of all major minerals (pyroxene, plagioclase, chromite, ilmenite, sulfides, metal) except silica (SiO_2) were made using the Cameca SX-50 electron microprobe at the University of Tennessee. Analytical conditions were: 15 kV, 20 or 30 nA, 1-μm beam for pyroxene, chromite, ilmenite, and metal; 15 kV, 20 nA, 5-μm beam for plagioclase and sulfides. ALH A81001 contained a silica-enriched plagioclase glass and this was analyzed at 15kV, 10nA, 1-μm beam. A correction was applied to the spinel analyses that contained vanadium, due to interference between the TiKβ and VKα peaks (Snetsinger et al., 1968). Tables 3-7 present representative analyses for each major mineral phase present in the sections studied. Previous studies of eucrites have reported the presence of tridymite (e.g. Delaney et al., 1984; Yamaguchi et al., 2001), cristobalite (e.g. Yamaguchi and Mikouchi, 2005; Chennaoui Aoudjehane and Jambon, 2007), and quartz (Treiman et al., 2004). However, in this study, we did not determine the mineralogy of the silica phase. Fe_2O_3 concentrations were not calculated for pyroxene or oxide minerals in these samples as previous bulk chemical analyses reported by Jarosewich (1990) did not find the presence of Fe_2O_3 in any HED meteorite. All reported analyses have good oxide totals (>98%) and stoichiometry. All errors reported for elemental compositions or ratios are given as 2σ, and are calculated from the counting errors associated with the analytical conditions used. All ternary diagrams in this paper were plotted using the freeware program Δplot (John, 2004).

4. Results

4.1 Textural Variations

All the mineral maps not used as figures accompanying this paper in Appendix II-A are given in Appendix II-B. Each map delineates plagioclase, pyroxenes, silica and opaque phases (chromite, ilmenite, troilite, kamacite, and taenite). These maps do not allow different pyroxene compositions to be distinguished, so both high- and low-Ca pyroxene are grouped together. Higher resolution maps allowing the differentiation between high- and low-Ca pyroxenes were collected only for those samples that will be included in the later spectral part of this study. Examples of the mineral maps, which cover the range of textures observed, are shown in Figure 1.

4.1.1 Basaltic Eucrite Textures

QUE 94484 is the only coarse-grained eucrite to contain elongate spherulitic plagioclase grains that in some areas reach over a millimeter in length. QUE 94484 (Figure 1a) contains abundant interstitial areas that are rich in silica and troilite, relative to other samples. These areas appear to be late-stage and probably represent residual melt pockets (*Antarctic Meteorite Newsletter 19-1*).

ALH A81001 (Figure 1b) is the finest-grained sample studied, with most grains being no larger than 200 μm. It has a vitrophyric texture and the "plagioclase" illustrated in Figure 1b is, in fact, glass having the composition of plagioclase plus silica. Pyroxene grains are lath-like, skeletal and often radiating (Figure 2a). Pyroxene phenocrysts reaching up to half a millimeter in size are found within this meteorite, although they are uncommon (Figure 2b) and probably crystallized before eruption. The map of ALH A81001 shows fine-grained areas with pyroxene grains typically between 50 and 100 μm.

These domains superficially resemble clasts, explaining its original polymict classification (Grossman, 1994). On closer microscopic inspection, however, pyroxene grains can be seen spanning the 'boundaries' between areas of different grain sizes, so the apparent clast relationship is an artifact and the sample can be described as texturally heterogeneous but unbrecciated. Fine-grained ilmenite is scattered throughout (Figure 2c), but it is not visible on the mineral map due to its small grain size (down to sub-micron in some grains) and it does not represent a significant modal component. Other fine-grained eucrites contain opaque phases (chromite, ilmenite, troilite, and kamacite) and silica on a scale that can be seen using the SEM mapping technique.

Coarser grained basalts are prevalent within the eucrites. Most of these samples exhibit a subophitic to ophitic texture (Table 1). Shock effects are relatively common and often cause granulation or fracturing of the samples. Chervony Kut (Figure 1c), a coarse-grained non-cumulate eucrite, retains its original igneous texture (sub-ophitic) despite being cataclasticized (Figure 2d). Previous authors have suggested that its origin can be attributed to comparatively slow magmatic crystallization followed by cataclasis and minor subsolidus recrystallization (Gooding et al., 1979). The unbrecciated eucrites show a range of features caused by shock metamorphism on their parent body. These range from fracturing, as described for Chervony Kut above, to mosaicism of grains. For example, MAC 02522 has mosaicized pyroxene. A few samples within the two-pyroxene eucrites contain shock-melted veins, such as LEW 85353 and EET 90029.

4.1.2 Granoblastic Textured Basaltic Eucrites

Five of the unbrecciated eucrites in this study have not completely preserved their original igneous textures. However, a range of metamorphic overprints is observed, from

Ibitira (Figure 1d), which exhibits an entirely granoblastic, fine-grained texture (Steele and Smith, 1976; Mittlefehldt, 2005), to BTN 00300 in which remnants of the original sub-ophitic texture remain (Mittlefehldt and Galindo, 2002). Both LEW 85305 and EET 90020 contain inequigranular granoblastic textures.

Ibitira also contains vesicles, which are an unusual feature in extraterrestrial basalts (McCoy et al., 2006). For terrestrial basalts that contain vesicles, the assumption is that they represent surface lava flows with CO, CO_2, or H_2O as the vesicle-forming gases (Wilkening and Anders, 1975); however, surface formation cannot necessarily be evoked for the vesicular eucrites. McCoy et al. (2006) concluded that vesicular basalts on asteroids require formation at depth. The lack of an atmosphere on these bodies means that there is no limit on the expansion of gas, so gas escape processes would be very efficient. Because of this unusual formation mechanism, in dikes at depth, vesicular eucrites may be a relatively uncommon occurrence.

One very interesting feature of this group is that only the samples with a granoblastic texture contain tabular silica grains. GRA 98098 (Figure 1e) is a relatively coarse-grained, texturally distinctive sample. Elongate white veins of silica can be seen in hand sample (Mittlefehldt and Lee, 2001). They appear to be a late-crystallizing phase as they overgrow or enclose the grains around them. In the section studied here, one lone silica grain is seen to cut across the entire thin section, so no conclusions can be made as to its overall length (Figure 1e). Smaller millimeter-sized tabular silica grains are found in Ibitira (Figure 1d). BTN 00300 also contains a few small tabular silica grains that crosscut the surrounding mineralogy, but not all the silica in the sample shows the same morphology. LEW 85305 contains an area in the section where silica is abundant and

poikilitcally encloses the minerals around it, suggestive of a large silica grain such as that in GRA 98098. However, it is harder to establish if this feature is one continuous grain.

4.1.3 Cumulate Eucrite Textures

Serra de Magé (Figure 1f) is one of the coarsest grained samples in this study, with pyroxene grains up to half a centimeter in size, whereas Moama has a much smaller grain size of under a millimeter. These samples show the coarsest exsolution lamellae of all the unbrecciated eucrites, as would be expected due to their slow cooling rate.

4.2 Modal Mineralogy

The unbrecciated eucrites are predominantly pyroxene-plagioclase basalts (Table 2), with lesser amounts of silica, ilmenite, chromite, troilite, and metal (kamacite in all but one sample) and rare late-stage phases such as fayalitic olivine, baddeleyite, and phosphates. Figure 3 illustrates the measured variation in pyroxene and plagioclase abundances and modal abundances for all the unbrecciated eucrites are given in Table 2. The majority of samples have <1 vol.% opaque minerals (oxides, troilite, and metal). The amount of silica in most thin sections is also low; however, this is much more variable with percentages ranging from 0 to <13 vol.%. GRA 98098 has a relatively high modal percentage of silica (8 vol.%) due to the one large grain that crosscuts the section. QUE 94484 and ALH A8100 have distinctive modal mineralogy: QUE 94484 has abundant late-stage phases relative to other samples (>2 vol.% opaque phases and >7 vol.% silica), and ALH A81001 contains no modally significant minor phases at all and has the lowest pyroxene to plagioclase ratio (Figure 3). Ilmenite is present (Figure 2c) in this sample but, as previously discussed, it is so fine grained that it is not shown on the SEM maps.

4.3 Mineral Chemistry

4.3.1 Pyroxenes

Compositional data for pyroxenes in all 29 unbrecciated eucrites are shown in Figure 4. It can be observed that orthopyroxene, pigeonite, and augite all occur within these samples.

The quadrilateral pyroxene compositions of all of the unbrecciated eucrites can be discussed in terms of the classification of Takeda and Graham (1991), who defined three main chemical zoning trends within the eucrite group (Figure 5 a-c). The majority of the unbrecciated eucrites in this study follow the Fe-Ca trend (Figure 5c), representing the variation from host pigeonite to exsolved augite in what have been called "ordinary" or equilibrated (Reid and Barnard, 1979) eucrites. QUE 94484, MAC 02522 (the zoned-pyroxene basalts) and, to a lesser extent, PCA 97053 (all shown in Figure 4) follow the Mg-Fe-Ca trend of Pun and Papike (1996), shown in Figure 5a. QUE 94484 pyroxenes show the most extensive zoning out of all the unbrecciated eucrites. Its compositions go from low-Ca, Mg-rich cores to more Fe-rich, low-Ca compositions and continue through increasing Ca contents. MAC 02522 pyroxenes, have one fairly uniform pyroxene composition and appear to have experienced Fe-Mg diffusion, suggesting partial equilibration, but they have not exsolved into two separate pyroxene compositions. PCA 97053 appears almost entirely equilibrated, with a few analyses indicating that some zonation may remain.

The cumulate eucrites can all be distinguished as they have more En-rich compositions. It was noted in the original classification of ALH A81313 that there appeared to be pyroxene- and plagioclase-rich layers present, suggesting a possible

cumulate origin (*Antarctic Meteorite Newsletter* 8-1). The quadrilateral pyroxene compositions would seem to support this suggestion, as ALH A81313 plots at compositions that mimic those of the cumulates, especially Serra de Magé (Figure 4). This sample should probably be reclassified as a cumulate eucrite.

ALH A81001 contains two populations of pyroxenes. It is the only sample that contains pyroxene phenocrysts, which are assumed to have formed before the magma reached the surface. These phenocrysts have a composition that is significantly lower in Ca than that of the rest of the sample, having Wo contents between 1 and 2%, compared to >20%. They do not represent a significant modal component but do appear to have compositions that are related to the primary pyroxene in the sample, as they plot on an extension of the tie line defined by non-phenocrysts in the pyroxene quadrilateral.

Plots of the minor elements Al, Cr, and Ti in pyroxenes were also constructed (smaller inset ternary plots in Figure 4). Despite most of the unbrecciated eucrites qualifying as equilibrated in terms of their quadrilateral components, a great diversity of compositions is observed among these minor elements. Some appear clustered (and therefore well equilibrated themselves), but most others show two trends (Figure 4). Trend 1 reflects a relatively constant Ti content with variation in Cr and Al contents (the most prevalent trend) and trend 2 a relatively constant Cr content with variation in Ti and Al contents. There are some samples, like LEW 88010, that appear to contain both trends. Chervony Kut demonstrates trend 1 well and, although it is seen in a number of other samples, it is not always as clearly defined. Trend 2 is less common among the unbrecciated eucrites, with LEW 85353 providing the best example. The possibility that these trends corresponded to a mixing line between high and low-Ca pyroxenes

(exsolution) was examined, but there appears to be no link between Ca content and minor element composition.

Pun and Papike (1996) discussed the expected crystallization sequence for the eucrites, in terms of their substitution couples. Basaltic assemblages begin at Cr-rich compositions, becoming more Al-rich as Cr is removed from the melt. This would involve both the $^{VI}Cr^{3+}$-$^{IV}Al^{3+}$ and $^{VI}Al^{3+}$-$^{IV}Al^{3+}$ couples, gradually shifting to the $^{VI}Al^{3+}$-$^{IV}Al^{3+}$ couple as Cr is depleted. When plagioclase starts to crystallize the pyroxene is competing for Al, resulting in a shift to the $^{VI}Ti^{3+}$-$^{IV}Al^{3+}$couple. The unbrecciated eucrites in this study that have not been equilibrated with respect to their minor element compositions appear to follow such a sequence. Trend 1 reflects early pyroxene crystallization before the onset of plagioclase, with little variation in Ti content, while trend 2 represents those pyroxenes crystallizing after plagioclase reached the solidus. Those unbrecciated eucrites that show minor-element pyroxene compositions that are a combination of both trends represent pyroxenes in that crystallized continuously before and after plagioclase crystallization began.

Fe/Mn ratios in pyroxenes are thought to be a diagnostic tool for determining if samples have a common planetary origin (Papike et al., 2003), as the primordial values of these elements are believed to remain constant throughout planetary differentiation (Papike, 1998). Oxygen isotopes are also commonly used to distinguish meteorites from different parent bodies. Wiechert et al. (2004) identified four eucrites (Pasamonte, Caldera, ALH A78132, and Ibitira) whose oxygen isotopic compositions deviated from those of the other eucrites. Mittlefehldt (2005) and Lentz et al. (2007) have investigated the possibility that samples with anomalous O isotope values also show distinct pyroxene

Fe/Mn ratios. Mittlefehldt (2005) found Ibitira's pyroxene Fe/Mn ratio differed from other eucrites, supporting its derivation from a different parent body. However, Pasamonte and Caldera appear indistinguishable from the general eucrite trend (Lentz et al., 2007). The Fe and Mn data for all pyroxenes in this study were plotted against Fe/Mg and Wo content and examined for distinct values (Figs. 6a and b).

The 29 unbrecciated eucrites define a much broader range of pyroxene Fe/Mn values than have previously been reported; values under 20 and up to almost 45 are measured (Figs. 6a and b). Ibitira pyroxene Fe/Mn ratios are the highest measured, but they overlap with the rest of the Fe/Mn pyroxene analyses. This diagram appears to allow cumulate and non-cumulate samples to be distinguished. Pyroxenes in each cumulate sample define a narrow range of Fe/Mg and Wo values but a large range in Fe/Mn, producing nearly vertical trends in Figure 6a and 6b. The narrow range of Fe/Mg values appear fairly diagnostic of the cumulate group. EET 92023 also demonstrates this pattern with just slightly more scatter in the data, although its origins are debated (see below). However, EET 87520, proposed as a partial cumulate (Mittlefehldt and Lindstrom, 2003), does not mirror the narrow Fe/Mg range seen in the cumulate eucrites. Of all the non-cumulate eucrites studied, QUE 94484 can be distinguished most easily; it has anomalously low pyroxene Fe/Mn ratios. In Figure 6c Fe is plotted directly against Mn and it can be seen that the low Fe/Mn values for QUE 94484 are a result of greater abundance of Mn rather than depletion of Fe. This sample was identified as unusual due to the high quantity of late-stage phases present, which are probable residual melt pockets.

4.3.2 Plagioclase

The range of plagioclase compositions, expressed as the An (Anorthite $CaAl_2Si_2O_8$) end-member, measured for all samples is shown in Figure 7. No sample has an Or (Orthoclase $KAlSi_3O_8$) content greater than Or_5, and most commonly there is no detectable Or component. The Or contents of analyzed feldspars (plotted as K in atomic formula units against An#) are compared in Figure 8a to the known trends for Moon/Vesta, Earth, and Mars (Papike, 1998; Papike et al., 2003). Most unbrecciated eucrite plagioclase compositions fall close to the previously defined Moon/Vesta line, although they appear to cluster slightly below it. ALHA 81001 is excluded from Figs. 7 and 8, as this sample actually contains a silica-enriched plagioclase composition glass rather than crystalline plagioclase. The overall range of $An_{73\text{-}96}$ compares well with previously reported ranges by Delaney et al. (1984) and Mittlefehldt et al. (1998), which were $An_{65\text{-}94}$ and $An_{75\text{-}93}$ respectively. Mittelfehldt (2005) reported that Ibitira had an unusually calcic composition when compared to other basaltic eucrites; however, in this study we see four other unbrecciated eucrites that have plagioclase compositions at, or above, An_{95}, suggesting that such feldspars are not as rare as previously thought. Of the 29 eucrites analyzed, over half appeared to contain zoned plagioclase, with grains typically becoming more An-poor from core to rim. Chervony Kut shows the most unequilibrated plagioclase of any of the unbrecciated eucrites, with some grains ranging from Ab_{91} at the core to Ab_{76} at the rim.

Figure 8b shows the measured range of Fe content within the eucrite plagioclase. The majority of the unbrecciated eucrites have Fe concentrations in their plagioclase that fall within the previous range defined by Papike (1998) of less than 0.06 afu Fe (Figure

8b). There are some samples that lie above this limit, e.g. Caldera, PCA 91078 and QUE 94484. The cumulate eucrites have relatively calcic plagioclase (An>90) and low Fe contents.

4.3.3 Oxides

The unbrecciated eucrites commonly contain ilmenite, ulvöspinel, chromite, troilite, and native-iron metal (Table 8). The chromites have varying compositions, ranging to more titaniferous chromites/ulvöspinel; however, they do not span the whole range of the ulvöspinel-chromite solid solution series (Figure 9a-c). Figure 9c provides a comparison of all these spinels with the work of Yamaguchi (2000), who analyzed the spinels of eucrites with different metamorphic histories. Most unbrecciated eucrites fall within the range of highly metamorphosed eucrites (type 4-6) and viewed as a group they contain compositions slightly poorer in Ti than those measured by Yamaguchi (2000). There are six samples whose compositions appear to lie partly in the field defined for types 1-2; these are LEW 88009, LEW 88010, PCA 97014, QUE 99658, PCA 91078, and MAC 02522. QUE 94484 does contain spinel minerals; however, this sample has undergone quite heavy terrestrial weathering and because of this the opaque phases are oxidized, so that we were unable to obtain good analyses.

Many of the basaltic unbrecciated eucrites show a range of chromite/ulvöspinel compositions within one sample. MAC 02522 has the widest range of all the unbrecciated eucrites analyzed. Spinels in the cumulate eucrites, as a group, vary in composition, but within each individual meteorite they are relatively constant. The granoblastic/highly-metamorphosed samples are richer in Cr than all other samples except MAC 02522, which shows a similar enrichment.

Ibitira, like the other granoblastic samples, shows relatively Ti-rich spinels; however, it also contains some spinels that compositionally lie between ulvöspinel and ilmenite, indicating more extreme Ti-enrichment. Annealing experiments (Arai et al., 1998) indicate the TiO_2 content of eucrite spinels increases at high temperature. It has already been observed that Ibitira has a metamorphic texture and, therefore, presumably was exposed to high temperatures, driving the spinel to more Ti-rich compositions. Yamaguchi et al. (1997a; 2000) previously concluded that the extreme Ti-enrichment seen in Ibitira spinels might be related to its complicated thermal history.

Ilmenite is a common minor phase in the unbrecciated eucrites (Table 8). Its composition varies both within and between samples. MgO contents range from 0.3 to over 5.2 wt. %, Cr_2O_3 from 0 to 5.5 wt. %, MnO from 0.59 to 1.5 wt. %, and ZrO_2 from 0 to 0.15 wt %. Rare Zr-rich grains were observed in association with spinels, usually within ilmenite, in a few samples. These grains were too small for accurate wavelength-dispersive electron microprobe analysis; however, a few were observed using energy-dispersive analysis and had a baddeleyite composition.

4.3.4 Troilite, Metal and Mesostasis

Eucrites commonly contain minor amounts of small metal grains, believed to form either during magmatic crystallization at low oxygen fugacity, or during later thermal metamorphism (Duke, 1965). As all the eucrites studied here are unbrecciated and none are believed to be impact melts, the metal they contain must be indigenous to the sample. The native-Fe metal is kamacite with very low Ni and Co contents (<1 wt.% of each in most samples), with the one exception of EET 92023 (see below). Kamacite is most often associated with troilite. The low-Ni metals in the eucrites most likely formed

by reduction of FeO in pyroxenes during thermal metamorphism (one of the mechanisms suggested by Duke, 1965). The close association of the metals with silica, which is another product of the breakdown reaction of pyroxene, supports this idea.

EET 92023 metal contains up to 50% Ni, making it the only sample in this study to contain taenite. Ni contents vary from 5 to 39% from core to rim, as also observed by Kaneda and Warren (1998). They also distinguished a compositional discontinuity near the grain edges and suggested that the outer rim, being richer in Ni, may in fact be tetrataenite. They concluded that the FeNi-metal dated from the original igneous crystallization of the rock (Kaneda and Warren, 1998). This compositional difference would seem to support the suggestion that EET 92023 is a clast from a mesosiderite (Mittlefehldt and Lindstrom 1991) and that the metal it contains was not formed by the same mechanism as seen in the rest of the unbrecciated eucrites.

Mesostasis assemblages occur within the unbrecciated eucrites, consisting of predominantly late-stage phases such as silica, olivine, ilmenite, and baddeleyite. Figure 2e shows an area of mesostasis in sample QUE 94484. This sample contains abundant mesostasis, consisting primarily of silica and troilite.

5. Discussion

5.1 Degree of Metamorphic Equilibration

The term ‘equilibrated,’ when applied to eucrites, refers only to the pyroxene quadrilateral compositions (Pun and Papike 1996). However, the plagioclase compositions measured in so-called equilibrated eucrites are not consistent with this description, as some grains show significant zoning. For example, Chervony Kut

plagioclase has an An content that varies by nearly 20 mole% (An_{75-94}), even though its pyroxenes are equilibrated. O'Neill and Delaney (1982) noted that plagioclase in eucrites was more resistant to thermal metamorphism than pyroxene due to the slow Si-Al diffusion kinetics in the coupled albite-anorthite substitution in plagioclase compared the kinetics of Fe-Mg diffusion in pyroxenes. As previously mentioned, the minor elements (Al, Ti, and Cr) in pyroxene (Figure 4) also show considerable variability, despite equilibration of the major elements. It may, therefore, be possible to obtain a more quantitative indicator of equilibration by considering both the major and minor elements of pyroxene as well as zoning within plagioclase. Table 9 compares the equilibration state of these three components. The table is ordered with respect to temperature, calculated for each sample using the QUILF two-pyroxene geothermometer (Andersen, 1993). Because these equilibration temperatures were calculated using pyroxene compositions from grains that are exsolved, the resulting output is the exsolution temperature and not that of original crystallization. The total column sums the "yes" values referring to whether pyroxene major elements (quadrilateral), pyroxene minor elements (Al, Cr, Ti), and plagioclase (An#) are equilibrated. As pyroxene equilibration temperature decreases, the overall equilibration of the eucrites does also. The succession shown in Table 9 indicates that the major elements in pyroxene become equilibrated first, followed by plagioclase, and then the minor elements in pyroxene. Taken together, these three equilibration indices thus provide a more sensitive estimate of the relative degree of metamorphism in eucrites.

Takeda and Graham (1991) also conducted a study of the homogenization of eucritic pyroxenes as a guide to their thermal history. They divided eucrites into six

types (Type 1 to 6), reflecting increasing degrees of metamorphism. They suggested that most eucrites have undergone at least one subsolidus-reheating event resulting from impact or lava flows extruded over a primary lava (Takeda and Graham, 1991). The results from this study also suggest widespread thermal metamorphism on Vesta, with most samples showing equilibration in at least the major elements in pyroxene. Most of the unbrecciated eucrites studied here, as previously mentioned, contain equilibrated, metamorphosed pyroxenes and, therefore, correspond to types 4-6 of Takeda and Graham (1991). QUE 94484, MAC 02522, and PCA 97053 to a lesser extent, are the only samples that exhibit less equilibrated compositions. If we re-examine those samples that contained spinel compositions overlapping the field defined by Yamaguchi (2000) for the type 1-2, least metamorphosed eucrites (LEW 88009, LEW 88010, QUE 99658, and MAC 02522), we observe that these samples do lie at the low temperature end of our equilibration table. Therefore, it would appear that despite widespread pyroxene equilibration the three indices used here can distinguish eucrites with different thermal histories.

Earlier we noted that tabular silica grains only occur in the granoblastic samples. Yamaguchi et al. (1997a) postulated that these were the result of partial melting at 1000-1100^{0}C. Barrat et al. (2007) observed that EET 90020 and Y-86763, which are both basaltic eucrites believed to have undergone partial melting, lack the mesostasis seen within other, less metamorphosed, basaltic eucrites. They suggest that metamorphism, partial melting, and then extraction of the partial melt from these samples produced these features. None of the granoblastic unbrecciated eucrites were observed to contain mesostasis and all of them have at least some tabular silica grains, indicating that the

formation of the silica grains is related to the high degree of metamorphism experienced by these samples. If Barrat et al. (2007) are correct, then silica may have formed from mobilization and crystallization of the remaining partial melt.

5.2 Understanding the Petrogenesis of the Basaltic Crust of Vesta

The eucrites are the key to understanding the petrogenesis of the basaltic upper crust of Vesta. Simplified cross-sections of Vesta commonly depict a howardite regolith, a eucrite upper crust, a diogenite lower crust or upper mantle, a dunite or harzburgite lower mantle, and a metal-rich core. Although this is a useful first-order model, each layer and its relationship to others must be fully understood and any model proposed for Vesta's differentiation must be capable of explaining these. In this study we have focused on the mineralogy and mineral chemistry of the unbrecciated eucrites, because it is these factors that will impact the spectra taken by the VIR aboard the Dawn spacecraft. As a result, we cannot draw any conclusions as to the origin of the magmas here, but we can glean information on their crystallization histories and environments of formation.

Yamaguchi et al. (1996) suggested that the widespread thermal metamorphism seen within the eucrites indicates that the crust of Vesta formed as a result of serial magmatism. They envisaged lava flows erupting and cooling rapidly at the surface only to be buried by subsequent lava flows, which underwent the same process. The lower units were then reheated by the lava flows above them, leaving only the uppermost flows unmetamorphosed. The period of volcanism was estimated to have lasted only a few Myr, and modeling suggests it produced a crust over 15 km thick (Yamaguchi et al., 1997b). The process of initial rapid cooling at the surface does not explain the formation of the cumulate eucrites, or coarser grained basaltic samples; however, these samples

could have intruded into the earlier buried flows as dikes or small magma chambers (Yamaguchi et al., 1997b). As was previously discussed, McCoy et al. (2006) invoked such a mechanism for the formation of those samples that contain vesicles at a depth of around 5 km. A model cross-section for the crust of Vesta is given in Figure 10.

The prevalence of some degree of metamorphic equilibration throughout the unbrecciated eucrites supports the hypothesis of serial magmatism and appears to be inconsistent with a magma ocean model. Although metamorphism caused by impact heating must have occurred on local scales, it seems unlikely that impacts can account for the near, if not total, global-scale heating event required (Keil et al., 1997). Zoned and rapidly cooled samples such as QUE 94484 and ALH A81001 are rare, suggesting that they were among the last lavas to crystallize on Vesta's surface. The ages of the basaltic eucrites are found to cluster around 4.47-4.48 Gyr (Blichert-Toft et al., 2002; Bogard et al., 2003), and the cumulates are ~100 Myr younger (Blichert-Toft et al., 2002). The close ages of all the basaltic eucrites also indicate that they were produced during a brief, but voluminous period of magmatism. However, it should be noted that serial magmatism alone might not be sufficient to explain the levels of re-equilibration seen in the unbrecciated eucrites. Serial magmatism occurs on Earth today in Hawaii, and most likely occurred on the Moon in the past, but neither Hawaiian nor lunar basalts show the same degree of metamorphic re-equilibration as the eucrites. Zoned pyroxenes are a common feature in basalts from both areas. This suggests that the internal heat of Vesta, driven by the presence of Al^{26} in the early Solar System, may have contributed significantly to the global-scale metamorphism on Vesta. The lava flows on the surface would then have acted as an insulation blanket, keeping the heat in Vesta, causing the

eucrites to become metamorphosed, and the elements within pyroxene and plagioclase to equilibrate.

The Fe/Mn ratios from pyroxenes within the unbrecciated eucrites have a wider range than has previously been reported and, used in conjunction with oxygen isotopes, indicate a more complex story. Previous authors have identified eucrites that show different Fe/Mn and oxygen isotopes to the majority of the eucrites (Mittlefehldt, 2005; Wiechert et al., 2004), and other eucrites with just different oxygen isotopes (Lentz et al., 2007). In this paper QUE 94484 was shown to exhibit lower Fe/Mn ratios compared to all other unbrecciated samples. If all the eucrites originate from a common parent body, the variations in oxygen isotopes and Fe/Mn ratios suggest widespread heterogeneity.

6. Summary

This paper discusses the petrology of the unbrecciated eucrites as part of a larger study into the relationship between the petrologic and spectral features of these meteorites. The unbrecciated eucrites were used to avoid the spectral complications of lithologic mixing that occurs with breccias. The eucrites are widely believed to originate from the basaltic crust of asteroid Vesta, one of the targets of the Dawn mission, and we can use these samples not only to explore the variety that exists within Vesta's complex crust, but also as a link to geologic context for the mission.

- The mineral chemistries, modal abundances, and textures of 29 unbrecciated eucrites were analyzed. A wide range of textures was observed, particularly in the Antarctic suite, with samples including quenched vitrophyric to coarse-grained basalts, and cumulate samples. This likely reflects only some of the diversity that

must exist within the basaltic crust of Vesta and hints at the complexity of the processes that went into forming the basaltic crust of 4 Vesta. At present we are only able to speculate on the real variety of rock-types that might currently exist on the surface and be seen by Dawn.

- With few exceptions, the unbrecciated eucrites have been thermally metamorphosed. The relative degree of metamorphic equilibration of the unbrecciated eucrites is assessed using pyroxene quadrilateral compositions, minor elements in pyroxene (Al, Ti, Cr) and the range of An content in plagioclase. These mineralogic components appear to have equilibrated at different rates as the eucrites cooled. These indicators of metamorphism correlate with pyroxene exsolution temperatures calculated by QUILF geothermometry.
- The almost ubiquitous metamorphism of the eucrite suite and the close ages of the basaltic eucrites (Blichert-Toft et al., 2002; Bogard et al., 2003) support the idea that they were formed during a time of serial magmatism (Yamaguchi et al., 1996), early in Solar System history.

Acknowledgments: Samples analyzed in this study were provided by the Smithsonian National Museum of Natural History. We thank Alan Patchen for all assistance with the electron microprobe, William Deane for editorial help, and Donald Lindsley for advice in using the QUILF program. This work was supported by a Graduate Fellowship at the Smithsonian to RGM and NASA Cosmochemistry grant NNG06GG36G to HYM.

References Cited

Adams J.B. 1974. Uniqueness of visible and near-infrared diffuse reflectance spectra of pyroxenes and other rock-forming minerals. *Journal of Geophysical Research* 79: 4829-4836.

Andersen D.J., Lindsley D.H., and Davidson P.M. 1993. QUILF: a PASCAL program to assess equilibria among Fe-Mg-Ti oxides, pyroxenes, olivine, and quartz. *Computers in Geoscience* 19:1333-1350.

Arai T., Takeda H., Lofgren G., and Miyamoto M. 1998. Metamorphic transformations of opaque minerals in some eucrites. *Antarctic Meteorite Research* 11:71-91.

Barrat J.A., Yamaguchi A., Greenwood R.C., Bohn M., Cotton J., Benoit M., and Franchi I.A. 2007. The Stannern trend eucrites: Contamination of Main Group eucritic magmas by crustal partial melts. 2007. *Geochimica et Cosmochimica Acta* 71:4108-4124.

Barrat J.A., Blichert-Toft J., Gillet PH., and Keller F. 2000. The differentiation of eucrites: The role of in situ crystallization. *Meteoritics and Planetary Science.* 35:1087-1100.

BVSP Basaltic Volcanism Study Project. 1981. *Basaltic Volcanism of the Terrestrial Planets.* Pergamon Press, Inc., New York., pp. 214-235.

Binzel R.P. and Xu S. 1993. Chips off asteroid 4 Vesta: Evidence for the parent body of basaltic achondrite meteorites. *Science* 260:186-191.

Binzel R.P., Gaffey M.J., Thomas P.T., Zellner B.H., Storrs A.D., and Wells E.N. 1997. Geologic mapping of Vesta from 1994 Hubble Space Telescope images. *Icarus* 28:95-103.

Blichert-Toft J., Boyet M., Télouk P., and Albaréde F. 2002. ^{147}Sm-^{143}Nd and ^{176}Lu-^{176}Hf in eucrites and the differentiation of the HED parent body. *Earth and Planetary Science Letters* 204:167-181.

Bogard D.D., and Garrison D.H. 2003. ^{39}Ar-^{40}Ar ages of eucrites and thermal history of asteroid 4 Vesta. *Meteoritics and Planetary Science* 38:669-710.

Bowman L.E., Papike J.J., and Spilde M.N. 1999. Diogenites as asteroidal cumulates: Insights from spinel chemistry. *American Mineralogist* 84:1020-1026.

Burns R.G. 1993. *Mineralogical Applications of Crystal Field Theory, 2nd edition*. New York: Cambridge University Press. 551 p.

Clayton R.N. and Mayeda T.K. 1996. Oxygen isotope studies of achondrites. *Geochimica et Cosmochimica Acta* 60:1999-2017.

Cloutis E.A. and Gaffey M.J. 1991. Pyroxene spectroscopy revisited: Spectral-compositional correlations and relationship to geothermometry. *Journal of Geophysical Research* 96:22,809-22,826.

Cloutis E.A., Gaffey M.J., Smith D.G.W., and Lambert R.St.J. 1990a. Metal silicate mixtures: Spectral properties and applications to asteroid taxonomy. *Journal of Geophysical Research* 95:8323-8338.

Cloutis E.A., Gaffey M.J., Smith D.G.W., and Lambert R.St.J. 1990b. Reflectance spectra of mafic silicate-opaque assemblages with applications to meteorite spectra. *Icarus* 84:315-333.

Chennaoui Aoudjehane H. and Jambon A. 2007. Determination of silica polymorphs in eucrites by cathodoluminescence. *Lunar and Planetary Science Conference XXXVIII***.** Lunar Planet. Inst., Houston. #1714 (abstract).

Consolmagno G.Y. and Drake M.J. 1977. Composition and evolution of the eucrite parent body: Evidence from rare earth elements. *Geochimica et Cosmochimica Acta* 41:1271-1282.

Delaney J.S., and Prinz M. 1984. The Polymict Eucrites. *Journal of Geophysical Research.* 89:C251-C288.

Drake M.J. 2001. The eucrite/Vesta story. *Meteoritics and Planetary Science* 36:501-513.

Duke M.B. 1965. Metallic iron in basaltic achondrites. *Journal of Geophysical Research* 70:1523-1529.

Fisk M.R. and Bence A.E. 1980. Experimental crystallization of chrome spinel in FAMOUS basalt 567-1-1. *Earth and Planetary Science Letters* 48:111-123.

Fowler G.W., Papike J.J., Spilde M.N., and Shearer C.K. 1994. Diogenites as asteroidal cumulates: Insights from orthopyroxene major and minor element chemistry. *Geochimica et Cosmochimica Acta* 18:3921-3929.

Gaffey M.J. 1976. Spectral reflectance characteristics of the meteorite classes. *Journal of Geophysical Research* 81:905-920.

Gaffey M.J. 1997. Surface lithologic heterogeneity of asteroid 4 Vesta. *Icarus* 127:30-157.

Gooding J.L., Prinz M., and Keil K. 1979. Mineralogy and petrology of the Chervony Kut eucrite. *Proceedings of the Lunar and Planetary Science Conference* 10:446-448.

Grossman J.N. 1994. The Meteoritical Bulletin, no. 76, 1994 January: The U.S. Antarctic meteorite collection. *Meteoritics* 29:100-143.

Hill R. and Roeder P. 1974. The crystallization of spinel from basaltic liquid as a function of oxygen fugacity. *Journal of Geology* 82:709-729.

Hsu W. and Crozaz G. 1996. Mineral chemistry and the petrogenesis of eucrites: I. Noncumulate eucrites. *Geochimica et Cosmochimica Acta* 60:4571-4591.

Jarosewich E. 1990. Chemical analyses of meteorites: A compilation of stony and iron meteorite analyses. *Meteoritics* 25:323-337.

John C.M. (2004) Plotting and analyzing data trends in ternary diagrams made easy, *EOS* 85:158. (Also available at http://www.agu.org/eos_elec/000562e.shtml).

Johnson, T.V., and Fanale, F.P. 1973. Optical properties of carbonaceous chondrites and their relationship to asteroids. *Journal of Geophysical Research* 78:8507-8518.

Kaneda K. and Warren P.H. 1998. Iron-nickel metal-bearing unique eucrite elephant moraine 92023: Its petrography, siderophile concentrations and petrogenesis. *Meteoritics and Planetary Science.* 33:A81-A82.

Keil K. 2002. Geological history of asteroid 4 Vesta: The "smallest terrestrial planet". In: *Asteroids III* (eds. W. Bottke, A. Cellino, P. Paolicchi, and R.P. Binzel). Arizona LPI Publishing, pp. 573-585

Kitts K. and Lodders K. 1998. Survey and evaluation of eucrite bulk compositions. *Meteoritics and Planetary Science* 33:A197-A213.

Lentz R.C.F., Scott E.R.D., and McCoy T.J. 2007. Anomalous eucrites: Using Fe/Mn to search for different parent bodies. *Lunar and Planetary Science Conference XXXVIII***.** Lunar and Planet. Institute, Houston. #1968 (abstract).

Mayne R.G., Sunshine J.M., McCoy T.J., and McSween H.Y. 2006. The VISNIR Spectra of Unbrecciated Antarctic Eucrites: A Preliminary Study. *Lunar and Planetary Science Conference XXXVII*. Lunar Planetary Institute, Houston #1796 (abstract).

Mason B. (1962) Meteorites. J. Wiley and Sons, New York.

McCord T.B., Adams J.B., and Johnson T.V. 1970. Asteroid Vesta: Spectral reflectivity and compositional implications. *Science* 168:1445-1447

McCoy T.J., Ketcham R.A., Wilson L., Benedix G.K., Wadhwa M., and Davis A.M. 2006. Formation of vesicles in asteroidal basaltic meteorites. *Earth and Planetary Science Letters* 246:102-108.

Mittlefehldt D.W. 1994. The genesis of diogenites and HED parent body petrogenesis. *Geochimica et Cosmochimica Acta* 58:1537-1552.

Mittlefehldt D.W. 2005. Ibitira: A basaltic achondrite from a distinct parent asteroid and implications for the Dawn mission. *Meteoritics and Planetary Science* 40:665-677.

Mittlefehldt D.W. and Galindo C. 2002. Petrology and geochemistry of unbrecciated metamorphosed eucrites. *Meteoritics and Planetary Science.* 37:A101 (abstract).

Mittlefehldt D.W. and Lee M.T. 2001. Petrology and geochemistry of unusual eucrite GRA 98098. *Meteoritics and Planetary Science.* 36:A136 (abstract).

Mittlefehldt D.W. and Lindstrom M.M. 1991. Generation of abnormal trace element abundances in Antarctic eucrites by weathering processes. *Geochimica et Cosmochimica Acta* 55:77-87.

Mittlefehldt D.W. and Lindstrom M.M. 2003. Geochemistry of basaltic eucrites, and Hf and Ta as petrogenetic indicators for altered Antarctic eucrites. *Geochimica et Cosmochimica Acta* 67:1911-1935.

Mittlefehldt D.W., McCoy T.J., Goodrich C.A., and Kracher A. 1998. Non-chondritic meteorites from asteroidal bodies. In *Planetary Materials* (ed. J.J. Papike). Washington D.C.: Mineralogical Society of America, pp. 4-1 to 4-195.

Miyamoto M., Mito A., and Takano Y. 1982. An attempt to reduce the effects of black materials from the spectral reflectance of meteorites and asteroids. *Memoirs National. Institute of Polar Research Special Issue* 20:345-361

Newsom H.E., and Drake M.J. 1982. The metal content of the eucrite parent body: Constraints from the partitioning behavior of tungsten. *Geochimica et Cosmochimica Acta* 46:2483-2489.

O'Neill C.O. and Delaney J.S. 1982. Zoning of eucritic feldspars. *Meteoritics* 17:265.

Papike J.J., Karner J.M., and Shearer C.K. 2003. Determination of planetary basalt parentage: A simple technique using the electron microprobe. *American Mineralogist* 88:469-472.

Papike J.J. 1998. Comparative planetary mineralogy: Chemistry of melt-derived pyroxene, feldspar, and olivine. In: *Planetary Materials* (ed. J.J. Papike). Washington D.C.: Mineralogical Society of America, pp. 7-1 to 7-11.

Pun A. and Papike J.J. 1996. Unequilibrated eucrites and the equilibrated Juvinas eucrite: Pyroxene systematics and major, minor, and trace element zoning. *American Mineralogist* 81:1438-1451.

Reid A.M. and Barnard B.M. 1979. Unequilibrated and equilibrated eucrites. *Proceedings of the 10th Lunar and Planetary Science Conference* pp. 1019-1021

Righter, K. and Drake, M.J. 1997. A magma ocean on Vesta: Core formation and petrogenesis of eucrites and diogenites. *Meteoritics and Planetary Science* 32:929-244

Roeder P.L. and Reynolds I. 1991. Crystallization of chromite and chromium stability in basaltic melts. *Journal of Petrology* 32:909-934.

Russell C.T., Coradini A., Feldman W.C., Jaumann R., Konopliv A.S., McCord T.B., McFadden L.A., McSween Jr. H.Y., Mottola S., Neukum G., Pieters C.M., Raymond C.A., Smith D.E., Sykes M.V., Williams B.G., and Zuber M.T. 2002. Dawn: A journey to the beginning of the solar system. *Proceedings of the Asteroids Comets and Meteors Conference* pp. 63-66.

Russell C.T., Capaccioni F., Coradini A., Christensen U., De Sanctis M.C., Feldman W.C., Jaumann R., Keller H.U., Konopliv A., McCord T.B., McFadden L.A., McSween H.Y., Mottola S., Neukum G., Pieters C.M., Prettyman T.H., Raymond C.A., Smith D.E., Sykes M.V., Williams B., and Zuber M.T. 2006. Dawn discovery mission to Vesta and Ceres: Present status. *Advances in Space Research* 38:2043-2048.

Ruzicka A., Synder G.A., and Taylor L.A. 1997. Vesta as the howardite, eucrite, and diogenite parent body: Implications for the size of a core and for large-scale differentiation. *Meteoritics and Planetary Science* 32:825-840.

Snetsinger K.G., Bunch T.E., and Keil K. 1968. Electron microprobe analysis of vanadium in the presence of titanium. *American Mineralogist* **53**, 1770-1773.

Steele I.M. and Smith I.M. 1976. Mineralogy of the Ibitira eucrite and comparison with other eucrites and lunar samples. *Earth and Planetary Science Letters* 33:67-78.

Stolper E. 1977. Experimental petrology of eucritic meteorites. *Geochimica et Cosmochimica Acta* 41:587-611.

Takeda H. and Graham A.L. 1991. Degree of equilibration of eucritic pyroxenes and thermal metamorphism of the earliest planetary crust. *Meteoritics* 26:129-134.

Treiman A.H., Lanzirotti A., and Xirouchakis D. 2004. Ancient water on asteroid 4 Vesta: evidence from a quartz veinlet in the Serra de Magé eucrite meteorite. *Earth and Planetary Science Letters* 219:189-199.

Wadhwa M., Srinivasan G., and Carlson R.W. 2006. Timescales of planetary differentiation in the early solar system. In: *Meteorites and the Early Solar System II* (eds. D.S. Lauretta and H.Y. McSween Jr.) University of Arizona Press, pp. 715-733.

Warren P.H., Kallemeyn G.W., and Arai T. 1996. Compositional investigation of quench-textured eucrites: Microporphyritic ALH 81001 and vesicular PCA 91007. *LPI Technical Reports 96-02,* 1:35-36.

Wiechert U.H., Halliday A., Palme H., and Rumble D. 2004. Oxygen isotope evidence for rapid mixing of the HED meteorite parent body. *Earth and Planetary Science Letters* 221:373-382.

Wilkening L.L. and Anders E. 1975. Some studies of an unusual eucrite – Ibitira. *Geochimica et Cosmochimica Acta* 39*:1205-1210.*

Yamaguchi A. 2000. Spinels in basaltic eucrites: Implication for crystallization and metamorphic history. *Meteoritics and Planetary Science.* 35:A174 (abstract).

Yamaguchi A. and Mikouchi T. 2005. Heating Experiments of the HaH 262 eucrite and implication for the metamorphic history of highly metamorphosed eucrites. *Lunar and Planetary Science Conference XXXVI***.** Lunar and Planetary Institute, Houston. #1574 (abstract).

Yamaguchi A., Taylor G.J., and Keil K. 1996. Global crustal metamorphism of the eucrite parent body. *Icarus* 124:97-112.

Yamaguchi A., Taylor G.J., Keil K., Bogard D.D. 1997a. Evidence for a large cratering event on the HED parent body (Vesta) ~4.5 GA ago. *Meteoritics and Planetary Science* 32:A144-A155.

Yamaguchi A., Taylor G.J., and Keil K. 1997b. Metamorphic history of the eucritic crust of 4 Vesta. *Journal of Geophysical Research* 102:13,381-13,386.

Yamaguchi A., Taylor G.J., Keil K., Floss C., Crozaz G., Nyquist L.E., Bogard D.D., Garrison D.H., Reese Y.D., Weismann H, and Shih C-Y. 2001. Post-crystallization reheating and partial melting of eucrite EET 90020 by impact into the hot crust of asteroid 4Vesta ~4.50Ga. *Geochimica et Cosmochimica Acta* 65:3577-3599.

Appendix II-A

Table II-1: Eucrite samples examined in this study. Thin-section numbers are given where available.

Sample	Section Number	SEM map Magnification	Sample Description
ALH A81001	10	70	Vitrophyric, skeletal pyroxene, few pyroxene micriphenocrysts
ALH A81313	1	40	Only sample with maskelynite, coarse-grained
BTN 00300	26	37	Granoblastic, some igneous texture remains, a few tabular silica grains
Caldera	USNM 6394-2	45	Gabbroic
Chervony Kut	USNM 6529-1	40	Sub-ophitic, highly fractured (shock)
EET 87520	18	37	Cumulate texture, coarse-grained
EET 90020	7	37	Predominantly equigranular, granoblastic
EET 90029	3	37	Microcrystalline, acicular plagioclase, shock veins
EET 92004	7	37	Sub-ophitic, fractured (shock)
EET 92023		35	Equigranular, cumulate
GRA 98098	18	30	Poikilitc quartz grain, inequigranular, granoblastic
GRO 95533	2	33	Granulated pyroxene, shocked, plagioclase undulose extinction
Ibitira	USNM 6153-1	100	Vesicular, granoblastic, tabular silica grains
LEW 85305		33	Possible poikilitc quartz grain
LEW 85353		40	Shock veins, granulated pyroxene
LEW 88009		80	Ophitic, acicular plagioclase
LEW 88010		40	Ophitic, variolitic plagioclase
MAC 02522	11	37	Pyroxene mosaicized, ophiticto sub-ophitic texture
MET 01081	14	37	Shock mosaicism of pyroxene and plagioclase
Moama	USNM 6376-1	4	Fine-grained cumulate
Moore County	USNM 929-5	40	Cumulate, some plagioclase poikilitically enclosed by pyroxene
PCA 82501		45	Sub-ophitic, fractured (shock)
PCA 91078	8	37	Sub-ophitic, coarse-grained
QUE 94484		50	Sub-ophitic, late-stage phases/mesostasis abundant, spherulitic plagioclase
QUE 97014		45	Ophitic, fractured (shock)
QUE 97053	6	43	Sub-ophitic, shocked, moasicized pyroxene, undulose plagioclase
QUE 99658	2	45	Sub ophitic, spherulitic plagioclase, shock veins. Fractured
RKP A80224	2	45	Ophitic, pyroxene partially mosaicized
Serra de Magé	USNM 839-3	45	Coarse grained cumulate

Table II-2: Average modal abundances of the twenty-nine unbrecciated eucrites studied[a]

	ALH A81001	ALH A81313	BTN 00300	CALDERA	CHERVONY KUT	EET 87520	EET 90020	EET 90029
Plagioclase	61 (2)	48 (0)	48 (0)	39 (0)	45 (0)	49 (0)	50 (0)	56 (0)
Pyroxene	39 (2)	51 (0)	46 (0)	47 (0)	52 (0)	50 (0)	49 (0)	39 (0)
Silica	0 -	<1 (0)	5 (0)	12 (0)	2 (0)	1 (0)	<1 (0)	4 (0)
OSM	0 -	<1 (0)	1 (0)	1 (0)	1 (0)	0 (0)	<1 (0)	<1 (0)

	EET 92004	EET 92023	GRA 98098	GRO 95533	IBITIRA	LEW 85305	LEW 85353	LEW 88009
Plagioclase	44 (0)	42 (0)	41 (0)	44 (0)	41 (0)	35 (0)	41 (0)	47 (0)
Pyroxene	55 (0)	55 (0)	50 (0)	52 (0)	53 (0)	60 (0)	54 (0)	51 (0)
Silica	<1 (0)	2 (0)	8 (0)	2 (0)	4 (0)	3 (2)	4 (0)	2 (0)
OSM	<1 (0)	1 (0)	<1 (0)	1 (0)	<1 (0)	2 (2)	1 (0)	0 (0)

	LEW88010	MAC 02522	MET 01081	MOAMA	MOORE COUNTY	PCA 82501	PCA 91007	PCA 91078
Plagioclase	41 (0)	41 (0)	40 (0)	55 (0)	44 (0)	44 (0)	41 (2)	46 (0)
Pyroxene	55 (0)	57 (0)	53 (0)	44 (0)	52 (0)	49 (0)	57 (2)	51 (0)
Silica	3 (0)	2 (0)	5 (0)	<1 (0)	3 (0)	5 (0)	2 (0)	3 (0)
OSM	1 (0)	<1 (0)	1 (0)	<1 (0)	<1 (0)	2 (0)	<1 (0)	<1 (0)

	PCA 91081	QUE 94484	QUE 97014	QUE 97053	QUE 99658	RKP A80224	SERRA DE MAGE
Plagioclase	56 (1)	46 (1)	58 (0)	51 (0)	50 (0)	41 (0)	53 (0)
Pyroxene	42 (1)	44 (1)	38 (0)	48 (0)	48 (0)	52 (0)	45 (0)
Silica	2 (0)	7 (0)	3 (0)	<1 (0)	1 (0)	4 (1)	<1 (0)
OSM	0 (0)	2 (0)	<1 (0)	<1 (0)	<1 (0)	3 (1)	1 (0)

[a]Figures in parentheses represent 1σ errors in the average modal abundance measurement, calculated from the variations between the three individual mode measurements that were taken.

n.d. = not detected

Table II-3: Representative pyroxene analyses[a].

	ALH A81001		ALH A81313		BTN 00300		Caldera		Chervony Kut		EET 87520		EET 90020	
	Low-Ca	High-Ca	Low-Ca	High-Ca	Low-Ca	High-Ca	Low-Ca	High-Ca	Low-Ca	High-Ca	Low-Ca	High-Ca	Low-Ca	High-Ca
SiO2	49.8	50.3	52.9	52.4	49.3	50.3	49.9	50.7	48.3	50.2	49.5	50.3	49.2	50.0
TiO2	0.09	0.33	0.21	0.30	0.25	0.44	0.36	0.74	0.37	0.32	0.21	0.47	0.51	1.03
Al2O3	0.27	0.70	0.43	0.94	0.31	0.66	0.27	0.84	0.46	0.94	0.21	0.79	0.49	1.29
Cr2O3	0.26	0.94	0.23	0.33	0.19	0.29	0.08	0.33	1.55	0.39	0.12	0.39	0.19	0.47
MgO	13.4	10.7	20.0	14.1	11.6	9.8	12.1	9.9	11.7	10.1	11.9	10.1	11.2	9.63
CaO	0.63	20.7	1.31	20.7	2.96	17.8	3.12	19.6	1.86	13.2	3.03	18.8	2.21	17.6
MnO	1.07	0.44	0.83	0.48	0.99	0.65	1.12	0.55	1.11	0.74	1.11	0.56	1.13	0.63
FeO	34.1	15.0	24.1	10.5	33.9	19.4	33.3	17.4	34.7	24.5	33.6	17.8	35.3	19.4
Na2O	<0.03	0.05	<0.03	0.07	0.03	0.06	<0.03	0.07	<0.03	<0.03	0.03	0.08	<0.03	0.10
Total	99.57	99.06	99.94	99.72	99.60	99.35	100.24	100.12	100.04	100.39	99.68	99.19	100.27	100.11
Si	1.98	1.95	1.99	1.97	1.98	1.97	1.98	1.96	1.94	1.97	1.98	1.96	1.97	1.94
Ti	0.00	0.01	0.01	0.01	0.01	0.01	0.01	0.02	0.01	0.01	0.01	0.01	0.02	0.03
Al	0.01	0.03	0.02	0.04	0.02	0.03	0.01	0.04	0.02	0.04	0.01	0.04	0.02	0.06
Cr	0.01	0.03	0.01	0.01	0.01	0.01	0.00	0.01	0.05	0.01	0.00	0.01	0.01	0.01
Mg	0.80	0.62	1.12	0.79	0.69	0.57	0.72	0.57	0.70	0.59	0.71	0.59	0.67	0.56
Ca	0.03	0.86	0.05	0.83	0.13	0.75	0.13	0.81	0.08	0.55	0.13	0.79	0.10	0.73
Mn	0.04	0.02	0.03	0.02	0.03	0.02	0.04	0.02	0.04	0.03	0.04	0.02	0.04	0.02
Fe	1.14	0.49	0.76	0.33	1.14	0.64	1.11	0.56	1.17	0.80	1.12	0.58	1.18	0.63
Na	n.d.	0.00	n.d.	0.01	0.00	0.00	n.d.	0.01	n.d.	0.00	0.00	0.01	0.00	0.01
Total	4.01	4.01	3.99	4.00	4.01	4.00	4.00	4.00	4.01	4.00	4.01	4.00	4.00	4.00
Wo	1.38	43.7	2.74	42.7	6.48	38.1	6.81	41.7	4.11	28.4	6.61	40.2	4.88	38.2
En	40.6	31.4	58.0	40.4	35.4	29.3	36.6	29.4	35.9	30.3	36.2	30.0	34.4	29.1
Fs	58.0	24.8	39.3	16.9	58.1	32.5	56.6	28.8	60.0	41.3	57.1	29.8	60.7	32.8

	EET 90029		EET 92004		EET 92023		GRA 98098		GRO 95533		Ibitira		LEW 85305	
	Low-Ca	High-Ca	Low-Ca	High-Ca	Low-Ca	High-Ca	Low-Ca	High-Ca	Low-Ca	High-Ca	Low-Ca	High-Ca	Low-Ca	High-Ca
SiO2	49.7	51.4	49.9	51.6	49.9	50.0	49.5	49.8	49.6	50.8	49.8	49.9	49.5	50.6
TiO2	0.22	0.40	0.13	0.23	0.47	0.81	0.49	0.79	0.12	0.27	0.60	1.16	0.44	0.52
Al2O3	0.24	0.47	0.17	0.46	0.56	1.23	0.54	1.12	0.13	0.48	0.40	1.44	0.48	0.73
Cr2O3	0.12	0.15	0.38	0.40	0.23	0.69	0.25	0.44	0.02	0.24	0.18	0.42	0.22	0.34
MgO	12.4	10.3	12.4	11.0	14.8	13.8	11.8	10.9	11.5	9.50	12.8	10.2	10.6	9.46
CaO	1.18	18.0	0.97	18.2	2.73	11.0	2.93	10.8	0.85	20.3	2.33	19.0	5.98	18.7
MnO	1.10	0.61	1.16	0.52	0.87	0.65	1.12	0.77	1.13	0.62	0.95	0.57	1.05	0.62
FeO	34.7	18.4	35.1	17.9	29.6	21.1	33.3	25.3	36.2	17.0	33.2	17.4	32.0	19.4
Na2O	<0.03	0.07	<0.03	0.06	<0.03	0.09	0.04	0.09	<0.03	0.05	<0.03	0.05	0.05	0.11
Total	99.72	99.88	100.12	100.30	99.20	99.46	99.97	99.87	99.56	99.24	100.24	100.03	100.35	100.54
Si	1.99	1.99	1.99	1.98	1.97	1.94	1.97	1.95	2.00	1.98	1.97	1.93	1.97	1.96
Ti	0.01	0.01	0.00	0.01	0.01	0.02	0.02	0.02	0.00	0.01	0.02	0.03	0.01	0.02
Al	0.01	0.02	0.01	0.02	0.03	0.06	0.03	0.05	0.01	0.02	0.02	0.07	0.02	0.03
Cr	0.00	0.01	0.01	0.01	0.01	0.02	0.01	0.01	0.00	0.01	0.01	0.01	0.01	0.01
Mg	0.74	0.59	0.74	0.63	0.87	0.80	0.70	0.64	0.69	0.55	0.76	0.59	0.63	0.55
Ca	0.05	0.75	0.04	0.75	0.12	0.46	0.13	0.45	0.04	0.85	0.10	0.79	0.26	0.78
Mn	0.04	0.02	0.04	0.02	0.03	0.02	0.04	0.03	0.04	0.02	0.03	0.02	0.04	0.02
Fe	1.16	0.60	1.17	0.57	0.98	0.68	1.11	0.83	1.22	0.56	1.10	0.56	1.07	0.63
Na	0.00	0.01	0.00	0.01	0.00	0.01	0.00	0.01	0.00	0.00	0.00	0.00	0.00	0.01
Total	4.00	3.99	4.00	4.00	4.00	4.00	4.00	3.99	4.00	4.00	4.00	4.00	4.00	4.00
Wo	2.57	38.6	2.11	38.4	5.87	23.6	6.46	23.6	1.90	43.4	5.07	40.6	13.1	39.8
En	37.9	30.6	37.8	32.2	44.3	41.1	36.1	33.2	35.5	28.2	38.7	30.4	32.2	28.0
Fs	59.6	30.8	60.1	29.4	49.8	35.3	57.4	43.2	62.6	28.4	56.2	29.0	54.7	32.2

	LEW 85353		LEW 88009		LEW 88010		MAC 02522	MET 01081		Moama		Moore County		PCA 82501	
	Low-Ca	High-Ca	Low-Ca	High-Ca	Low-Ca	High-Ca		Low-Ca	High-Ca	Low-Ca	High-Ca	Low-Ca	High-Ca	Low-Ca	High-Ca
SiO2	49.8	50.5	49.5	52.0	49.5	50.6	48.1	48.7	49.2	52.3	51.9	51.2	51.5	49.0	50.8
TiO2	0.32	0.86	0.17	0.19	0.09	0.59	0.66	0.48	0.70	0.24	0.41	0.36	0.63	0.23	0.33
Al2O3	0.16	1.16	0.18	0.43	0.41	0.33	1.00	0.51	1.06	0.43	0.70	0.27	0.76	0.23	0.38
Cr2O3	0.05	0.20	0.33	0.24	0.77	0.37	0.25	0.25	0.40	0.25	0.35	0.11	0.33	1.42	0.22
MgO	13.3	11.0	12.4	10.4	12.9	11.6	9.63	11.7	11.0	19.6	13.7	15.7	12.2	12.3	10.9
CaO	0.82	21.0	0.73	21.0	0.75	14.4	6.64	2.31	9.68	1.45	21.2	3.06	20.1	1.77	16.6
MnO	1.01	0.43	1.12	0.53	1.07	0.65	0.97	1.07	0.90	0.89	0.49	0.87	0.58	1.07	0.52
FeO	34.7	14.5	35.9	16.1	34.2	20.9	31.9	34.5	26.1	24.9	11.1	28.3	13.9	34.2	19.9
Na2O	<0.03	0.06	<0.03	0.06	<0.03	0.03	0.04	<0.03	0.06	<0.03	0.06	<0.03	0.09	<0.03	0.05
Total	100.22	99.67	100.33	100.89	99.64	99.42	99.18	99.48	99.06	100.07	99.89	99.98	99.96	100.19	99.72
Si	1.98	1.94	1.98	1.99	1.98	1.97	1.95	1.96	1.95	1.98	1.96	1.99	1.96	1.96	1.98
Ti	0.01	0.03	0.01	0.01	0.00	0.02	0.02	0.01	0.02	0.01	0.01	0.01	0.02	0.01	0.01
Al	0.01	0.05	0.01	0.02	0.02	0.02	0.05	0.02	0.05	0.02	0.03	0.01	0.03	0.01	0.02
Cr	0.00	0.01	0.01	0.01	0.02	0.01	0.01	0.01	0.01	0.01	0.01	0.00	0.01	0.05	0.01
Mg	0.79	0.63	0.74	0.59	0.77	0.67	0.58	0.70	0.65	1.11	0.77	0.91	0.69	0.73	0.63
Ca	0.04	0.87	0.03	0.86	0.03	0.60	0.29	0.10	0.41	0.06	0.86	0.13	0.82	0.08	0.69
Mn	0.03	0.01	0.04	0.02	0.04	0.02	0.03	0.04	0.03	0.03	0.02	0.03	0.02	0.04	0.02
Fe	1.15	0.47	1.20	0.51	1.14	0.68	1.08	1.16	0.87	0.79	0.35	0.92	0.44	1.14	0.65
Na	n.d.	0.00	n.d.	0.00	0.00	0.00	0.00	0.00	0.01	0.00	0.00	n.d.	0.01	0.00	0.00
Total	4.01	4.01	4.01	4.00	4.00	4.00	4.01	4.01	4.00	4.00	4.01	4.00	4.00	4.01	4.01
Wo	1.77	44.1	1.58	43.8	1.65	30.8	14.8	5.09	21.4	3.02	43.3	6.49	42.0	3.90	35.2
En	39.9	32.2	37.4	30.1	39.6	34.4	29.8	35.8	33.7	56.7	39.0	46.5	35.4	37.6	32.0
Fs	58.3	23.7	61.0	26.2	58.7	34.8	55.4	59.1	44.9	40.3	17.7	47.0	22.6	58.5	32.8

	PCA 91078		QUE 94484		QUE 97014		QUE 97053		QUE 99658		RKP A80224		Serra de Mage	
	Low-Ca	High-Ca	High-Mg	Low-Mg/Ca	High-Ca	Low-Ca	High-Ca	Low-Ca	High-Ca	Low-Ca	High-Ca	Low-Ca	High-Ca	Low-Ca	High-Ca
SiO2	49.6	50.8	52.4	49.2	49.1	49.4	50.9	50.0	49.5	49.6	51.1	49.3	51.0	52.4	52.9
TiO2	0.18	0.23	0.20	0.26	0.62	0.08	0.34	0.16	0.45	0.08	0.15	0.16	0.19	0.15	0.27
Al2O3	0.24	0.41	1.82	0.84	1.66	0.09	0.54	0.30	1.36	0.09	0.31	0.13	0.44	0.29	0.70
Cr2O3	0.18	0.16	0.94	0.32	0.76	0.01	0.23	0.13	0.47	0.07	0.14	0.06	0.20	0.12	0.29
MgO	12.16	10.1	21.4	10.7	9.59	11.5	10.3	13.0	10.1	11.7	10.4	12.1	10.2	19.6	14.0
CaO	2.79	19.52	2.63	5.64	14.6	0.82	20.5	1.90	13.9	1.51	19.5	1.04	20.4	1.02	22.1
MnO	0.94	0.5	0.77	1.47	0.97	1.11	0.50	0.98	0.83	1.09	0.57	0.99	0.58	0.95	0.38
FeO	33.9	17.74	20.2	32.0	22.7	36.7	16.2	33.9	23.3	36.2	17.6	36.0	16.5	25.3	9.84
Na2O	n.m.	n.m.	<0.03	<0.03	0.05	<0.03	0.07	0.03	0.07	<0.03	0.04	<0.03	0.06	<0.03	0.06
Total	100.04	99.47	100.39	100.41	100.05	99.75	99.55	100.32	99.92	100.35	99.80	99.81	99.52	99.88	100.51
Si	1.98	1.98	1.94	1.96	1.93	1.99	1.97	1.98	1.94	1.99	1.98	1.98	1.98	1.99	1.97
Ti	n.m.	n.m.	0.01	0.01	0.02	0.00	0.01	0.01	0.01	0.00	0.00	0.01	0.01	0.00	0.01
Al	0.01	0.01	0.08	0.04	0.08	0.00	0.03	0.01	0.06	0.00	0.01	0.01	0.02	0.01	0.03
Cr	0.01	0.02	0.03	0.01	0.02	0.00	0.01	0.00	0.02	0.00	0.00	0.00	0.01	0.00	0.01
Mg	0.01	0.01	1.19	0.64	0.56	0.69	0.60	0.77	0.59	0.70	0.60	0.72	0.59	1.11	0.78
Ca	0.72	0.58	0.11	0.24	0.62	0.04	0.85	0.08	0.58	0.07	0.81	0.05	0.85	0.04	0.88
Mn	0.12	0.81	0.02	0.05	0.03	0.04	0.02	0.03	0.03	0.04	0.02	0.03	0.02	0.03	0.01
Fe	0.03	0.02	0.63	1.07	0.75	1.24	0.53	1.12	0.77	1.21	0.57	1.21	0.54	0.81	0.31
Na	1.13	0.58	0.00	0.00	0.00	n.d.	0.01	0.00	0.01	n.d.	0.00	n.d.	0.00	n.d.	0.01
Total	4.01	4.00	4.00	4.01	4.01	4.00	4.01	4.01	4.01	4.01	4.01	4.01	4.01	4.00	4.01
Wo	95.01	96.4	5.5	12.4	5.5	12.41	32.0	1.78	43.1	4.07	30.1	3.29	40.8	2.27	43.0
En	0.8	0.8	61.8	32.7	61.8	32.7	29.2	35.2	30.3	38.9	30.5	35.4	30.4	36.6	29.9
Fs	4.2	2.8	32.7	54.8	32.7	54.8	38.7	63.0	26.6	57.0	39.4	61.3	28.8	61.1	27.1

[a]n.d. = not detected

Table II-4: Representative analyses for plagioclase[a].

	ALH A81001	ALH A81313	BTN 00300	Caldera	Chervony Kut	EET 87520	EET 90020	EET 90029	EET 92004	EET 92023	GRA 98098	GRO 95533	Ibitira	LEW 85305	LEW 85353
SiO2	69.8	44.6	45.3	45.4	46.8	45.3	46.5	45.8	47.9	46.0	47.2	45.1	45.1	46.4	45.4
Al2O3	19.0	34.0	34.2	34.0	33.4	34.4	32.7	34.3	32.8	34.4	33.3	34.5	35.0	33.7	34.3
MgO	0.08	<0.03	0.04	<0.03	0.03	<0.03	0.05	<0.03	<0.03	0.04	0.05	<0.03	<0.03	<0.03	<0.03
CaO	10.5	19.7	18.3	18.4	17.5	18.1	18.0	18.4	16.6	18.1	17.4	18.5	19.1	17.5	17.9
FeO	0.92	0.19	0.18	0.19	0.04	0.15	0.45	0.32	0.16	0.14	0.34	0.01	0.50	0.34	0.11
Na2O	0.23	0.60	1.11	0.99	1.61	1.11	1.29	0.97	2.13	1.19	1.64	1.00	0.54	1.49	1.30
K2O	0.03	<0.03	0.05	0.06	0.11	0.10	0.06	0.06	0.19	0.06	0.15	0.07	0.03	0.07	0.05
Total	100.54	99.20	99.23	99.16	99.44	99.17	99.06	99.87	99.70	99.89	100.09	99.18	100.26	99.46	99.07
Si	3.01	2.08	2.10	2.11	2.16	2.11	2.16	2.11	2.20	2.12	2.17	2.10	2.08	2.15	2.11
Al	0.96	1.87	1.88	1.87	1.82	1.88	1.80	1.87	1.78	1.87	1.81	1.89	1.91	1.84	1.88
Mg	0.01	0.00	0.00	0.00	0.00	0.00	0.00	0.00	0.00	0.00	0.00	0.00	0.00	0.00	0.00
Ca	0.48	0.99	0.91	0.92	0.87	0.90	0.90	0.91	0.82	0.89	0.86	0.92	0.94	0.87	0.89
Fe	0.03	0.01	0.01	0.01	0.00	0.01	0.02	0.01	0.01	0.01	0.01	0.00	0.02	0.01	0.00
Na	0.02	0.05	0.10	0.09	0.15	0.10	0.12	0.09	0.19	0.11	0.15	0.09	0.05	0.13	0.12
K	0.00	0.00	0.00	0.00	0.01	0.01	0.00	0.00	0.01	0.00	0.01	0.00	0.00	0.00	0.00
Total	4.52	5.01	5.01	5.00	5.00	5.00	5.00	5.00	5.01	5.00	5.01	5.00	4.99	5.00	5.01
An	95.8	94.7	89.9	90.8	85.1	89.5	88.1	91.0	80.3	89.0	84.8	90.7	95.0	86.3	88.2
Ab	3.76	5.18	9.83	8.79	14.3	9.94	11.5	8.68	18.7	10.7	14.4	8.88	4.84	13.3	11.5
Or	0.40	0.10	0.29	0.40	0.69	0.60	0.39	0.30	1.08	0.30	0.79	0.39	0.20	0.40	0.30

	LEW 88009	LEW 88010	MAC 02522	MET 01081	Moama	Moore County	PCA 82501	PCA 91078	QUE 94484	QUE 97014	QUE 97053	QUE 99658	RKP A80224	Serra de Mage
SiO2	47.2	47.3	46.4	45.2	44.7	45.7	48.5	48.0	47.6	45.5	47.2	46.2	46.3	44.9
Al2O3	32.9	31.9	33.4	34.5	34.5	33.9	32.3	32.3	32.2	34.4	32.9	33.9	34.1	35.1
MgO	<0.03	<0.03	n.m.	<0.03	0.05	0.05	0.04	0.06	<0.03	<0.03	<0.03	<0.03	<0.03	0.04
CaO	16.9	16.7	17.9	18.3	19.4	18.6	16.0	16.9	17.3	18.2	16.9	17.1	18.0	19.3
FeO	0.45	0.45	0.24	0.19	0.11	0.07	0.25	0.23	0.43	0.11	0.20	0.15	0.06	0.06
Na2O	1.77	1.99	1.21	1.04	0.63	0.96	2.04	1.83	1.61	1.13	1.69	1.61	1.32	0.61
K2O	0.13	0.08	0.04	0.04	0.02	0.05	0.48	0.15	0.14	0.09	0.14	0.10	0.06	0.02
Total	99.28	98.37	99.08	99.33	99.41	99.42	99.70	99.48	99.28	99.48	99.03	99.02	99.79	100.00
Si	2.18	2.21	2.15	2.10	2.08	2.12	2.23	2.21	2.21	2.11	2.19	2.14	2.14	2.07
Al	1.80	1.76	1.83	1.89	1.89	1.85	1.75	1.76	1.76	1.88	1.80	1.86	1.85	1.91
Mg	0.00	0.00	n.m.	0.00	0.00	0.00	0.00	0.00	0.00	0.00	0.00	0.00	0.00	0.00
Ca	0.84	0.84	0.89	0.91	0.97	0.93	0.79	0.84	0.86	0.90	0.84	0.85	0.89	0.96
Fe	0.02	0.02	0.01	0.01	0.00	0.00	0.01	0.01	0.02	0.00	0.01	0.01	0.00	0.00
Na	0.16	0.18	0.11	0.09	0.06	0.09	0.18	0.16	0.15	0.10	0.15	0.15	0.12	0.05
K	0.01	0.01	0.00	0.00	0.00	0.00	0.03	0.01	0.01	0.01	0.01	0.01	0.00	0.00
Total	5.00	5.00	4.99	5.00	5.00	5.00	5.00	4.99	4.99	5.00	4.99	5.01	5.00	5.00
Ab	83.4	81.9	88.8	90.5	94.3	91.2	79.0	82.9	84.9	89.4	84.0	84.9	88.0	94.6
An	15.8	17.6	10.9	9.24	5.57	8.47	18.2	16.2	14.4	10.1	15.2	14.5	11.7	5.34
Or	0.80	0.49	0.30	0.30	0.10	0.30	2.80	0.89	0.79	0.49	0.80	0.60	0.30	0.10

[a]n.d. = not detected

Table II-5: Representative analyses for metal and sulfides[a].

	ALH A81313		BTN 00300		Caldera	Chervony Kut	EET 87520	EET 90020		EET 90029	EET 92004	EET 92023			GRO 95533		Ibitira	LEW 85305
	Metal	Sulfide	Metal	Sulfide	Sulfide	Sulfide	Sulfide	Metal	Sulfide	Sulfide	Sulfide	Metal	Ni-rich Metal	Sulfide	Metal	Sulfide	Metal	Metal
Fe	100.1	63.8	100.2	63.0	64.0	62.7	62.1	100.2	63.9	63.8	62.9	95.2	51.9	63.7	99.6	63.7	99.1	99.8
Si	<0.03	<0.03	<0.03	0.03	<0.03	0.17	<0.03	<0.03	<0.03	<0.03	<0.03	<0.03	<0.03	<0.03	<0.03	<0.03	<0.03	0.04
Ni	0.49	<0.03	0.04	0.03	<0.03	<0.03	<0.03	0.20	<0.03	<0.03	0.07	5.15	48.31	0.10	0.43	0.05	1.06	0.25
Co	0.26	0.08	0.37	0.36	<0.03	<0.03	<0.03	<0.03	<0.03	<0.03	<0.03	1.37	0.25	<0.03	0.04	<0.03	0.49	0.09
S	<0.03	35.8	<0.03	35.5	35.5	35.9	34.2	<0.03	<0.03	35.9	36.0	<0.03	<0.03	36.3	<0.03	<0.03	<0.03	<0.03
P	<0.03	<0.03	<0.03	<0.03	<0.03	<0.03	<0.03	<0.03	35.2	<0.03	<0.03	<0.03	<0.03	<0.03	<0.03	35.5	<0.03	<0.03
Total	100.93	99.67	100.72	99.00	99.47	98.71	96.39	100.48	99.10	99.71	99.03	101.79	100.48	100.13	100.04	99.23	100.66	100.16
Fe	99.2	50.6	99.5	50.3	50.9	49.9	51.0	99.8	51.0	50.5	50.0	93.8	52.9	50.2	99.5	50.7	98.5	99.6
Si	0.04	0.00	0.04	0.04	0.02	0.26	0.01	n.d.	n.d.	0.01	n.d.	0.03	0.02	0.01	0.02	0.03	0.01	0.07
Ni	0.46	n.d.	0.04	0.03	n.d.	n.d.	n.d.	0.19	n.d.	n.d.	0.05	4.83	46.83	0.07	0.40	0.03	1.00	0.24
Co	0.25	0.06	0.35	0.27	n.d.	0.01	n.d.	0.02	n.d.	0.02	n.d.	1.28	0.24	n.d.	0.03	n.d.	0.46	0.08
S	0.02	49.4	0.06	49.4	49.1	49.8	49.0	n.d.	n.d.	49.5	49.9	0.02	n.d.	49.7	0.00	0.01	0.04	n.d.
P	n.d.	0.02	0.01	0.03	0.00	n.d.	n.d.	0.02	48.97	0.00	0.02	n.d.	n.d.	n.d.	n.d.	49.25	n.d.	0.00
Total	100.00	100.00	100.00	100.00	100.00	100.00	100.00	100.00	100.00	100.00	100.00	100.00	100.00	100.00	100.00	100.00	100.00	100.00

	LEW 85353	LEW 88009	LEW 88010	MET 01081		Moama	Moore County		PCA 82501		PCA 91078	QUE 94484	QUE 97014		QUE 99658	RKP A80224	Serra de Mage
	Sulfide	Sulfide	Sulfide	Metal	Sulfide	Sulfide	Metal	Sulfide	Metal	Sulfide	Sulfide	Sulfide	Metal	Sulfide	Sulfide	Sulfide	Sulfide
Fe	63.1	63.2	62.9	100.2	63.0	99.2	100.1	63.3	100.7	63.6	62.4	63.4	100.3	63.4	62.0	63.0	63.7
Si	<0.03	0.09	0.04	<0.03	<0.03	0.11	<0.03	<0.03	<0.03	<0.03	<0.03	<0.03	<0.03	<0.03	0.11	<0.03	<0.03
Ni	0.03	<0.03	0.04	<0.03	<0.03	0.15	0.05	0.06	<0.03	<0.03	<0.03	<0.03	<0.03	<0.03	0.11	<0.03	<0.03
Co	<0.03	<0.03	0.13	0.42	0.02	0.16	0.42	<0.03	0.04	<0.03	<0.03	<0.03	0.15	0.04	0.24	0.45	0.04
S	35.2	35.7	36.2	0.03	36.0	<0.03	<0.03	35.7	<0.03	34.7	35.9	35.1	<0.03	34.3	35.8	36.3	34.8
P	<0.03	<0.03	<0.03	<0.03	<0.03	<0.03	<0.03	<0.03	<0.03	<0.03	<0.03	<0.03	<0.03	<0.03	<0.03	<0.03	<0.03
Total	98.29	99.01	99.28	100.64	99.06	99.64	100.56	99.03	100.78	98.34	98.36	98.52	100.46	97.68	98.25	99.71	98.58
Fe	50.7	50.3	49.9	99.5	50.1	99.5	99.5	50.5	99.9	51.3	49.9	50.9	99.8	51.5	49.7	49.7	51.2
Si	n.d.	0.14	0.06	n.d.	0.01	0.22	0.01	n.d.	n.d.	0.03	0.01	0.04	0.03	0.01	0.18	0.03	0.02
Ni	0.02	n.d.	0.03	n.d.	n.d.	0.14	0.05	0.04	n.d.	0.02	0.00	n.d.	0.01	n.d.	0.08	0.02	n.d.
Co	0.01	n.d.	0.10	0.39	0.02	0.15	0.40	n.d.	0.03	0.01	n.d.	0.00	0.14	0.03	0.18	0.34	0.03
S	49.3	49.5	49.9	0.04	49.8	n.d.	n.d.	49.5	0.02	48.7	50.1	49.1	n.d.	48.5	49.9	49.9	48.8
P	0.01	n.d.	0.01	0.03	0.01	n.d.	0.02	n.d.	n.d.	0.01	0.03	n.d.	n.d.	n.d.	n.d.	n.d.	n.d.
Total	100.00	100.00	100.00	100.00	100.00	100.00	100.00	100.00	100.00	100.00	100.00	100.00	100.00	100.00	100.00	100.00	100.00

[a]n.d. = not detected

Table II-6: Representative analyses for ilmenite[a].

	BTN 00300	Caldera	Chervony Kut	EET 87520	EET 90020	EET 90029	EET 92004	EET 92023	GRA 98098	GRO 95533	Ibitira	LEW 85305
SiO2	<0.03	0.03	<0.03	<0.03	<0.03	<0.03	<0.03	<0.03	<0.03	<0.03	0.04	<0.03
TiO2	52.9	52.4	52.8	52.6	53.2	52.7	52.2	52.3	52.7	52.4	52.3	52.2
ZrO2	<0.03	<0.03	<0.03	<0.03	0.05	<0.03	<0.03	<0.03	0.09	<0.03	0.12	0.04
Al2O3	<0.03	<0.03	<0.03	0.04	<0.03	<0.03	<0.03	<0.03	<0.03	<0.03	0.03	<0.03
Cr2O3	0.15	0.61	0.09	0.37	0.11	0.08	0.11	0.43	0.09	0.03	0.34	0.42
MgO	1.36	1.33	0.47	1.38	0.75	0.93	0.60	1.03	0.77	0.58	0.86	1.05
CaO	0.03	0.06	<0.036	0.16	<0.039	0.04	0.03	<0.03	<0.03	<0.031	0.07	0.06
MnO	0.80	0.81	0.96	0.81	0.72	0.90	0.93	1.04	0.71	0.97	0.59	0.79
FeO	44.3	44.0	44.7	43.8	44.3	45.4	45.5	44.5	45.1	45.2	44.8	44.4
Total	99.62	99.26	99.13	99.24	99.13	100.08	99.36	99.38	99.41	99.27	99.11	98.97
Si	n.d.	0.00	n.d.	n.d.	n.d.	n.d.	n.d.	0.00	0.00	0.00	0.00	n.d.
Ti	1.00	0.99	1.01	1.00	1.01	1.00	1.00	0.99	1.00	1.00	1.00	0.99
Zr	n.d.	n.d.	n.d.	n.d.	0.00	n.d.	n.d.	n.d.	0.00	n.d.	0.00	n.d.
Al	0.00	n.d.	n.d.	0.00	0.00	n.d.	n.d.	0.00	n.d.	n.d.	0.00	n.d.
Cr	0.01	0.01	0.00	0.01	0.00	0.00	0.00	0.01	0.00	0.00	0.01	0.01
Mg	0.05	0.05	0.02	0.05	0.03	0.04	0.02	0.04	0.03	0.02	0.03	0.04
Ca	0.00	0.00	n.d.	0.00	0.00	0.00	0.00	n.d.	n.d.	0.00	0.00	0.00
Mn	0.02	0.02	0.02	0.02	0.02	0.02	0.02	0.02	0.02	0.02	0.01	0.02
Fe	0.93	0.93	0.95	0.92	0.93	0.95	0.96	0.94	0.95	0.96	0.95	0.94
Total	2.00	2.00	1.99	2.00	1.99	2.00	2.00	2.00	2.00	2.00	2.00	2.00

	LEW 85353	LEW 88010	MET 01081	Moore County	PCA 82501	PCA 91078	PCA 91081	QUE 94484	QUE 97014	QUE 97053	QUE 99658	RKP A80224	Serra de Mage
SiO2	<0.03	<0.03	0.04	0.00	0.04	<0.03	<0.03	<0.03	<0.03	<0.03	0.04	<0.03	<0.03
TiO2	52.7	52.9	51.0	52.2	53.1	52.8	52.3	52.7	52.2	53.2	52.8	52.2	51.5
ZrO2	<0.03	<0.03	<0.03	<0.03	<0.03	<0.03	<0.03	<0.03	<0.035	<0.03	<0.03	<0.03	<0.03
Al2O3	<0.03	<0.03	0.07	0.11	<0.03	0.04	<0.03	<0.03	<0.03	<0.03	<0.03	<0.03	0.08
Cr2O3	0.18	0.07	1.29	2.47	0.05	0.29	0.08	0.03	<0.03	0.18	0.18	0.06	1.93
MgO	0.85	0.68	0.40	2.32	0.79	1.14	0.60	0.82	0.55	0.98	0.51	0.57	1.92
CaO	<0.037	0.03	0.32	<0.03	0.06	0.00	0.15	<0.03	0.05	0.07	0.15	<0.03	<0.03
MnO	0.87	0.88	0.98	0.84	0.90	0.82	0.88	1.34	0.94	0.91	0.80	0.89	1.03
FeO	45.2	45.3	44.8	41.7	44.6	44.1	45.5	44.6	45.0	44.6	45.0	45.4	42.5
Total	99.82	99.83	98.91	99.60	99.54	99.18	99.55	99.54	98.75	99.97	99.47	99.17	98.98
Si	n.d.	n.d.	0.00	n.d.	0.00	n.d.	0.00	0.00	n.d.	n.d.	0.00	n.d.	0.00
Ti	1.00	1.00	0.98	0.98	1.00	1.00	0.99	1.00	1.00	1.00	1.00	1.00	0.97
Zr	n.d.	n.d.	n.d.	n.d.	n.d.	n.d.	n.d.	n.d.	n.d.	n.d.	n.d.	n.d.	n.d.
Al	n.d.	0.00	0.00	0.00	n.d.	0.00	0.00	n.d.	n.d.	n.d.	0.00	0.00	0.00
Cr	0.00	0.00	0.03	0.05	0.00	0.01	0.00	0.00	0.00	0.00	0.01	0.00	0.04
Mg	0.03	0.03	0.02	0.09	0.03	0.04	0.02	0.03	0.02	0.04	0.02	0.02	0.07
Ca	n.d.	0.00	0.01	n.d.	0.00	n.d.	0.00	n.d.	0.00	0.00	0.00	n.d.	0.00
Mn	0.02	0.02	0.02	0.02	0.02	0.02	0.02	0.03	0.02	0.02	0.02	0.02	0.02
Fe	0.95	0.95	0.95	0.87	0.94	0.93	0.96	0.94	0.96	0.93	0.95	0.96	0.89
Total	2.00	2.00	2.01	2.00	1.99	2.00	2.01	2.00	2.00	2.00	2.00	2.00	2.00

[a]n.d. = not detected

Table II-7: Representative analyses for ulvöspinel[a].

	ALH A81001	ALH A81313	BTN 00300	Caldera	Chervony Kut	EET 87520	EET 90020	EET 90029	EET 92004	EET 92023	GRA 98098	GRO 95533	Ibitira
SiO2	0.86	0.12	<0.03	<0.03	<0.03	<0.03	0.03	<0.03	0.07	0.05	<0.03	<0.03	<0.03
TiO2	2.15	2.98	12.2	15.3	12.1	12.1	16.7	5.67	3.60	5.35	21.7	7.58	12.0
ZrO2	<0.03	<0.03	<0.03	<0.03	<0.03	<0.03	<0.03	<0.03	<0.03	<0.03	<0.03	<0.03	<0.03
Al2O3	9.66	9.43	5.49	4.55	5.49	5.36	5.44	7.73	8.24	10.91	4.15	7.20	7.11
V2O3	0.64	0.64	0.81	0.81	0.58	0.56	0.58	0.83	0.89	0.43	0.51	0.56	0.63
Cr2O3	49.9	52.2	37.3	33.0	37.8	38.1	28.0	47.3	49.5	43.7	<0.03	44.2	35.3
MgO	0.36	2.34	1.01	0.98	1.08	1.08	0.43	0.72	0.46	1.25	0.69	0.69	0.70
CaO	0.20	<0.03	<0.03	<0.03	0.04	0.06	<0.03	0.06	0.03	0.14	0.00	<0.03	0.04
MnO	0.57	0.56	0.59	0.55	0.47	0.52	0.61	0.47	0.52	0.53	0.55	0.59	0.48
FeO	33.9	32.1	42.0	44.6	41.5	41.5	47.4	36.5	35.4	35.9	51.5	38.2	42.8
Total	98.24	100.39	99.42	99.79	99.01	99.29	99.16	99.29	98.74	98.29	99.07	99.04	99.10
Si	0.03	0.00	0.00	0.00	0.00	0.00	n.d.	n.d.	0.00	0.00	n.d.	0.00	n.d.
Ti	0.06	0.08	0.33	0.42	0.33	0.33	0.46	0.15	0.10	0.14	0.60	0.21	0.33
Zr	n.d.	n.d.	n.d.	n.d.	n.d.	n.d.	n.d.	n.d.	n.d.	n.d.	n.d.	n.d.	n.d.
Al	0.41	0.39	0.24	0.20	0.24	0.23	0.24	0.33	0.35	0.46	0.18	0.31	0.31
V	n.d.	n.d.	0.00	0.00	0.02	0.02	0.00	0.00	n.d.	n.d.	0.00	0.00	0.00
Cr	1.42	1.45	1.08	0.95	1.08	1.09	0.81	1.36	1.43	1.24	0.58	1.27	1.02
Mg	0.02	0.12	0.06	0.05	0.06	0.06	0.02	0.04	0.03	0.07	0.04	0.04	0.04
Ca	0.01	n.d.	0.00	n.d.	0.00	0.00	0.00	0.00	0.00	0.01	n.d.	0.00	0.00
Mn	0.02	0.02	0.02	0.02	0.01	0.02	0.02	0.01	0.02	0.02	0.02	0.02	0.01
Fe	1.02	0.94	1.28	1.36	1.26	1.26	1.46	1.11	1.08	1.07	1.59	1.16	1.30
Total	2.99	3.00	3.01	3.00	3.00	3.00	3.01	3.00	3.01	3.01	3.01	3.00	3.01

	LEW 85305	LEW 85353	LEW 88009	LEW 88010	MAC 02522	MET 01081	Moama	Moore County	PCA 91078	QUE 97014	QUE 99658	RKP A80224	Serra de Mage
SiO2	<0.03	<0.03	<0.03	<0.03	1.08	0.04	<0.03	<0.03	<0.03	<0.03	0.06	<0.03	<0.03
TiO2	17.0	2.59	13.0	2.51	22.6	6.93	5.25	11.1	2.80	2.93	2.14	3.37	3.19
ZrO2	<0.03	<0.03	<0.03	<0.03	<0.03	<0.03	<0.03	<0.03	<0.03	<0.03	<0.03	<0.03	<0.03
Al2O3	4.21	8.46	4.32	8.54	3.51	7.89	7.59	5.89	11.64	8.14	12.87	8.12	8.43
V2O3	0.61	0.75	0.89	0.67	0.43	1.12	0.80	0.85	0.00	0.95	0.56	0.93	0.63
Cr2O3	29.4	53.0	37.9	53.5	17.9	43.1	49.5	39.8	47.9	51.1	48.8	51.0	51.4
MgO	0.71	0.60	0.45	0.38	0.99	0.35	2.42	1.87	1.00	0.50	0.83	0.43	1.87
CaO	<0.03	<0.03	0.12	<0.03	0.13	0.08	<0.03	0.00	<0.03	0.12	0.11	0.05	<0.03
MnO	0.50	0.45	0.60	0.47	0.58	0.59	0.63	0.53	0.55	0.58	0.50	0.57	0.58
FeO	46.8	33.8	43.1	33.9	51.6	38.6	33.1	39.0	34.5	34.3	34.2	35.1	32.3
Total	99.15	99.65	100.40	100.01	98.89	98.73	99.21	99.14	98.41	98.66	100.05	99.55	98.42
Si	n.d.	n.d.	0.00	0.00	0.04	0.00	n.d.	n.d.	n.d.	n.d.	0.00	n.d.	n.d.
Ti	0.47	0.07	0.36	0.07	0.62	0.19	0.14	0.30	0.08	0.08	0.06	0.09	0.09
Zr	n.d.	n.d.	n.d.	n.d.	n.d.	n.d.	n.d.	n.d.	n.d.	n.d.	n.d.	n.d.	n.d.
Al	0.18	0.36	0.19	0.36	0.15	0.34	0.32	0.25	0.49	0.35	0.53	0.35	0.36
V	0.00	0.00	0.00	0.00	0.00	0.03	0.00	0.00	0.00	0.00	0.00	0.00	0.00
Cr	0.86	1.51	1.09	1.52	0.52	1.24	1.40	1.14	1.35	1.48	1.35	1.46	1.46
Mg	0.04	0.03	0.02	0.02	0.05	0.02	0.13	0.10	0.05	0.03	0.04	0.02	0.10
Ca	0.00	n.d.	0.00	0.00	0.01	0.00	n.d.	n.d.	n.d.	0.00	0.00	0.00	n.d.
Mn	0.02	0.01	0.02	0.01	0.02	0.02	0.02	0.02	0.02	0.02	0.01	0.02	0.02
Fe	1.44	1.02	1.32	1.01	1.59	1.17	0.99	1.18	1.03	1.05	1.00	1.06	0.97
Total	3.01	3.00	3.00	2.99	3.00	3.01	3.00	3.00	3.01	3.01	3.00	3.00	3.00

[a]n d. = not detected

Table II-8: The opaque minerals present within the unbrecciated eucrites[a].

Group	Samples	Chr/Usp	Ilmenite	Sulphide	Metal
Basaltic	ALH A81001	N	Y[b]	N	N
	ALH A81313	Y	N	Y	Y
	BTN 00300	Y	Y	Y	Y
	Caldera	Y	Y	Y	N
	Chervony Kut	N	Y	Y	N
	EET 87520	Y	Y	Y	N
	EET 90020	Y	Y	Y	Y
	EET 90029	Y	Y	Y	N
	EET 92004	Y	Y	Y	N
	EET 92023	Y	Y	Y	Y
	GRA 98098	Y	Y	N	N
	GRO 95533	Y	Y	Y	Y
	Ibitira	Y	Y	N	Y
	LEW 85305	Y	Y	N	Y
	LEW 85353	Y	Y	Y	N
	LEW 88009	Y	N	Y	N
	LEW 88010	Y	Y	Y	N
	MAC 02522	Y	N	N	N
	MET 01081	Y	Y	Y	Y
	PCA 82501	N	Y	Y	Y
	PCA 91007	Y	Y	N	N
	PCA 91078	Y	Y	Y	N
	PCA 91081	Y	N	N	N
	QUE 94484	Y[c]	Y	Y	N
	QUE 97014	Y	Y	Y	Y
	QUE 97053	Y	Y	N	N
	QUE 99658	Y	Y	Y	N
	RKP A80224	Y	Y	Y	N
Cumulate	Moama	Y	N	N	Y
	Moore County	Y	Y	Y	Y
	Serra de Mage	Y	Y	Y	N

[a]Y indicates that mineral is present and analyzed. N indicates that it was not observed in that sample, Chr/Usp = Chromite/Ulvöspinel

[b] This mineral was analyzed but good totals could not be achieved due to grain size.

[c] This minerals was analyzed but good totals could not be achieved due to oxidation.

Table II-9: Degree of metamorphic equilibration in the unbrecciated eucrites[a].

Sample	Group	Exsolution T °C		Pyx Major	Pyx Minor	Plag <5%An	Total
EET 90020	Granoblastic	1095	±75	Y	Y	Y	3
Caldera	Basaltic	1034	±88	Y	Y	Y	3
BTN 00300	Granoblastic	1024	±74	Y	Y	Y	3
PCA 91078	Basaltic	1012	±68	Y	N	N	1
EET 87520	Basaltic	1010	±94	Y	Y	Y	3
GRA 98098	Granoblastic	985	±78	Y	Y	N	2
Ibitira	Granoblastic	979	±54	Y	Y	Y	3
Moore County	Cumulate	934	±54	Y	Y	Y	3
MET 01081	Basaltic	919	±72	Y	Y	Y	3
Moama	Cumulate	906	±33	Y	Y	Y	2
ALH A81313	Basaltic	891	±29	Y	Y	Y	2
PCA 91007	Basaltic	872	±28	Y	N	N	2
LEW 85305	Granoblastic	834	±39	Y	Y	N	2
EET 90029	Basaltic	817	±32	Y	N	Y	2
QUE 97053	Basaltic	801	±24	Y	N	N	1
PCA 91081	Basaltic	800	±10	Y	N	N	1
Serra De Mage	Cumulate	794	±24	Y	Y	Y	3
PCA 82501	Basaltic	784	±36	Y	N	N	1
EET 92004	Basaltic	738	±39	Y	N	N	1
GRO 95533	Basaltic	706	±30	Y	N[a]	N	1
RKP A80224	Basaltic	698	±21	Y	N	Y	2
LEW 85353	Basaltic	692	±17	Y	N	Y	2
Chervony Kut	Basaltic	685	±32	Y	N	Y	2
PCA 97014	Basaltic	685	±7	Y	N	Y	2
ALH A81001	Basaltic	680	±23	Y	N	N/A	1[b]
QUE 99658	Basaltic	677	±31	Y	N	N	1
LEW 88009	Basaltic	654	±29	Y	N	N	1
LEW 88010	Basaltic	654	±46	Y	N	N	1
QUE 94484	Basaltic	N/A		N	N[a]	N	0
MAC 02522	Basaltic	N/A		N	N	N	0

[a]Y denotes sample is equilibrated with respect to that component, N denotes that it is not.
[b]These components are very close to being judged as equilibrated.

Figure II-1: Compiled SEM mineral maps for six unbrecciated eucrites showing the wide range of textures seen within the samples studied. Each map consists of superimposed Fe, Si, and Al elemental X-ray maps. Blue/purple – pyroxene, lilac – plagioclase, green – silica, red – oxides, sulfides and metal. (a) QUE 94484. (b) ALH A81001. (c) Chervony Kut. (d) Ibitira. (e) GRA 98098. (f) Serra de Magé.

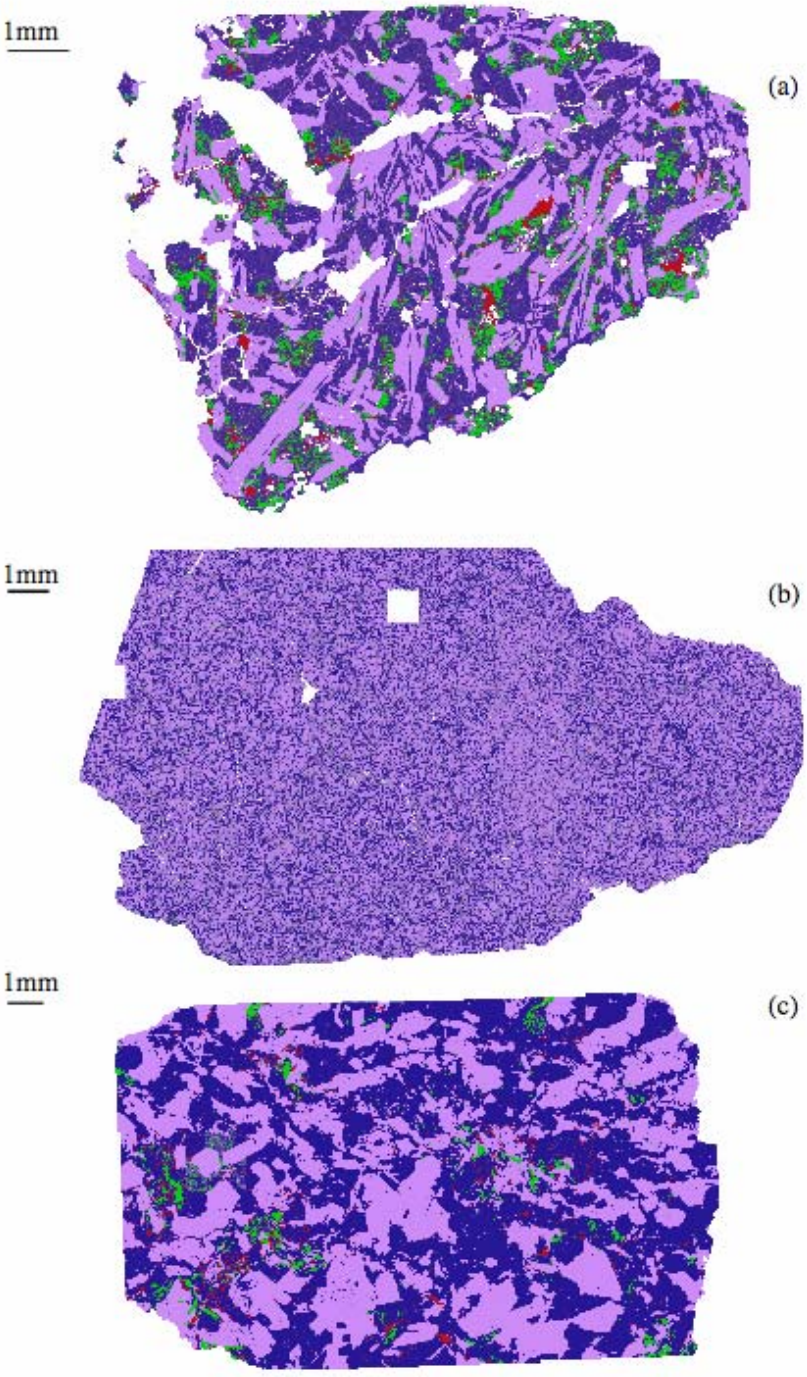
1mm
(a)
1mm
(b)
1mm
(c)

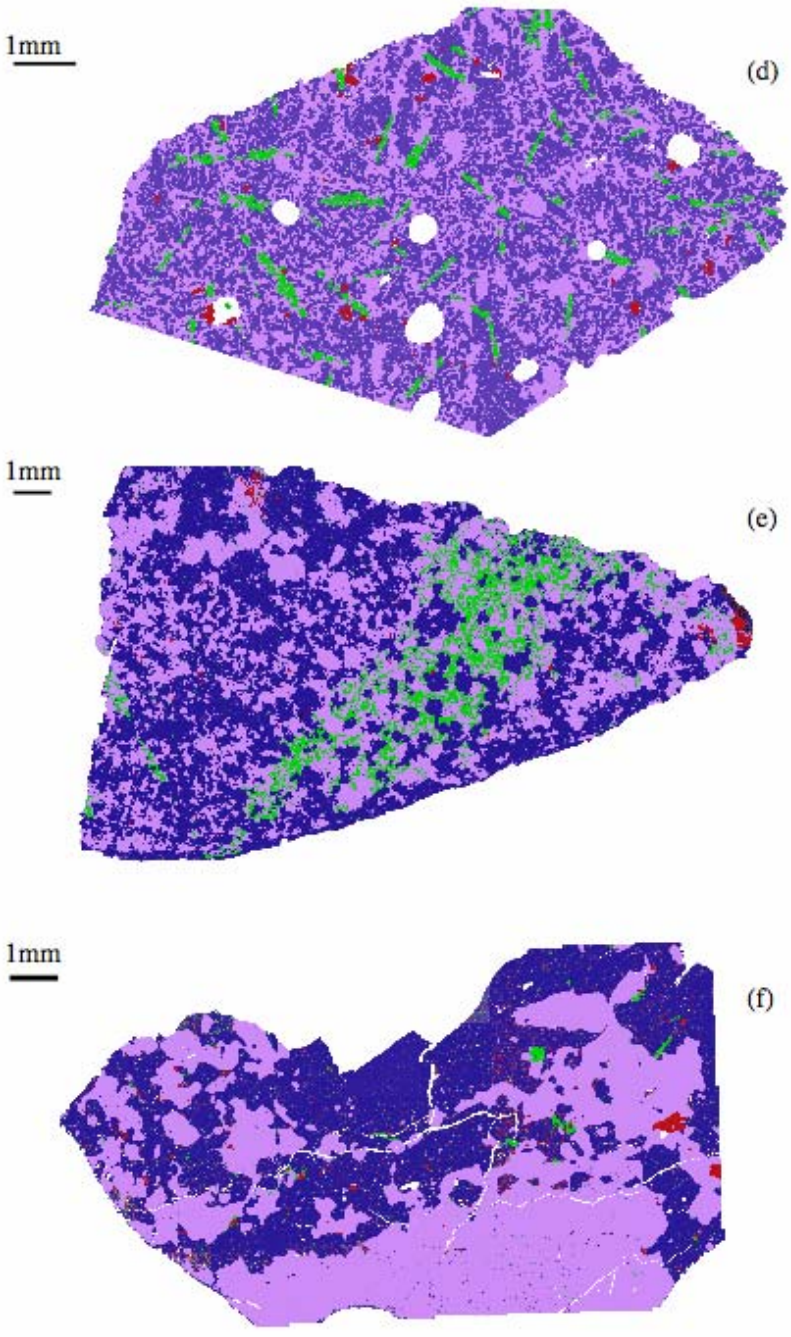
1mm
(d)
1mm
(e)
1mm
(f)

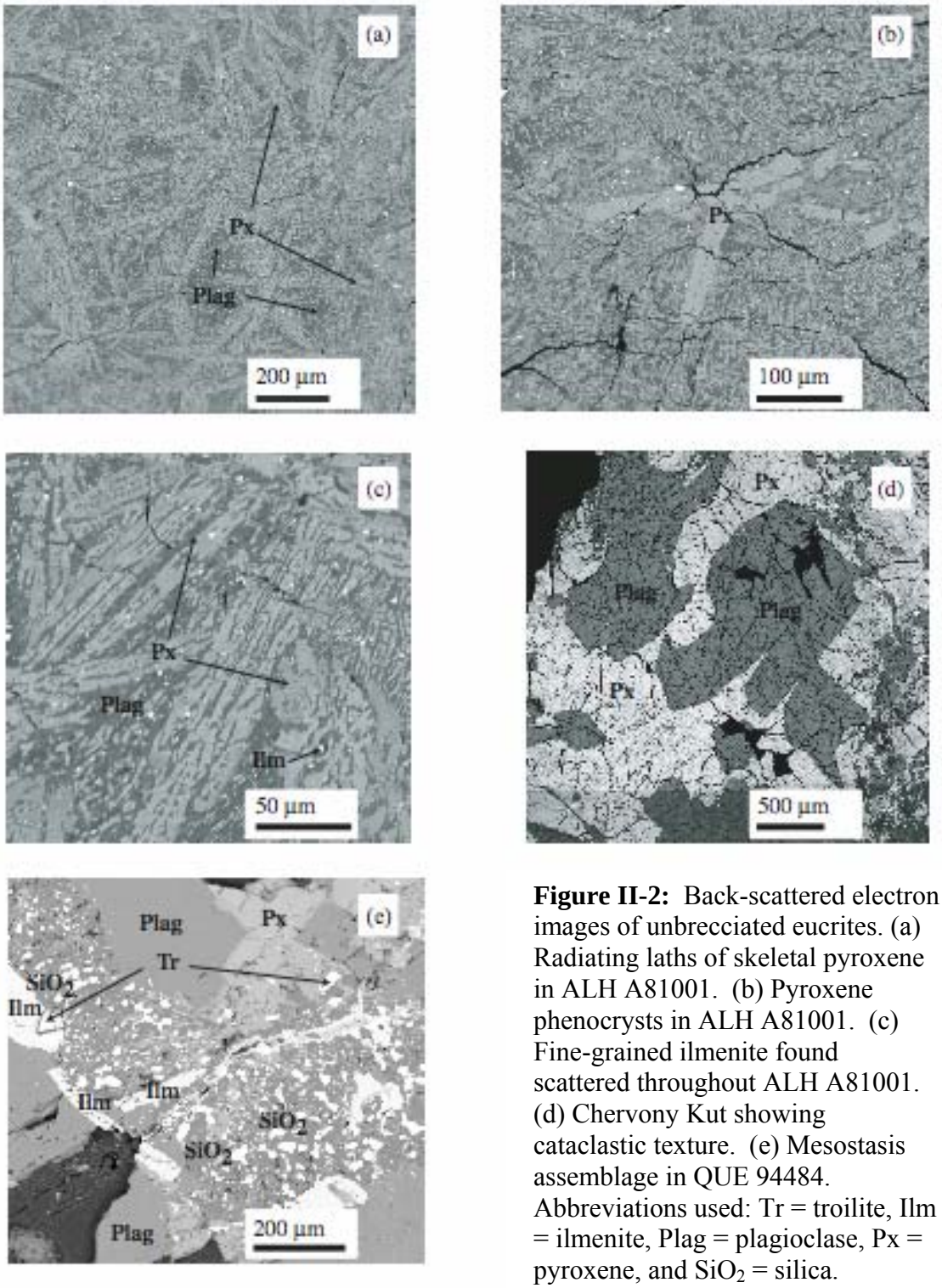

Figure II-2: Back-scattered electron images of unbrecciated eucrites. (a) Radiating laths of skeletal pyroxene in ALH A81001. (b) Pyroxene phenocrysts in ALH A81001. (c) Fine-grained ilmenite found scattered throughout ALH A81001. (d) Chervony Kut showing cataclastic texture. (e) Mesostasis assemblage in QUE 94484. Abbreviations used: Tr = troilite, Ilm = ilmenite, Plag = plagioclase, Px = pyroxene, and SiO_2 = silica.

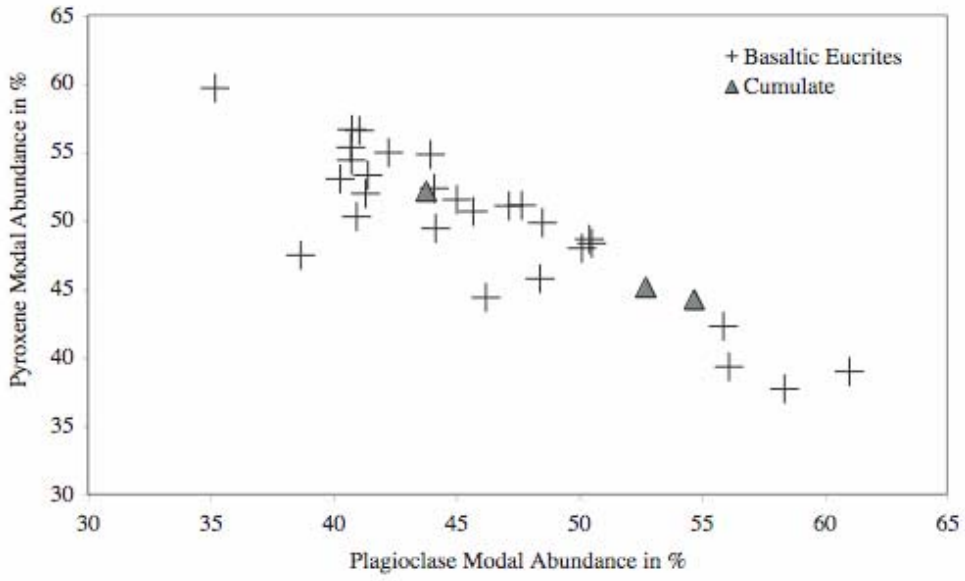

Figure II-3: A comparison of the relative modal abundances of plagioclase and pyroxene in the unbrecciated eucrites. Basaltic samples are denoted by crosses and the cumulate eucrites by triangles.

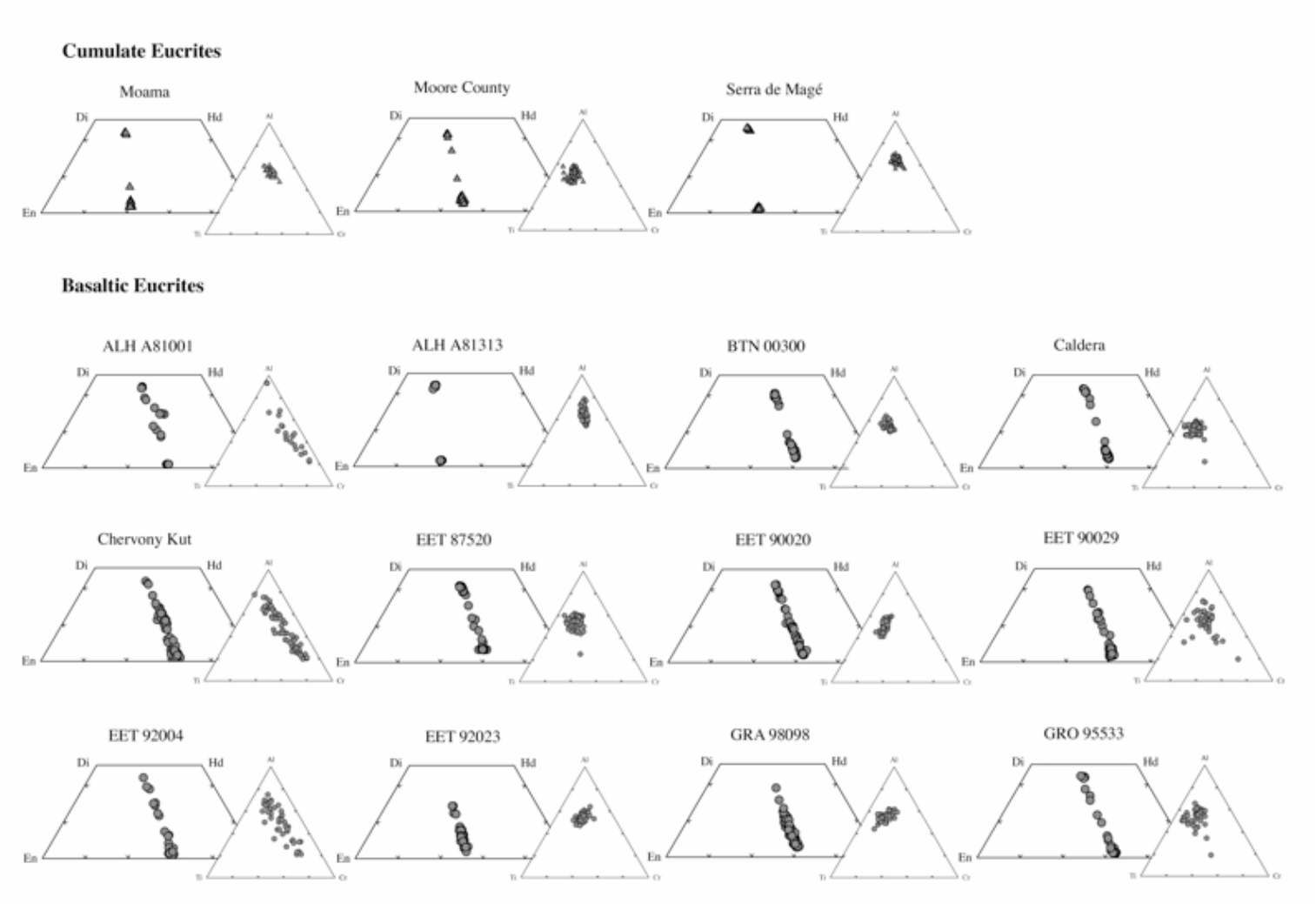

Figure II-4: Major (quadrilateral) and minor (Al, Cr, Ti) element compositions in pyroxenes of the unbrecciated eucrites.

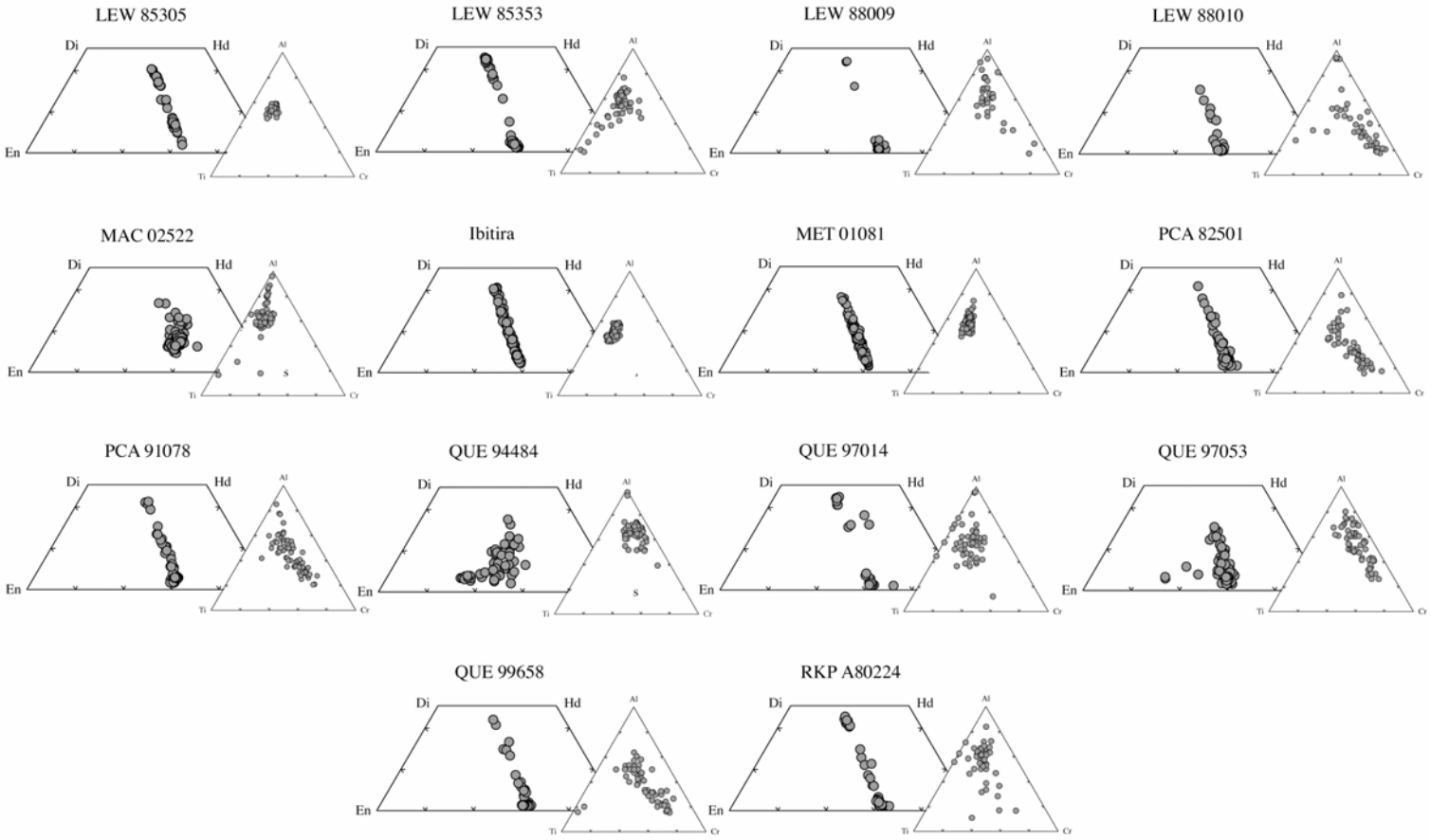

Figure II-4 continued: Major (quadrilateral) and minor (Al, Cr, Ti) element compositions in pyroxenes of the unbrecciated eucrites.

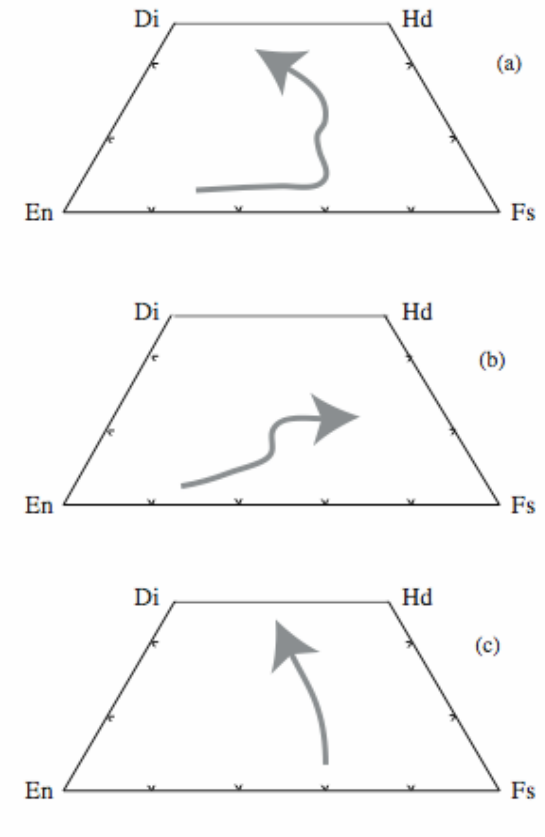

Figure II-5: Primary chemical zoning trends of pyroxene, after Pun and Papike (1996). (a) Mg-Fe-Ca trend. Mg-rich cores to Fe-rich rims. (b) Mg-Fe trend. (c) Fe-Ca trend, showing tie lines between host pigeonite to exsolved augite in ordinary eucrites. These are considered to be equilibrated, as chemical zoning is no longer present.

Figure II-6: All pyroxene elemental composition analyses and ratio plots for the unbrecciated eucrites studied. (a) Fe/Mn versus Fe/Mg. (b) Fe/Mn versus Wo content. (c) Mn versus Fe content in atomic formula units. All values plotted here are above the detestion limit on the electron micrprobe. Counting errors lead to a 2σ of $\pm 9.7\%$ for Fe/Mn, due to the larger counting error for Mn, which is only a minor element in eucrite pyroxenes. This error still does not account for the distinct Fe/Mn ratio seen in QUE 94484 in all three of these plots.

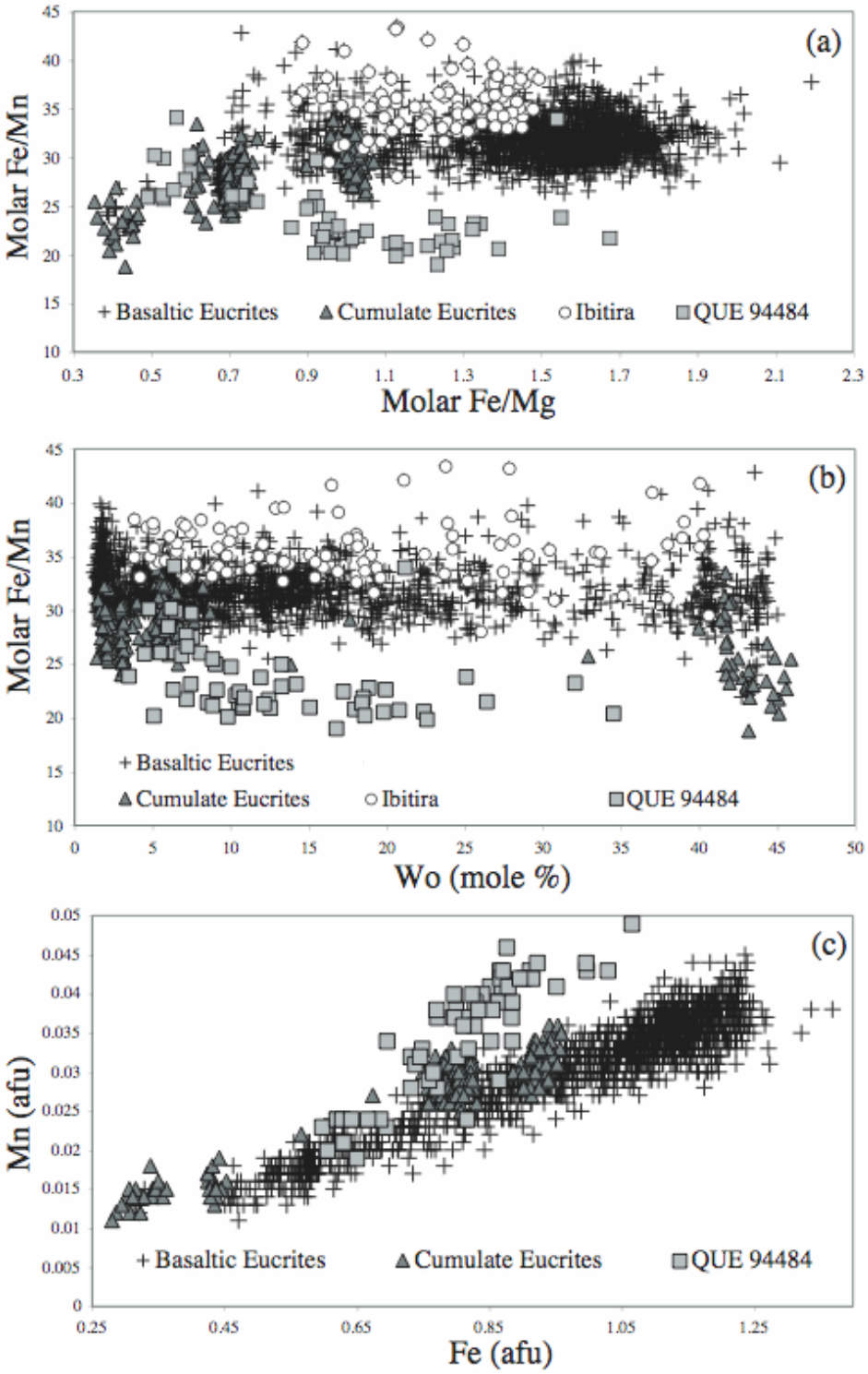
(a)
Molar Fe/Mn
Molar Fe/Mg
+ Basaltic Eucrites
▲ Cumulate Eucrites
○ Ibitira
■ QUE 94484
(b)
Molar Fe/Mn
Wo (mole %)
+ Basaltic Eucrites
▲ Cumulate Eucrites
○ Ibitira
■ QUE 94484
(c)
Mn (afu)
Fe (afu)
+ Basaltic Eucrites
▲ Cumulate Eucrites
■ QUE 94484

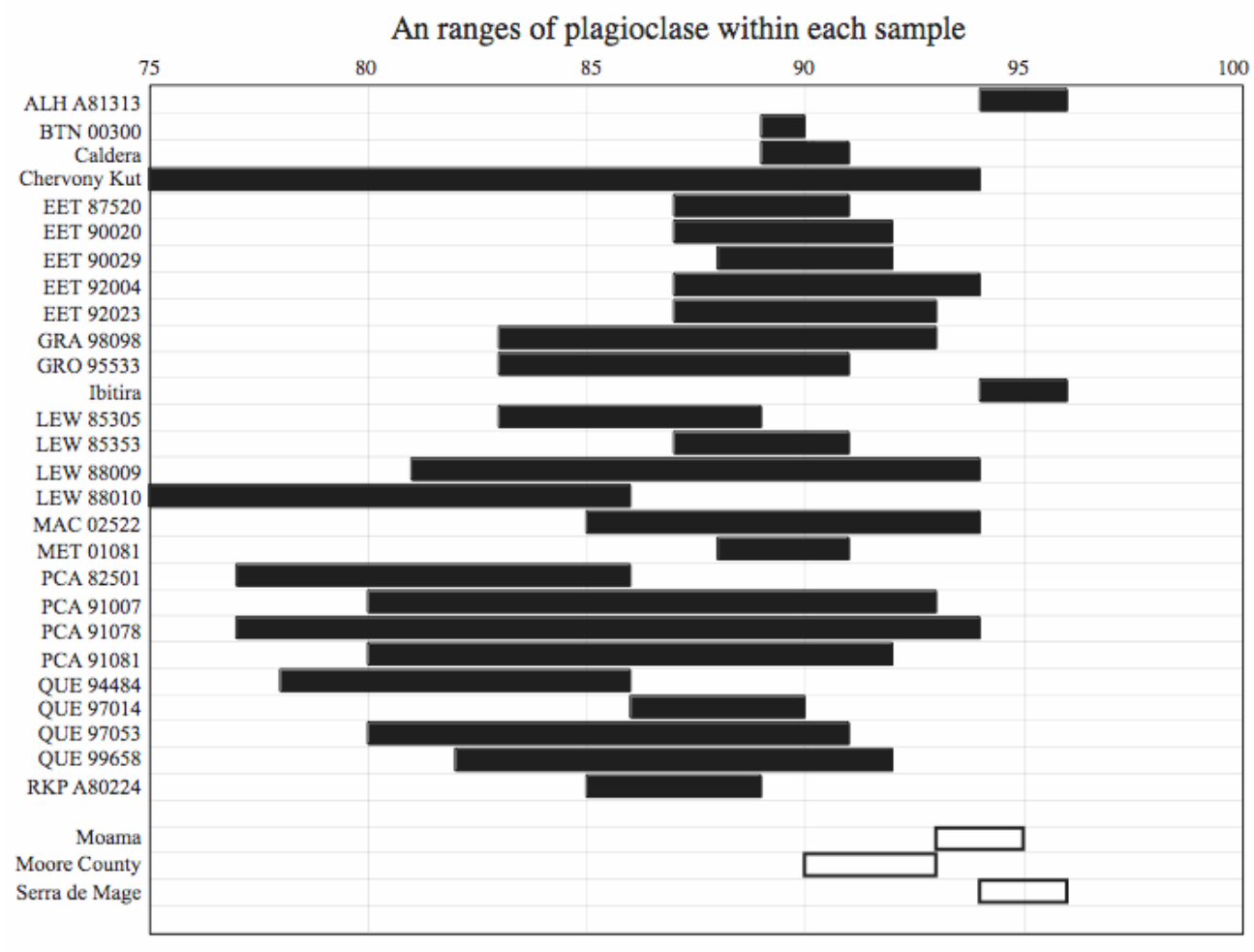

Figure II-7: Anorthite (An) ranges for plagioclase analyses in the unbrecciated eucrites. Basaltic eucrites are shown using filled-in black bars and the cumulates with unfilled bars.

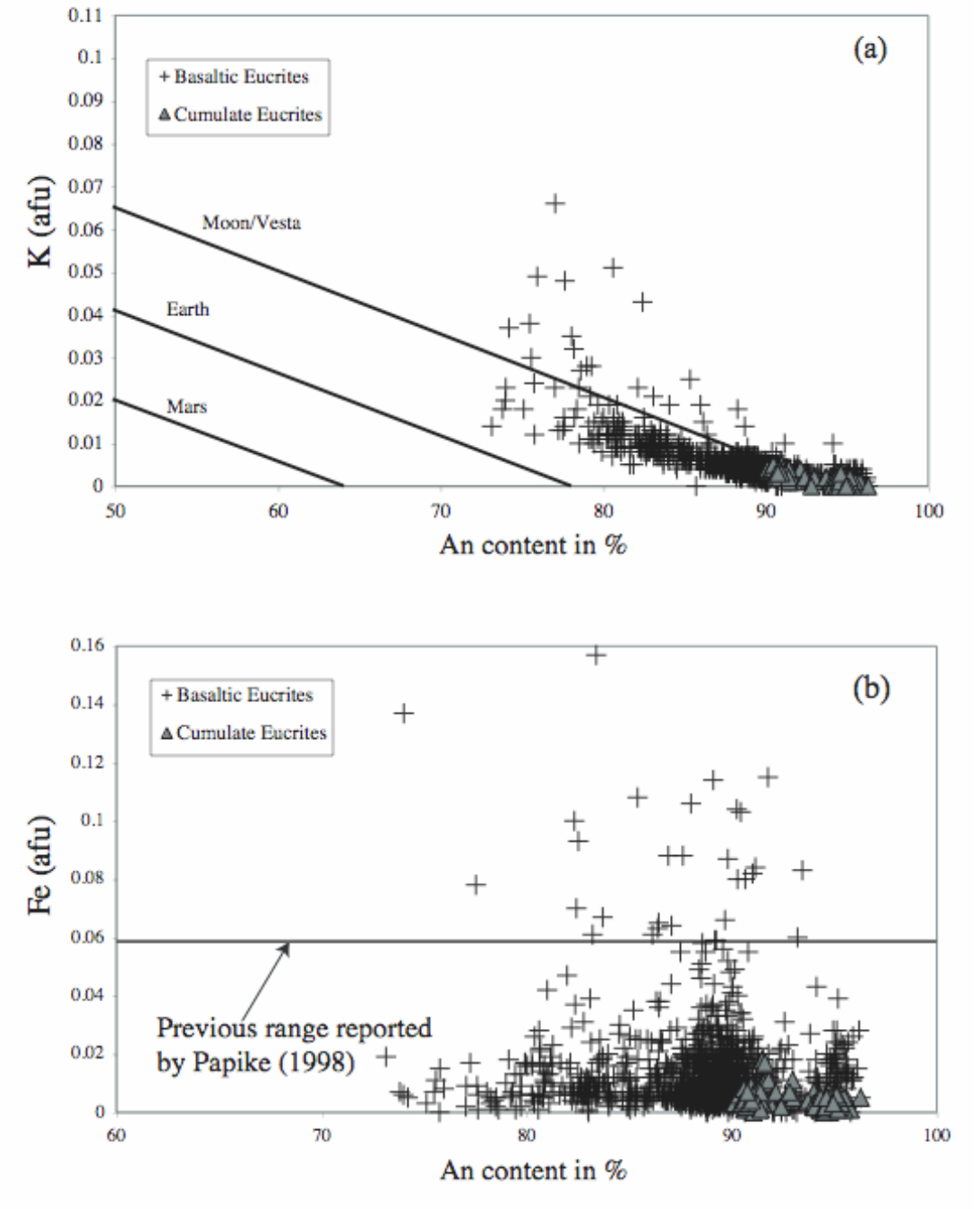

Figure II-8: Elemental compositions of plagioclase in the unbrecciated eucrites studied. (a) K (atoms per formula unit) vs. An content. (b) Fe (atoms per formula unit) vs. An content. The detection limits of these elements on the electron microprobe are 0.003 afu for K and 0.001 afu for Fe.

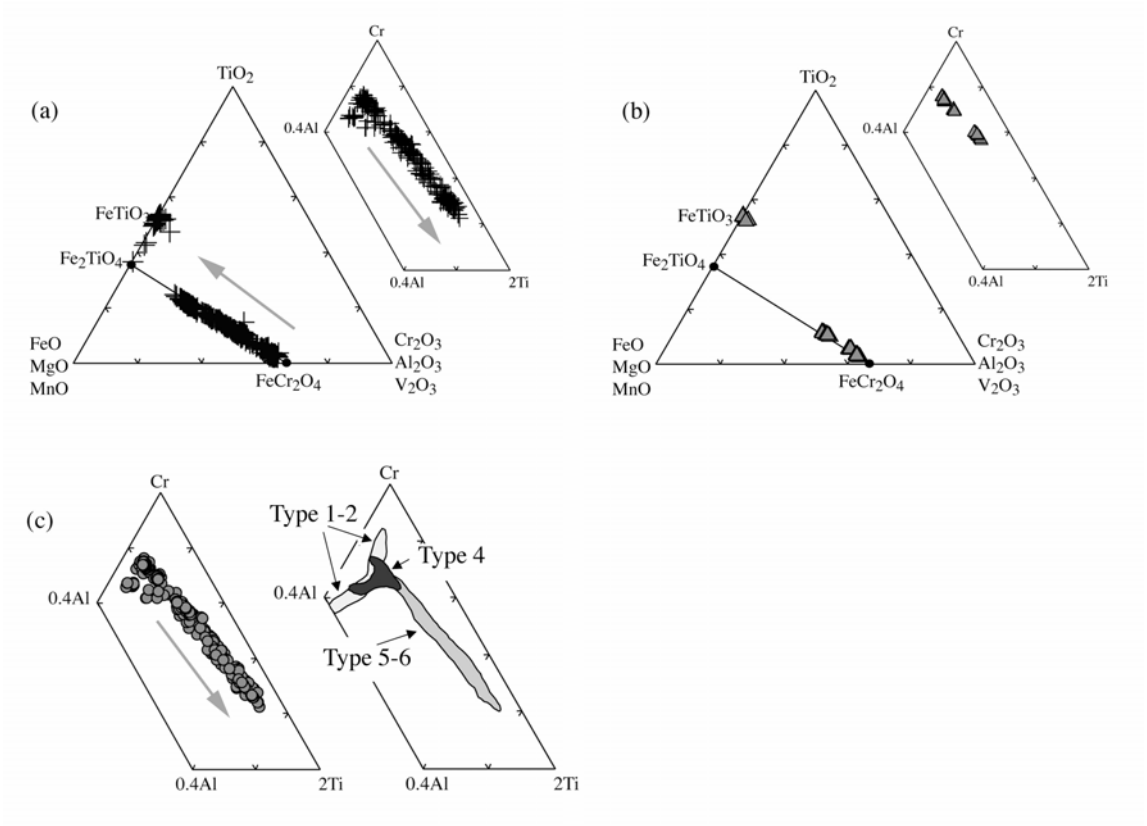

Figure II-9: All spinel analyses for the unbrecciated eucrites studied. (a) All basaltic eucrites in this study. (b) All cumulate eucrites in this study. (c) All analyses compared to the spinel compositions of the petrographic types of Yamaguchi. The grey arrows indicate the compositional trends with increasing crystallization.

Figure II-10: Model cross-section through the basaltic crust of 4 Vesta shortly after its formation. The petrology of the unbrecciated eucrites supports the suggestion that the crust formed through a combination of serial magmatism and intrusive processes (Yamaguchi et al., 1996; Yamaguchi et al., 1997b).

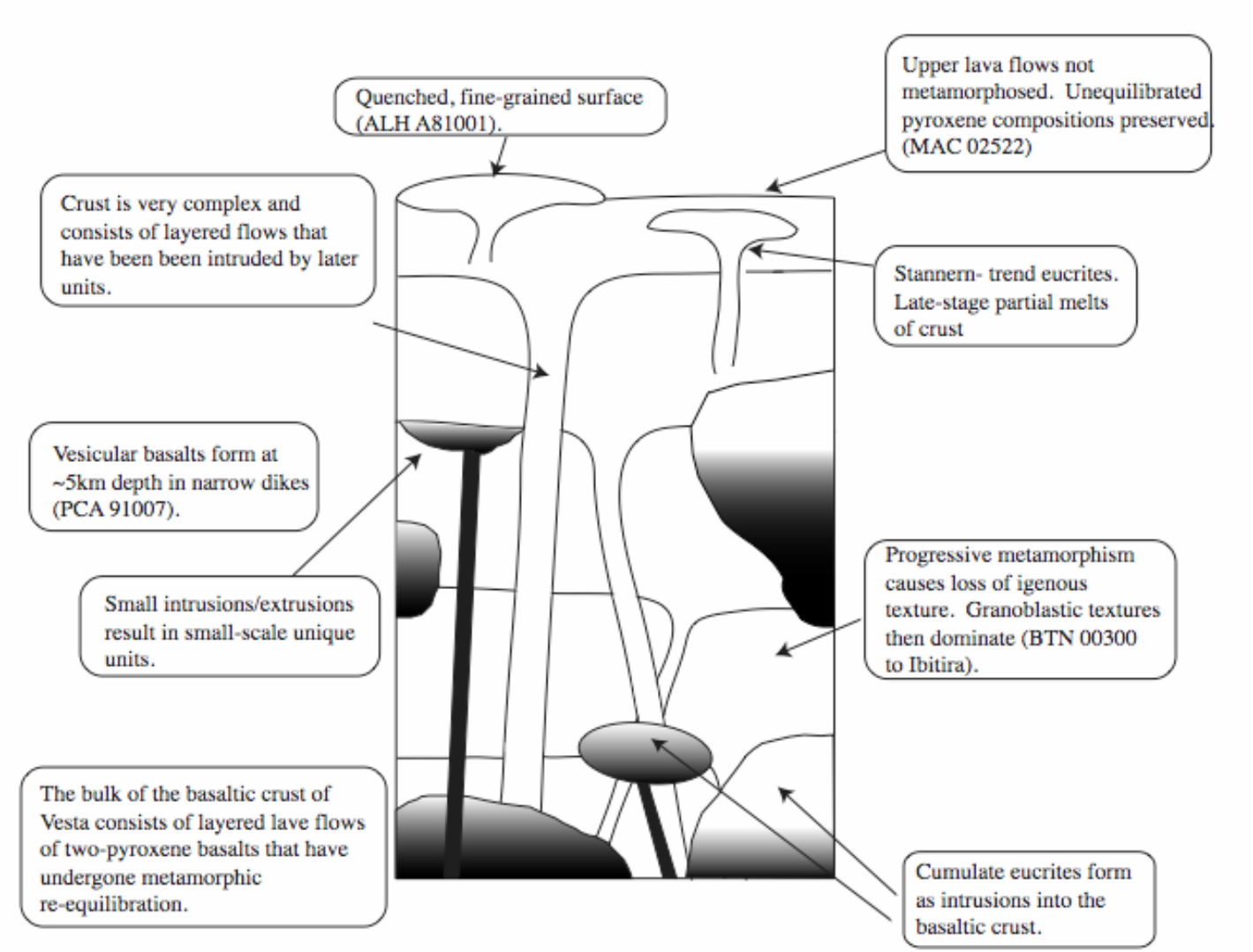
Quenched, fine-grained surface (ALH A81001).
Upper lava flows not metamorphosed. Unequilibrated pyroxene compositions preserved. (MAC 02522)
Crust is very complex and consists of layered flows that have been been intruded by later units.
Stannern- trend eucrites. Late-stage partial melts of crust
Vesicular basalts form at ~5km depth in narrow dikes (PCA 91007).
Small intrusions/extrusions result in small-scale unique units.
Progressive metamorphism causes loss of igenous texture. Granoblastic textures then dominate (BTN 00300 to Ibitira).
The bulk of the basaltic crust of Vesta consists of layered lave flows of two-pyroxene basalts that have undergone metamorphic re-equilibration.
Cumulate eucrites form as intrusions into the basaltic crust.

Appendix II-B

Key to SEM Mineral Maps

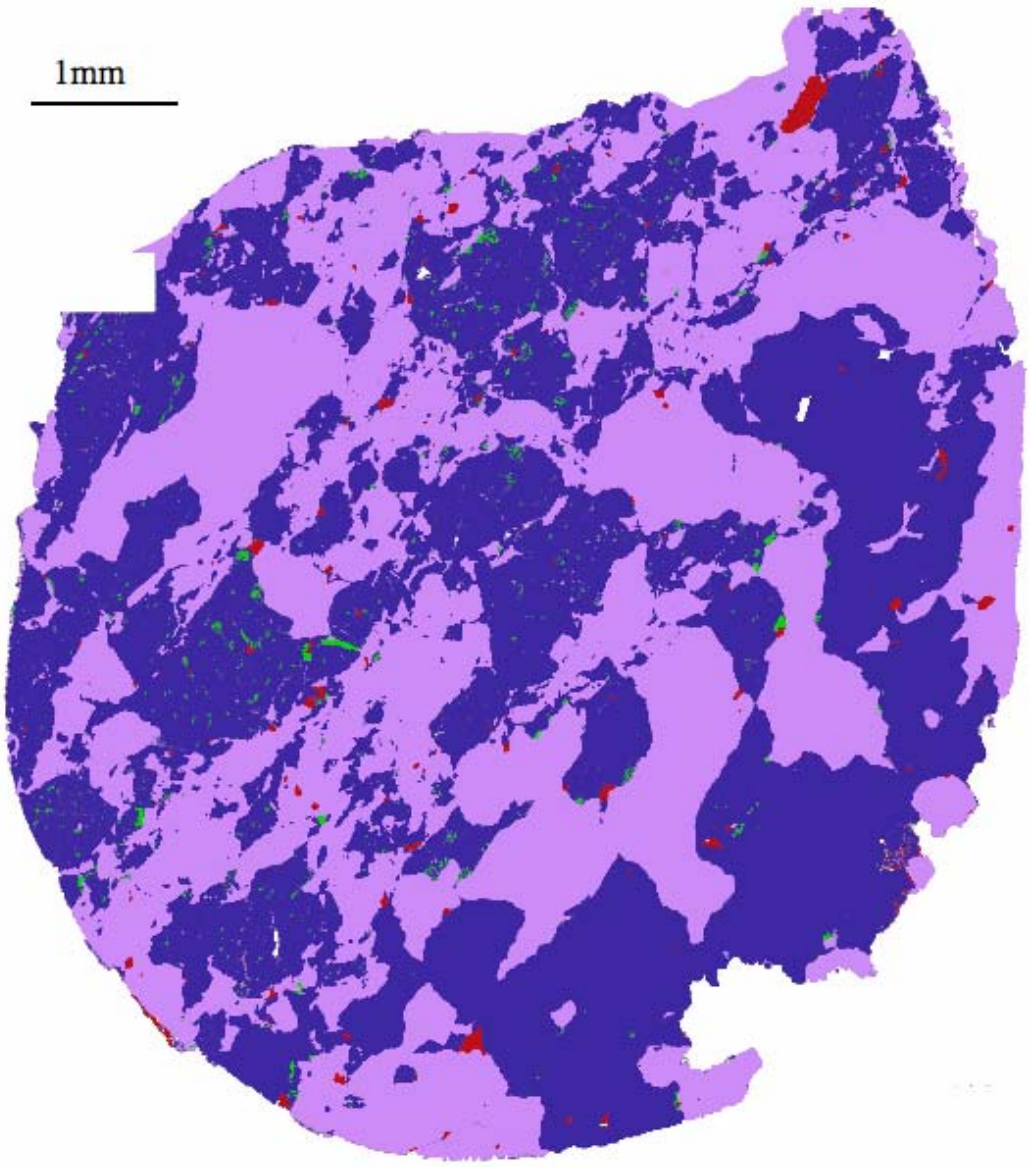

ALH A81313

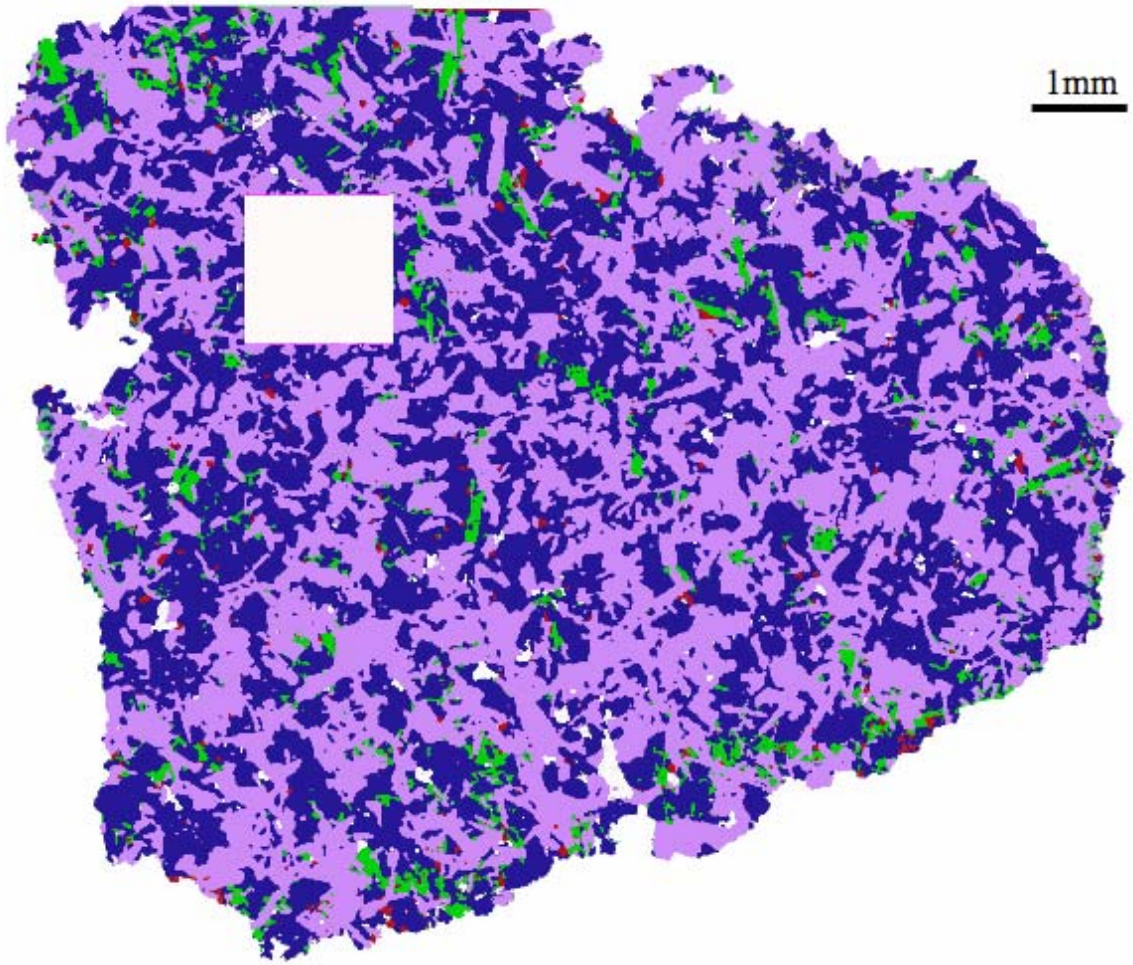

BTN 00300

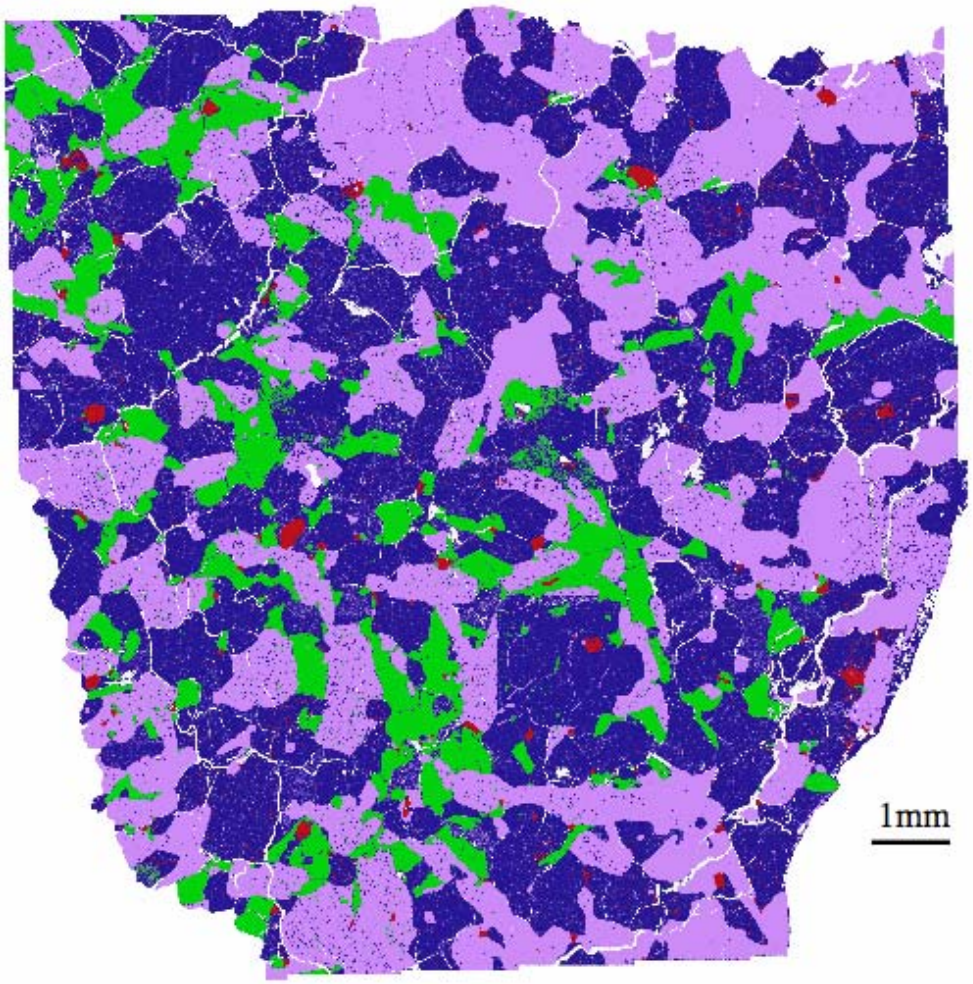

Caldera

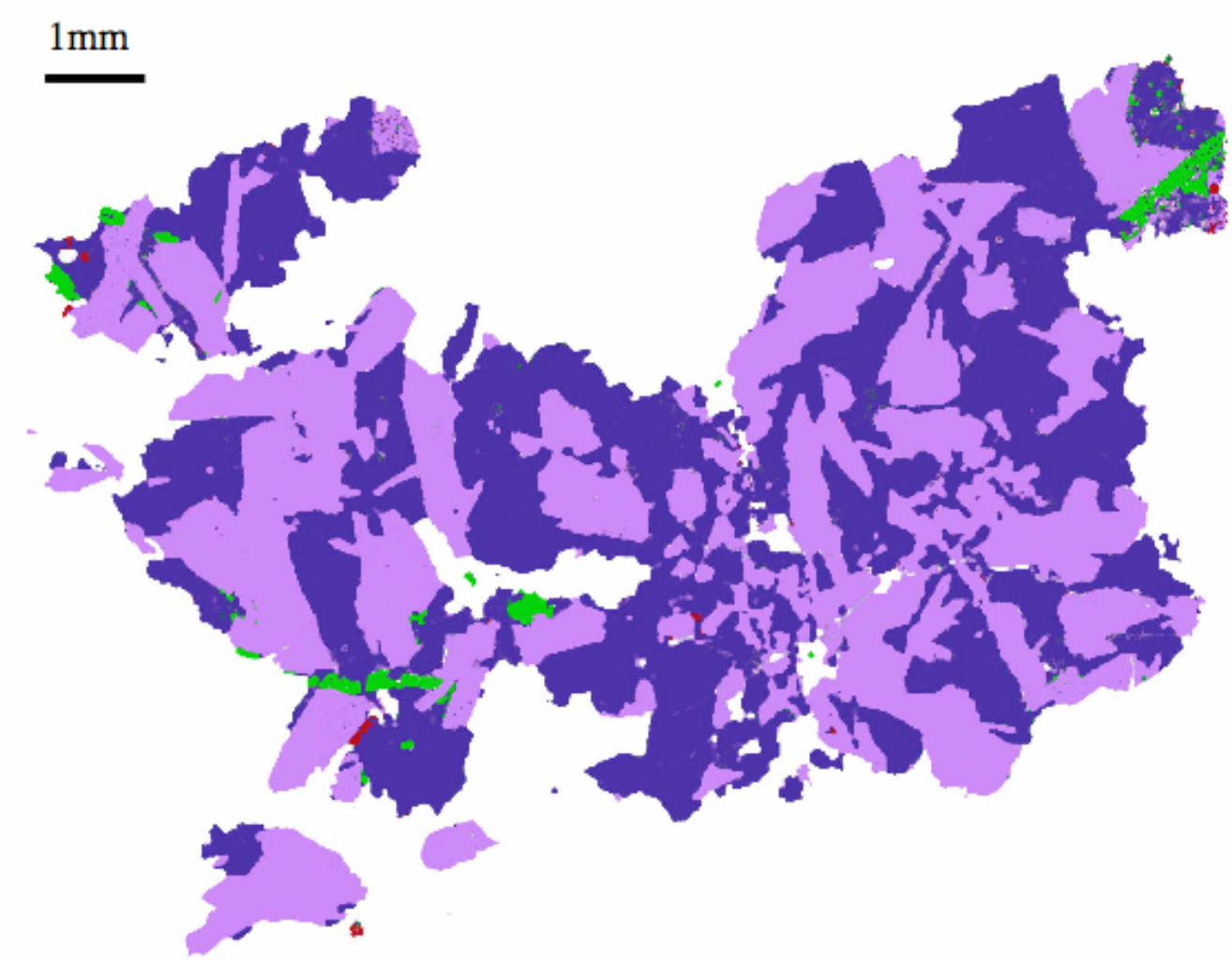

EET 87520

N.B. This sample was not mapped at the same resolution as all other maps and consequently is not of the same quality.

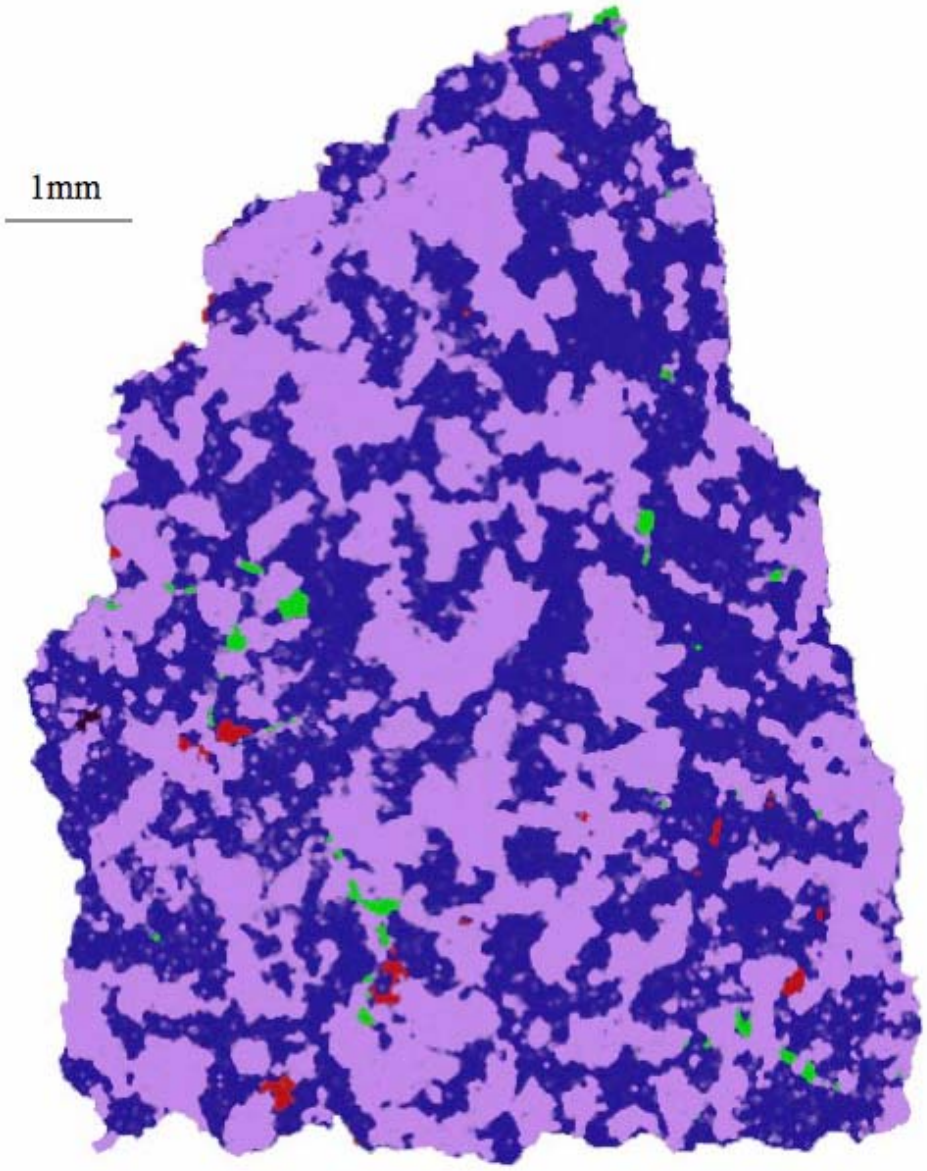

EET 90020

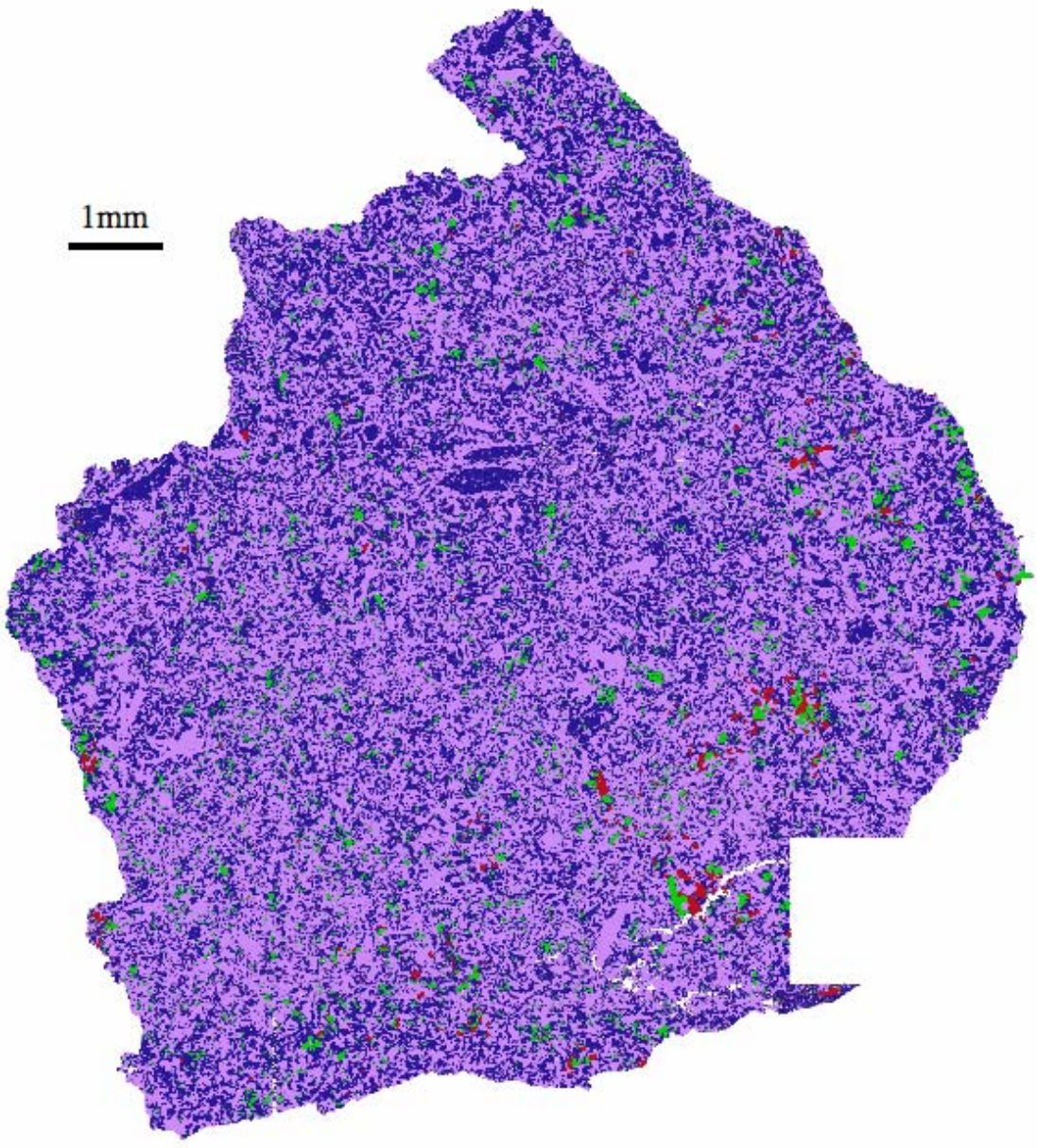

EET 90029

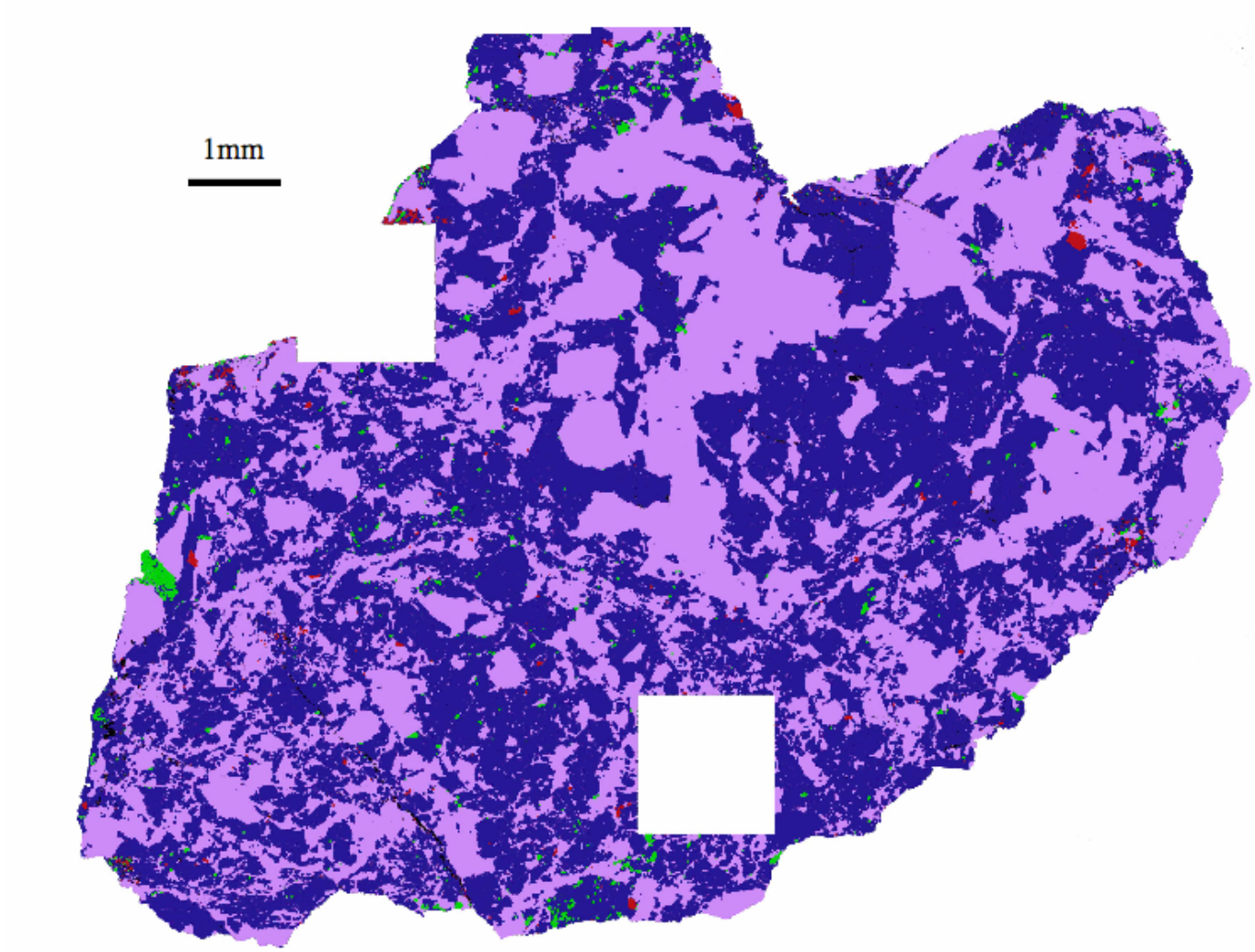

EET 92004

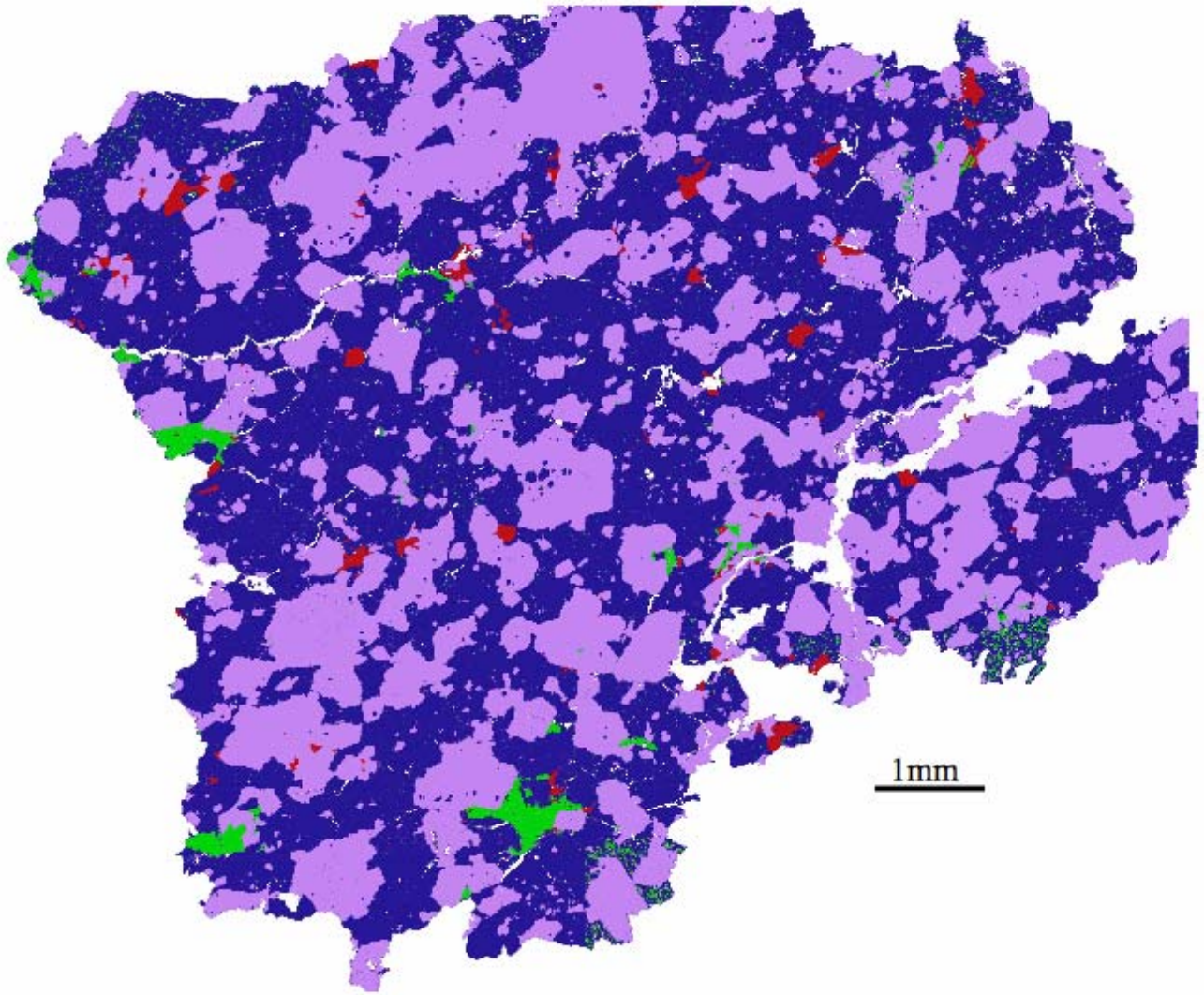

EET 92023

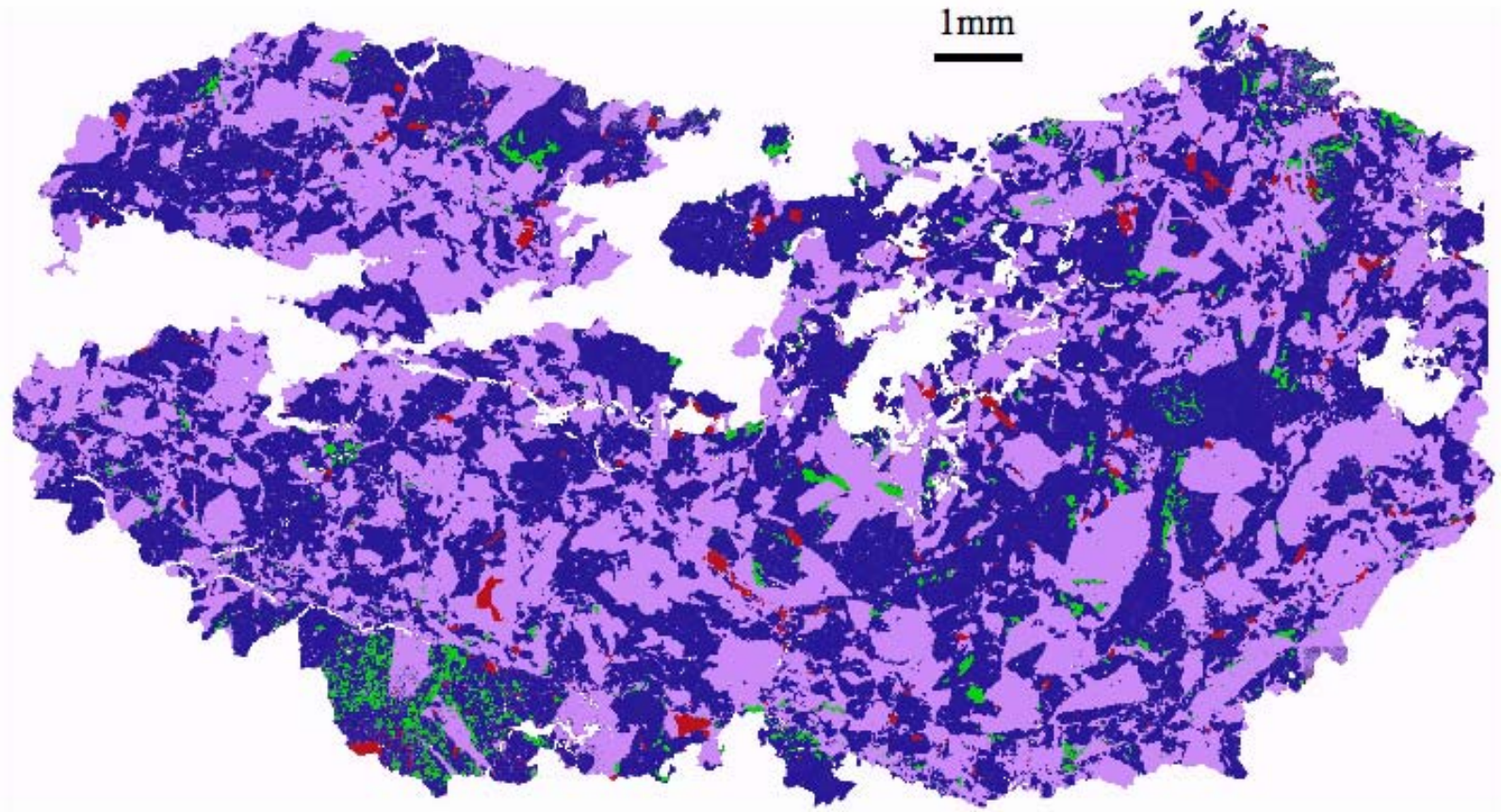

GRO 95533

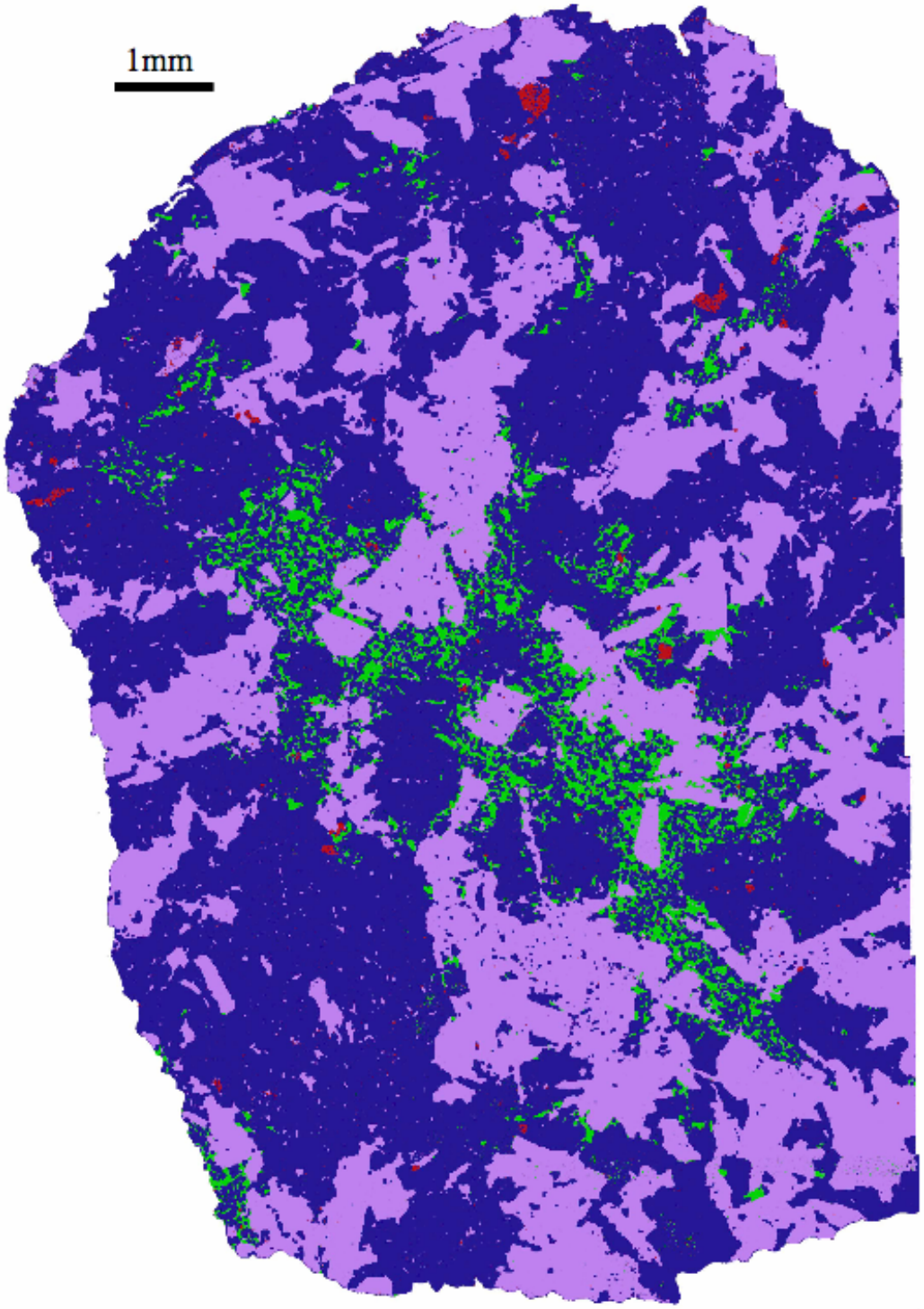

LEW 85305

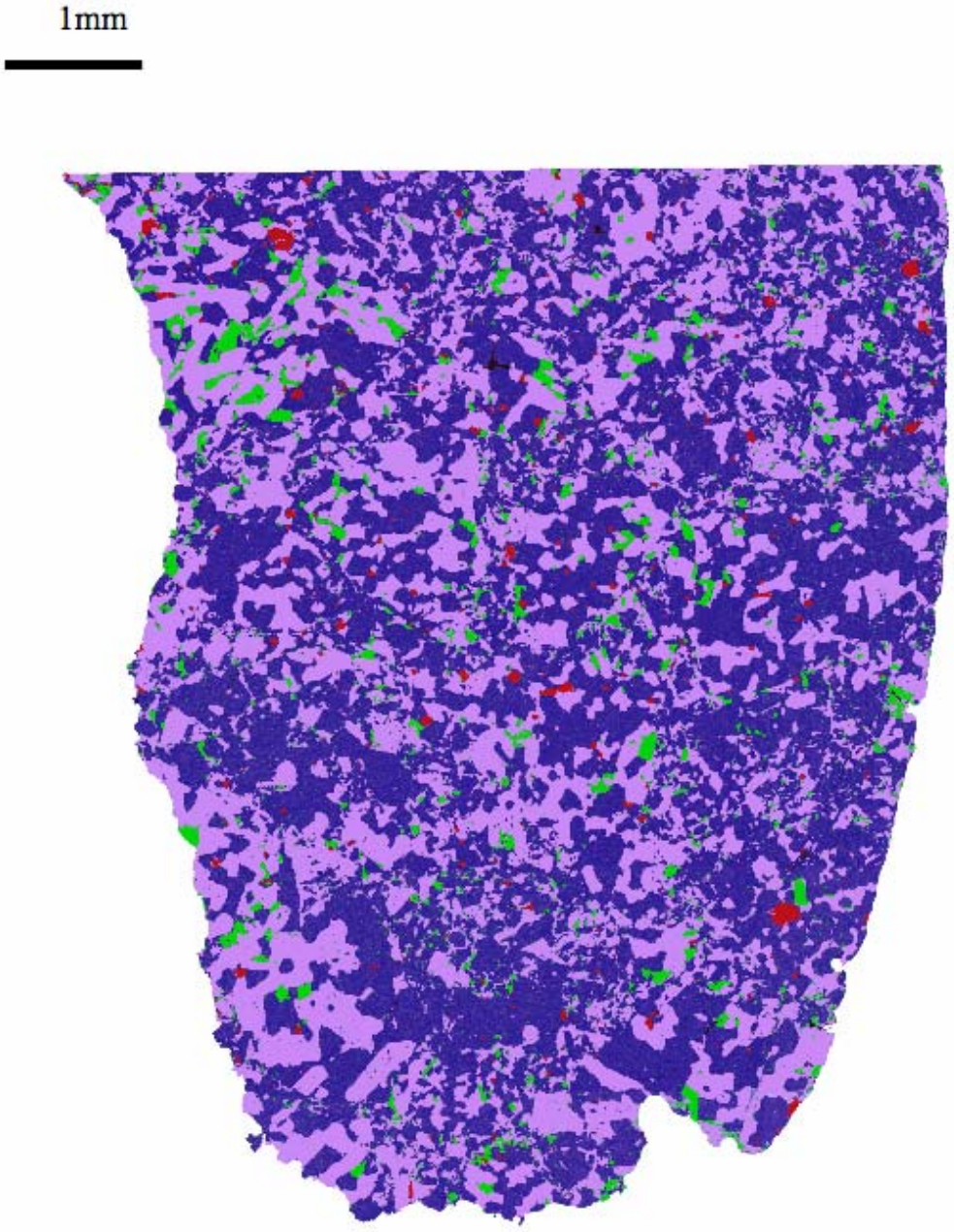

LEW 85353

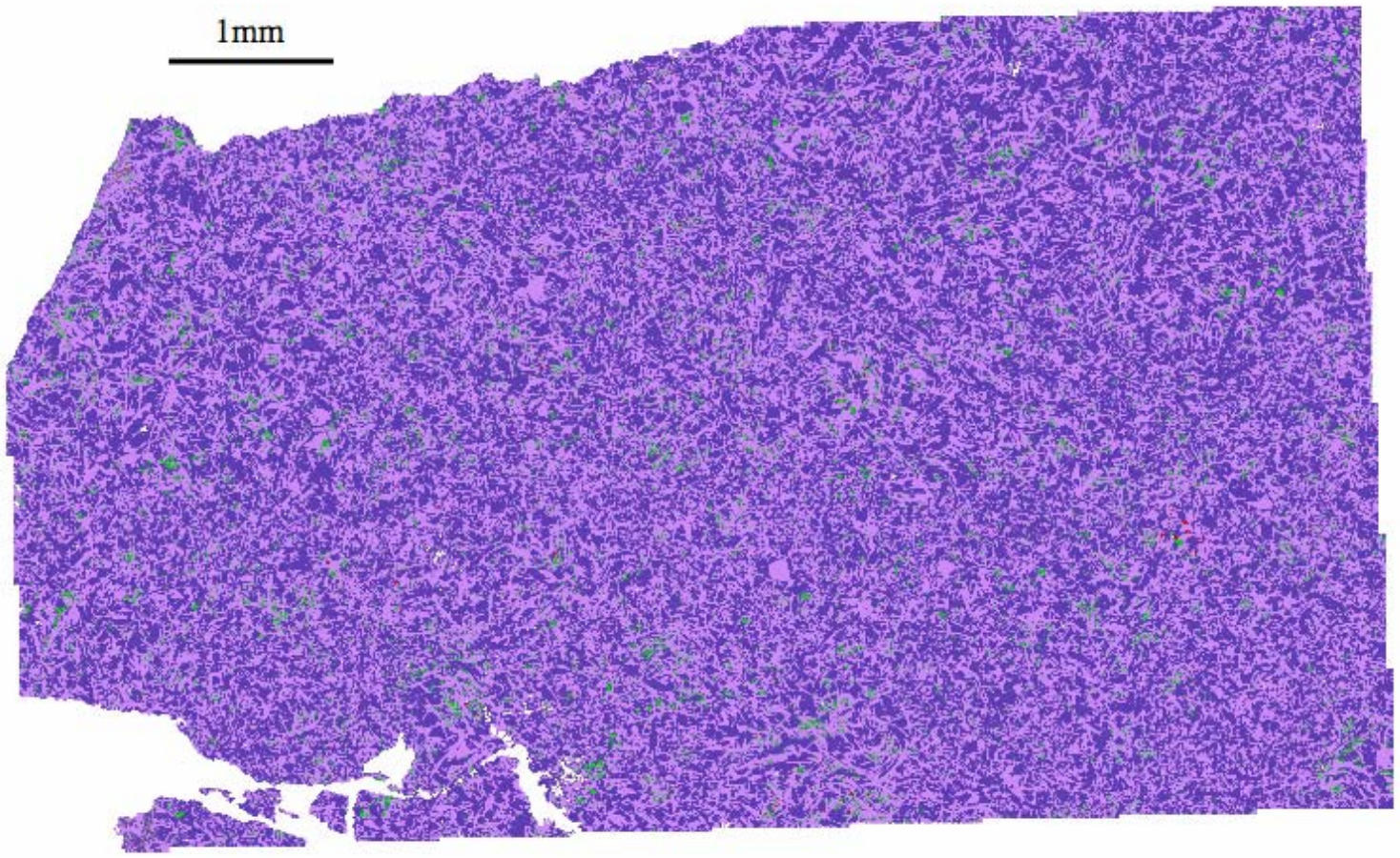

LEW 88009

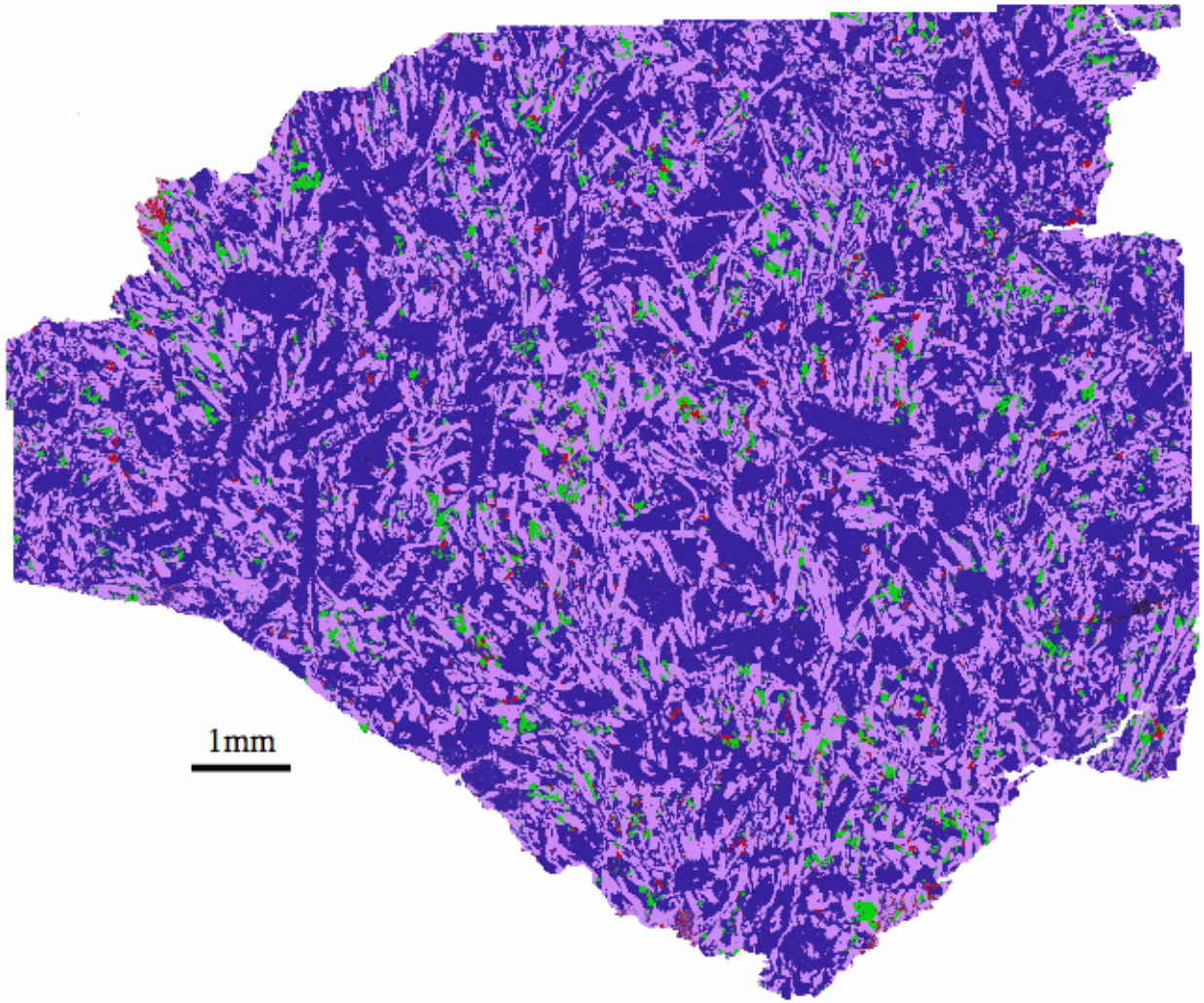

LEW 88010

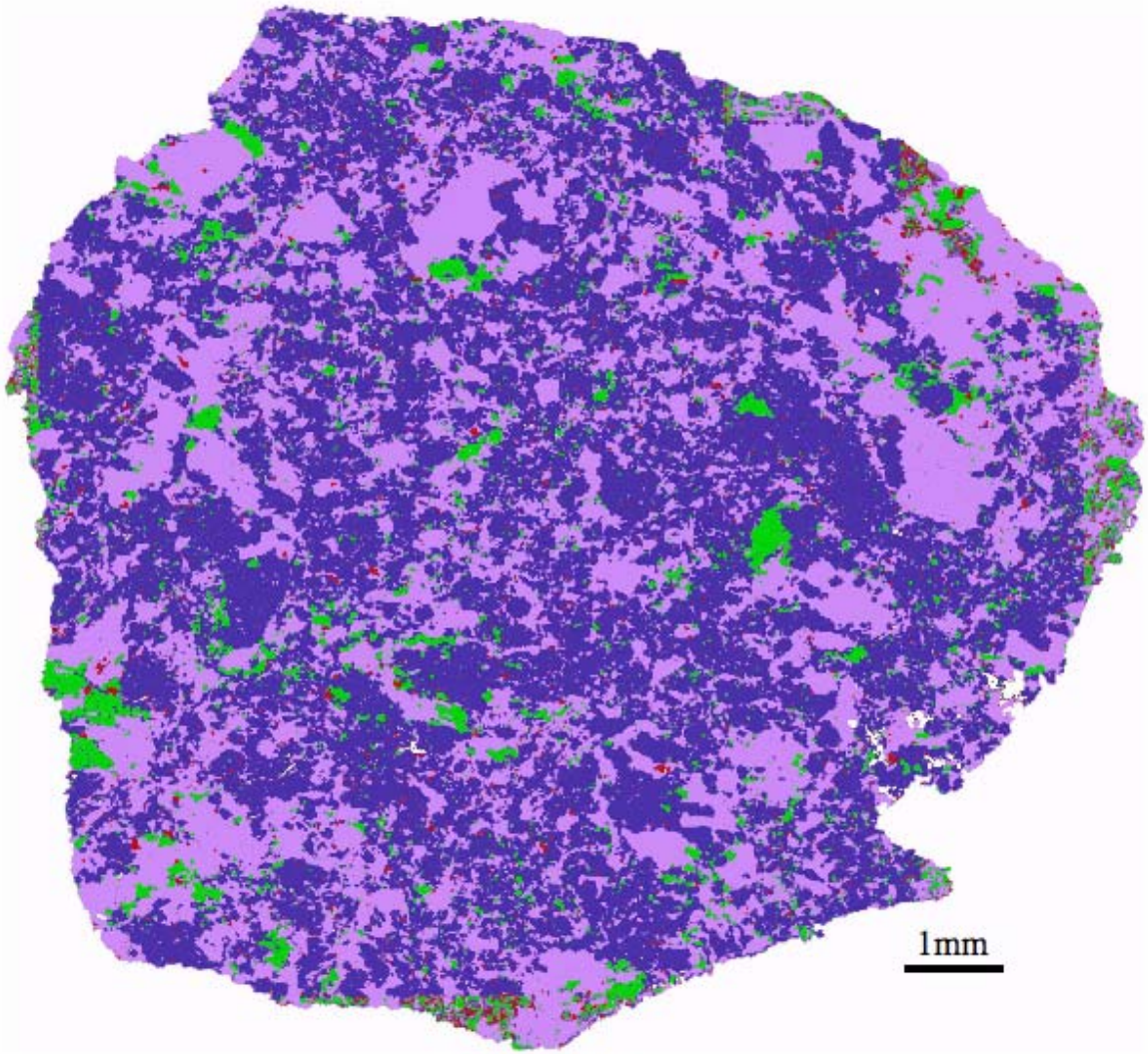

MET 01081

Moama

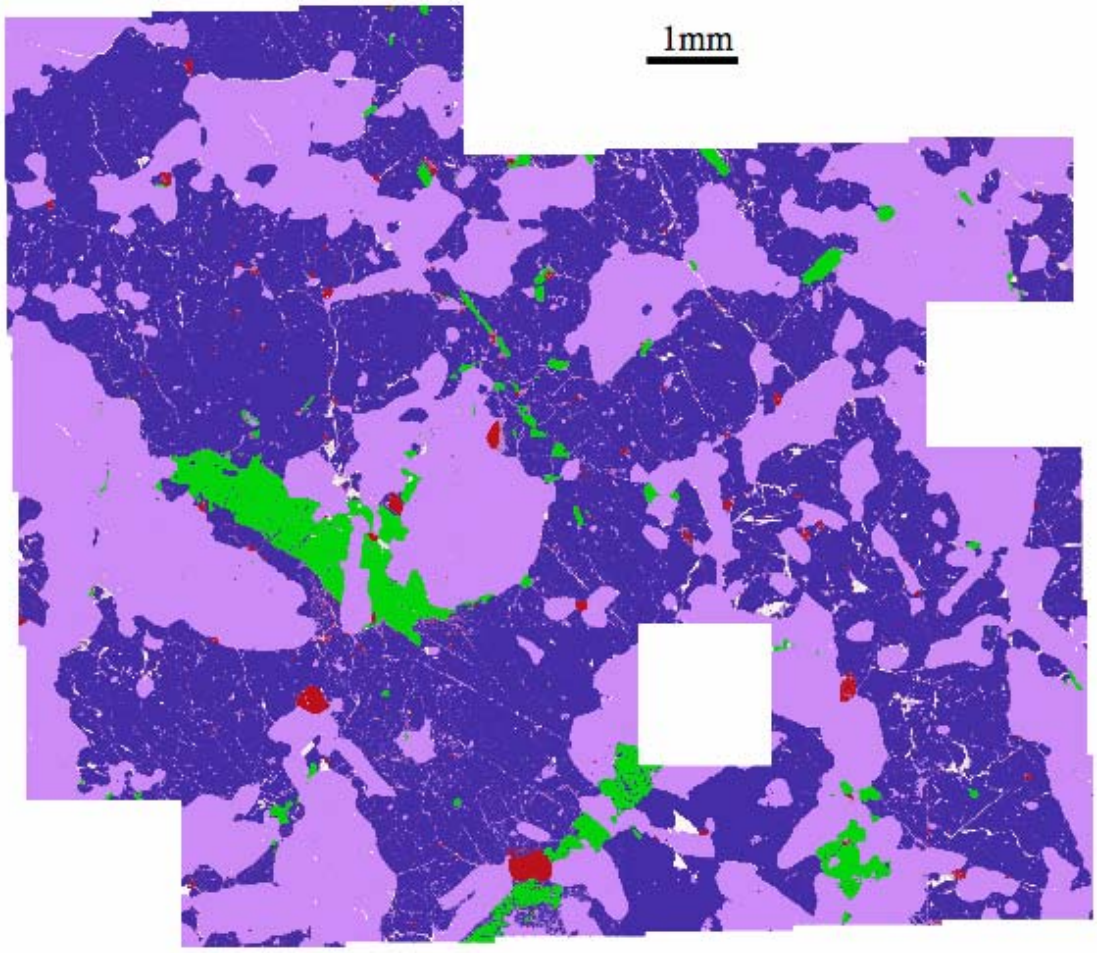

Moore County

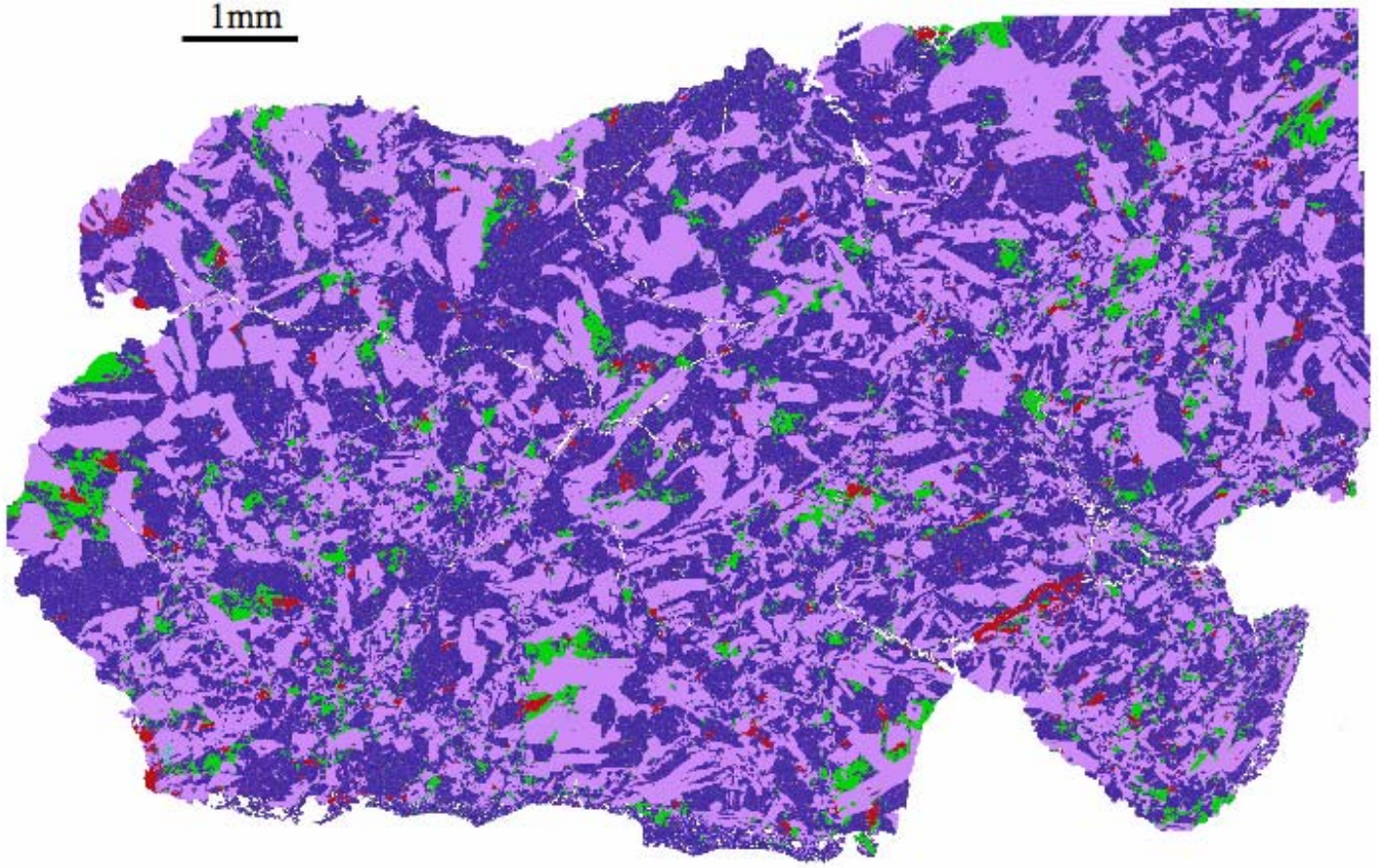

PCA 82501

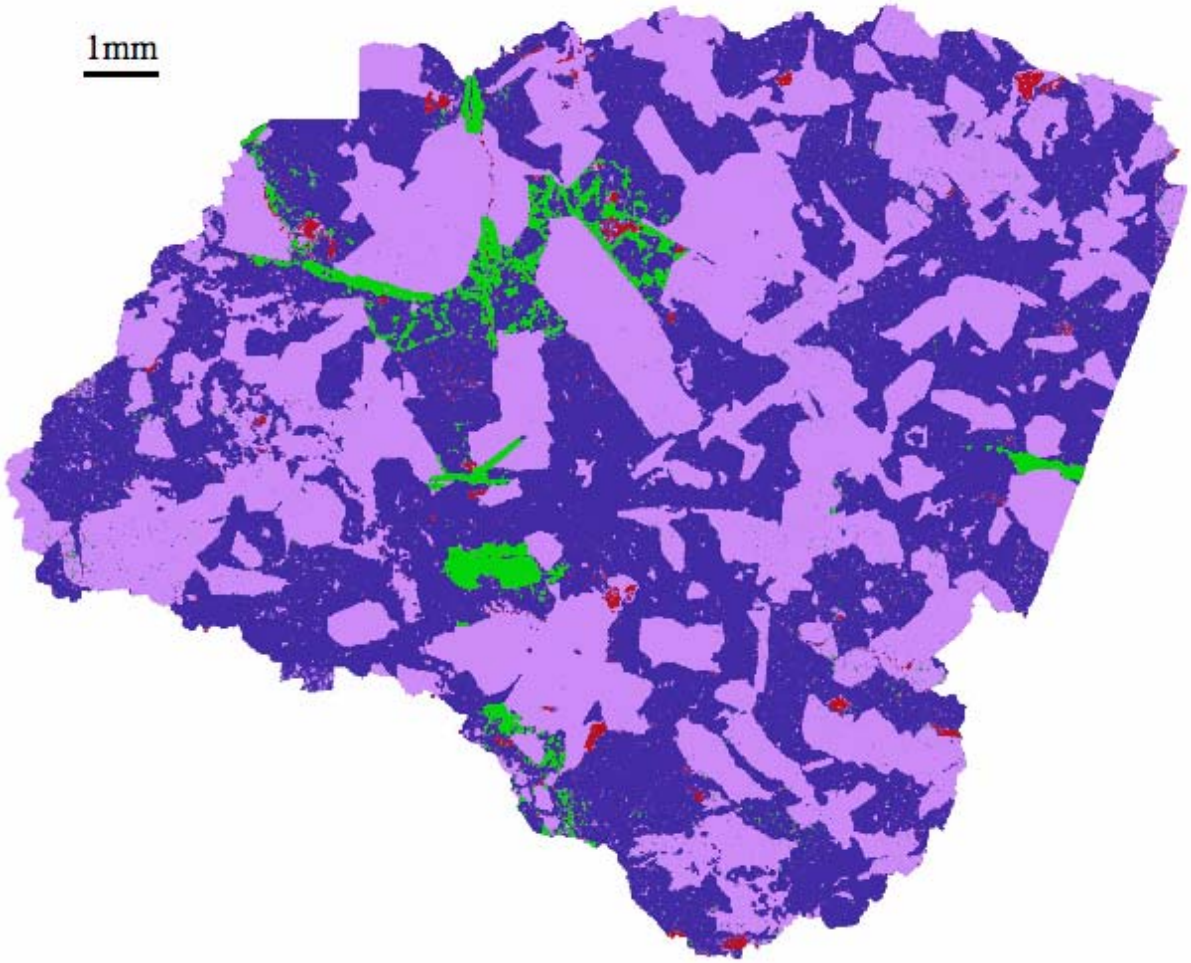

PCA 91078

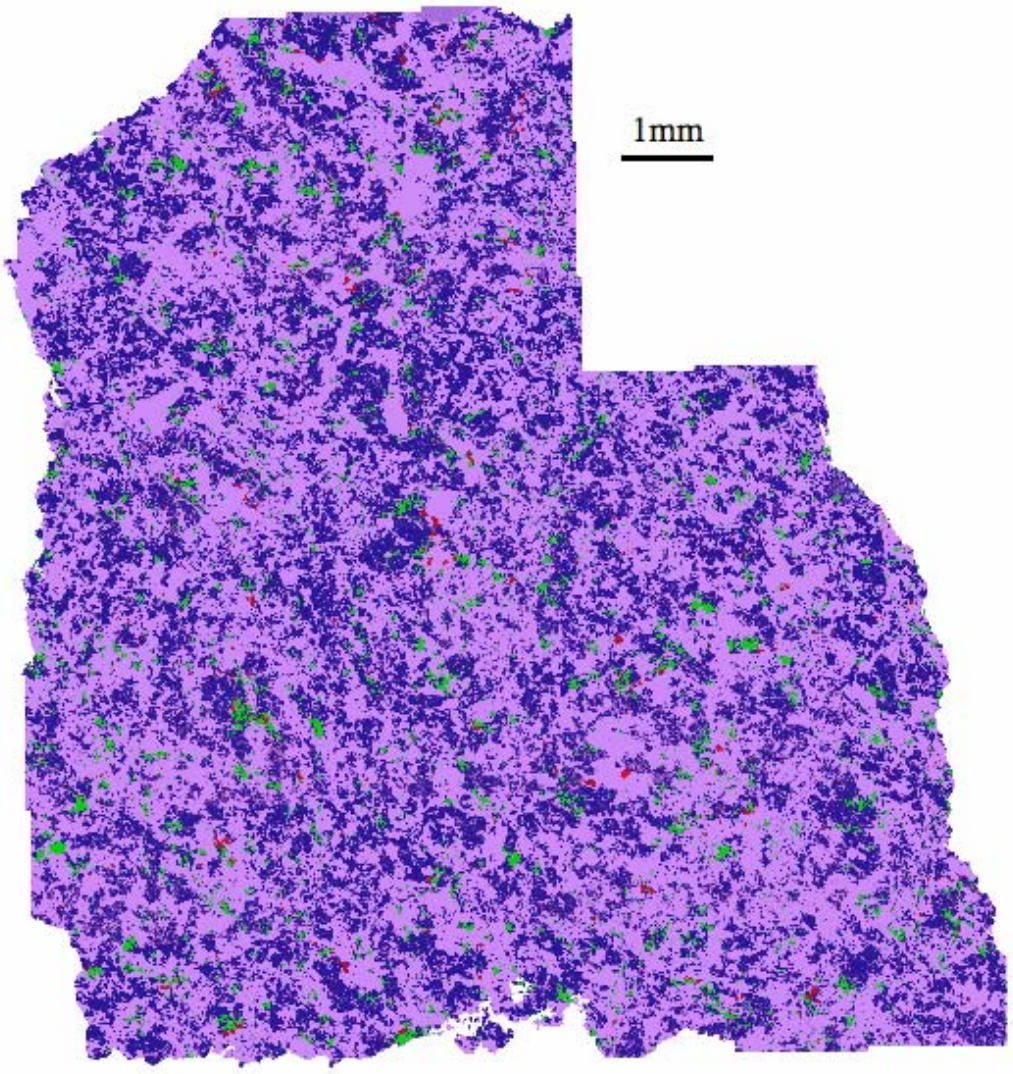

QUE 97014

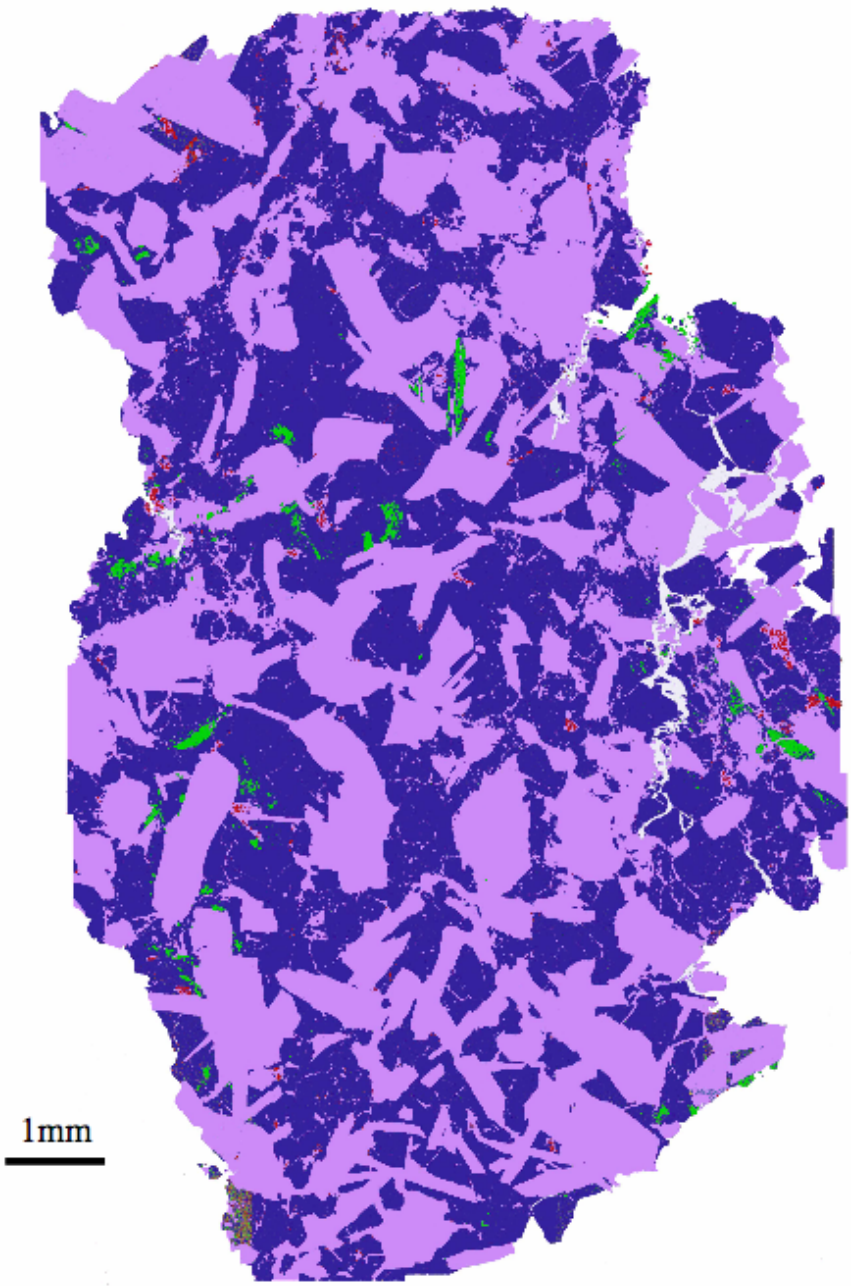

QUE 97053

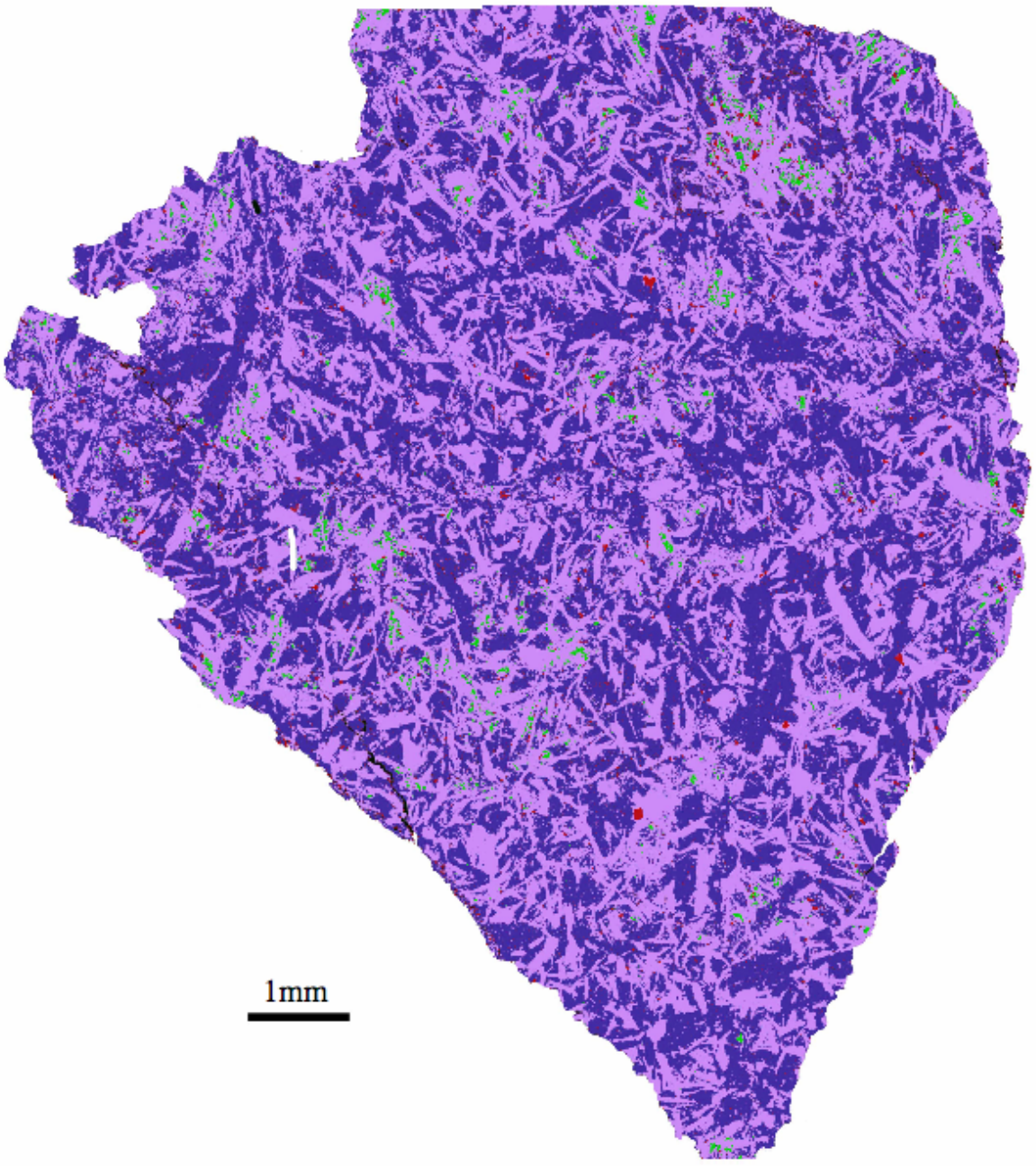

QUE 99658

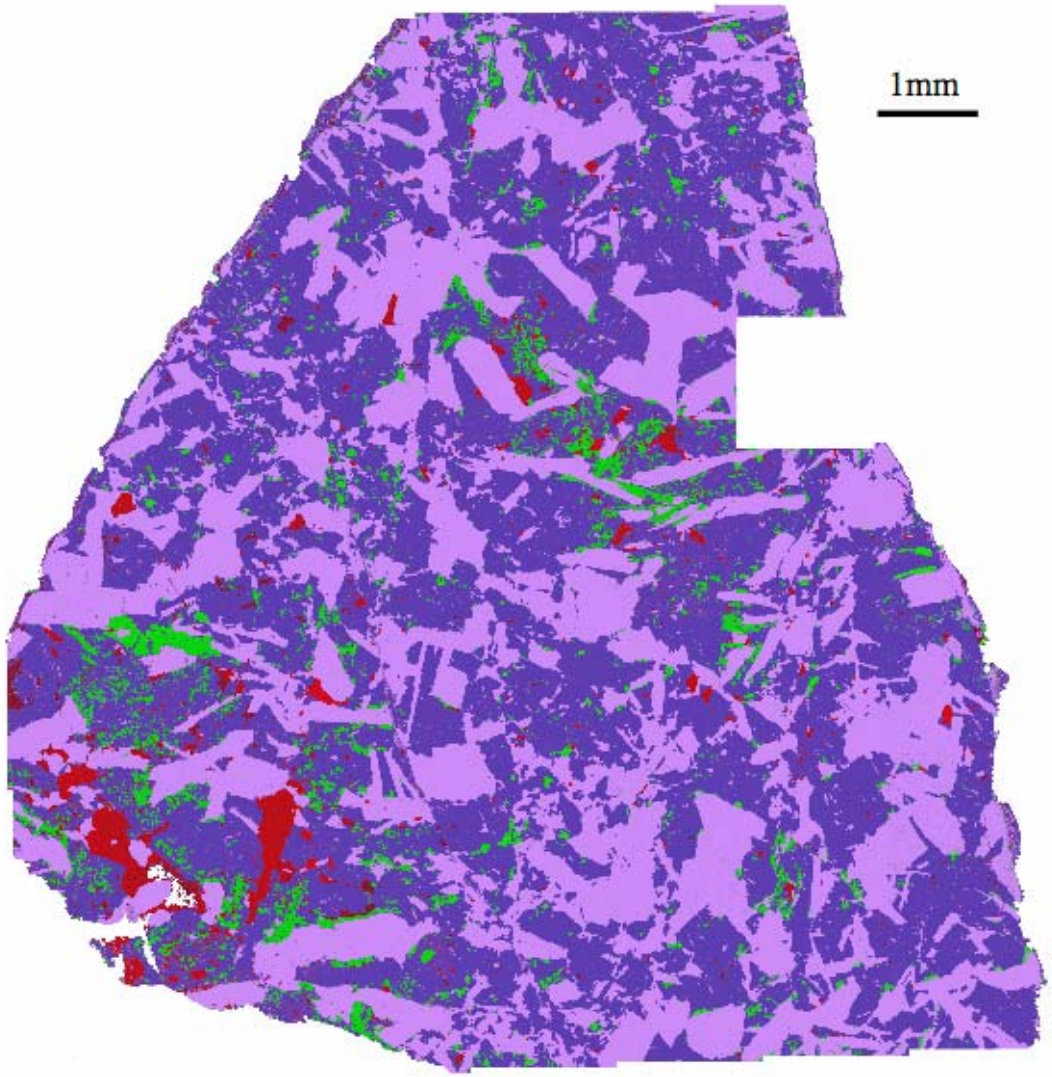

RKP A80224

III. Petrologic Insights from the Spectra of the Unbrecciated Eucrites: Implications for Vesta

This chapter is a reformatted version of a paper, by the same name, to be submitted to the journal Meteoritics and Planetary Science by Rhiannon G. Mayne, Jessica M. Sunshine, Harry Y. McSween, Timothy J. McCoy, Catherine M. Corrigan, Allison Gale, and M. Darby Dyar.

Mayne R.G., Sunshine J.M., McSween H.Y. Jr., McCoy T.J., Corrigan C.M., Gale A., Dyar M.D. Spectra of the Unbrecciated Eucrites.

Abstract

We investigate the relationship between the petrology and visible-near infrared (VIS-NIR) spectra of the unbrecciated eucrites and pyroxene-plagioclase mixtures, to establish what information can be extracted about the mineral chemistries and thermal histories of a sample from their spectra alone. The unbrecciated eucrites were characterized petrologically in a previous study, in terms of the factors believed to impact spectra the most (mineral chemistries, modal mineralogies, and textures). The VIS-NIR spectra of 11 unbrecciated eucrites were collected and band centers and band area ratios were measured. All spectra were then subject to analysis with the Modified Gaussian Model (MGM) to assess how well we can predict pyroxene compositions and modal abundances, particular focus was given to the effect of the amount plagioclase on the spectra of the pyroxene-plagioclase mixtures. The results show that plagioclase has little effect on VIS-NIR spectra. However, information on not only the mineralogy, but also the magmatic history (e.g. fast cooling vs. slow-cooling, early crystallization from melt vs. late, highly metamorphosed and equilibrated eucrites vs. unequilibrated) can be obtained from the spectra of the unbrecciated eucrites.

1. Introduction

Asteroid 4 Vesta has been the focus of much research since McCord (1970) noted the spectral similarities between its spectrum and that of the howardites, eucrites, and diogenites (HEDs) and it is now one of the targets for Dawn mission, which launched in September 2007. Several lines of evidence have been put forward to support the hypothesis that the HEDs derive from Vesta, such as the fact that they lie on the same oxygen isotope fractionation line (Clayton and Mayeda, 1996), the evidence for significant impact excavation from the surface (Thomas et al., 1997), common cosmic-ray exposure ages (Eugster and Michel, 1995), and the discovery of Vesta-like asteroids (Vestoids) bridging the gap between it and the 3:1 resonance (Binzel and Xu, 1993). The HEDs therefore enable us to collect detailed mineralogical, petrological and geochemical information about Vesta. This information, in turn, allows us to better constrain models for its formation, which is still not well understood (Mittlefehldt and Lindstrom, 2003).

Gaffey (1997) observed sub-hemispheric color and spectral variations across the surface of Vesta, corresponding to regions of differing mineralogies. He was able to produce a generalized lithologic map of Vesta using these results and infer whether regions on the surface were dominated by eucrite or diogenite components. He suggested that an olivine unit had been exposed within the large crater in the south-pole region of Vesta. Binzel et al. (1997), using higher spatial resolution Hubble Space Telescope data, produced a similar geologic map of the surface. The 1-μm band was observed to be subtly deeper and broader in the area suggested by Gaffey (1997) as olivine, and they

concluded that, whilst the results were consistent with an olivine-rich component, the surface does not consist of olivine alone (Binzel et al., 1997).

Here we quantify the effects that differing modal mineralogy, mineral compositions, and textures of eucrites have upon their spectra. However, most eucrites are polymict breccias and, consequently, their spectra represent a mixture of lithologies. As a result, the unbrecciated eucrites are key when trying to establish any spectral-mineralogical relationship because direct comparisons can be made between the petrologic characteristics and spectral features of the same material. An earlier phase of this study documents the textures, modal mineralogy, and mineral chemistries of 29 unbrecciated eucrites (Mayne et al., 2008 – Part II of this dissertation).

If we are able to distinguish the type of eucrite that a particular spectrum represents and we understand the petrologic history of such samples, then it may be possible to draw conclusions about the mineralogies and mineral chemistries from measurements by the Dawn VIR (Visible Infrared) spectrometer. Armed with this knowledge we may be able to decipher the petrographic significance of mapped units on the surface of Vesta and understand the processes behind the formation of its basaltic crust. This study aims to quantify how much information can be extracted from the spectra of the unbrecciated eucrites by analyzing the spectra of petrologically well-characterized samples.

2. Background

2.1 The Dawn Mission

The HED-Vesta connection is one of the primary reasons that Vesta was chosen as one of the targets for the Dawn mission, which launched in September 2007. The instrumentation onboard was designed primarily to provide information about its surface morphology, and composition, with one of the science goals being to provide a geologic context for the HEDs (Russell et al., 2004). However, more importantly Dawn aims to provide us with a better understanding of the processes that occurred to form a large, differentiated asteroid. Mineralogic information will be derived primarily from the VIR spectrometer, which has ranges both in the visible (0.25-1.0 μm) and infrared (0.95-5.0 μm) wavelengths and a spatial resolution of 0.25 mrad, with spectral resolution ($\lambda/\Delta\lambda$) between 30 and 170 (Russell et al., 2006). The baseline mission at Vesta includes three orbits at varying planetocentric radii (2700km, 950km, and 460km), with orbit 2 representing the best opportunity for collecting high spatial resolution data with the VIR, at a spatial sampling of 170m. Nearly global coverage is expected (Russell et al., 2006).

2.2 Eucrite Spectra

The eucrites are basalts and gabbros comprised primarily of plagioclase and pyroxenes. Some kinds of plagioclase have a weak absorption feature that occurs within the visible and near-infrared (VIS-NIR) range. This feature, lying between 1.1 and 1.3 μm, has been attributed to minor amounts of Fe^{2+} incorporated into the crystal structure of plagioclase (Adams and Goullaud, 1978). This feature has been used to infer the presence of plagioclase in spectra from Vesta (McCord et al., 1970), along with other

basaltic asteroids (Hardersen et al., 2004). However, as discussed below, this spectral region is also the location of a weak pyroxene absorption band (Sunshine and Pieters, 1993), causing ambiguity in the interpretation of the spectra at ~1.2 μm.

Pyroxene spectra are much more readily interpretable. The pyroxenes produce VIS-NIR spectra with distinctive absorption features near 1 and 2 μm (Adams, 1974; Burns, 1993). The positions of the absorption bands are directly proportional to the cations in the octahedral sites, primarily Ca^{2+}, Mg^{2+}, and Fe^{2+}, although other lesser cations such as Ti^{4+}, Cr^{3+} and Al^{3+} may also have an effect (Adams, 1974; Burns, 1993). Both 1 and 2-μm bands shift to longer wavelengths with an increase in calcium content (Adams, 1974; Burns, 1993; Cloutis and Gaffey, 1991). The presence of trivalent phases such as Fe^{3+}, $Al^{3+}$and, Ti^{3+} is believed to result in a band shift to much longer wavelengths compared to bands of other calcic pyroxenes of a similar iron content (Adams, 1974). Fe^{2+} in the M2 site with its greater asymmetry has a much stronger 1-μm feature, and is also solely responsible for the 2-μm feature (Burns 1993). In the low-calcium pyroxenes (LCP) Fe^{2+} occurs principally in the M2 site, whereas in the more high-calcium pyroxenes (HCP) Ca^{2+} preferentially fills the M2, resulting in Fe^{2+} being concentrated in the M1 (Burns, 1993). Fe^{2+} in the M1 site causes a weak absorption in the 1-μm region due to the symmetry in the M1 octahedral site (more symmetry leads to a weaker absorption feature) and a second feature centered at 1.2 μm (Burns 1993).

The other phases that may influence the reflectance spectra of eucrites are the opaque minerals (primarily ilmenite and chromite, with lesser amounts of native iron-nickel metal and troilite). The low albedos of some meteorite spectra are associated with the presence of opaque minerals (Johnson and Fanale, 1973), as they are often dark and

spectrally featureless (Cloutis et al, 1990). The presence of opaque minerals can suppress the absorption bands from the major Fe^{2+} silicates (Miyamoto et al., 1981). This effect will vary depending on the composition of the opaque minerals present, their overall modal abundance, and grain size.

3. Methodology

3.1 Assessing the Degree of Terrestrial Weathering

For this spectral study each of the original 29 unbrecciated eucrite thin-sections studied by Mayne et al. (2008 – Part II of this dissertation) were examined to determine the degree of terrestrial weathering. Some lesser-studied Antarctic eucrites were also examined in hand sample. Weathered samples have terrestrial-contaminated spectra, which typically show a change in spectral slope (e.g. Salisbury and Hunt 1974; Gooding 1981) caused by weathering products, such as rust formed around the opaque minerals. Therefore, all samples found to contain evidence of terrestrial weathering were not considered for spectral work. The remaining unweathered, unbrecciated eucrites were then narrowed to 10 samples believed to best represent the unbrecciated eucrite suite (Table 1). GRA 98098, although somewhat weathered, was chosen as the eleventh sample for spectral analysis because it is texturally unique. It contains elongate silica grains that overgrow or enclose the grains around them. In hand sample these can be seen as white veins (Mittlefehldt and Lee, 2001) and in one of the thin-sections examined a single grain crosscuts the whole section (Mayne et al., 2008 – Part II of this

dissertation). Although other unbrecciated eucrites contain similar tabular grains of silica, to our knowledge, none have any on this scale.

3.2 Pyroxene Characterization

Chemical analyses of pyroxene were made using the Cameca SX-50 electron microprobe at the University of Tennessee. Analytical conditions were: 15 kV, 30 nA, and 1-μm beam size. All ternary compositional diagrams in this paper were plotted using the freeware program Δplot (John, 2004).

SEM mineral maps have been compiled for all the eucrites in this study (Mayne et al., 2008 – Part II of this dissertation); however, these maps did not allow determination of the low-calcium pyroxene to high calcium pyroxene ratio (LCP:HCP). The eucrites contain HCP (augite) most commonly as an exsolving phase, but also as individual grains. In many of the unbrecciated eucrites in this study the exsolution occurred on a very-fine scale and resolving this requires high-resolution SEM mapping, which is time-intensive and, for the petrologic study, was not deemed necessary for all 29 samples. However, the LCP:HCP ratio is one of the petrologic factors that we can estimate spectrally. Therefore, high-resolution elemental X-ray maps were collected for all eleven sections using the JOEL (Japan Electron Optics Laboratory) JSM-840 scanning electron microscope (SEM) in the Mineral Sciences Department of the Smithsonian Institution. If the actual proportions of LCP and HCP within the eucrites are known then they can be used to test the accuracy with which spectra can predict the mineralogy of a sample. To this end, the elemental X-ray maps of Ca, Si, and Al were combined to distinguish LCP and HCP and the relative proportions of each calculated

3.3 Mössbauer Spectroscopy

Mössbauer spectra were collected for three of the eleven samples; BTN 00300, MAC 02522, and EET 87520. BTN 00300 and MAC 02522 were chosen because of unique spectral or mineralogical characteristics; BTN 00300 was the most complex spectrum to model, as discussed below, and MAC 02522 is the only eucrite in this study with one-pyroxene. EET 87520 was included as a control because its spectrum was modeled well and it contains two-pyroxenes, similar in composition to the majority of the unbrecciated eucrites. Mössbauer spectroscopy was used to investigate if any differences in their spectra were due to differing site occupancies in pyroxene.

Sample mounts were prepared by gently crushing 20-26 mg of whole-rock sample under acetone, then mixing with a sugar-acetone solution designed to form sugar coatings around each grain and prevent preferred orientation (Dyar and Burns, 1986). Because there is so much more iron in the pyroxene than in the feldspar, it was not necessary to handpick mineral separates for the Mössbauer study. Grains were gently heaped in a sample holder confined by Kapton tape. Mössbauer spectra were acquired using the method outlined in Dyar et al. (2007).

Run times were 12-24 hours for each spectrum, and baseline counts were 2.7-5.5 million after the Compton correction, as needed to obtain reasonable counting statistics on these very low Fe samples. Data were collected in 2048 channels and corrected for nonlinearity via interpolation to a linear velocity scale, which is defined by the spectrum of the 25 μm Fe foil used for calibration. Data were then folded before fitting, using a procedure that folds the spectrum about the channel value that produces the minimum least squares sum difference between the first half of the spectrum and the reflected

second half of the spectrum. Spectra were processed using the MEX_FielDD program (as developed at the University of. Ghent by E. DeGrave and T. Van Alboom), which uses Lorentzian line shapes and solves full Hamiltonians for isomer shift and quadrupole splitting distributions in each of two valence states. Isomer shifts (IS), and quadrupole splittings (QS) of the doublets were allowed to vary, and widths of all four peaks were coupled to vary in unison.

3.4 Visible and Near-Infrared Data and Modeling

Chips off eight of the eleven unbrecciated eucrites were ground to a <45-μm dry powder and VIS-NIR (0.32 – 2.55 μm) spectra were collected using the Bi-directional Reflectance Spectrometer at the NASA/Keck Reflectance Experiment Laboratory (RELAB) at Brown University (Pieters, 1993; Pieters and Hiroi, 2004). All samples were measured with an incidence angle of 30º and an emission angle of 0º over the wavelength range 0.32-2.55 μm at 5-nm intervals. The remaining three eucrite samples (Moore County, Ibitira, and Serra de Magé) were available for download from the RELAB database and were measured from <25-μm powders over the wavelength range 0.3-2.6 μm. All raw data were ratioed with a calibrated halon reference standard spectrum to produce reflectance values.

A straight-line continuum was removed from both the 1 and 2-μm bands by the following method. The beginning and ending wavelengths of the regions containing continuum like endpoints were defined, a second order polynomial was then fit across, and tangent point locations defined for the continuum. The band centers were determined from the continuum-removed spectrum by selecting the relevant fraction from the bottom of the band to be fit by the second order polynomial, noisier data requires a larger

fraction for a good fit. The resulting band centers, which are the wavelength position of the point of lowest reflectance (Cloutis and Gaffey, 1991), shall be referred to as 'continuum-removed band centers' throughout the rest of this paper. The band area ratio (BAR), the ratio of the area of band 2 (2 -μm region) to band 1 (1-μm region), was also calculated using the straight-line continuum defined by the method outlined above. BARs are commonly used to estimate the relative abundance of olivine and LCP in a sample (e.g. Cloutis et al., 1986; Gastineau-Lyons et al., 2002; Burbine et al., 2003). However, in this study we are examining the effect of the abundance of plagioclase on the BAR. If the 1.2-μm feature is a result of plagioclase then we might expect the area of band 1 to increase relative to band 2 with increasing plagioclase content. The VIS-NIR spectral data used here extend to only 2.55 or 2.6 μm and, it is therefore possible that the full extent of the 2μm band was not measured, i.e. that the continuum-line was not tangent at the end of the spectrum; however, the same end point of 2.55 μm was used for each spectrum in the BAR calculation.

The collected spectra were also analyzed using the Modified Gaussian Model, hereafter referred to as MGM (Sunshine et al. 1990; Sunshine and Pieters 1993). MGM models each spectrum as a continuum and a series of modified Gaussian distribution curves, with each distribution curve representing a specific absorption band characterized by three parameters: band strength, band center, and band width (Sunshine et al. 1990). This approach has been shown to successfully resolve the absorptions of overlapping bands (Mustard, 1992; Sunshine and Pieters, 1993; Sunshine et al., 1993; Schade and Wäsch, 1999a; Kanner et al., 2007; Klima et al, 2007). Therefore, MGM offers a useful approach for modeling the spectra of the eucrites, which are dominated by overlapping

absorptions due to the presence of both LCP and HCP bands in both the 1 and 2-μm regions. The separate LCP and HCP band centers from MGM are referred to here as 'MGM-derived band centers'.

Two sets of mixtures were produced containing LCP, HCP, and plagioclase, with one set having an LCP:HCP ratio of 50:50, and the other 85:15. For each of the two sets a sequence of mixtures was prepared with different proportions of plagioclase, ranging from 10 to 50% for 85:15 and from 10 to 60% for 50:50, increasing in increments of 10%. The standards used within the mixtures were Johnstown hypersthene from the Johnstown meteorite and the terrestrial Kakanui augite and Lake County plagioclase (Table 2) (Jarosewich et al., 1979). These samples were chosen as they are part of the Smithsonian Microprobe Standard Reference Collection and have been chemically well characterized and are in common use as mineralogical standards. The eucrites are predominantly LCP, HCP, and plagioclase mixtures and, therefore, the mixtures used here lend themselves well to comparisons with eucrite spectra.

All the standards were all ground to <45-μm powders and the sieve used was sonicated for ten minutes in between standards to ensure there was no cross contamination. Spectra were collected of both the mixtures and the individual standards that compose them using the same method as described for the eucrites. BARs, continuum-removed and MGM- derived band centers were also collected as described above.

4. Results

4.1 Pyroxene Chemistry and Modal Mineralogy

The pyroxenes in the eleven eucrites are plotted according to their quadrilateral compositions and their minor elements (Figure 1). A full discussion of pyroxene compositional differences within the unbrecciated eucrites can be found in Mayne et al. (2008 – Part II of this dissertation).

The modal mineralogy for all eleven unbrecciated eucrites calculated from a combination of previously reported SEM mineral maps and the high-resolution pyroxene mapping is given in Table 1. Examples of mapped tiles showing LCP and HCP are given in Figure 2. The LCP:HCP ratios for Chervony Kut, Moore County, and Serra de Magé were found to be in close agreement with those collected by Delaney and Prinz (1984) using electron microprobe analyses. These three samples are the coarsest grained eucrites in this study. Comparison of our modal data with that collected previously confirms the validity of the SEM map method, not only for the three samples for which they overlap, but also for those with fine-grained exsolution.

The percentage of HCP varies from grain to grain (Figure 2a). This variation is taken into account in the mode by averaging over the entire area collected. This process was not applied to MAC 02522 as it contains pyroxene of a relatively homogeneous composition. As mentioned above the unbrecciated eucrites contain HCP as both an exsolved phase within LCP and as individual grains (Figure 2b). Different exsolution morphologies are also present within and between individual meteorites as some contain HCP blebs, and others more elongate lamellae (Figure 2c). There is a wide range in the modal abundances of LCP and HCP; HCP varies from 5.4-29.0%. Overall the cumulate

eucrite Serra de Magé has the lowest percentage of HCP and this percentage did not vary greatly from grain to grain within the thin-section. ALH A81001 is the only unbrecciated eucrite studied that contains phenocrysts, they have a LCP composition (Wo_{1-2}) compared to the pyroxene in the rest of the sample ($Wo_{>20}$) (Mayne et al. 2008 – Part II of this dissertation). This meteorite has a low modal percentage of HCP (11%).

4.2 Mössbauer Spectroscopy

All three Mössbauer spectra are dominated by Fe^{2+} in pyroxene, with very small doublets assigned to Fe^{3+} in pyroxene and Fe^{2+} in ilmenite (Table 3, Figure 3). Errors on isomer shifts and quadrupole splitting are estimated at ±0.04 mm/s for all four doublets. Errors on $^{M1}Fe^{2+}$ and $^{M2}Fe^{2+}$ pyroxene peak areas based on repeated fits using different constraints and fitting models are ±0.3% absolute for these well-resolved spectra. These are the same errors reported in pyroxene studies by Skogby et al. (1992) and Dyar et al. (2007). However, the areas of the smaller components relative to the total area are accurate only to within ±1-3% absolute. Thus, they occur just at the resolution limit of this technique. It is possible that the small amount of Fe^{3+} detected in all three samples could be attributed to small amounts of peak asymmetry. This seems likely as Fe^{3+} is not present in the HED meteorites (Jarosewich, 1990) and these samples were chosen because they did not show signs of terrestrial weathering.

The final Mössbauer peak areas were corrected to account for thickness and differential recoil-free fractions (*f*) of $^{[M1]}Fe^{2+}$ and $^{[M2]}Fe^{2+}$ using the formulation of Bancroft (1969), as outlined in Dyar et al. (2007). Values for the recoil-free fraction (*f*) are specific to mineral groups (and perhaps, species) and must be experimentally determined. For this study, we chose to use a value of $C = 1.068$ (see Dyar et al., 2007

for explanation). As is apparent in Table 3, the corrections for thickness and differential recoil-free fraction resulted in a small change in the areas of the M1 and M2 doublets for Fe^{2+}. The areas of the paired peaks in each doublet are proportional to the abundance of Fe in the site (e.g. Dyar, 2007). All three samples show approximately the same M1:M2 area ratio suggesting that they have very similar site occupancies. This would suggest that any differences in the spectra cannot be accounted for using site occupancy differences.

4.3 Pyroxene-Plagioclase Mixtures

Individual spectra of the pyroxene and plagioclase standards used to construct the mixtures were collected (Figure 4a). The Lake County plagioclase spectrum shows a broad absorption feature between 1.2 to 1.3 μm, which is not found in all plagioclases. Pieters et al. (2005) measured VIS-NIR spectra of mineral separates from cumulate eucrite Y-980318 and observed no absorption feature at 1.2 μm in the plagioclase. The 1.2-μm feature in pyroxene spectra, as discussed above, is a result of Fe^{2+} in the M1 site and whilst it is only visually apparent in the Kakanui augite spectrum it is also a contributor to the overall Johnstown hypersthene spectrum. As expected the Kakanui augite (HCP) has band centers at significantly longer wavelengths than the Johnstown hypersthene (LCP), due to the greater Ca content within its structure.

The spectra of the mixtures are dominated by the two pyroxenes and to the naked eye there is no discernable feature around 1.2 μm (Figures 4b and c). Both sets of mixture spectra show no significant shift in continuum-removed band centers with the addition of extra plagioclase (Table 4). The overall reflectance of the spectra increases with increasing plagioclase content, and overall the 85:15 mixtures have higher

reflectance than the 50:50. The BAR decreases with increasing plagioclase content for both sets of mixture (Table 4a), although, as discussed below, this cannot be used as a calibration tool to determine the amount of plagioclase present in a sample.

The pyroxene-plagioclase mixtures were all subject to modeling using MGM (Figure 5). Each spectrum required a two-pyroxene model and in each case the weak 1-μm M1 band could be distinguished from the M2 band in this region. Because the 1-μm M1 band is often masked by the large 1-μm M2 band it commonly does not require a separate band in MGM. A previous study of martian meteorites showed that HCP from Nakhla also required this additional band (Sunshine et al., 2004). However, none of the spectra required an additional band in the 1.2-μm region to account for the presence of plagioclase. LCP:HCP ratios (the ratio of the relative strength of the LCP band to the relative strength of the HCP band for either the 1 or 2-μm region) calculated using the MGM models matched those of the samples within ~6% (Table 4b). The MGM-derived band centers for the separate LCP and HCP bands remain constant with increasing plagioclase content, as do the relative strengths of the two bands (LCP/HCP at 1 and 2 μm)(Table 4a). The band widths for all the bands in the MGM model used for the mixtures also do not change with plagioclase content.

4.4 Modeling of the Unbrecciated Eucrites

As with the mixtures, initial modeling of all eleven spectra revealed that none of the eucrite spectra required an additional band for plagioclase (Figure 6). Six of the unbrecciated eucrites were fit well using a two-pyroxene, nine-band model (Table 5). Both BTN 00300 and Chervony Kut required the addition of the M1 band in the 1-μm region for a good fit, as with the pyroxene mixtures. These two samples have the lowest

LCP:HCP ratio (Table 1), i.e. the greatest modal abundance of HCP relative to LCP, and it is most likely that it is the high-Ca content of the pyroxenes which results in the M1 1 -µm band being required in the model for these samples. Ca^{2+} preferentially fills the M2 site, pushing Fe^{2+} into the M1 (Burns, 1993), resulting in a stronger M1 band in the 1-µm region. Increased Ca-content pyroxene also pushes the band 1 and band 2 centers to at longer wavelengths (Adams, 1974; Cloutis and Gaffey, 1991), which may act to further distinguish the M1 band. MGM-derived band centers and relative strengths for the unbrecciated eucrites are given in Table 5a. The separate MGM-derived LCP and HCP band centers are compared to the continuum-removed band centers for pyroxenes in Figure 7a.

MAC 02522, the only sample containing zoned pyroxene, was one of two samples that did not require a model with bands for two-pyroxenes. This sample was fit well by one HCP, with a broad band in the 2-µm region (0.7 µm compared to <0.6µm for all other samples)(Table 6). A separate 1-µm M1 band was again needed. The ALH A81001 spectrum was modeled well using a one-pyroxene, seven-band model (Figure 6). ALH A81001 actually contains two pyroxenes, despite being modeled well by only one. It is possible that the chip chosen did not contain one of the LCP phenocrysts observed in thin-section.

Chervony Kut, GRA 98098, Moore County, and Serra De Magé all show a non-random residual error in the 1-µm region of the MGM model. The peak error occurs at the same point as the MGM-derived band center. This is possibly indicative of band saturation and not missing absorption bands, which tend to be offset and much larger (Sunshine and Pieters, 1993). However, we are only examining major absorption

features here and it is possible that the addition of extra bands, such as those that represent spin forbidden pyroxene features, may also improve upon this error.

BTN 00300 was the most complicated eucrite spectrum to model. The best MGM fit required the LCP bands to be weaker than that of the HCP in the 1 and 2-μm region. It is the only eucrite measured for which this is the case, it is also the only one that had a negative slope between the peaks either side of the 1-μm absorption. The MGM-derived LCP band center in the 2-μm region is at much shorter wavelengths than the other eucrites, causing BTN 00300 to plot above the curve in Figures 7a and b. The mössbauer spectroscopy results suggest that these differences cannot be attributed to differences in the site occupancies of the pyroxenes.

5. Discussion

5.1 Grain-size effects

Grain size is known to affect the VIS-NIR spectrum of a sample (e.g. Adams and Felice 1967); however it does not appear to be an important factor in the spectra of the unbrecciated eucrites. For example, the spectra of Ibitira and EET 87520 (Figure 8) are very similar and yet Ibitira is a fine-grained (≤0.3mm) granoblastic sample, and EET 87520 a coarse-grained (≤1mm) partial cumulate. The main difference between the two spectra, their band positions, can be attributed to their differing pyroxene compositions and the fact that the spectra here are also collected from <45-μm powders, which negates much of the difference in grain-size between samples. Therefore, the effect of grain size appears to be negligible.

5.2 The Role of Plagioclase

The effect of pyroxene on spectra is well understood and has been investigated by many authors (e.g. Burns 1993; Adams 1974; Klima 2006); however, the spectral effect of plagioclase in a plagioclase-pyroxene mixture such as the eucrites is poorly understood. It is thought by some to have little or no effect on the spectra (e.g. Sunshine et al 1993), but others have attributed the 1.2-µm feature seen in the spectra of plagioclase-pyroxene mixtures to Fe^{2+} in plagioclase (e.g. Gaffey, 1976; McFadden and Gaffey, 1978; Hardersen et al., 2004). Not all plagioclases contain iron and this feature is absent in the spectra of such samples.

Gaffey (1976) noted that the 1.2-µm absorption was seen most strongly in the spectra of eucrites, which have the highest modal abundance of plagioclase, that it was weaker in the spectra of howardites, corresponding to a lesser amount of plagioclase, and absent in the spectra of diogenites, which lack plagioclase altogether. Although all these observations are true, it is important to also consider mineral chemistries. Mayne et al. (2008 – Part II of this dissertation) showed that the plagioclase in cumulate eucrites generally has lower iron content than the plagioclase in basaltic eucrites. An exception is MAC 02522, a basaltic eucrite with plagioclase iron content equivalent to the cumulates, and yet it still exhibits the 1.2-µm feature in its spectrum. The unbrecciated cumulate and basaltic eucrites have a very similar relative abundances of pyroxene and plagioclase, but the 1.2-µm feature is seen in all the basaltic eucrite spectra but not in the cumulates. Therefore, the mineralogical evidence suggests that the 1.2-µm absorption feature is not caused by plagioclase in the HED meteorites.

The synthetic pyroxene-plagioclase mixtures contain two phases (augite and plagioclase) with observable features at ~1.2 μm (Figure 4a); however, no 1.2-μm feature can be discerned visually in any of the mixture spectra (Figure 4b and c). Therefore, even when the individual plagioclase spectrum has an observable feature, in a mixture with pyroxene it is masked by the dominant pyroxene absorptions. Both the 85:15 and the 50:50 mixtures with 50% plagioclase are good approximations to the mineralogy of the eucrites, which have a varying LCP:HCP ratio (Table 1) and roughly equal amounts of plagioclase and pyroxene.

The strength of the 1.2-μm band feature, normalized to the strength of the 2-μm HCP band, as derived from MGM is plotted for both the eucrites and the mixtures in Figures 9a and b against plagioclase content. The relative strength of the 1.2-μm band actually decreases with increasing plagioclase content. If the presence of plagioclase was the cause of the 1.2-μm band then the strength of this band would be expected to increase with plagioclase content and not decrease. Eucrite plagioclase is not even thought to have a 1.2-μm feature, as discussed earlier. The mixtures (in Figure 9b) show no change in the relative strength of the 1.2-μm band with plagioclase content, further suggesting that this absorption feature is unrelated to plagioclase.

Even though the 1.2-μm absorption cannot be attributed to plagioclase, we considered the possibility that information about its abundance might still be extracted from the overall spectrum using calibration curves created from the mixtures. The BAR decreases linearly with increasing plagioclase content for the mixtures (Figure 9c); however, it cannot be used as a calibration tool for several reasons. Firstly, the lines defined by increasing plagioclase content differ for the 85:15 and 50:50 mixtures;

therefore, to use these as a calibration tool for the amount of plagioclase the LCP:HCP ratio would have to be known. If we then plot the BAR values for unbrecciated eucrites with a similar LCP:HCP ratio to that of the 50:50 mixtures we can see that they span a wide-range of values. MET 01081 appears to lie close to the line defined by the 50:50 mixtures; however, PCA 91078 and GRA 98098 do not plot close to it. This suggests that the eucrites, despite having relatively similar modal abundances of plagioclase and pyroxene, contain mineral compositions that differ enough from the mixtures to make their BAR values far more difficult to predict.

The inability to produce useful calibration curves for plagioclase abundance for a range of LCP:HCP, suggests that in the VIS-NIR range the presence of plagioclase cannot be detected on the surface of Vesta, much less an estimate of its proportion relative to pyroxene. However, the Dawn VIR spectrometer will be capable of taking measurements into the mid-IR (to 5 μm) (Russell et al., 2006). Plagioclase is known to have absorption features in the mid IR and one at ~4.4 μm (Salisbury et al., 1992), may permit its identification on the surface of Vesta (C.M. Pieters, Pers. Comm.).

5.3 Spectral Classes and Features

We have grouped the collected spectra according to shared characteristics. These groups are compared with the petrologic data to assess what mineralogic aspects control spectral features. The four main features studied here are:

1. Relative positions of bands 1 and 2.
2. Presence or absence of a 600 nm absorption feature.
3. Strength of the 1.2-μm absorption band
4. Relative spectral contrast.

5.3.1 Relative Positions of Bands 1 and 2

AS discussed earlier, shifts in band positions in the 1 and 2-μm regions within eucrite spectra (Figure 10), reflect different pyroxene compositions (e.g. Adams, 1974; Cloutis and Gaffey, 1991; Burns, 1993). Continuum-removed band positions lie between 0.93 and 0.97 μm in the 1-μm region and 1.97 to 2.13 μm in the 2-μm, with Serra de Magé lying at the shortest wavelengths and MAC 02522 at the longest (Figure 7a). The majority of the unbrecciated eucrites are clustered at the shorter end of the wavelength range with MAC 02522 offset from the rest. Separate band centers for LCP and HCP were resolved using MGM and, as expected, lie on either side of the continuum-removed band centers. MAC 02522 and ALH A81001 were best fit using one-pyroxene models and, as such, do not have separate HCP and LCP bands. The MGM-derived band centers for both ALH A81001 spectra lie close to their continuum-removed band centers; whereas, MAC 02522 has MGM-derived band centers at slightly longer wavelengths than the continuum-removed ones. BTN 00300 plots separately from the majority of the basaltic eucrites in terms of its LCP band centers, due to its short wavelength LCP band in the 2-μm region.

The basaltic (non-cumulate) eucrites all have relatively similar continuum-removed band 1 and band 2 centers and the cumulate eucrites lie at the shortest wavelengths of all (Figure 7b); however, the transition from basaltic to cumulate is not distinct. The shorter wavelengths for cumulate eucrites can be attributed to both their more Mg-rich compositions and their lower modal HCP component, with the latter being the most important. Another factor which illustrates that the calcium content, or rather the LCP:HCP ratio, is the principle spectral variable is that of the MGM-derived LCP and

HCP band centers, which plot with those of the rest of the basaltic unbrecciated eucrites. The LCP and HCP compositions in the cumulate eucrites have similar calcium contents to the basaltic eucrites, with variation occurring in the En and Fs components.

MAC 02522 contains continuum-removed band centers at much longer wavelengths than those in the other ten samples (Figure 7b). This eucrite contains one, relatively homogeneous pigeonite. It is the only unbrecciated eucrite in this study that is not equilibrated with respect to the quadrilateral elements of pyroxene (Fe, Mg, and Ca), although some Fe-Mg diffusion has reduced its original compositional zoning. This sample has the highest average iron content in its pyroxenes (Figure 1), resulting in the longer wavelength for the continuum-removed band centers. It was fit well in MGM using one HCP; however, this spectrum requires a fit with extremely wide absorption bands. Anomalously wide bands are a characteristic of continuous zoning and rapid cooling (Sunshine and Pieters, 1993). Both its MGM-derived and continuum-removed band centers plot intermediate between the separate modeled LCP and HCP (Figure 7a) of the other eucrites, reflecting its overall pyroxene composition which has a calcium content that lies between the exsolved HCP and LCP of the other eucrites on the quadrilateral (Figure 1).

5.3.2 Presence or Absence of an Observable 600-nm (0.6-µm) Absorption Feature

The PCA 91078, Chervony Kut and ALH A81001 spectra contain a feature at around 600 nm, which, although present in all the spectra, is not observable in the other unbrecciated eucrites (Figure 6, Figure 11a). Cr^{3+} in octahedral coordination in the pyroxene M1 site is known to have absorption features in this region (Rossman, 1980; Burns, 1993; Cloutis, 2002). A study by Cloutis (2002) concluded that for this

absorption to appear LCP required less Cr^{3+} to be present (0.38 wt%) when compared to HCP (0.9 wt%), although the resulting absorption is much weaker in the LCP. To investigate whether this feature is consistent with Cr^{3+} in the pyroxene of the unbrecciated eucrites the chromium contents of all the pyroxene analyses were compared to calcium contents (Figure 11b). Only PCA 91078, Chervony Kut, and ALH A81001, the three samples exhibiting the observable 600 nm absorption, contain some pyroxene analyses with chromium contents over 0.02 afu (atomic formula units), which corresponds to approximately 0.65 wt %. The 'Cr-threshold value', e.g. the chromium content at which the absorption appears in the spectrum (0.02 afu or 0.65 wt%), lies between the two values reported by Cloutis (2002) because the unbrecciated eucrites contain a mixture of both HCP and LCP.

The chromium contents of pyroxene may provide information on the magmatic evolution of specific eucrites. In the eucrite basaltic melt chromium would have behaved as a compatible element as it has a strong affinity for pyroxene. Therefore, as crystallization of pyroxene proceeded the amount of chromium available in the melt decreased. This means that early-crystallized eucrites have more Cr-rich pyroxenes when compared to more fractionated eucrites. ALH A81001 supports this interpretation, as it not only contains Cr-rich pyroxenes, but also is the most Mg-rich member of the Stannern trend (a geochemical grouping used to sub-divide the eucrites), and, as such, is considered to be the most primitive (Mittlefehldt, Pers. Comm.). This indicates that PCA 91078 and Chervony Kut also crystallized from a primitive magma. Therefore, the presence or absence of an observable ~600 nm absorption can be used as a proxy for the relative magmatic evolution of the unbrecciated eucrites.

However, as was already noted above, the degree of equilibration of the unbrecciated eucrites in terms of the minor elements in pyroxene (Al, Ti, and Cr) varies. The samples that show the Cr-feature are also those that are unequilibrated with respect to these elements (Figure 1). Equilibration redistributes the elements throughout the pyroxene and, in so doing, erases the original crystallization trend, and, with it, the areas that originally had Cr-rich compositions. In the insets in Figure 1, those eucrites that are equilibrated show compositions closest to the Al corner and clumped in the center between Ti and Cr. Therefore, the presence of an observable 600 nm feature reveals not only that the eucrite crystallized from a primitive magma but also that it is not equilibrated with respect to its minor elements, and, therefore, underwent relatively fast-cooling without later metamorphism. This initially seems counter-intuitive as it would suggest that these primitive meteorites were among the last to form on Vesta, not the first, since they have not been subject to the high-degree of metamorphism that is common in the eucrites as a whole. This suggests that these samples may have formed from partial melts, late in the formation history of the basaltic crust, which would allow them to have mineral chemistries reflecting relatively primitive magmas, and yet not undergo the widespread metamorphism suggested for the surface of Vesta (e.g. Takeda and Graham, 1991; Yamaguchi et al., 1996.

5.3.3 Strength of 1.2-µm Band

Many of the unbrecciated eucrite spectra show an absorption band at around 1.2 µm. This feature was discussed above in regards to the plagioclase and any link between it and the amount of plagioclase was not proven. Fe^{2+} in the M1 site of pyroxenes is also known to cause a weak absorption at around 1.2 µm (Burns 1993). The pyroxenes in

basaltic eucrites have higher-Fe contents and a larger modal percentage of HCP than the cumulate eucrites. The basaltic eucrites are also the samples that contain a visually obvious 1.2-µm absorption, whereas the cumulate eucrites, with their more Mg-rich compositions and lower modal HCP component, do not (Figure 12).

Klima et al. (2008) have characterized the 1.2-µm band of pyroxene standard and HED spectra and suggest a relationship between its depth and the cooling history of the sample. They define the M1 intensity ratio, which is calculated by dividing the strength of the 1.2-µm band by that of the combined strengths of the 1.2-µm and 2-µm bands. It was found that those samples that underwent slow cooling (the cumulate eucrites and diogenites) had a much lower M1 intensity ratio than those that cooled faster (the basaltic eucrites). This feature, therefore, serves as a tool for distinguishing basaltic eucrites from cumulates. However, all their HED spectra were modeled with a one-pyroxene fit (Klima et al., 2008) and so the results of this study cannot be compared to their work.

5.3.4 Relative Spectral Contrast

The unbrecciated eucrite spectra show a wide range in spectral contrast. MET 01081 and BTN 00300 show a much lower absolute reflectance relative to the other samples, as illustrated in Figure 13. ALH A81001 shows muted bands and overall reduced contrast relative to the other eucrites but does not have the same overall low value of normalized reflectance. MET 01081 and BTN 00300 have among the highest modal opaque mineral contents (chromite, ilmenite, troilite, and Fe-Ni metal) of the eleven unbrecciated eucrites. These minerals probably darken the spectra of these rocks (Cloutis et al, 1990). GRA 980998 actually has the highest modal content of opaque minerals (8.2%), however, unlike MET 01081 and BTN 00300, no Fe-metal or troilite

was observed in this sample, suggesting that it is these phases, and not chromite and ilmenite, that result in the reduced spectral contrast.

As mentioned previously, the spectral contrast of ALH A81001 is also distinct from the rest of the samples but it has no modally significant opaque mineral content. Instead, this eucrite is extremely fine-grained and contains ilmenite grains a few micrometers in size, distributed ubiquitously throughout. The widespread distribution of the ilmenite in this eucrite most likely accounts for the reduced contrast, rather than the amount present. Therefore, a reduced spectral contrast can be related to high modal content of metals and sulfides or widely distributed very fine-grained ilmenite.

5.4 Predicting Mineralogies

MGM has been used in the past as a tool for modeling the relative proportions of LCP and HCP from spectra. Sunshine et al. (1993) used MGM to model the spectra of the dual lithologies within martian meteorite EET A79001 and found that they were able to predict the modal abundance of LCP and HCP within ±5-10% of those obtained from petrographic methods. More recently, Kanner et al. (2007) used MGM to model laboratory data for martian pyroxenes and were also able to estimate the modal abundance of LCP and HCP with ±10%. We have compared the strengths of the modeled LCP and HCP bands in the 1 and 2-μm region in both the mixture and eucrite spectra, and applied the calibration of Sunshine and Pieters (1993). MGM was able to estimate the LCP:HCP ratio in both the 50:50 and 85:15 pyroxene-plagioclase mixtures to well within the 5-10% accuracy range reported by Sunshine et al. (1993)(Table 4b).

The eucrites represent more complex mixtures of LCP-HCP-plagioclase-opaque minerals. Their calculated HCP abundances from MGM are given in Table 4b. The

majority of these abundances are higher than those measured using SEM maps of the actual samples. The LCP:HCP ratios of all of the samples bar one, PCA 91078, are predicted within ±15% of the actual value by both the 1-μm and 2-μm region band strengths. PCA 91078 is relatively coarse grained and it is likely that the thin section used for the measurement of modal abundances was not representative of the sample as a whole, or of the chip used for spectral measurement. Overall MGM gives a relatively good estimate of the relative modal abundances of LCP and HCP in the eucrites, although it has a tendency to over predict the HCP component. However, the original calibration study by Sunshine and Pieters (1993) did not use pyroxenes with iron-rich compositions, as seen in the eucrites. The spectral contrast of the unbrecciated eucrites does appear to give an indication of the opaque mineral content; however, high modal abundance of metal and sulfide versus widespread micrometer-sized ilmenite grains cannot be distinguished.

Pyroxene compositions can be estimated using both MGM fits and continuum-removed band centers. Two-pyroxene basalts can be distinguished from samples with one-pyroxene using the number of bands required in the MGM fit. Eucrites that contain pyroxenes retaining some of their original compositional zonation (e.g. MAC 02522), can be distinguished by the larger band widths required, especially in the 2-μm region. Samples with continuum-removed band centers at shorter wavelengths (cumulate eucrites) have pyroxenes that are Fs-poor in comparison to those at longer wavelengths (basaltic eucrites).

We have demonstrated the presence of plagioclase cannot be determined from the VIS-NIR spectra of pyroxene-plagioclase mixtures, or the eucrites. This means that its

modal abundance cannot be quantified. There is also the possibility, as mentioned above, that a feature at ~4.4 μm in the mid-IR may aid in the identification and quantification of plagioclase (Pieters et al., 2005). Lim et al. (2005) have also measured the thermal infrared (8-13 μm) spectrum of Vesta, which is outside of the range of the Dawn VIR spectrometer but also contains absorptions attributed to plagioclase (e.g. Sprague et al, 1992; Sprague et al, 1997; Milam et al., 2004). They made no mineralogical interpretations of this spectrum; however, preliminary work by Donaldson Hanna and Sprague (2008) using the Ramsey and Christiansen (1998) spectral deconvolution algorithm suggests that plagioclase can be detected on the surface.

5.5 The Surface of Vesta

It is probable that much of Vesta's surface will be covered with regolith, reflected by the abundance of howardites in current collections. The global distribution, and degree of mixing in this regolith will have an effect on what the VIR instrument aboard Dawn can detect on the surface, but it does not mean that valuable petrologic information cannot be extracted. The Moon is known for its abundant regolith, and yet various studies using remote sensed data have been able to not only characterize different terrains on the surface (Jolliff et al., 2000), but also map distinct basaltic units (Staid and Pieters, 2000; Kramer et al., 2008), and even obtain estimates of flow thickness (Heather and Dunkin, 2002). Both Gaffey (1997) and Binzel et al. (1997) were able to detect areas on the surface of Vesta that had spectra akin to the eucrites, and others that were more like the diogenites. This suggests that the surface is not a globally homogenized regolith, but may instead reflect the local lithologies. It is also possible that there will be places on the

surface, such as in the walls of the large southern crater or as surficial flows, where in-situ basaltic units will be found.

5.6 Testing Models for the Petrogenesis of Vesta

The two models originally proposed for the formation of Vesta are those of partial melting (Stolper, 1977) and fractional crystallization (Mason, 1962). However, neither model can completely explain the formation of the HEDs. Partial melting models are unable to explain the eucrite siderophile element abundances (Mittlefehldt and Lindstrom, 2003), whereas fractional crystallization models cannot reproduce all the geochemical groups found within the eucrites (Ruzicka et al., 1997; Mittelfehldt and Lindstrom, 2003). More recently the idea of a magma ocean on Vesta has been proposed (e.g. Ruzicka et al.1997; Righter and Drake, 1997), invoking equilibrium crystallization (Righter and Drake, 1997) and fractional crystallization (Ruzicka et al., 1997). However, in general it appears that no one model proposed thus far is capable of producing the Stannern and main group-Nuevo Laredo trends by a single crystallization process (Mittlefehldt and Lindstrom, 2003). In order to be able to test the models for the formation of Vesta using the instrumentation aboard Dawn, it is necessary to think about how the geologic context of the rocks resulting from each model vary, as opposed to the geochemical links between them.

Mayne et al. (2008 – Part II of this dissertation) stated that the petrology of the eucrites supported the serial magmatism theory put forward by Yamaguchi (1996), which could play a role in any one of the models suggested for Vesta's formation. This would produce a layered crust, with different eucrite lava flows stacking up upon one another. Lithologic variation should be expected, therefore, to be on a smaller scale vertically than

horizontally. The least metamorphosed basaltic eucrites, those preserving the observable 600nm absorption, would be at the surface. The cumulate eucrites are then formed as later intrusions into the basaltic crust and would therefore be seen to crosscut different eucrite layers with depth but be on a smaller lithologic scale horizontally. The cumulates can be identified through their lack of an observable 1.2 μm feature, higher LCP:HCP ratios, and shorter band centers.

Partial melting would, most likely, produce small-scale local units both at the surface and with depth, whereas a magma ocean would be expected to produce more globally homogeneous lithologies with a large lateral extent. For example, in the magma ocean model the diogenites are envisaged to form by crystal accumulation (Ruzicka et al., 1997); therefore, intrusion of diogenite material into the eucritic crust should be limited if this model is correct. The southern crater provides an ideal window into the crust, and possibly the upper mantle, of Vesta (Binzel et al., 1997; Gaffey, 1997). The walls of the crater may allow mapping of in-situ units at depth within Vesta and give a measure of their spatial extent, i.e. can we trace one unit around the whole crater (layered crust, suggestive of a magma ocean) or are there multiple intrusions and lithologies (vertically and laterally heterogeneous, indicating partial melting)?

.

6. Implications for Spectral Interpretation

The primary goal for the Dawn mission is to gain a better understanding of the formation of large asteroidal bodies, and for Vesta this will, most likely, focus on the processes that produced the crust on this large differentiated asteroid. Here we have

examined the relationship between the petrology of the HEDs and their spectra, to establish what petrologic information we may be able glean from Dawn. If in-situ units are found on Vesta on a scale larger than the spatial resolution of the VIR instrument then we can expect to extract information about the mineral chemistries and modal mineralogy of the units; however, this study has shown that we can also use the spectral data to map the processes that formed the crust of Vesta itself. Basaltic eucrites are easily distinguished from their cumulate counterparts, using the continuum-removed band centers and the presence and strength of the 1.2-μm M1 pyroxene band. The 600-nm (0.6-μm) absorption allows identification of early crystallizing eucrites (high Cr) from those that crystallized later in Vesta's differentiation history. The presence of a 600 nm absorption also indicates that the sample was not greatly affected by later metamorphism, which is widespread throughout the eucrites and, therefore, suggested to be a major process in the formation of the basaltic crust. Such information about not only the mineral make-up of units, but also their magmatic history and stratigraphic relationships to one another on the surface of Vesta may enable us to test the models for its petrogenesis.

Acknowledgments: This work was supported by PGG grant NNX06AH69G to JMS and NASA Cosmochemistry grant NNG06GG36G and UCLA subcontract 2090-S-JB694 for Dawn to HYM. All meteorite spectra were collected at Brown University's KECK/NASA Reflectance Experiment Laboratory (RELAB).

References cited

Adams J.B. 1974. Uniqueness of visible and near-infrared diffuse reflectance spectra of pyroxenes and other rock-forming minerals. *Journal of Geophysical Research* 79: 4829-4836.

Adams J.B. 1975. Interpretation of visible and near-infrared diffuse reflectance spectra of pyroxenes and other rock-forming minerals. In: *Infrared and Raman Raman Spectroscopy of Lunar and Terrestrial Materials*. Edited by: C. Karr Jr., Academic, New York. pp. 91-116.

Adams J.B. and Filice A. 1967. Spectral reflectance 0.4 to 2.0 microns of silicate rock powders. *Journal of Geophysical Research* 72:5705-5715.

Adams J.B. and Goullaud L.H. 1978. Plagioclase feldspars: Visible and near infrared diffuse reflectance spectra as applied to remote sensing. *Proceedings Lunar and Planetary Science Conference* 9:2901-2909.

Bancroft G.M. 1969. Quantitative site populations in silicate minerals by the Mössbauer effect. *Chemical Geology* 5:255-58.

Binzel R.P. and Xu S. 1993. Chips off asteroid 4 Vesta: Evidence for the parent body of basaltic achondrite meteorites *Science* 260**:**186-191.

Binzel R.P., Gaffey M.J., Thomas P.T., Zellner B.H., Storrs A.D., and Wells E.N. (1997) Geologic mapping of Vesta from 1994 Hubble Space Telescope images. *Icarus* 128:95-103.

Burbine T.H., Buchanan P.C., Binzel R.P., Bus S.J., Hiroi T., Hinrichs J.L. Meibom A., and McCoy T.J. 2001. Vesta, Vestoids, and the howardite, eucrite, diogenite

group: Relationships and the origin of spectral differences. *Meteoritics and Planetary Science* 36:761-781.

Burbine T.H., McCoy T.J., Jarosewich E., and Sunshine J.M. 2003. Deriving asteroid mineralogies from reflectance spectra: Implications for the MUSES-C target asteroid. *Antarctic Meteorite Research* 16:185-195.

Burns R.G. 1993. *Mineralogical Applications of Crystal Field Theory, 2nd edition*. New York: Cambridge University Press. 551 p.

Clayton R.N. and Mayeda T.K. 1996. Oxygen isotope studies of achondrites. *Geochimica et Cosmochimica Acta* 60:1999-2017.

Cloutis E.A. 2002. Pyroxene reflectance spectra: Minor absorption bands and effects of elemental substitutions. *Journal of Geophysical Research* 107:E6 doi:10.1029/2001/JE001590.

Cloutis E.A. and Gaffey M.J. 1991. Pyroxene spectroscopy revisited: Spectral-compositional correlations and relationship to geothermometry. *Journal of Geophysical Research* 96:22,809-22,826.

Cloutis E.A., Gaffey M.J., Jackowski T.L., and Reed K.L. 1986. Calibration of phase abundance, composition, and particle size distribution for olivine-orthopyroxene mixtures from reflectance spectra. *Journal of Geophysical Research* 91:11641–11653.

Cloutis E.A., Gaffey M.J., Smith D.G.W., and Lambert R.St.J. 1990b. Reflectance spectra of mafic silicate-opaque assemblages with applications to meteorite spectra. *Icarus* 84:315-333.

Delaney J.S., and Prinz M. (1984) The Polymict Eucrites. *Journal of Geophysical Research* 89:C251-C288.

Donaldson Hanna K.L. and Sprague A.L. 2008. Mineralogy of Vesta and howardite, eucrite, and diogenite (HED) meteorites determined by spectral Deconvolution. *Lunar and Planetary Science* XXXIX, Abstract # 1410.

Drake M.J. 2001. The eucrite/Vesta story. *Meteoritics and Planetary Science* 36:501-513.

Dyar M.D. and Burns, R.G. 1986. Mössbauer spectral study of ferruginous one-layer trioctohedral micas. *American Mineralogist* 71:955-965.

Dyar M.D., Klima R.L., Lindsley D., and Pieters C.M. 2007. Effects of differential recoil-free fraction on ordering and site occupancies in Mössbauer spectroscopy of orthopyroxenes. *American Mineralogist* 92:424-428.

Eugster O. and Michel Th. 1995. Common asteroid break up events of eucrite, diogenite, and howardite, and the cosmic ray production rates for noble gases in achondrites. *Geochimica et Cosmochimica Acta* 59:177-199.

Gaffey M.J. 1976. Spectral reflectance characteristics of the meteorite classes. *Journal of Geophysical Research* 81:905-920.

Gaffey M.J. 1993. Mineralogic variations within the S-type asteroid class. *Icarus* 106:573-602.

Gaffey M.J. 1997. Surface lithologic heterogeneity of asteroid 4 Vesta. *Icarus* 127:130-157.

Gastineau-Lyons, H.K., McSween, H.Y. Jr., and Gaffey, M.J. 2002. A critical evaluation of oxidation versus reduction during metamorphism of L and LL group

chondrites, and implications for asteroid spectroscopy. *Meteoritics and Planetary Science* 37:75-89.

Gooding J.L. 1981. Mineralogic changes during terrestrial weathering of Antarctic chondrites. *Proceedings of the 12th Lunar Science Conference* pp. 1105-1122.

Hardersen P.S., Gaffey M.J., and Abell P.A. 2004. Mineralogy of asteroid 1459 Magnya and implications for its origin. *Icarus* 167:170-177.

Hazen R.M., Bell P.M., and Mao H.K. 1978. Effects of compositional variation on absorption spectra of lunar pyroxenes. *Lunar and Planetary Science IX*:483-484.

Heather D.J. and Dunkin S.K. 2002. A stratigraphic study of southern Oceanus Procellarum using Clementine multispectral data. *Planetary and Space Science* 50:1299-1309.

Klima R.L., Pieters C.M. and Dyar M.D. 2007. Spectroscopy of synthetic Mg-Fe pyroxenes I: Spin-allowed and spin-forbidden crystal bands in the visible and near-infrared. *Meteoritics and Planetary Science* 42:235-253.

Jarosewich E., Nelen J., and Norberg J. 1979. Electron microprobe reference samples for mineral analysis. *Smithsonian Institution Contributions to the Earth Sciences* 22:68-72.

Jarosewich E. 1990. Chemical analyses of meteorites: A compilation of stony and iron meteorite analyses. *Meteoritics* 25:323-337.

John C.M. 2004. Plotting and analyzing data trends in ternary diagrams made easy, *EOS* 85:158. (Also available at http://www.agu.org/eos_elec/000562e.shtml).

Johnson T.V., and Fanale F.P. 1973. Optical properties of carbonaceous chondrites and their relationship to asteroids. *Journal of Geophysical Research* 78:8507-8518

Jolliff B.L., Gillis J.J., Haskin L.A., Korotev R.L., and Wieczorek M.A. 2000. Major lunar crustal terranes: Surface expressions and crust-mantle origins. *Journal of Geophysical Research* 105:4197-4216.

Kanner L.C., Mustard J.F., and Gendrin A. 2007. Assessing the limits of the Modified Gaussian Modal for remote spectroscopic studies of pyroxenes on Mars. *Icarus* 187:442-456.

Klima R.L., Pieters C.M., and Dyar M.D. 2008. Characterization of the 1.2-μm M1 pyroxene band: Extracting cooling history from near-IR spectra of pyroxenes and pyroxene-dominated rocks. *Meteoritics and Planetary Science* Submitted.

Klima R.L., Pieters C.M., and Dyar M.D. 2007. Spectroscopy of synthetic Mg-Fe pyroxenes I: Spin-allowed and spin-forbidden crystal field bands in the visible and near-infrared. *Meteoritics and Planetary Science* 42:235-253.

Kramer G.Y., Jolliff B.L., and Neal C.R. 2008. Distinguishing high-alumina basalts using Clementine UVVIS and Lunar Prospector GRS data: Mare Moscoviense and Mare Nectaris. *Journal of Geophysical Research* 113:E01002, doi:10.1029/2006JE002860.

Lim L.F., McConnochie T.H., Bell J.F., and Hayward T.L. 2005. Thermal infrared (8-13 μm) spectra of 29 asteroids: The Cornell Mid-Infrared Asteroid Spectroscopy (MIDAS) Survey. *Icarus* 173:385-408.

Mason B. (1962) Meteorites. J. Wiley and Sons, New York.

Mayne R.G., McSween H.Y., McCoy T.J., and Gale A. 2008. Petrology of the unbrecciated eucrites. *Geochimica et Cosmochimica Acta* Submitted.

McCord, T.B., Adams, J.B., and Johnson, T.V. 1970. Asteroid Vesta: Spectral reflectivity and compositional implications. *Science* 168:1445-1447.

McFadden L.A. and Gaffey M.J. 1978. Calibration of quantitative mineral abundances determined from meteorite reflectance spectra and applications to Solar System objects. *Meteoritics* 13:556-557.

Milam K.A., McSween H.Y., Hamilton V.E., Moersch J.E., and Christensen P.R. 2004. Accuracy of plagioclase compositions from laboratory and Mars spacecraft thermal emission spectra, *Journal of Geophysical Research* 109:E04001, doi:10,1029/2003JE002097.

Mittlefehldt D.W. and Lee M.T. 2001. Petrology and geochemistry of unusual eucrite GRA 98098. *Meteoritics and Planetary Science* 36:A136.

Mittlefehldt D.W. and Lindstrom M.M. 2003. Geochemistry of basaltic eucrites, and Hf and Ta as petrogenetic indicators for altered Antarctic eucrites. *Geochimica et Cosmochimica Acta* 67:1911-1935.

Miyamoto M., Mito A., and Takano Y. 1982. An attempt to reduce the effects of black materials from the spectral reflectance of meteorites and asteroids. *Memoirs National. Institute of Polar Research Special Issue* 20:345-361.

Mustard J.F. 1992. Chemical analysis of actinolite from reflectance spectra. *American Mineralogist* 77:345-358.

Pieters C.M. 1983. Strength of mineral absorption features in the transmitted component of near-infrared reflected light: First results from RELAB. *Journal of Geophysical Research* 88:9534-9544.

Pieters C.M. and Hiroi T. 2004. RELAB (Reflectance Experiment Laboratory): A NASA multi-user spectroscopy facility. *Lunar and Planetary Science* XXXV, Abstract #1720.

Pieters C.M., Binzel R.P., Bogard D., Hiroi T., Mittlefehldt D.W., Nyquist L., Rivkin A., Takeda H. 2005. Asteroid-meteorite links: The Vesta conundrum(s). *Asteroids, Comets, Meteors Proceedings, IAU Symposium* 229:273-288.

Ramsey M.S. and Christensen P.R. 1998. Mineral abundance determination: Quantitative deconvolution of thermal emission spectra. *Journal of Geophysical Research* 103:577-596.

Righter, K. and Drake, M.J. 1997. A magma ocean on Vesta: Core formation and petrogenesis of eucrites and diogenites. *Meteoritics and Planetary Science* 32:929-244.

Rossman G.R. 1980. Pyroxene spectroscopy. In: *Reviews of Mineralogy, Pyroxenes* (eds. C. Prewitt). pp. 93-115

Russell C.T., Coradini A., Christensen U., De Sanctis M.C., Feldman W.C., Jaumann R., Keller H.U., Konopliv A., McCord T.B., McFadden L.A., McSween H.Y., Mottola S., Neukum G., Pieters C.M., Prettyman T.H., Raymond C.A., Smith D.E., Sykes M.V., Williams B., Wise J., Zuber M.T. 2004. Dawn: A journey in space and time. *Planetary Space Science* 52:465-489.

Russell C.T., Capaccioni F., Coradini A., Christensen U., De Sanctis M.C., Feldman W.C., Jaumann R., Keller H.U., Konopliv A., McCord T.B., McFadden L.A., McSween H.Y., Mottola S., Neukum G., Pieters C.M., Prettyman T.H., Raymond C.A., Smith D.E., Sykes M.V., Williams B., and Zuber M.T. (2006) Dawn

discovery mission to Vesta and Ceres: Present status. *Advances in Space Research* 38:2043-2048.

Ruzicka, A., Synder, G.A., and Taylor, L.A. 1997. Vesta as the howardite, eucrite, and diogenite parent body: Implications for the size of a core and for large-scale differentiation. *Meteoritics and Planetary Science* 32:825-840.

Salisbury J.W. and Hunt G.R. 1974. Meteorite spectra and weathering. *Journal of Geophysical Research* 79:4439-4441.

Salisbury J.W., Walter L.S., Vergo N. and D'Aria D.M. 1992. *Infrared (2.1 - 25 um) Spectra of Minerals.* The Johns Hopkins University Press, Baltimore. 267 pp.

Schade U. and Wäsch R. 1999. Near-infrared reflectance spectra from bulk samples of the two SNC meteorites Zagami and Nakhla. *Meteoritics and Planetary Science* 34:417-424.

Skogby H., Annersten H., Domeneghetti M.C., Molin G.M., and Tazzoli V. 1992. Iron distribution in orthopyroxene: A comparison of Mössbauer spectroscopy and X-ray refinement results. *European Journal of Mineralogy* 4:441-452.

Sprague A.L., Witteborn F.C., Kozlowski R.W., Cruikshank D.P., Bartholomew M.J., and Graps A.L. 1992. The Moon: Mid-Infrared (7.5 to 11.4 μm) spectroscopy of selected regions. *Icarus* 100:73-84.

Sprague A.L., Nash D.B., Witeborn F.C., and Cruikshank D.P. 1997. Mercury's feldspar connection mid-IR measurements suggest plagioclase. *Advanced Space Research* 19:1507-1510.

Staid M.I. and Pieters C.M. 2000. Integrated spectral analysis of mare soils and craters; Applications to eastern nearside basalts. *Icarus* 145:122-139.

Stolper E. (1977) Experimental petrology of eucritic meteorites. *Geochimica et Cosmochimica Acta* 41:587-611.

Sunshine J.M. and Pieters C.M. 1993. Estimating modal abundances from the spectra of natural and laboratory pyroxene mixtures using the Modified Gaussian Model. *Journal of Geophysical Research* 98:9075-9087.

Sunshine J.M., Pieters C.M., and Pratt S.F. 1990. Deconvolution of mineral absorption bands: an improved approach. *Journal of Geophysical Research* 95:6955-6966.

Sunshine J.M., McFadden L.A., Pieters C.M. 1993. Reflectance spectra of the Elephant Moraine A79001 meteorite: Implications for remote sensing of planetary bodies. *Icarus* 105:79-91.

Sunshine J.M., Bishop J., Dyar M.D., Hiroi T., Klima R., and Pieters C.M. 2004. Near-infrared spectra of martian pyroxene separates: First results from Mars Spectroscopy Consortium. *Lunar and Planetary Science* XXXV, Abstract # 1636.

Thomas P.C., Binzel R.P., Gaffey M.J., Storrs A.R., Wells E.N., and Zellner B.H. 1997. Impact excavation on asteroid 4 Vesta: Hubble Space Telescope results. *Science* 277:1492-1495.

Yamaguchi A., Taylor G.J., and Keil K. 1996. Global crustal metamorphism of the eucrite parent body. *Icarus* 124:97-112.

Appendix III

Table III-1: Modal mineralogy for the unbrecciated eucrites selected for spectral study.

	Modal Mineralogy					
	Plag	Px	LCP	HCP	Si	OSM
ALH A81001	61.0		28.0	11.0	0.0	0.0
BTN 00300	48.4		18.7	27.0	4.8	1.0
Chervony Kut	45.0		22.5	29.0	1.9	1.5
EET 87520	48.5		28.6	21.2	1.4	0.2
GRA 98098	41.0		25.9	24.3	8.2	0.6
Ibitira	41.4		28.6	24.7	4.4	0.9
MAC 02522	41.1	56.6			1.6	0.7
MET 01081	40.3		25.6	27.4	5.5	1.2
Moore County	43.8		29.6	22.5	3.4	0.7
PCA 91078	45.7		25.4	25.3	2.9	0.8
Serra de Mage	52.7		39.7	5.4	0.7	1.5

Where OSM = oxides, sulfides, and metal, Si = SiO_2, Plag = plagioclase, Px = pyroxene, LCP = low-calcium pyroxene, HCP = high –calcium pyroxene.

Table III-2: Compositional data for end-members used in the pyroxene-plagioclase mixtures.

	Johnstown Hypersthene	**Kakanui Augite**	**Lake Co. Plagioclase**
SiO_2	54.09	50.73	51.25
Al_2O_3	1.23	8.73	30.91
Fe_2O_3		1.08	0.34
FeO	15.22	5.37	0.15
MgO	26.79	16.65	0.14
CaO	1.52	15.82	13.64
Na_2O	<0.05	1.27	3.45
K_2O	<0.05	0.00	0.18
TiO_2	0.16	0.74	0.05
P_2O_5			
MnO	0.49	0.13	0.01
Cr_2O_3	0.75		
H_2O	0.00	0.04	0.05
Total	100.25	100.56	100.17
Wo	3.00	36.01	
En	73.56	52.72	
Fs	23.44	11.27	
An			80.86
Ab			18.51
Or			0.64

The compositional data given here is from Jarosewich et al. (1979).

Table III-3: Mössbauer spectroscopy results.

		BTN 00300	MAC 02522	EET 87520
Fe^{2+} Px M2	d (mm/s)	1.13	1.12	1.13
	D (mm/s)	2	1.94	1.99
	G (mm/s)	0.24	0.28	0.26
	% Area	52	53	56
Fe^{2+} Px M1	d (mm/s)	1.17	1.18	1.18
	D (mm/s)	2.53	2.5	2.54
	G (mm/s)	0.24	0.22	0.22
	% Area	42	44	41
Fe^{2+} Ilm	d (mm/s)	1.1	1.09	1.11
	D (mm/s)	0.73	0.73	0.73
	G (mm/s)	0.25	0.24	0.24
	% Area	3	1	10
Fe^{3+} Px	d (mm/s)	0.14	0.19	0.11
	D (mm/s)	0.39	0.67	0.73
	G (mm/s)	0.24	0.24	0.24
	% Area	4	1	1
	c^2	1.29	1.24	0.95
$^{M2}Fe^{2+}$ corrected*		59	57	60
$^{M1}Fe^{2+}$ corrected*		41	43	40

*doublet areas corrected for thickness and recoil-free fraction, using a value of f = 1.068 from Dyar et al. (2007)

Table III-4a: MGM results for plagioclase-pyroxene mixtures.

	50-50 (LCP-HCP)							85-15 (LCP-HCP)					
% Plagioclase	0	10	20	30	40	50	60	0	10	20	30	40	50
MEASURED BAND CENTERS (μm):													
Band 1	0.94	0.92	0.92	0.92	0.92	0.92	0.94	0.92	0.94	0.94	0.94	0.94	0.94
Band 2	1.92	1.89	1.89	1.89	1.89	1.89	1.93	1.89	1.92	1.92	1.93	1.93	1.92
BAR	1.60	1.95	1.91	1.88	1.86	1.82	1.39	1.88	1.60	1.56	1.51	1.52	1.48
MGM BAND CENTERS (μm):													
LCP at 1	0.92	0.92	0.92	0.92	0.92	0.92	0.92	0.92	0.93	0.93	0.92	0.92	0.92
HCP at 1	1.02	1.01	1.02	1.02	1.01	1.01	1.01	1.01	1.01	1.01	1.01	1.01	1.01
1.2 Feature	1.16	1.17	1.17	1.17	1.17	1.18	1.18	1.14	1.14	1.14	1.14	1.14	1.14
LCP at 2	1.88	1.88	1.88	1.88	1.88	1.88	1.89	1.87	1.87	1.87	1.87	1.87	1.87
HCP at 2	2.32	2.32	2.33	2.32	2.31	2.30	2.30	2.23	2.23	2.23	2.23	2.23	2.23
MGM BAND STRENGTHS (log reflectance):													
LCP at 1	-0.55	-0.52	-0.47	-0.43	-0.39	-0.33	-0.28	-0.85	-0.80	-0.76	-0.69	-0.62	-0.60
HCP at 1	-0.27	-0.30	-0.26	-0.22	-0.21	-0.19	-0.17	-0.04	-0.04	-0.04	-0.04	-0.03	-0.03
1.2 Feature	-0.13	-0.13	-0.11	-0.10	-0.09	-0.09	-0.71	-0.10	-0.10	-0.09	-0.08	-0.07	-0.06
LCP at 2	-0.43	-0.41	-0.37	-0.32	-0.30	-0.26	-0.23	-0.58	-0.58	-0.55	-0.47	-0.42	-0.39
HCP at 2	-0.20	-0.20	-0.18	-0.15	-0.14	-0.13	-0.10	-0.10	-0.10	-0.09	-0.08	-0.07	-0.06
LCP/HCP at 1	2.03	1.74	1.83	1.91	1.83	1.72	1.71	19.41	18.91	21.60	16.94	18.12	21.47
LCP/HCP at 2	2.20	2.06	1.99	2.07	2.15	2.10	2.32	5.76	5.76	6.37	6.17	6.35	6.94
MGM BAND WIDTHS (μm):													
LCP at 1	0.19	0.19	0.19	0.19	0.19	0.19	0.19	0.19	0.19	0.19	0.19	0.19	0.19
HCP at 1	0.20	0.20	0.20	0.20	0.20	0.20	0.20	0.20	0.20	0.20	0.20	0.20	0.20
1.2 Feature	0.28	0.28	0.28	0.28	0.28	0.28	0.28	0.28	0.28	0.28	0.28	0.28	0.28
LCP at 2	0.54	0.54	0.54	0.54	0.54	0.54	0.54	0.56	0.56	0.56	0.55	0.55	0.55
HCP at 2	0.57	0.57	0.57	0.57	0.57	0.57	0.57	0.57	0.57	0.57	0.57	0.57	0.57

Table III-4b: Predicted HCP content* from MGM, compared to the measured mode in the sample.

Sample	HCP	HCP MGM 1 μm	HCP MGM 2 μm
Mixture 1	50	50	45
Mixture 2	15	10	19
ALH A81001	28	N/A	N/A
BTN 00300	59	73	71
Chervony Kut	56	61	61
EET 87520	43	65	63
GRA 98098	48	55	59
Ibitira	46	56	44
MAC 02522	N/A	N/A	N/A
MET 01081	52	55	57
Moore County	43	47	35
PCA 91078	50	63	67
Serra de Mage	12	18	25

* where % HCP and LCP have been normalised to 100%

Table III-5a: MGM initial parameters for mixtures.

Continuum	0.47			
Continuum Slope	-1.25E-06			
	Absorption	Band Center (μm)	Band width (μm)	Band Strength
Band 1	Charge transfer	0.284	0.095	-1.046
Band 2	Charge transfer	0.403	0.328	-0.48
Band 3	Cr^{3+}	0.662	0.145	-0.102
Band 4	Additional M1	0.878	0.188	-0.156
Band 5	LCP 1 μm	0.908	0.188	-0.156
Band 6	HCP 1 μm	1.014	0.193	-0.551
Band 7	1.2 μm	1.148	0.278	-0.068
Band 8	LCP 2 μm	1.832	0.56	-0.137
Band 9	HCP 2 μm	2.266	0.563	-0.449
Band 10	Adsorbed water band	2.666	0.563	-0.449

Table III-5b: Bands required in MGM for each of the unbrecciated eucrite spectra.

	Absorption	ALH A81001	BTN 00300	Chervony Kut	EET 87520	GRA 98098	Ibitira	MAC 02522	MET 01081	Moore County	PCA 91078	Serra de Mage
Band 1	Charge transfer	Y	Y	Y	Y	Y	Y	Y	Y	Y	Y	Y
Band 2	Charge transfer	Y	Y	Y	Y	Y	Y	Y	Y	Y	Y	Y
Band 3	Cr^{3+}	Y	Y	Y	Y	Y	Y	Y	Y	Y	Y	Y
Band 4	Additional M1	N	Y	Y	N	N	N	Y	N	N	N	N
Band 5	LCP 1 µm	N/A*	Y	Y	Y	Y	Y	N/A*	Y	Y	Y	Y
Band 6	HCP 1 µm	N/A*	Y	Y	Y	Y	Y	N/A*	Y	Y	Y	Y
Band 7	1.2 µm	Y	Y	Y	Y	Y	Y	Y	Y	Y	Y	Y
Band 8	LCP 2 µm	N/A*	Y	Y	Y	Y	Y	N/A*	Y	Y	Y	Y
Band 9	HCP 2 µm	N/A*	Y	Y	Y	Y	Y	N/A*	Y	Y	Y	Y
Band 10	Adsorbed water band	Y	Y	Y	Y	Y	Y	Y	Y	Y	Y	Y

N/A* for band numbers 5, 6 and 7,9 denotes eucrites that only needed one pyroxene in the model and, therefore, did not have separate LCP and HCP bands in these regions

All the unbrecciated eucrite spectra require bands at 600nm (Cr^{3+}) and 1.2 µm for good MGM fits. However, these two features are not observable in the overall spectrum of all of the eucrites (see sections 5.3.2 and 5.3.3 for more details).

Table III-6: MGM results for unbrecciated eucrites.

	ALH A81001	BTN 00300	Chervony Kut	EET 87520	GRA 98098	Ibitira	MAC 02522	MET 01081	Moore County	PCA 91078	Serra de Mage
MEASURED BAND CENTERS (μm):											
Band 1	0.94	0.95	0.94	0.95	0.94	0.94	0.97	0.94	0.94	0.96	0.93
Band 2	2.01	2.01	2.01	2.02	2.01	2.00	2.13	2.00	1.99	2.02	1.97
BAR	2.64	1.15	2.39	1.35	1.34	1.29	1.18	1.46	1.60	2.15	1.69
MGM BAND CENTERS (μm):											
Extra M1		0.83	0.87				0.88				
LCP at 1		0.91	0.92	0.90	0.90	0.90		0.90	0.91	0.89	0.92
HCP at 1	0.93	1.01	0.99	1.01	1.01	1.01	0.99	1.01	0.99	1.01	1.00
1.2 Feature	1.19	1.21	1.19	1.20	1.20	1.20	1.12	1.21	1.18	1.20	1.17
LCP at 2		1.81	1.91	1.91	1.90	1.93		1.89	1.93	1.89	1.94
HCP at 2	2.02	2.20	2.22	2.24	2.12	2.21	2.15	2.22	2.23	2.24	2.24
MGM RELATIVE STRENGTHS (log reflectance):											
Extra M1		-0.56	-0.26				-0.36				
LCP at 1		-0.89	-0.51	-0.74	-1.03	-0.78		-0.92	-0.77	-0.88	-0.58
HCP at 1	-0.54	-0.98	-0.37	-0.61	-0.63	-0.50	-0.90	-0.58	-0.40	-0.67	-0.10
1.2 Feature	-0.09	-0.73	-0.20	-0.26	-0.34	-0.21	-0.23	-0.34	-0.15	-0.34	-0.07
LCP at 2		-0.95	-0.57	-0.49	-0.57	-0.43		-0.59	-0.49	-0.62	-0.40
HCP at 2	-0.35	-0.98	-0.41	-0.37	-0.40	-0.20	-0.37	-0.38	-0.17	-0.56	-0.09
LCP/HCP at 1		0.91	1.37	1.22	1.62	1.57		1.59	1.93	1.31	6.03
LCP/HCP at 2		0.97	1.39	1.30	1.43	2.17		1.54	2.88	1.11	4.30
MGM BAND WIDTHS (μm):											
Extra M1							0.14				
LCP at 1	0.00	0.20	0.19	0.19	0.18	0.18		0.19	0.19	0.19	0.19
HCP at 1	0.19	0.20	0.18	0.18	0.17	0.18	0.19	0.19	0.18	0.18	0.19
1.2 Feature	0.32	0.32	0.28	0.28	0.31	0.28	0.34	0.29	0.28	0.29	0.28
LCP at 2	0.00	0.58	0.56	0.55	0.57	0.56		0.56	0.56	0.55	0.56
HCP at 2	0.60	0.56	0.56	0.56	0.56	0.56	0.70	0.56	0.56	0.56	0.56

Figure III-1: Unbrecciated eucrite pyroxene compositions. Major-element pyroxene compositions (Fe, Mg, Ca) are shown in the quadrilaterals and minor-element compositions (Ti, Al, Cr) are overlain in the form of ternary plots.

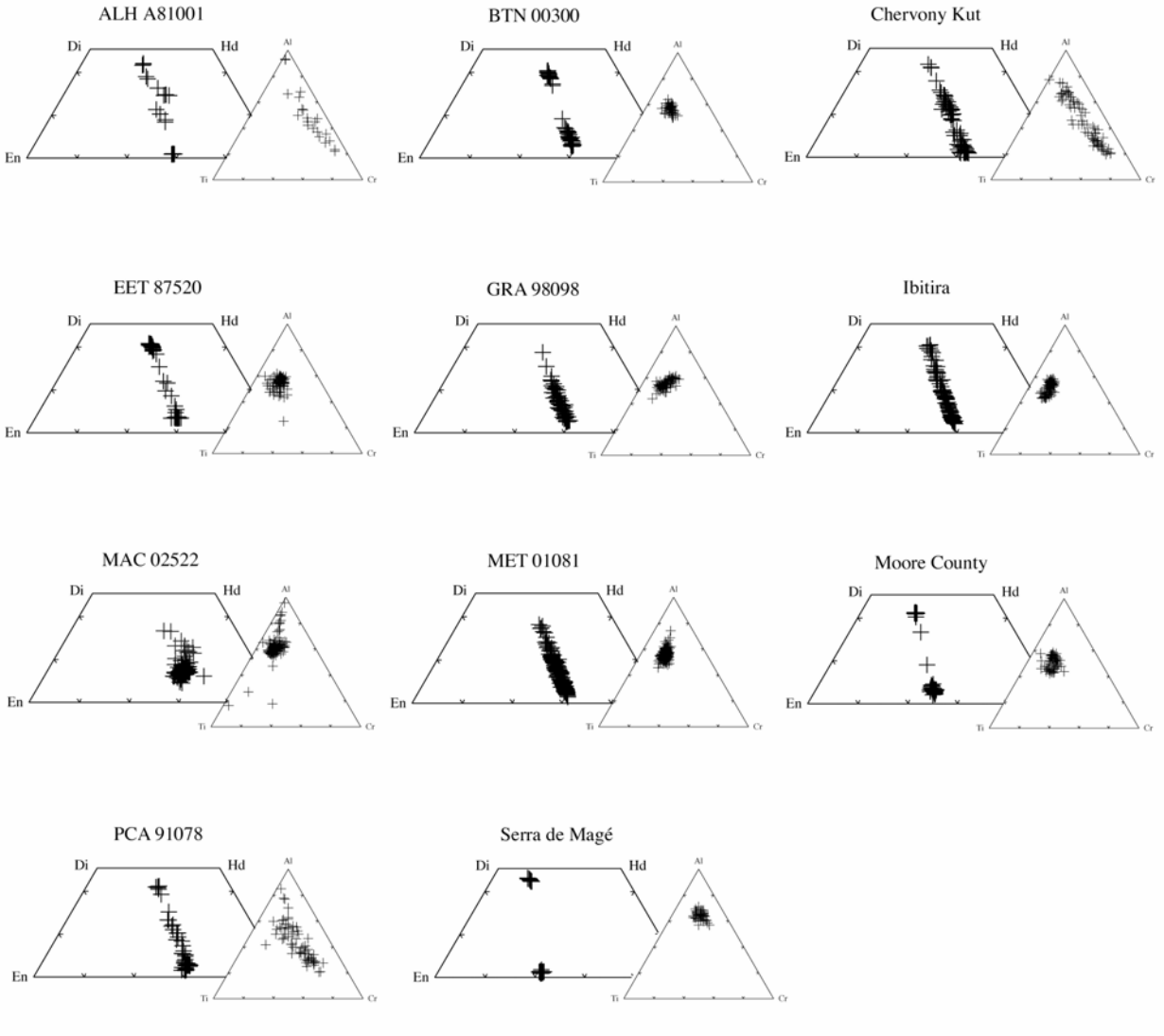
ALH A81001
BTN 00300
Chervony Kut
EET 87520
GRA 98098
Ibitira
MAC 02522
MET 01081
Moore County
PCA 91078
Serra de Magé
Di
Hd
En
Al
Ti
Cr

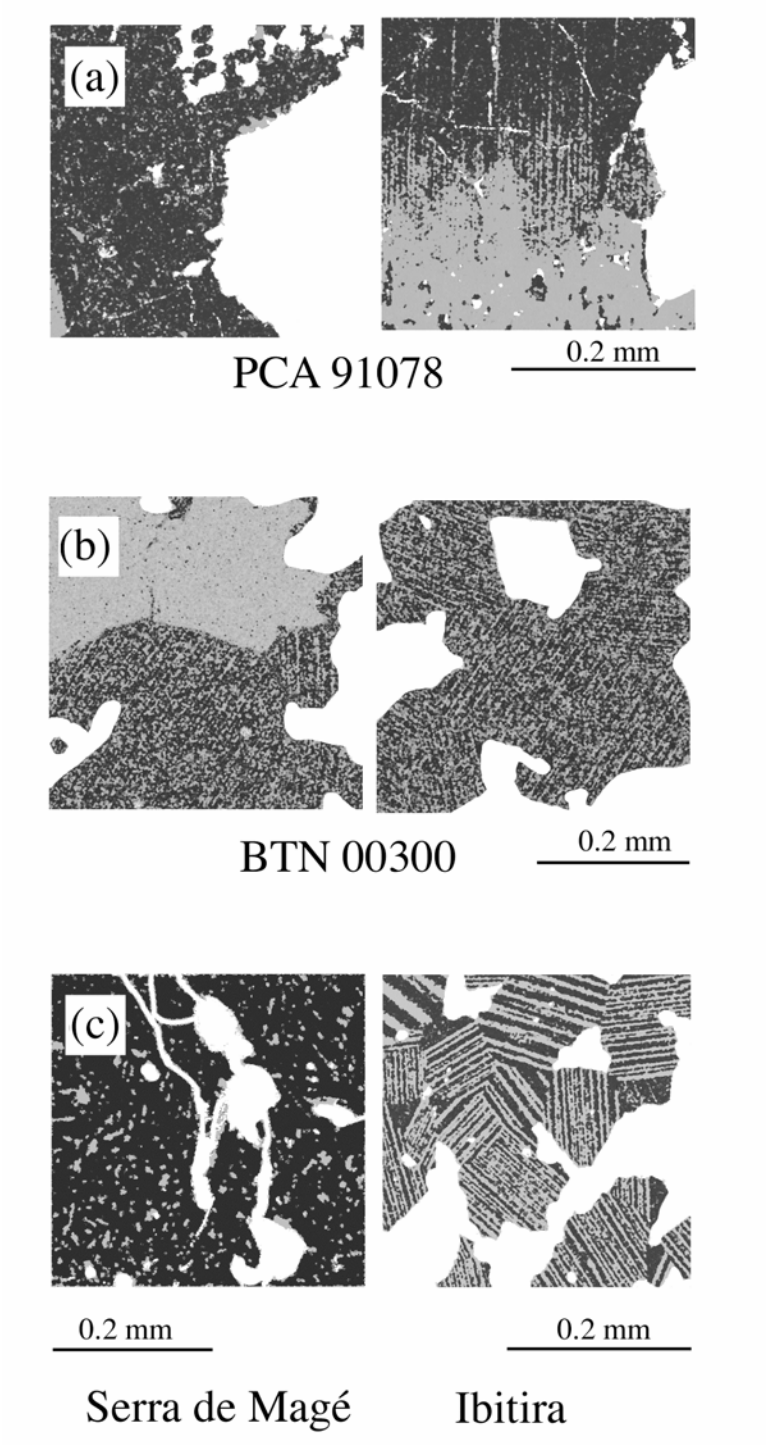

Figure III-2: High-resolution mineral maps of pyroxene compiled using SEM X-ray maps. (a) Variations in the proportions of LCP and HCP within different grains. (b) Individual grains of HCP and HCP exsolved from LCP. (c) Different exsolution morphologies.

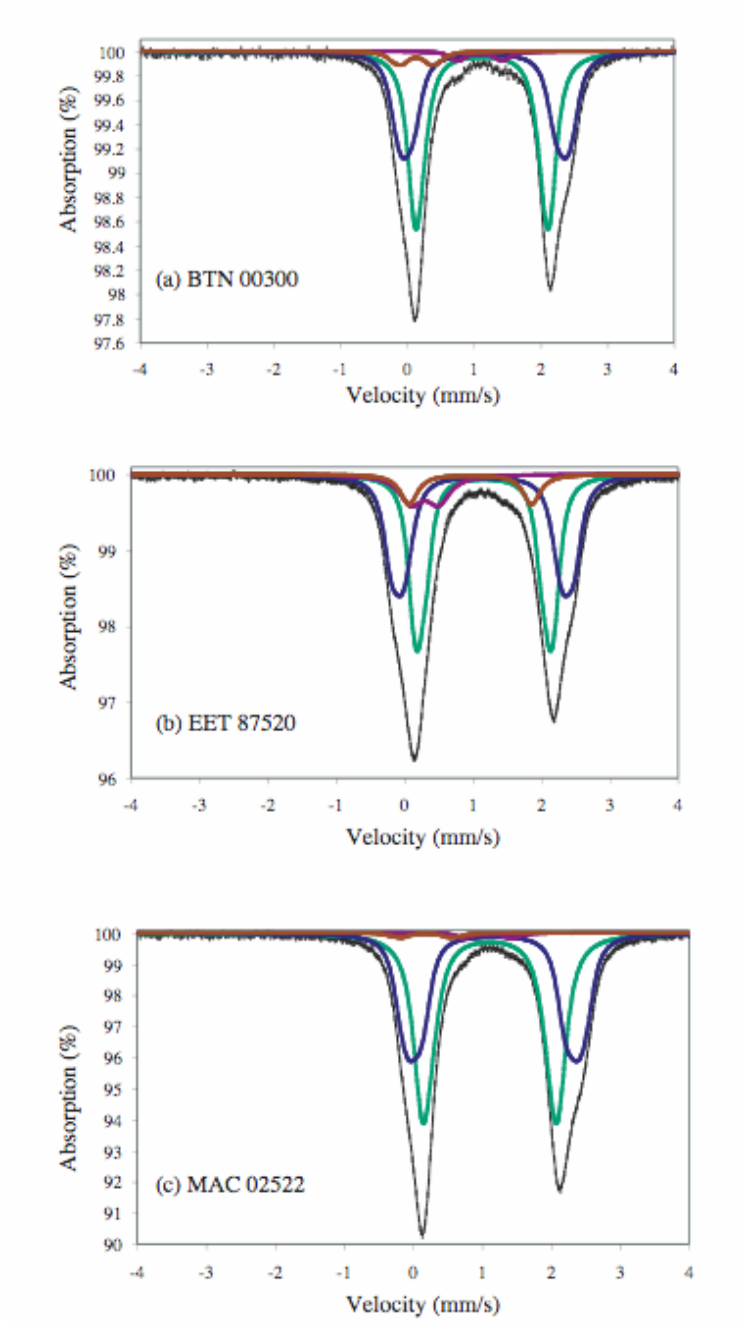

Figure III-3: Mössbauer spectra for three unbrecciated eucrites (a) BTN 00300 (b) EET 87520 (c) MAC 02522. The M1 ferrous doublet is shown in blue, the M2 ferrous doublet in green. Ferric iron in pyroxene is given in brown, and in ilmenite in purple.

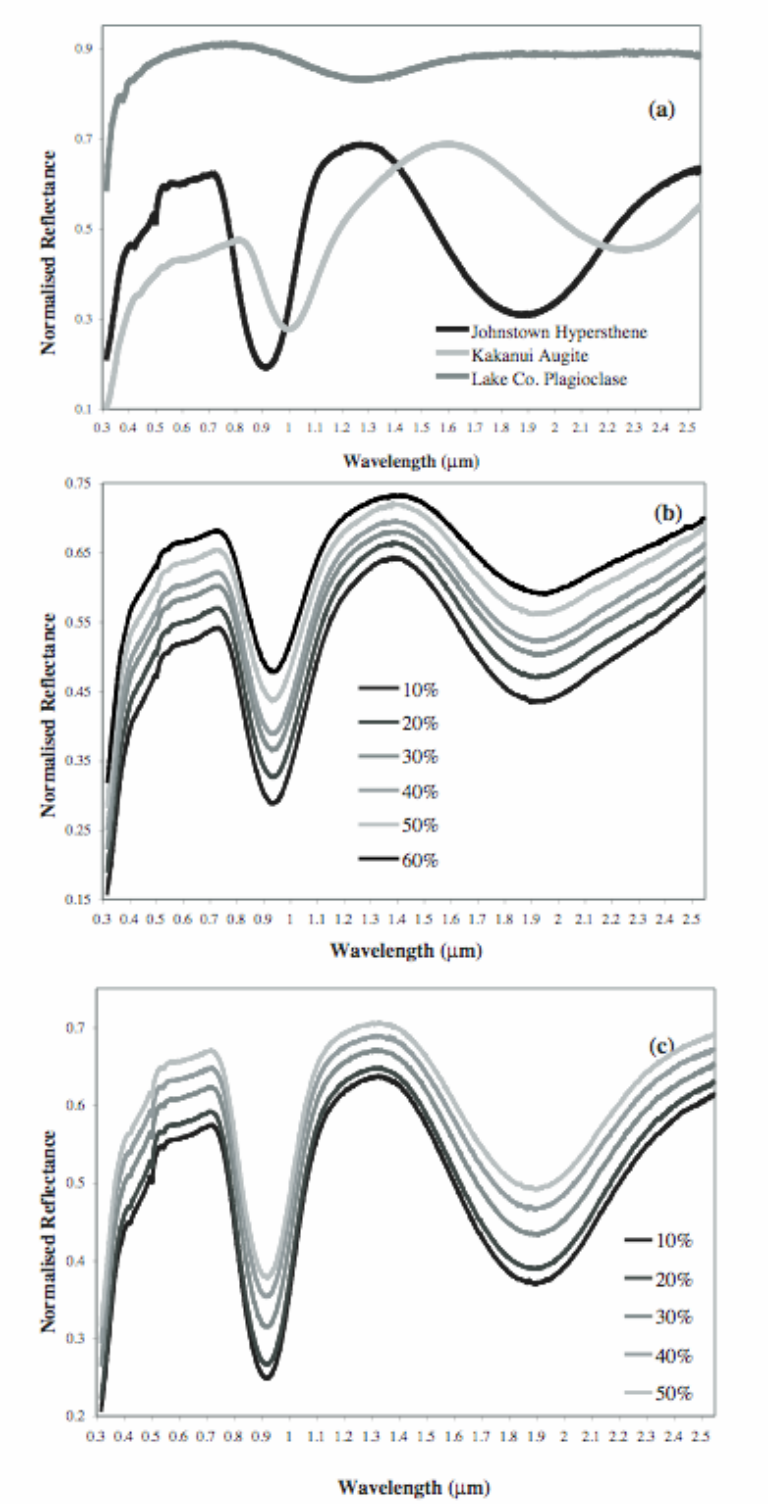

Figure III-4: Reflectance spectra of: (a) End members used in the mixtures. (b) 50:50 LCP:HCP mixtures; (c) 85:15 LCP:HCP mixtures.

Figure III-5: MGM results for all mixture spectra. The individual absorption bands modeled by modified Gaussians are shown in dark grey. The upper black line represents the residual error of the model; the lower black line represents the continuum. The measured spectrum is plotted with grey +'s, and the black is the modeled value. A large arrow is used to denote the LCP band in the 1 and 2-μm region, and a small arrow for HCP.

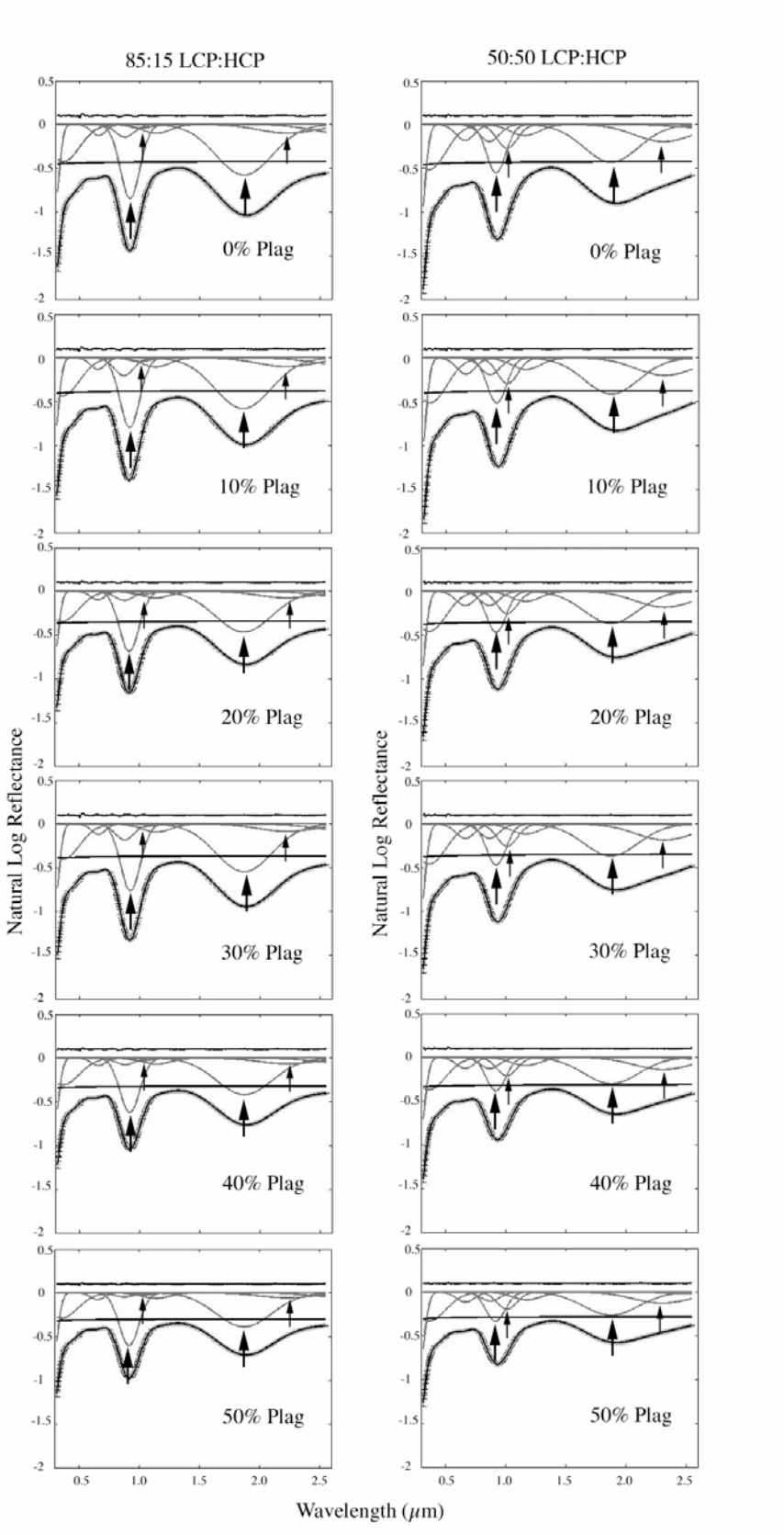
85:15 LCP:HCP
50:50 LCP:HCP
0% Plag
10% Plag
20% Plag
30% Plag
40% Plag
50% Plag
Natural Log Reflectance
Wavelength (μm)

Figure III-6: MGM results for all eucrite spectra. The individual absorption bands modeled by modified Gaussians are shown in dark grey. The upper black line represents the residual error of the model; the lower black line represents the continuum. The measured spectrum is plotted with grey +'s, and the black is the modeled value. A large arrow is used to denote the LCP band in the 1 and 2-μm region, and a small arrow for HCP.

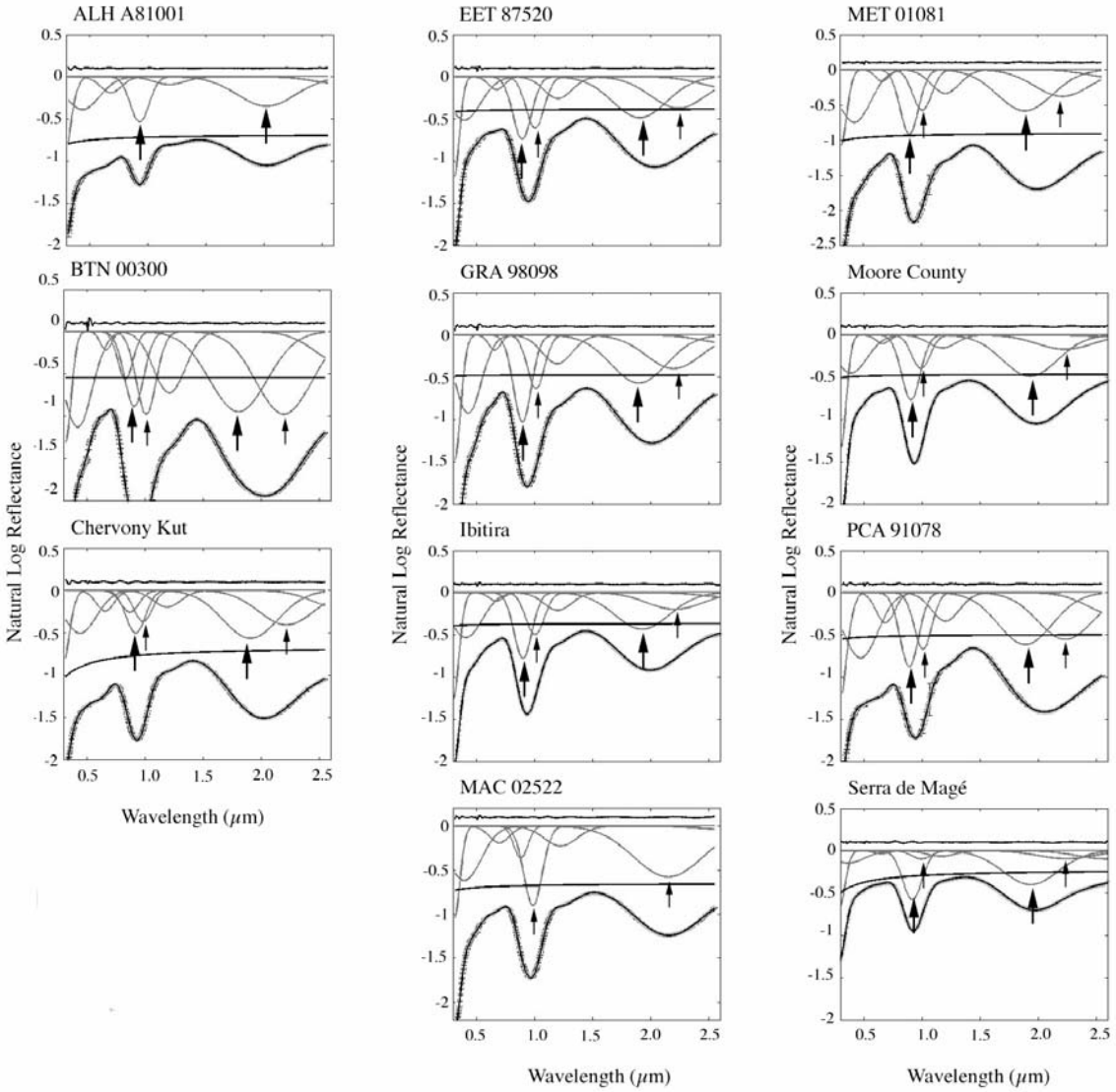
ALH A81001
EET 87520
MET 01081
BTN 00300
GRA 98098
Moore County
Chervony Kut
Ibitira
PCA 91078
MAC 02522
Serra de Magé
Natural Log Reflectance
Wavelength (μm)

Figure III-7: Eucrite continuum-removed and MGM-derived band centers. (a) Band centers for the unbrecciated eucrites are superimposed on data from previous studies, showing shift in band center values with increasing calcium contents. Solid symbols for data from Adams (1974;1975), Cloutis and Gaffey (1991), and Hazen (1978) represent those pyroxenes with Wo<11% and open symbols Wo>11%. The eucrite data continuum-removed band centers are shown in large solid circles, and the MGM-derived in large solid squares. (b) The unbrecciated eucrite band centers divided into cumulate (triangles) and basaltic (squares). Continuum-removed values are shown as filled symbols and open symbols represent MGM-derived band centers.

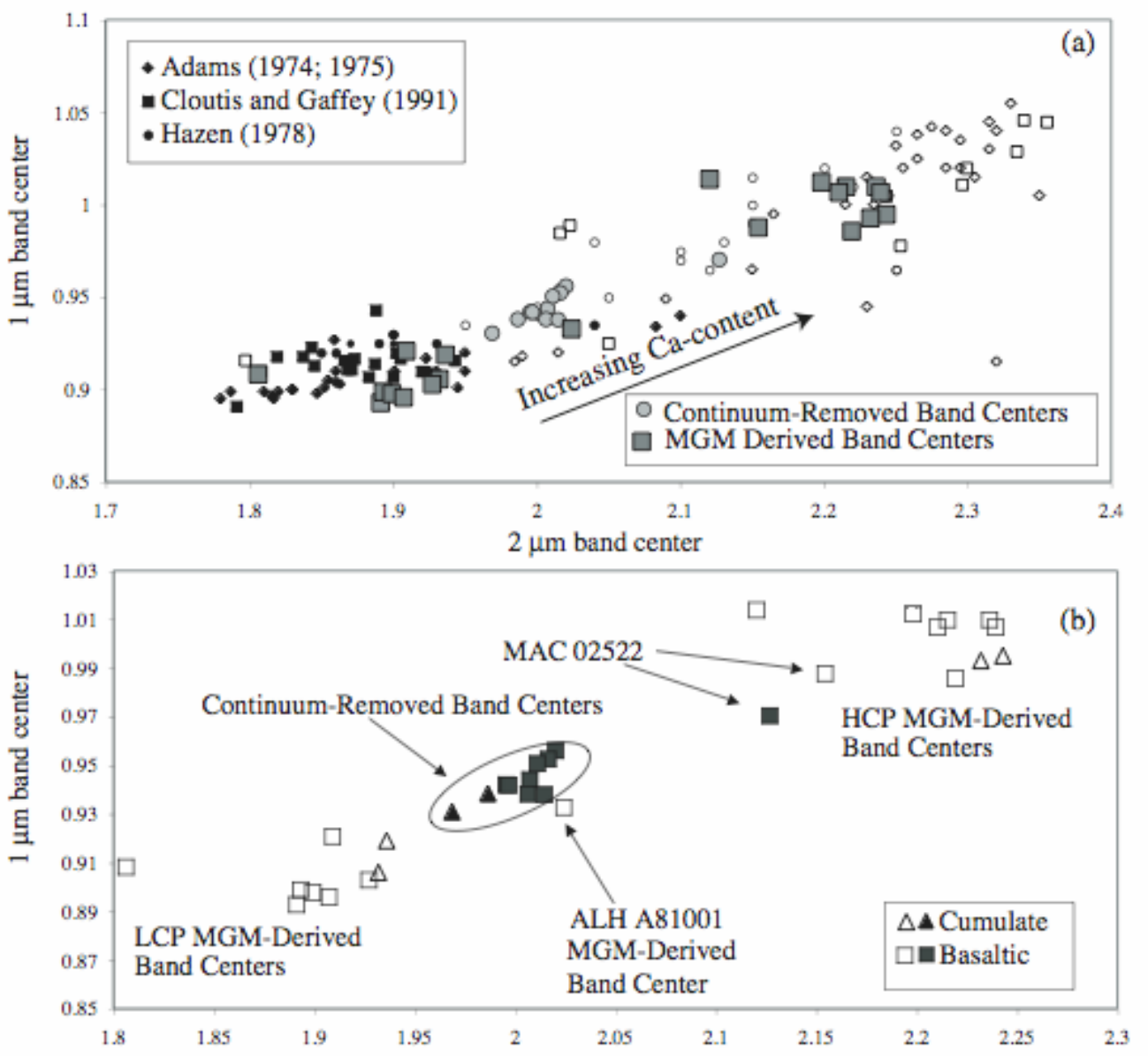
(a)
Adams (1974; 1975)
Cloutis and Gaffey (1991)
Hazen (1978)
Increasing Ca-content
Continuum-Removed Band Centers
MGM Derived Band Centers
1 µm band center
2 µm band center
1.1
1.05
1
0.95
0.9
0.85
1.7
1.8
1.9
2
2.1
2.2
2.3
2.4
(b)
MAC 02522
Continuum-Removed Band Centers
HCP MGM-Derived
Band Centers
LCP MGM-Derived
Band Centers
ALH A81001
MGM-Derived
Band Center
Cumulate
Basaltic
1 µm band center
1.03
1.01
0.99
0.97
0.95
0.93
0.91
0.89
0.87
0.85
1.8
1.85
1.9
1.95
2
2.05
2.1
2.15
2.2
2.25
2.3

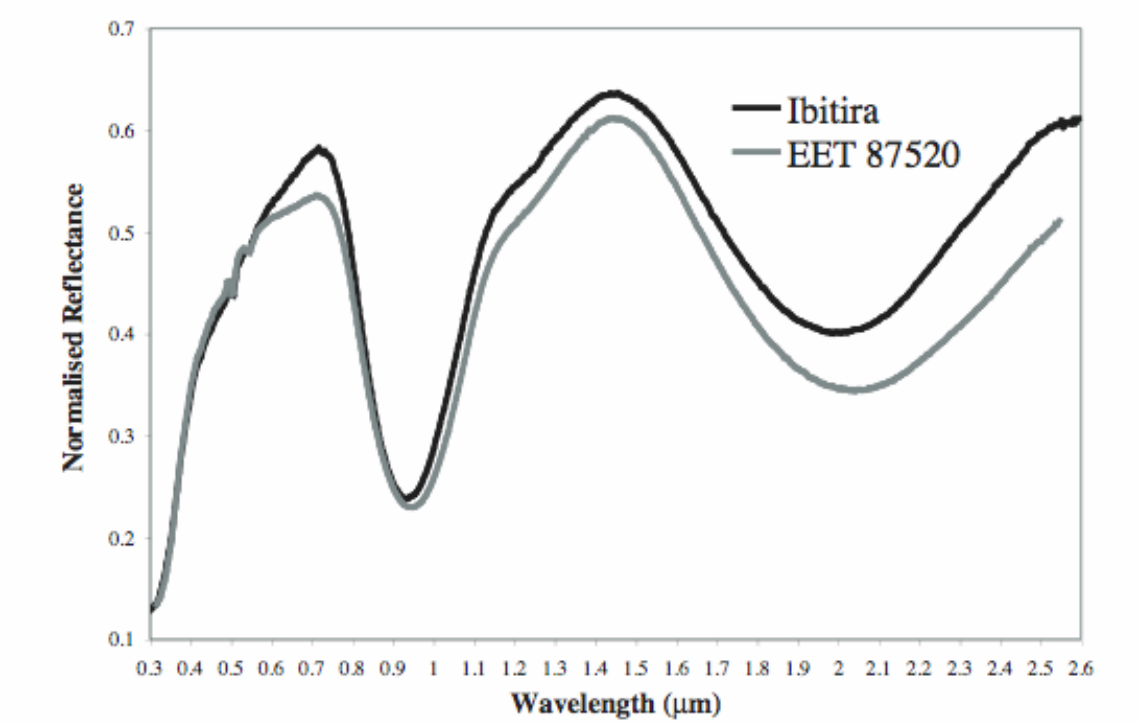

Figure III-8: Graph showing the spectral similarity between Ibitira and EET 87520.

Figure III-9: (a) The relative strength of the 1.2-µm band against plagioclase content for the unbrecciated eucrites. The strength of the 1.2-µm band is normalized to the strength of the 2-µm HCP band (1.2/(1.2+2 HCP)); therefore, only those eucrites modeled by two pyroxenes are plotted here. A trend line is plotted to show the decrease in strength of he 1.2-µm band with plagioclase content. This relationship is the inverse of what would be expected if the 1.2-µm band was caused by plagioclase. (b) The relative strength of the 1.2-µm band against plagioclase content for the pyroxene-plagioclase mixtures. The strength of1.2-µm band is normalized to the strength of the 2-µm HCP band (1.2/(1.2+2 HCP)). (c) BAR plotted against plagioclase composition for the two sets of pyroxene-plagioclase mixtures. Three unbrecciated eucrites with a LCP:HCP ratio similar to that of the 50:50 mixtures are shown to demonstrate that the BAR values of the mixtures cannot be used as a calibration tool for plagioclase content in the eucrites.

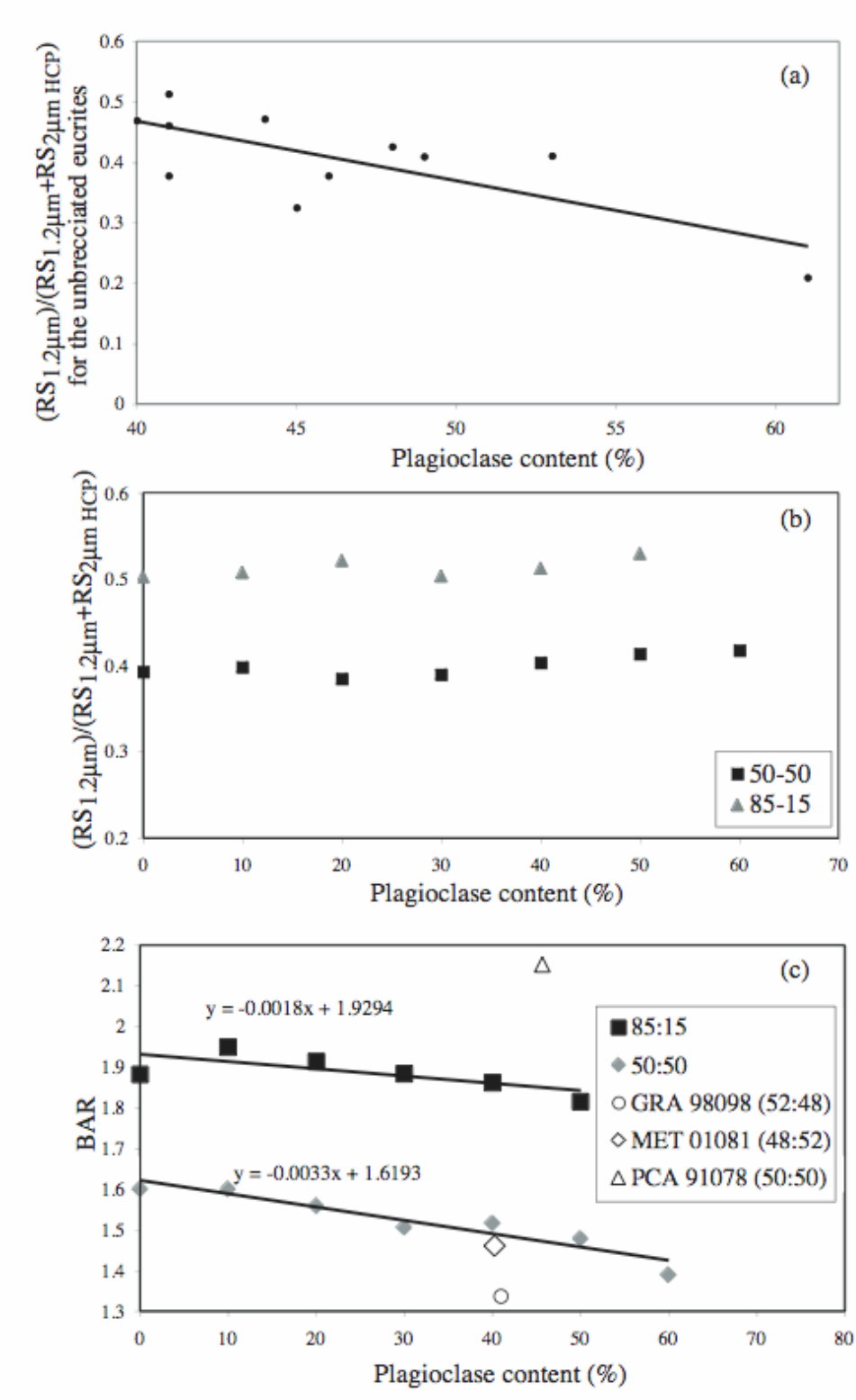
(a)
(RS1.2µm)/(RS1.2µm+RS2µm HCP) for the unbrecciated eucrites
Plagioclase content (%)
(b)
(RS1.2µm)/(RS1.2µm+RS2µm HCP)
50-50
85-15
Plagioclase content (%)
(c)
y = -0.0018x + 1.9294
y = -0.0033x + 1.6193
BAR
85:15
50:50
GRA 98098 (52:48)
MET 01081 (48:52)
PCA 91078 (50:50)
Plagioclase content (%)

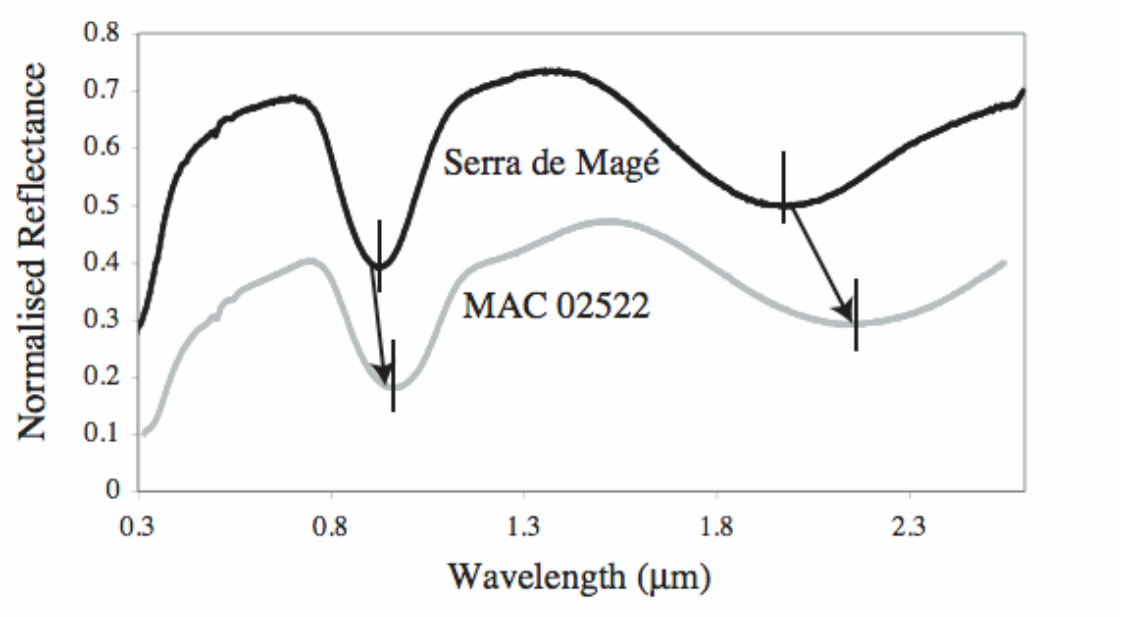

Figure III-10: Shift in 1 and 2-µm continuum-removed band centers between Serra de Magé and MAC 02522, the unbrecciated eucrites in this study with the shortest and longest values respectively.

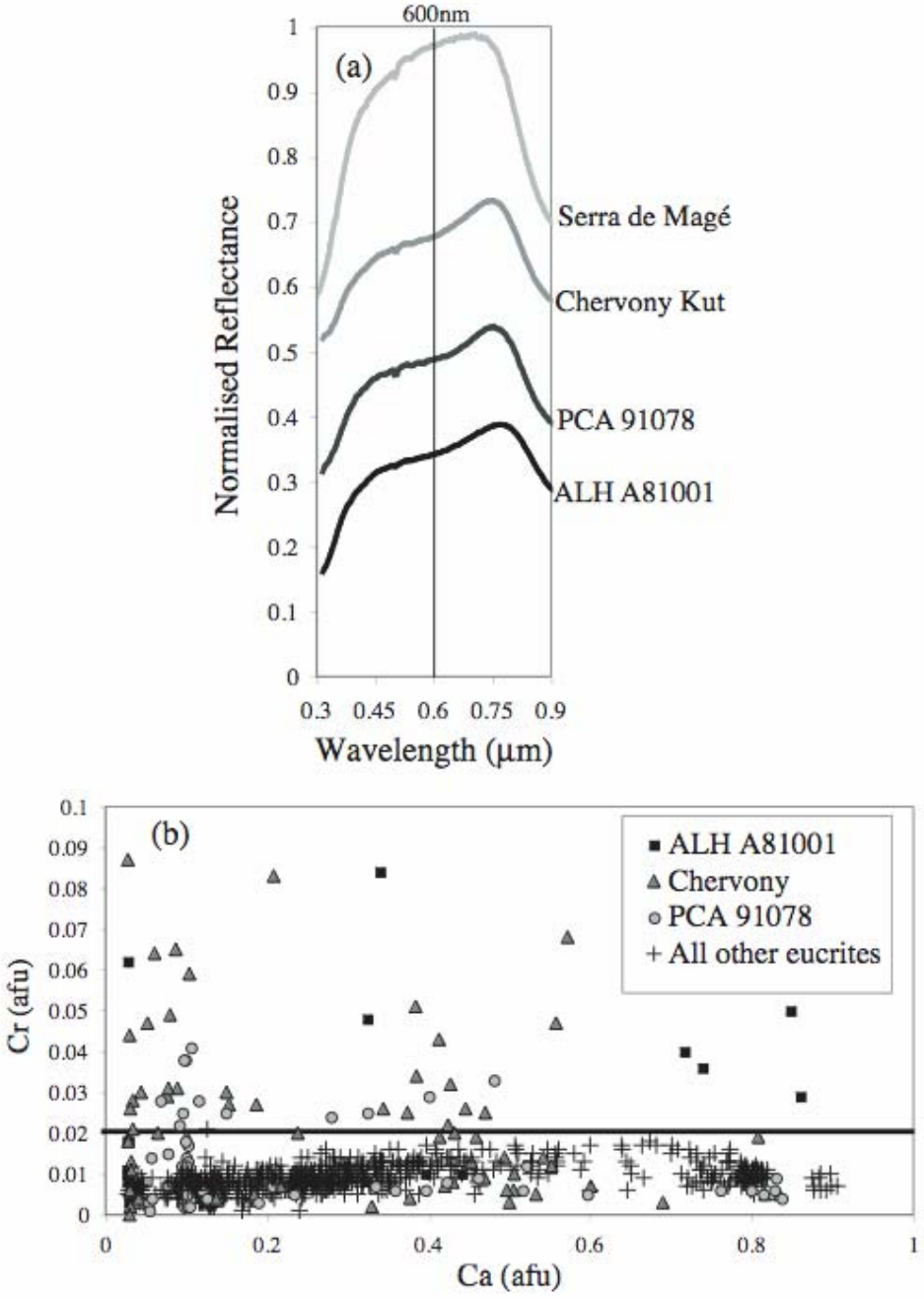

Figure III-11: Presence of the 600-nm (0.6-µm) Cr^{3+} feature in the spectra of the unbrecciated eucrites. (a) Portion of VIS-NIR spectra for the unbrecciated eucrites showing the 600-nm (0.6-µm) absorption. The Serra de Magé spectrum is illustrated as an example of a spectrum with no absorption visually present. (b) Plot of Ca vs. Cr in atomic formula units for the pyroxenes in the unbrecciated eucrites. The detection limit of Cr_2O_3 on the electron microprobe is around 0.03 wt.%, which translates to 0.001 - 0.002 afu.

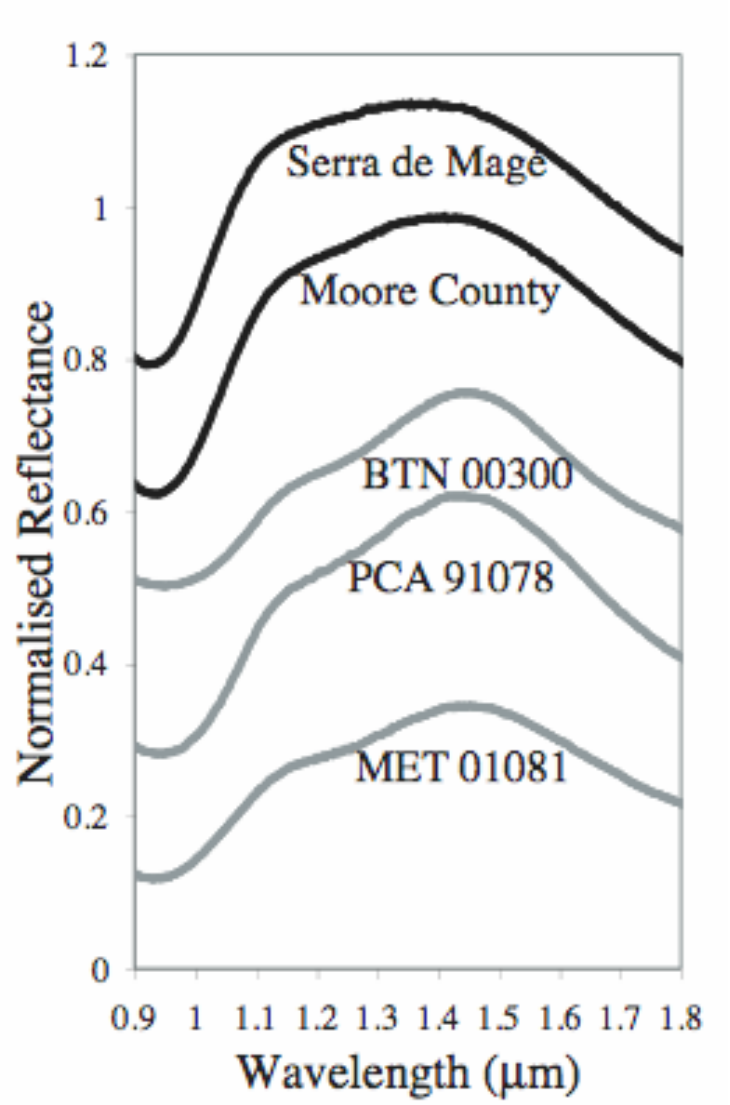

Figure III-12: Portion of VIS-NIR spectra for unbrecciated eucrites showing the 1.2-µm absorption. The spectra of Serra de Magé and Moore County are illustrated as examples of spectra without a visible 1.2-µm feature.

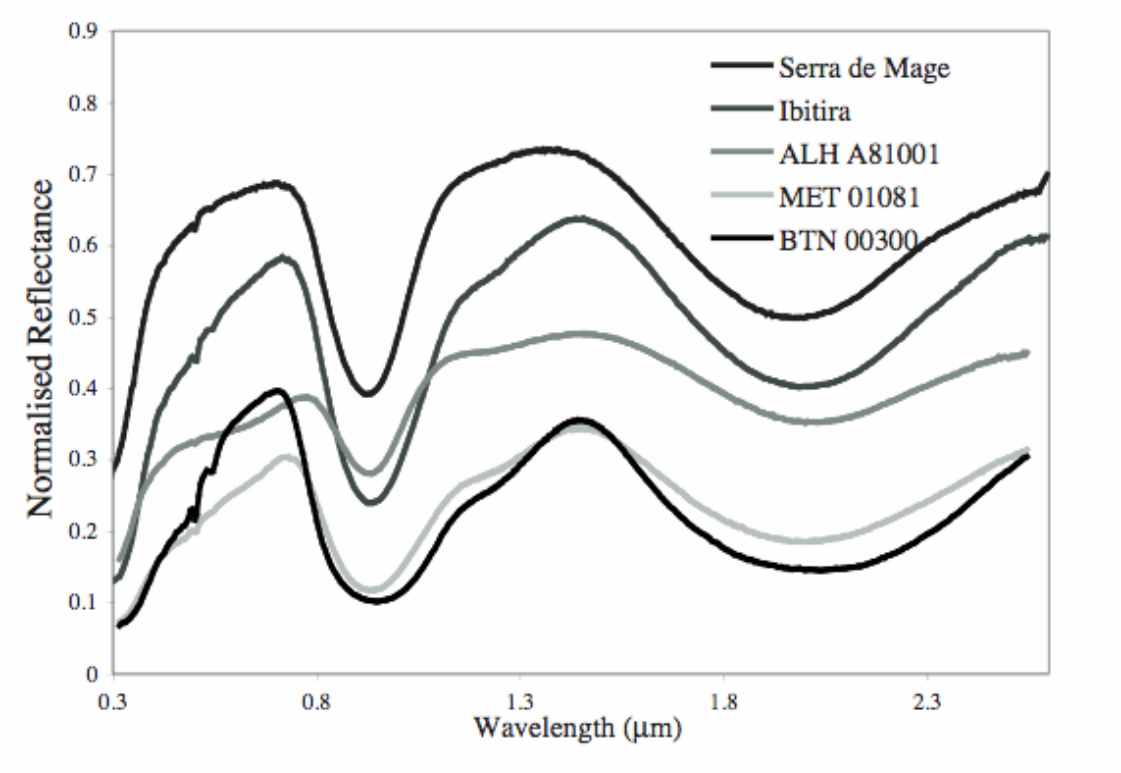

Figure III-13: VIS-NIR Reflectance spectra of 5 unbrecciated eucrites showing the difference in reflectance values and spectral contrast between samples.

IV. The Compositional Diversity of Vestoids and their Implications for the Heterogeneity on the Surface of 4 Vesta

This chapter is a reformatted version of a paper, by the same name, to be submitted to the journal Icarus by Rhiannon G. Mayne, Jessica M. Sunshine, Harry Y. McSween Jr., Schelte J. Bus, and Timothy J. McCoy.

Mayne R.G., Sunshine J.M., McSween H.Y. Jr., Bus S.J., and McCoy T.J. The compositional diversity of Vestoids and their implications for the heterogeneity of the surface of 4 Vesta.

Abstract

4 Vesta is a unique asteroid, not only because of its large size and differentiated nature, but also because we have meteorites that are believed to originate there, the HEDs (howardites, eucrites, and diogenites). It is also one of the targets for the Dawn mission, which launched in September 2007. High quality spectra of 15 Vestoids, small asteroids that are believed to originate from Vesta, were collected and compared to laboratory spectra and compositional data for selected HED meteorites. The Vestoids indicate that both large-scale homogeneous units and smaller-scale heterogeneity exist on the surface of Vesta, as both monomineralogic (eucrite or diogenite material alone) and mixed (both eucrite and diogenite) spectra are observed. Most Vestoid spectra appear to represent a mixture of both eucrite and diogenite material. This may reflect the formation of the Vestoids themselves, as rubble piles made up of ejecta from their parent Vesta, or it may indicate that the majority of the Vestoids are in fact howardite-dominated. However, mixed sub-hemispheric spectral signatures may also mean that during the formation of Vesta's crust, processes were operating that produced both large and small-scale units, a greater understanding of which could help to decipher the petrogenesis of Vesta itself.

1. Introduction

The howardites, eucrites, and diogenites (HEDs) have long been identified spectrally with 4 Vesta, the second largest asteroid in the main-belt (McCord, 1970). The link between Vesta and the HEDs was debated for several decades, as it was not initially believed to be dynamically possible to deliver fragments from Vesta to Earth (Wasson and Wetherill, 1979). Binzel and Xu (1993) identified a group of 'Vestoids', small asteroids that are spectrally similar and dynamically linked to Vesta. These smaller bodies were observed to bridge the gap between Vesta and the 3:1 resonance with Jupiter, which provides a pathway for the delivery of the HED meteorites to Earth. They also have been observed to have spectral characteristics consistent with surface compositions of both the eucrites and howardites (Burbine et al., 2001). Other basaltic asteroids that are similar to with the asteroid Vesta, but which lie outside its dynamical family, have since been identified and have led more recent asteroid taxonomies to refer to those asteroids with spectra similar to that of Vesta as V-type (e.g. Tholen and Barucci, 1989; Bus and Binzel, 2002b). However, those asteroids that appear most similar to diogenites, with deep narrow 1-μm features, are denoted by the separate classification of J-type (Binzel and Xu, 1993). In the past few years, evidence for differentiation has also been found on asteroidal bodies that have no apparent relationship to Vesta, suggesting that there may be a large population of differentiated asteroids yet to be discovered (Hardersen et al., 2004; Sunshine et al., 2004). Here we present new data on fifteen members of the Vestoid family.

Recent work has been carried out to quantify both the petrology (Mayne et al., 2008a – Part II of this dissertation) and visible near-infrared (VIS-NIR) spectra (Mayne et al., 2008b; Mayne et al., 2008a – Part III of this dissertation) of the unbrecciated eucrites, in order to better understand the variability and petrogenesis of the basaltic crust of Vesta and assess how much we can learn about both from spectroscopy. The topic of Vesta and the HEDs is particularly relevant now that the Dawn spacecraft, which will orbit and spectrally map Vesta's surface, has launched. Here we present VIS-NIR data (~0.4-2.5 μm) for 15 Vestoids believed to have originated from Vesta. Their spectra are modeled and compared with those for selected HED meteorites to constrain the heterogeneity we should expect to see from Dawn. The Vestoids reflect lithologies that were once present both on the surface of Vesta and also at depth. If the Vestoid spectra suggest that more than one type of material is present, i.e. the spectral signature of both eucrites and diogenites, have been averaged over the asteroid being measured, then the sizes of individual igneous provinces on Vesta must be smaller than the size of the Vestoids. The size of individual units can then be used to interpret the formation of the basaltic crust of Vesta, as the processes that form small-scale units are different from those that produce larger-scale ones. Therefore, these asteroids offer an opportunity to learn more about the surface of Vesta and the layering and petrogenesis of the crust than we can by studying their parent asteroid alone, before Dawn arrives in 2011.

2. Background

2.1 Howardite-Eucrite-Diogenite Family

The HED meteorite family consists of cumulate orthopyroxenites (diogenites), basalts, and gabbros (eucrites), as well as regolith breccias (howardites), which contain clasts of both materials. Many lines of evidence suggest that the HEDs all originated from the same parent body: all three groups lie on the same oxygen isotope mass fractionation line (Clayton and Mayeda, 1996); howardites consist of a mixture of material from eucrites and diogenites, suggesting comminution on a single parent body (Drake, 2001); they share common exposure ages, implying ejection from the same parent body (Eugster and Michel, 1995); HST observations demonstrate that significant impact excavation has occurred from the surface of Vesta (Thomas et al., 1997); the Vestoids bridge the gap between Vesta and the 3:1 resonance, which is a proposed delivery path for getting meteorites to Earth (Binzel and Xu, 1993)

2.2 HED spectra

Pyroxene has two main absorption features, caused by the presence of Fe^{2+} in its structure, in visible and near-infrared (VIS-NIR) spectra near 1 and 2 μm (Adams, 1974; Burns 1993). The positions of the absorption bands are directly proportional to the concentrations of cations within the octahedral sites, primarily Ca^{2+}, Mg^{2+}, and Fe^{2+}, although other cations in smaller abundances (Ti^{4+}, Cr^{3+} and Al^{3+}) may have an effect (Adams, 1974; Burns, 1993). Both the 1 and 2-μm bands shift to longer wavelengths with an increase in calcium content. Fe^{2+} in the asymmetric M2 site gives rise to a strong feature at 1 μm and is solely responsible for the 2-μm absorption in pyroxene (Burns, 1993). The M1 site of pyroxenes is more symmetrical and, therefore, does not cause

absorption features of the same strength as the M2 bands. Fe^{2+} in the M1 gives rise to two overlapping absorptions, a relatively weak one in the 1-μm region and another centered near 1.2 μm (Burns, 1993). Diogenite spectra tend to have band centers at shorter wavelengths than howardites and eucrites as they contain pyroxenes with a low-calcium composition. Eucrites commonly contain both low- and high-calcium pyroxene compositions, and the basaltic members are iron-rich in comparison to the diogenites and the cumulate eucrites.

The absorption at 1.2 μm varies in strength among the HED family. It is seen most strongly in the spectra of basaltic eucrites, is weaker in the spectra of cumulate eucrites and howardites, and is absent in the spectra of diogenites (Gaffey, 1976). Previous authors have attributed this feature to the presence of iron within the plagioclase structure (e.g. Gaffey, 1976; McFadden and Gaffey, 1978; Hardersen et al., 2004); however, the M1 band in pyroxene, as mentioned above, also gives rise to an absorption in the 1.2-μm region (Burns, 1993). Recent work has attempted to resolve the spectral ambiguity of the 1.2-μm feature and has shown that it can be explained entirely by the presence of Fe^{2+} in the M1 site of pyroxene (e.g. Sunshine et al., 1993; Klima et al., 2007, 2008; Mayne et al., 2008b – Part III of this dissertation)

2.3 Temperature Effects

It has been demonstrated that absorption band positions of silicate minerals vary with temperature (e.g. Singer and Roush; 1985, Roush and Singer, 1987; Schade and Wäsch 1999; Moroz et al., 2000). Hinrichs et al. (1999) calculated that the surface temperature of an asteroid at Vesta's position in the main-belt (2.36 AU) will be ~200 K, if a fine-grained regolith is present. This is based on the assumption that the surface

temperature of an asteroid will fall somewhere between that of the fast and slow rotating end-members of the simple radiative balance model (Encrenaz et al., 1991). A fast rotator radiates heat on both its day and night side (high thermal inertia) and a slow rotator has a surface that is in instantaneous equilibrium with sunlight (low thermal inertia)(Encrenaz et al., 1991; Hinrichs et al., 1999). Laboratory spectra are commonly collected at room temperature ~ 293 K. Singer and Roush (1985) showed that the 2-μm region in pyroxenes is affected by temperature changes. In orthopyroxenes (low-calcium pyroxenes) the band shifts to shorter wavelengths with decreasing temperature, whereas the opposite effect occurs with clinopyroxenes (high-calcium pyroxenes) (Roush and Singer, 1985; Moroz et al., 2000). Singer and Roush (1985) observed that over the temperature range 80-448 K the shift of the 2-μm band minimum for both HCP and LCP was about 0.1 μm. Here we compare laboratory-collected HED spectra with those for Vestoids and it is important to consider any temperature effects that may produce differences between the two data sets.

Diogenite-composition Vestoids, consisting of only low-calcium pyroxene (LCP), would be expected to have a shorter wavelength 2-μm absorption band than their meteorite counterparts. However, the majority of the Vestoid spectra should be expected to reflect the presence of both LCP and HCP, and the temperature effects on the spectra of such mineralogies are difficult to quantify as they act in opposite directions and may, in fact, partially cancel each other out. For this reason no temperature correction has been applied to the Vestoid spectra collected. Fortunately, the 1-μm band is believed to be mostly unaffected by temperature changes for mixed high and low-calcium pyroxene (HCP and LCP) mineralogies like the HEDs (e.g. Singer and Roush; 1985, Roush and

Singer, 1987). Therefore, more consideration has been given to the differences, or similarities, that exist between the spectra of the Vestoids and HEDs in the 1-μm region.

3. Methodology

3.1 Collection of Asteroid Spectra

The VIS-NIR asteroid data are taken in two different surveys, the Small Main-belt Asteroid Spectroscopic Survey, Phase II (SMASSII), that covers the visible region and the SpeX NIR asteroid survey (0.82 - 2.49 μm)(where SpeX refers to the instrument name). These two datasets were taken at two different observatories using a total of three different telescopes. The SMASSII data were taken at the MDM observatory (so called as it is jointly operated by the University of Michigan, Dartmouth College, and MIT) on Kitt Peak in Arizona, using the two telescopes: the 1.3-m McGraw-Hill telescope, and the 2.4-m Hiltner telescope. The NIR data were taken with the NASA Infrared Telescope Facility (IRTF), a 3.0-m telescope on Mauna Kea in Hawaii.

The two different surveys (SMASSII and the SpeX NIR survey) use different instruments / cameras. For SMASSII, a low-resolution grism spectrograph was used, and two possible different CCD cameras were attached to this spectrograph to actually record the data (different CCDs with different pixel dimensions and scales). The two CCD cameras that were used are:

1. a camera utilizing a SITE 1024 x 1024 thinned, backside illuminated CCD with 24-micron pixels.
2. a camera utilizing at Loral 2048 x 2048 thick, frontside illuminated CCD with 15-micron pixels.

For both of these cameras, the pixels were binned on readout, giving a spatial resolution (along the length of the slit) of about 0.5 arcsec per pixel. The spectra were consistently taken with a wide 4.5 arcsecond slit, producing a spectral resolving power of R ~ 100 ($\lambda/\Delta\lambda$). The detailed methodology of the SMASSII observations can be found in Bus & Binzel (2002).

The NIR data were taken with SpeX, the low- to medium-resolution spectrograph and imager. The spectrograph part of this instrument uses a Raytheon Aladdin 3 1024 x 1024 pixel InSb array with 27-micron pixels. In the low-resolution prism mode data taken with SpeX, the spatial image scale (along the slit direction) is 0.15 arcsec per pixel, and the spectral resolving power is again about R ~ 100 when using the 0.8 arcsec slit. Because the sky and seeing conditions on Mauna Kea are better than they are on Kitt Peak, a much narrower slit size is used (4.5 arcsecond-wide, vs. 0.8 arcsecond with SpeX). Because of the difference in design of these two different spectrographs, these two different slit widths give about the same spectral resolution of R ~ 100. Further details on the instrumentation used in the SpeX asteroid survey can be found in Rayner et al. (2003). Exposures were taken in pairs and had a maximum integration time of 120 seconds. A near-simultaneous measurement of the sky background is provided by the image pairs, which can then be subtracted during the data reduction process. Several image pairs are combined to obtain a good signal-to-noise level for each asteroid observation. Each night, a set of 3 to 5 solar-like stars were observed, along with flat-field and Ar-lamp images that were used in calibrating the asteroid spectra. The steps used in extracting and calibrating the near-infrared asteroid spectra from the SpeX survey

are outlined in more detail in Sunshine et al. (2004). A detailed observation table for the spectra presented here is given in Table 1.

The data from both surveys are completely reduced and extracted to 1-D spectra, calibrated as relative reflectance vs. wavelength. The combining of these two spectra simply uses the overlap region from 0.82 - 0.92 microns that were sampled in both datasets. Since the spectra in both surveys were binned/resampled at uniform wavelengths at 0.005 microns, there are (at most) 21 points that overlap between the two wavelength regions. Each NIR spectrum is scaled to match the corresponding VIS spectrum (which has been normalized to unity at 0.55 μm) using a mean scaling factor determined from those 21 overlap points. Normalizing at a specific wavelength (usually 0.55 microns, which is the center of the V photometric band) is standard procedure for asteroid spectra. The actual albedos for most asteroids are unknown, and for those that we do have albedos, they are not necessarily very accurate. Without accurate albedos, we cannot plot the spectra in terms of absolute reflectivity. Therefore, all plots of asteroid spectra use units of "relative reflectance" plotted vs. wavelength.

There are 15 V-type asteroids, not including Vesta, that have been observed so far in the SpeX NIR asteroid survey. This survey is designed to observe representative asteroids of all taxonomic types, and is NOT focused just on V-types or Vestoids. The objects observed were chosen simply because they were appropriately placed in the sky and bright enough to observe at times when telescope time was available. Collection of the NIR spectrum for an asteroid was limited to those that had a visible spectrum already taken in the earlier SMASSII survey. Of the V-types observed, only one (3908 Nyx) is a planet crossing V-type. Therefore in this study we present the spectra of 14 "Vestoids",

ie: members of the Vesta family, and one planet crossing V-type asteroid. The Vesta family was estimated to have 372 members in 1995 (Zappala et al., 1995). However, the number of known members of the Vesta family is constantly increasing and may currently be ten times greater than the number given by Zappala et al. (1995)(S.J. Bus, Pers. Comm.)

3.2 Collection of Laboratory Spectra

VISNIR (0.3-2.55 μm) spectra for howardites, eucrites, and diogenites were collected using the Bi-directional Reflectance Spectrometer (BDR) at the NASA/Keck Reflectance Experiment Laboratory (RELAB) at Brown University (Pieters, 1993; Pieters and Hiroi, 2004). This research utilizes spectra acquired for the diogenites and howardites, which were available for download from the RELAB database, as well as those for eight of the unbrecciated eucrites (ALH A81001, BTN 00300, Chervony Kut, EET 87520, GRA 98098, MET 01081, MAC 02522, and PCA 91078), which were presented in Mayne et al. (2008b – Part III of this dissertation). All diogenite and howardite spectra were reported to have been collected from powders with a <45-μm particle size (RELAB database).

3.3 VISNIR Spectroscopy and Modeling

Band centers of the HED and Vestoid spectrum were calculated for the 1 and 2-μm regions. A straight-line continuum was removed from both the 1 and 2-μm bands by defining the beginning and ending wavelengths of the regions containing continuum like endpoints. Tangent point locations were then defined for the continuum. The band centers were determined from the continuum-removed spectrum by selecting a fraction from the bottom of the band to be fit by a second order polynomial. If there is noise in

the data then a larger fraction of the band will be required for a good fit. The resulting band centers, which are the wavelength positions of the points of lowest reflectance (Cloutis and Gaffey, 1991), shall be referred to as 'continuum-removed band centers' throughout the rest of this paper. All HED and Vestoid spectra were also modeled using the Modified Gaussian Model, hereafter referred to as MGM (Sunshine et al. 1990; Sunshine and Pieters 1993). MGM fits for the spectra of the unbrecciated eucrites are presented in Mayne et al. (2008b - Part III of this dissertation), the Vestoids and selected diogenites and howardites are presented below.

MGM models each spectrum as a continuum and a series of modified Gaussian distributions, with each distribution representing a specific absorption feature characterized by three parameters: band strength, band center, and band width (Sunshine et al. 1990). Band center values produced by MGM will be referred to here as MGM-derived band centers. This approach has been shown to successfully resolve the absorptions of overlapping bands (Mustard, 1992; Sunshine and Pieters, 1993; Schade and Wäsch, 1999b; Sunshine et al., 1990. 2004; Kanner et al., 2007;; Klima et al., 2007), such as those seen in the HED and Vestoid spectra. Only three diogenites (EET A79002, LAP 91900, GRO 95555) and howardites (EET 87503, QUE 94200, Y-791573) were fit using MGM. These samples were selected for additional spectral work because there was previously published data on their pyroxene compositions. The results of MGM were then used to estimate the relative proportions of LCP and HCP from the spectra that required a two-pyroxene model (e.g. Sunshine and Pieters, 1993; Sunshine et al., 2004; Kanner et al., 2007).

3.4 Calculation of Vestoid Size

The physical parameters of asteroids are not well known because of their small sizes and large numbers (JPL small-body database). Commonly, the absolute magnitude (H) is the only physical parameter available for small bodies, this value is defined as the magnitude that the object would have if it was 1 AU from the Earth and 1 AU from the Sun, whilst having a phase angle of 0°. The diameter of an asteroid can be estimated from its absolute magnitude; however, this calculation (Equation 1; Bowell et al., 1989) also requires the value for the asteroid's visual albedo (ρ) to be known.

$$D \approx 10^{((6.259-0.4H-\log\rho)/2))} \qquad \text{(Equation 1)}$$

In this study we adopt the practice used by previous studies of the Vestoids (e.g. Burbine et al., 2001) and take the value of the visual albedo to be 0.42 for all Vestoids, which is Vesta's Infrared Astronomical Satellite albedo. Values of H and ρ were taken from the JPL small-body database (http://ssd.jpl.nasa.gov/sbdb.cgi). Therefore, the calculated diameters are dependent on the chosen value for the visual albedo. For example, if the visual albedo value is incorrect by up to a factor of 2 (actual value lies between 0.21 to 0.84) then what was calculated as a 7 km diameter asteroid could actually lie between 4.9 and 9.9 km. The calculation of absolute magnitude is also subject to error as it relies on simplified assumptions relating to the phase relation of the asteroid and typically assumes a flat lightcurve (Bowell et al., 1989).

4. Results

4.1 HED Pyroxene Compositions

Compositional data for the pyroxenes in howardites and diogenites that were fit using MGM are presented in Table 2. The three diogenites contain low-calcium pyroxenes of a similar composition. The howardites, as breccias, contain a wide range of pyroxene compositions, the end members of which are given in Table 2. Pyroxene compositions for all the unbrecciated eucrites used in this study are presented in Mayne et al. (2008a Part II of this dissertation).

4.2 Spectral Modeling

The spectra of all HEDs and Vestoids are dominated by the characteristic 1 and 2-μm pyroxene absorption features (Figures 1-4). Continuum-removed band centers for the HEDs and Vestoids, and MGM-derived band centers and band strengths for the spectra that were modeled, are given in Tables 3 and 4. The relationship between the continuum-removed band 1 (~1 μm) and band 2 (~2 μm) center positions for all HED spectra is shown in Figure 5a. The Vestoid continuum-removed band centers are superimposed upon the fields defined by the HEDs plotted in Figure 5b. The majority of the Vestoids studied here have band centers that overlap the field defined by howardites (Figure 5), suggesting that they reflect a mixture of diogenite and eucrite materials. However, 3155 Lee and 2851 Harbin lie within the same wavelength range as the diogenites, and 2579 Spartacus and 2763 Jeans have band centers at the longest wavelengths and appear similar to eucrites. The continuum-removed band centers are then compared to previous data, collected by Adams (1974; 1975), Cloutis and Gaffey (1991), and Hazen et al. (1978,) for pyroxenes of known composition in Figure 5c and include a distinction

between LCP and HCP (at Wo_{11}; Cloutis and Gaffey, 1991). As expected, all eucrite spectra lie on the high-calcium side of the compositional trend, and diogenite spectra on the low-calcium side, with the howardites and Vestoids bridging the two.

The three diogenite spectra selected were all well fit with MGM using a one-pyroxene model (Tables 3 and 5). The diogenite models all show a non-random residual error in the 1-μm region, with the peak error occurring at the same wavelength as the modeled band center (Figure 6). This is likely to be due to band saturation rather than missing absorption bands, which are offset and much larger (Sunshine and Pieters, 1993). All howardite spectra required a two-pyroxene model to achieve a good fit (Tables 3 and 5, Figure 6). All eucrite spectra were modeled by Mayne et al. (2008b - Part III of this dissertation) and the resulting model parameters are given in Table 3, with three examples given in Figure 6. The Vestoids required either one- or two-pyroxene fits (Table 4, Figure 7). 3155 Lee and 3782 Celle were best modeled using a one-pyroxene model with an extra band to account for the M1 absorption in the 1-μm region (Tables 4 and 5). Why only these two Vestoids require the presence of the M1 1-μm band is unclear. Its presence was predicted by Burns (1993), but its location is close to that of the strong M2 band so it cannot often be distinguished. Three of the five samples that only needed a one-pyroxene model fit lie at the shortest 1-μm band center wavelengths: 3155 Lee, 2851 Harbin, and 3782 Celle (Table 6). These spectra may reflect a predominantly diogenite composition.

The relative strengths of the LCP and HCP MGM-derived bands at both 1 and 2-μm can be used to estimate the proportion of high-calcium pyroxene in the sample, if a two-pyroxene model is needed. The estimated modes can then be compared to actual

HCP and LCP modes measured for the eucrite meteorites (Mayne et al., 2008a - Part II of this dissertation), to assess the accuracy of this calculation for the HEDs and Vestoids. HCP and LCP modes were not available in the literature for the howardite samples and diogenites contain only one pyroxene. Less than 30% of the pyroxene in howardites is spectrally estimated to have a high-calcium composition, compared to greater than 44% for basaltic eucrites (Tables 3 and 4). Estimates of high-calcium pyroxene abundance from the relative band strengths are within ±15% of the actual values based upon previously collected data on the unbrecciated eucrites (Mayne et al., 2008b - Part III of this dissertation). The HCP calculation yields similar values for all of the Vestoids. 2579 Spartacus and 3908 Nyx have the largest proportion of high-calcium pyroxene (using the value estimated from their 1-μm band) of 59% and 46% respectively, giving them similar abundances to that of the basaltic eucrites (Tables 3 and 4). All other HCP values correspond to the range shown by howardites and cumulate eucrites, suggesting that only two of the fifteen Vestoids studied have a significant basaltic eucrite component in their spectra.

The 1.2-μm absorption feature, as discussed above, is in all the HED and Vestoid spectra, although it is deepest within the eucrites. This has been attributed to the high modal abundance of plagioclase within these samples (e.g. Gaffey, 1976; McFadden and Gaffey, 1978; Hardersen et al., 2004). However recent work on well characterized pyroxene-plagioclase mixtures suggests it is, in fact, more likely due to the larger amount of HCP (Mayne et al., 2008b - Part III of this dissertation). All Vestoid spectra were examined for the presence of an observable 1.2-μm absorption feature, i.e. one that can be seen in the overall spectrum with the naked eye, and the results are given in Table 6.

The feature was most easily observed in those Vestoids with longer wavelength band centers, which is consistent with more eucritic, or high-calcium pyroxene, material. The relative strength (RS) of the 1.2-µm band ($RS_{1.2\ \mu m}/(\ RS_{1.2\ \mu m} + RS_{1.2\ \mu m\text{-}LCP})$) is plotted against the strength of the 2-µm HCP band for all eucrites, howardites, and Vestoids that require a two-pyroxene model in Figure 8. It can be observed that the relative strength of the 1.2-µm band increases with increasing HCP content. Therefore, the eucrites have the strongest 1.2-µm band relative to the 2-µm HCP band as they have the highest proportion of HCP relative to LCP. The two-pyroxene Vestoids have a 1.2-µm relative band strength that overlaps both howardite and eucrite fields, which is unsurprising as they probably represent material from both groups.

5. The Mineralogy of Vestoids

The above analysis of the spectra of 15 Vestoids indicates clear compositional differences, most likely reflecting different lithologies on or near the surface of their parent asteroid, Vesta. However, it is possible that excavation from a large crater may have liberated material from deeper within the asteroid. For example, the south-pole crater on Vesta is calculated to have a depth of 13 km (Thomas et al., 1997). Gaffey (1997) produced a mineralogic map of the surface of Vesta, using sub-hemispheric spectral and color variations, and suggested that the large crater excavated down to an olivine-bearing layer, possibly representing upper mantle material. Binzel et al. (1997), looking at higher resolution Hubble Space Telescope images, observed that the 1-µm band in this proposed olivine region was broader and deeper than elsewhere on the

surface, indicating olivine may be present, although probably not as a monomineralic unit.

In spectra reflecting a mixture of LCP and olivine compositions the BAR can be used to estimate the amount of olivine (Cloutis et al., 1986). Duffard et al. (2004) used the equation given in Gaffey et al. (2002) to calculate the relative abundance of olivine in various Vestoid spectra and found that five asteroids (2763 Principia, 2851 Harbin, 2045 Peking, 4796 Castalia, and 4815 Anders) that had olivine contents of around 30%. However, as Duffard et al. (2004) acknowledge, this method does not work in the presence of HCP. HCP is a significant modal component in the eucrites and, therefore, is abundant in howardites, depending on the rock-types that make up that particular breccia. It does not seem possible to apply these equations to the Vestoids, and any olivine content that is estimated from them is probably not real. Therefore, estimation of olivine contents from the BAR values of Vestoid spectra will not be used here.

In HCP-LCP mixtures the presence of olivine can best be detected by a longer wavelength 1-μm feature (Gaffey, 2002). We would then expect an olivine-bearing Vestoid to be offset in a plot comparing continuum-removed band 1 and band 2 centers. This is not seen for any of the samples including three of those identified to have ~30% olivine by Duffard et al. (2004): 2045 Peking, 2753 Jeans, and 2851 Harbin (Figure 5b). This is further supported by MGM analyses of the fifteen Vestoids, which do not require bands suggestive of olivine to achieve a good fit. The lack of olivine in any of the Vestoid spectra suggests that the south-pole excavation did not sample major mantle material. This would imply that the crater-floor lithology might not be as olivine-rich as previously suggested.

Of the fifteen Vestoid spectra studied here, there appear to be seven asteroids that consist entirely of either eucrites or diogenites. 2579 Spartacus and 2763 Jeans are most likely eucrite material as they have 1 and 2-μm band centers at long wavelengths, overlapping those of the eucrite meteorite samples. In addition, a large proportion (60%) of the pyroxene in 2579 Spartacus is calculated to be of high-calcium composition. 3155 Lee, 2851 Harbin, 3782 Celle, 4215 Kamo, and 2511 Patterson are suggested to be diogenite asteroids. All five have spectra that are fit well with a one-pyroxene model (low-calcium in composition), and all except 2511 Patterson have band centers equivalent to those of the diogenites. A previous study by Burbine et al. (2001) did not identify 2851 Harbin as a diogenite asteroid; however, they employed predominantly spectral feature and continuum-removed band center comparison techniques and it is the MGM fit of this Vestoid, which requires only one pyroxene that lends weight to the theory that it most-likely diogenite material.

The remaining eight Vestoids appear to represent mixtures of both eucrite and diogenite materials. 1929 Kollaa has previously been suggested to have compositional characteristics similar to those of cumulate eucrites (Kelley et al., 2003). However, there is a great deal of similarity between the spectra of howardites and cumulate eucrites. As mentioned above, both contain a 1.2-μm feature that, though present, is often not visible to the naked eye. Cumulate eucrites contain pyroxenes with lower iron contents, which give them shorter wavelength band centers, the same effect that the addition of low-calcium pyroxene (diogenite) would have on a basaltic eucrite. This results in overlap between the band centers of howardites and cumulate eucrites, and asteroids that also have band center values close to this region could consist of either material (see Figure

5). Only two cumulate eucrite spectra are included here, so their band center range is not well defined. More work should be done on the spectral differences between these two groups before conclusions can be drawn as to whether any of these asteroids are dominated by cumulate eucrites.

6. Implications for the Surface of Vesta

One of the major goals of the Dawn mission is to provide a geologic context for HED meteorites. The results will be limited both by the resolution of the instruments and the sizes of individual rock-units on the surface. The highest resolution geologic map currently available for the surface of Vesta was generated using the rotational variations in its spectra from Hubble Space Telescope data, with a resolution of 52 km/pixel (Binzel et al., 1997). Therefore, our knowledge of the variation on the surface is limited at present. The presence of regions with dominant eucrite and dominant diogenite components has been suggested (Gaffey, 1997), and olivine signatures have been suggested within the large crater in the south-pole region of Vesta (Gaffey, 1997; Binzel et al., 1997). In advance of Dawn's arrival at Vesta, the Vestoids provide a means of examining the variability that can be expected on Vesta's surface, as well as an opportunity to study the mechanisms behind its formation. They also potentially offer an opportunity to study the mineralogy of Vesta at depth as rock-types that exist on the surface of an asteroid may, in fact, reflect lithologies that came from depth within Vesta, i.e. surface variations on the Vestoids could reflect vertical changes within Vesta.

The diameters of the Vestoids are given in Table 6. Asteroid 3908 Nyx is by far the smallest with a diameter of less than 1 km, with all others having diameters between

4.5 and 7.5 km. Of the 15 Vestoids studied, seven appear to consist of diogenite or eucrite alone, supporting the idea that there are large regions predominated by one HED type on or within Vesta. It should be emphasized that although the spectra of these asteroids point to a single lithology (diogenite or eucrite), there may be multiple eucrite or multiple diogenite types within it. However, the fact that there are domains, greater than 5km in size, that consist of either diogenite or eucrite suggests that there is large-scale homogeneity not only laterally on the surface of Vesta, but also vertically, with depth. This is broadly consistent with a layered crust morphology.

The remaining ten asteroids probably represent mixtures of eucrite and diogenite, which could suggest any one, or a mixture, of three different things.

1. ***Surface heterogeneity:*** Approximately half (eight of the fifteen) of the Vestoids have spectra that indicate that both diogenite and eucrite material is present. It is, therefore, possible that the spectra collected are hemispherically averaged compositions of distinct terrains. If this is the case, then we know that the size of each individual lithology contributing to the averaged composition must be smaller than the surface being measured. 3908 Nyx, at less than 1 km in diameter, is the smallest Vestoid in this study, suggesting that mixing is present on a sub-kilometer scale. This would indicate that there are areas on Vesta, which have smaller-scale heterogeneity.

2. ***Vestoids dominated by howardite material:*** It is not possible to tell if the 'mixed' Vestoid spectra, i.e. those that suggest both eucrite and diogenite are present, represent a combination of individual units of both lithologies on the Vestoid surface, or an asteroid that is composed of howardite. The latter situation would require a thick, consolidated regolith on Vesta. However, only 15% of the HED meteorites by mass have been

classified as howardites (Burbine, 2001), and as the Vestoids are believed to be the delivery pathway for the HED meteorites, it would then seem likely that this number would be higher if they were primarily howardites themselves.

3. ***Asteroidal rubble piles:*** The processes of impact excavation and ejection of material are key to the formation of the Vestoids. It is possible that the majority of the Vestoids are, in fact, re-accumulated piles of homogenized rock, effectively howardite rubble piles that formed after their ejection from the surface of Vesta. This mechanism was suggested by Michel et al. (2001) as a way to produce asteroidal families. This would mean that the few proposed here as monolithic, represent preserved impact ejecta blocks. Further work on the mechanics of cratering and ejection would be needed in order to see if this formation mechanism is likely for the Vestoids.

In this study we saw no evidence of olivine being present in any of the Vestoid spectra, indicating that no mantle material was ejected from Vesta, which calls into question the suggestion of an olivine-rich area within the south-pole crater. It is equally possible that the slight broadening and deepening in the 1-μm region observed in the crater (Gaffey, 1997; Binzel et al., 1997) could be due to a higher abundance of HCP. A greater HCP content would result in a stronger 1.2-μm absorption feature, which may, in turn, make the 1-μm band appear broader.

The formation of Vesta is not well understood, and numerous models have been put forward (e.g. Mason, 1962; Stolper, 1977; Righter and Drake, 1997; Ruzicka et al., 1997). Remotely sensed data of both Vesta and the Vestoids offer the opportunity to test these models, with respect to the units exposed on their surface. The processes that create small and large scale igneous units are different. A magma-ocean formation model

(Righter and Drake, 1997; Ruzicka et al., 1997) would predict widespread homogeneity, whereas partial melting might be expected to produce a more heterogeneous body with multiple intrusions and plutons of basaltic melt in the upper mantle and lower crust. The crater in the south-pole region on Vesta will, hopefully, expose fresh, regolith-free material in the crater walls, which will allow us to see the lithologic changes that occur with depth in Vesta (Mayne et al., 2008b – Part III of this dissertation).

The Vestoids show evidence of both large-scale (>5 km) homogeneity (just eucrite or diogenite) and small-scale (<1 km) heterogeneity (eucrite and diogenite) on their surface, representing changes both laterally and vertically within Vesta. This is consistent with the evidence from the petrology of the unbrecciated eucrites, which suggest serial magmatism played a role in the formation of the basaltic crust of Vesta (Figure 9)(Mayne et al., 2008a – Part II of this dissertation). However, the presence of serial magmatism does not eliminate either the partial melting or magma ocean model, as it could have occurred in both. The VIR instrument aboard Dawn has a resolution of 170-615 m/pixel, depending on the planetocentric radius of the orbit (Russell et al., 2006), which will allow us to detect different lithologies on a much smaller scale. This may mean that individual rock-units on the surface of Vesta will be at or above the size that can be detected by the VIR, vastly improving our knowledge of the spectral and petrologic variability of the surface of Vesta. This variability can then be used to test the various models for the petrogenesis of Vesta by comparing what is observed to what each model predicts (Mayne et al., 2008b – Part III of this dissertation).

Acknowledgments: This work was supported by PGG grant NNX06AH69G to JMS, a NASA Cosmochemistry grant NNG06GG36G and UCLA subcontract 2090-S-JB694 for Dawn to HYM. All meteorite spectra were collected at Brown University's KECK/NASA Reflectance Experiment Laboratory (RELAB).

References Cited

Adams J.B. 1974. Uniqueness of visible and near-infrared diffuse reflectance spectra of pyroxenes and other rock-forming minerals. *Journal of Geophysical Research* 79: 4829-4836.

Adams J.B. 1975. Interpretation of visible and near-infrared diffuse reflectance spectra of pyroxenes and other rock-forming minerals. In: *Infrared and Raman Raman Spectroscopy of Lunar and Terrestrial Materials*. Edited by: C. Karr Jr., Academic, New York. pp. 91-116.

Binzel, R.P. and Xu, S. 1993. Chips off asteroid 4 Vesta: Evidence for the parent body of basaltic achondrite meteorites *Science* 260**:**186-191.

Binzel R.P., Gaffey M.J., Thomas P.T., Zellner B.H., Storrs A.D., and Wells E.N. (1997) Geologic mapping of Vesta from 1994 Hubble Space Telescope images. *Icarus* 128:95-103.

Bowell E., Hapke B., Domingue D., Lumme K., Peltoniemi J., and Harris A.W. 1989. Application of photometric models to asteroids. In *Asteroids II* (eds. R.P. Binzel, T. Gehrels, and M.S. Matthews), pp. 524-556. University of Arizona Press, Tucson, Arizona, USA.

Burbine T.H., Buchanan P.C., Binzel R.P., Bus S.J., Hiroi T., Hinrichs J.L., Meibom A., and McCoy T.J. 2001. Vesta, Vestoids, and the howardite, eucrite, diogenite group: Relationships and the origin of spectral differences. *Meteoritics and Planetary Science* 36:761-781.

Burns R.G. 1993. *Mineralogical Applications of Crystal Field Theory, 2nd edition*. New York: Cambridge University Press. 551 p.

Bus S.J., and Binzel R.P. 2002. Phase II of the small main-belt asteroid spectroscopic survey: a feature based taxonomy. *Iacrus* 158:146-177.

Clayton R.N. and Mayeda, T.K. 1996. Oxygen isotope studies of achondrites. *Geochimica et Cosmochimica Acta* 60:1999-2017.

Cloutis E.A. and Gaffey M.J. 1991. Pyroxene spectroscopy revisited: Spectral-compositional correlations and relationship to geothermometry. *Journal of Geophysical Research* 96:22,809-22,826.

Cloutis E.A., Gaffey M.J., Jackowski T., Reed K.J. 1986. Calibrations of phase abundance, composition, and particle size distribution for olivine-orthopyroxene mixtures from reflectance spectra. *Journal of Geophysical Research* 95: 8323-8338.

Drake M.J. 2001. The eucrite/Vesta story. *Meteoritics and Planetary Science* 36:501-513.

Duffard R., Lazarro D, Licandro J., De Sanctis M.C., Capria M.T., and Carvano J.M. 2004. Mineralogical characterization of some basaltic asteroids in the neighborhood of (4) Vesta: first results. *Icarus* 171:120-132.

Encrenaz T. and Bibring J.P. 1991. *Solar System*. Springer-Verlag Berlin and Heidelberg GmbH & Co. KG. 330 pp.

Eugster O. and Michel Th. 1995. Common asteroid break up events of eucrite, diogenite, and howardite, and the cosmic ray production rates for noble gases in achondrites. *Geochimica et Cosmochimica Acta* 59:177-199.

Gaffey M.J. 1976. Spectral reflectance characteristics of the meteorite classes. *Journal of Geophysical Research* 81:905-920.

Gaffey M.J. 1997. Surface lithologic heterogeneity of asteroid 4 Vesta. *Icarus* 127:130-157.

Gaffey M.J., Cloutis E.A., Kelley M.S., Reed K.L. 2002. Mineralogy of the Asteroids. In: *Asteroids III* (W.F. Bottke, A. Cellino, P. Paolicchi, R.P. Binzel, eds.), 183-204. University of Arizona, Tucson

Hardersen P.S., Gaffey M.J., and Abell P.A. 2004. Mineralogy of asteroid 1459 Magnya and implications for its origin. *Icarus* 167:170-177.

Hazen R.M., Bell P.M., and Mao H.K. 1978. Effects of compositional variation on absorption spectra of lunar pyroxenes. *Lunar and Planetary Science IX*:483-484

Hinrichs J.L., Lucey P.G., Robinson M.S., Meibom A., and Krot A.N. 1999. Implications of temperature-dependent near-IR spectral properties of common minerals and meteorites for remote sensing of asteroids. *Geophysical Research Letters* 26:1661-1664.

Kanner L.C., Mustard J.F., and Gendrin A. 2007. Assessing the limits of the Modified Gaussian Modal for remote spectroscopic studies of pyroxenes on Mars. *Icarus* 187:442-456.

Kelley M.S., Vilas F., Gaffey M.J., Abell P.A. 2003. Quantified mineralogy evidence for a common origin of 1929 Kollaa with 4 Vesta and the HED meteorites. *Icarus* 165:215-218.

Klima R. L., Pieters C.M. and Dyar M.D. 2007. Spectroscopy of synthetic Mg-Fe pyroxenes I: Spin-allowed and spin-forbidden crystal field bands in the visible and near-infrared, *Meteoritics and Planetary Science* 42:235-253

Klima R.L., Pieters C.M., and Dyar M.D. 2008. Characterization of the 1.2-μm M1 pyroxene band: Extracting cooling history from near-IR spectra of pyroxenes and pyroxene-dominated rocks. *Meteoritics and Planetary Science* Submitted.

Lord S. 1992. A new software tool for computing Earth's atmospheric transmission of near- and far-infrared radiation. NASA Technical Memorandum 103957.

Mason B. (1962) Meteorites. J. Wiley and Sons, New York.

Mayne R.G., McSween H.Y., McCoy T.J., and Gale A. 2008a. Petrology of the unbrecciated eucrites. *Geochimica et Cosmochimica Acta* Submitted.

Mayne R.G., Sunshine J.M., McSween H.Y., McCoy T.J., Corrigan C.M., Gale A. and Dyar M.D. 2008b. Spectra of the unbrecciated eucrites. *Meteoritics and Planetary Science* Submitted.

McCord T.B., Adams J.B., and Johnson T.V. (1970) Asteroid Vesta: Spectral reflectivity and compositional implications. *Science* 168:1445-144.

McFadden L.A. and Gaffey M.J. 1978. Calibration of quantitative mineral abundances determined from meteorite reflection spectra and applications to Solar System objects. *Meteoritics* 13:556.

Michel P., Benz W., Tanga P., and Richardson D.C. 2001. Collisions and gravitational reaccumulation: Forming asteroid families and satellites. *Science* 294:1696-1700.

Moroz L., Schade U., and Wäsch R. 2000. Reflectance spectra of olivine-orthopyroxene bearing assemblages at decreased temperatures: Implications for remote sensing of asteroids. *Icarus* 147:79-93.

Mustard J.F. 1992. Chemical analysis of actinolite from reflectance spectra. *American Mineralogist* 77:345-358.

Pieters C.M. 1983. Strength of mineral absorption features in the transmitted component of near-infrared reflected light: First results from RELAB. *Journal of Geophysical Research* 88:9534-9544.

Pieters C.M. and Hiroi T. 2004. RELAB (Reflectance Experiment Laboratory): A NASA multi-user spectroscopy facility. *Lunar and Planetary Science* XXXV, Abstract #1720.

Rayner J.T., Toomey D.W., Onaka P.M., Denault A.J., Stahlberger W.E., Vacca W.D., Cushing M.C., and Wang S. 2003. SpeX: A medium resolution 0.8-5.5 micron spectrograph and imager for the NASA Infra-red telescope facility. *Publications of the Astronomical Society of the Pacific* 115:362-382.

Righter K. and Drake M.J. 1997. A magma ocean on Vesta: Core formation and petrogenesis of eucrites and diogenites. *Meteoritics and Planetary Science* **32**, 929-244.

Rothman L.S., Jacquemart D., Barbe A., Benner C., Birk M., Brown L.R., Carleer M.R., Chackerian C., Chance K., Coudert L.H., Dana V., Devi V.M., Flaud J.-M., Gamache R.R., Goldman A., Hartmann J.-M., Jucks K.W., Maki A.G., Mandin J.-Y., Massie S.T., Orphal J., Perrin A., Rinsland C.P., Smith M.A.H., Tennyson J., Tolchenov R.N., Toth R.A., Vander Auwera J., Varanasi P., and Wagner g. 2005.

The HITRAN 2004 molecular spectroscopic database. *Journal of Quantitative Spectroscopy and Radiative Transfer* 96:139-204.

Roush T.L. and Singer R.B. 1987. Possible temperature variation effects on the interpretation of spatially resolved reflectance observations of asteroid surfaces. *Icarus* 69:571-574.

Russell C.T., Capaccioni F., Coradini A., Christensen U., De Sanctis M.C., Feldman W.C., Jaumann R., Keller H.U., Konopliv A., McCord T.B., McFadden L.A., McSween H.Y., Mottola S., Neukum G., Pieters C.M., Prettyman T.H., Raymond C.A., Smith D.E., Sykes M.V., Williams B., and Zuber M.T. 2006. Dawn discovery mission to Vesta and Ceres: Present status. *Advances in Space Research* 38: 2043-2048.

Ruzicka A., Synder G.A., and Taylor L.A. 1997. Vesta as the howardite, eucrite, and diogenite parent body: Implications for the size of a core and for large-scale differentiation. *Meteoritics and Planetary Science* **32**, 825-840

Schade U. and Wäsch R. 1999a. Near-infrared reflectance spectroscopy if mafic minerals in the temperature region between 80 and 473 K. *Advances in Space Research* 23:1253-1256.

Schade U. and Wäsch R. 1999b. Near-infrared reflectance spectra from bulk samples of the two SNC meteorites Zagami and Nakhla. *Meteoritics and Planetary Science* 34:417-424.

Singer R.B. and Roush T.L. 1985. Effects of temperature on remotely sensed mineral absorption features. *Journal of Geophysical Research* 90:12434-12444.

Stolper E. (1977) Experimental petrology of eucritic meteorites. *Geochimica et Cosmochimica Acta* **41**, 587-611.

Sunshine J.M., Pieters C.M., and Pratt S.F. 1990. Deconvolution of mineral absorption bands: an improved approach. *Journal of Geophysical Research* 95:6955-6966.

Sunshine J.M. and Pieters C.M. 1993. Estimating modal abundances from the spectra of natural and laboratory pyroxene mixtures using the Modified Gaussian Model. *Journal of Geophysical Research* 98:9075-9087.

Sunshine J.M., Bus S.J., McCoy T.J., Burbine T.H., Corrigan C.M., and Binzel R.P. 2004. High-calcium pyroxene as an indicator of igneous differentiation in asteroids and meteorites. *Meteoritics and Planetary Science* 39:1343-1357.

Tholen D. and Barucci M.A. 1989. Asteroid Taxonomy. In: *Asteroids II* (R.P. Binzel, T. Gerhels, and M.S. Matthews, eds.), 298-315. University of Arizona, Tucson.

Thomas P.C., Binzel R.P., Gaffey M.J., Storrs A.R., Wells E.N., and Zellner B.H. 1997. Impact excavation on asteroid 4 Vesta: Hubble Space Telescope results. *Science* 277:1492-1495.

Wasson J.T. and Wetherill G.W. 1979. Dynamical, chemical, and isotopic evidence regarding the formation locations of asteroids and meteorites. In: *Asteroids* (T. Gehrels, ed.), 926-974. University of Arizona, Tucson.

Xu S., Binzel B.P., Burbine T.H., and Bus S.J. 1995. Small main-belt asteroid spectroscopy survey: Initial results. *Icarus* 115:1-35.

Zappalà V., Bendjoya P., Cellino A., Farinella P., and Froeschlé C. 1995. Asteroid families: search of a 12,487-asteroid sample using two different clustering techniques, *Icarus* 116:291–314.

Appendix IV

Table IV-1: Observational data for Vestoid spectra

Asteroid	Spectral Range	UT Date	Exposure (sec)	Mean Airmass	Precipitable Water (mm)	Heliocentric Distance (AU)	Phase Angle (deg)	V magnitude
4 Vesta	Vis	18-Apr-96	3.5	1.33		2.18	11.9	5.9
	NIR	9-Oct-00	600	1.45	0.9	2.26	25.9	7.3
1929 Kollaa	Vis	22-Feb-97	1800	1.06		2.18	19.3	15.6
	NIR	19-Feb-01	1440	1.04	0.9	2.21	14.4	15.3
2045 Peking	Vis	23-Nov-97	1800	1.13		2.51	18.6	16.4
	NIR	14-Jan-02	2400	1.02	4.7	2.48	21.7	16.7
2511 Patterson	Vis	15-Apr-97	1800	1.07		2.27	15.0	15.8
	NIR	7-May-04	1920	1.04	1.3	2.23	21.2	16.1
2566 Kirghizia	Vis	26-Nov-96	1800	1.08		2.43	12.8	16.2
	Vis	30-Nov-96	1800	1.08		2.42	14.3	16.3
	NIR	8-May-02	1920	1.12	2.5	2.41	9.8	16.0
2579 Spartacus	Vis	30-Apr-96	2700	1.57		2.09	10.9	15.5
	NIR	10-Oct-00	1680	1.15	1.2	2.22	18.9	16.4
2653 Principia	Vis	13-Apr-97	2700	1.56		2.43	19.6	16.2
	NIR	26-Nov-02	2880	1.13	4.4	2.53	17.8	16.3
	NIR	16-Jul-05	1680	1.24	1.5	2.59	3.1	15.5
2763 Jeans	Vis	23-Nov-97	1800	1.19		1.96	28.0	16.0
	NIR	26-Jun-04	1920	1.44	3.6	2.24	12.6	15.7
2795 Lepage	Vis	9-Sep-96	1800	1.06		2.33	20.4	17.0
	NIR	9-Apr-05	1440	1.16	0.9	2.26	4.7	15.9
2851 Harbin	Vis	29-Apr-96	1800	1.57		2.77	5.4	16.2
	NIR	24-Aug-01	1680	1.30	2.0	2.42	8.7	15.6
	NIR	12-Jan-03	2880	1.03	1.3	2.20	16.0	15.9
2912 Lapalma	Vis	17-Jan-97	1800	1.04		2.29	17.5	16.3
	NIR	20-Feb-01	1920	1.01	0.9	2.14	8.7	15.3
3155 Lee	Vis	12-Apr-97	1800	1.40		2.54	4.0	16.0
	NIR	22-Jun-01	1680	1.59	2.9	2.56	8.4	16.2
	NIR	14-Jul-05	1680	1.56	2.3	2.43	7.9	15.9
3782 Celle	Vis	13-Sep-97	1800	1.28		2.39	10.7	15.9
	NIR	26-Nov-02	1920	1.03	5.5	2.60	17.1	16.8
	NIR	25-Jun-04	1680	1.38	3.9	2.19	13.3	15.5
3908 Nyx	Vis	9-Sep-96	1800	1.25		1.15	30.2	15.1
	Vis	12-Oct-96	900	1.07		1.05	48.5	13.9
	NIR	26-Jul-04	3120	1.22	2.2	1.44	3.7	16.7
	NIR	11-Sep-04	1920	1.18	1.4	1.17	46.1	16.6
4188 Kitezh	Vis	8-Feb-96	1800	1.16		2.55	0.4	15.8
	NIR	14-Aug-01	1680	1.29	1.5	2.10	10.8	15.3
4215 Kamo	Vis	8-Apr-97	2700	1.77		2.34	16.5	16.0
	NIR	11-Nov-02	3840	1.03	5.3	2.52	17.3	16.5
	NIR	15-Jul-05	2400	1.23	2.9	2.51	3.2	15.6

Spectral range: Visible spectra cover 0.44 to 0.92 micron, and were taken with either the 1.3-m or 2.4-m telescope at MDM Observatory on Kitt Peak using a low-resolution grism spectrograph with CCD camera. Near-IR spectra cover 0.82 to 2.42 μr and were taken with the 3.0-m NASA IRTF on Mauna Kea using SpeX.

Amount of precipitable water above Mauna Kea was determined from fits to telluric water absorption bands in the SpeX data using the ATRAN (**A**tmospheric **TRAN**smission) modeling routine (Lord, 1992) that utilizes the HITRAN (**HI**gh resolution **TRAN**smission) database (Rothman et al., 2005).

Table IV-2: Pyroxene compositions of the howardites and the diogenites modeled using MGM.

		Orthopyroxene			Pigeonite		
		Wo	En	Fs	Wo	En	Fs
Howardites*	EET 87503[1]	2	75	23	12	38	50
	QUE 94200[2]	1	81	18	11	46	43
	Y-791573[3]	2	83	15	44	48	8

		Pyroxene Composition		
		Wo	En	Fs
Diogenites	EET A79002[4]	2	76	22
	LAP 91900[5]	2	75	23
	GRO 95555[6]	2	74	24

* The pyroxene compositions given for the howardites represent the end-members of the range seen within the sample as opposed to discrete separate compositions. All eucrite compositions are given in Mayne et al (2008a - Part II of this dissertation)

[1]*Antarctic Meteorite Newsletter 11(2)* (1988); [2]*Antarctic Meteorite Newsletter 18(2)* (1995); [3]*Meteorite Newsletter J9(1)* (2000)

[4] *Antarctic Meteorite Newsletter 3(3)* (1980); [5]*Antarctic Meteorite Newsletter 15(2)* (1992); [6]*Antarctic Meteorite Newsletter 19(2)* (1996)

Table IV-3: Continuum-removed band 1 and band 2 centers, BARs, and MGM-derived band centers and band strengths for the HEDs.

	ALH A81001	BTN 00300	Chervony Kut	EET 87520	GRA 98098	Ibitira	MAC 02522	MET 01081	Moore County	PCA 91078	Serra de Mage	EET 87503	QUE 94200	Y-791573	EET A79002	LAP 91900	GRO 95555
Meteorite Type	Eucrite	Eucrite	Eucrite	Eucrite	Eucrite	Eucrite	Eucrite	Eucrite	Cumulate Eucrite	Eucrite	Cumulate Eucrite	Howardite	Howardite	Howardite	Diogenite	Diogenite	Diogenite
CONTINUUM REMOVED BAND CENTERS (µm):																	
Band 1	0.94	0.95	0.94	0.95	0.94	0.94	0.97	0.94	0.94	0.96	0.93	0.93	0.92	0.93	0.92	0.92	0.92
Band 2	2.01	2.01	2.01	2.02	2.01	2.00	2.13	2.00	1.99	2.02	1.97	1.96	1.93	1.95	1.90	1.91	1.91
BAR	1.64	1.15	2.39	1.35	1.34	1.29	1.18	1.46	1.60	2.15	1.69	1.58	2.03	1.99	1.90	1.84	1.92
MGM BAND CENTERS (µm):																	
1 µm M1		0.83	0.87				0.88										
LCP at 1		0.91	0.92	0.90	0.90	0.90		0.90	0.91	0.89	0.92	0.92	0.92	0.92	0.92	0.92	0.92
HCP at 1	0.93	1.01	0.99	1.01	1.01	1.01	0.99	1.01	0.99	1.01	1.00	1.03	1.00	1.01			
1.2 Feature	1.19	1.21	1.19	1.20	1.20	1.20	1.12	1.21	1.18	1.20	1.17	1.23	1.18	1.19	1.17	1.17	1.16
LCP at 2		1.81	1.91	1.91	1.90	1.93		1.89	1.93	1.89	1.94	1.93	1.91	1.92	1.90	1.91	1.91
HCP at 2	2.02	2.20	2.22	2.24	2.12	2.21	2.15	2.22	2.23	2.24	2.24	2.08	2.15	2.22			
MGM BAND STRENGTHS (log reflectance):																	
Extra M1		-0.56	-0.26				-0.36										
LCP at 1		-0.89	-0.51	-0.74	-1.03	-0.78		-0.92	-0.77	-0.88	-0.58	-0.53	-0.73	-0.71	-1.11	-1.10	-1.14
HCP at 1	-0.54	-0.98	-0.37	-0.61	-0.63	-0.50	-0.90	-0.58	-0.40	-0.67	-0.10	-0.10	-0.07	-0.09			
1.2 Feature	-0.09	-0.73	-0.20	-0.26	-0.34	-0.21	-0.23	-0.34	-0.15	-0.34	-0.07	-0.09	-0.09	-0.09	-0.10	-0.10	-0.12
LCP at 2		-0.95	-0.57	-0.49	-0.57	-0.43		-0.59	-0.49	-0.62	-0.40	-0.27	-0.45	-0.42	-0.74	-0.70	-0.71
HCP at 2	-0.35	-0.98	-0.41	-0.37	-0.40	-0.20	-0.37	-0.38	-0.17	-0.56	-0.09	-0.07	-0.07	-0.09			
% HCP from 1*		73	61	65	55	56		55	47	63	18	20	14	16			
% HCP from 2*		71	61	63	59	44		57	35	67	25	26	19	22			
MGM BAND WIDTHS (µm):																	
Extra M1							0.14										
LCP at 1	0.00	0.20	0.19	0.19	0.18	0.18		0.19	0.19	0.19	0.19	0.17	0.18	0.18	0.18	0.19	0.20
HCP at 1	0.19	0.20	0.18	0.18	0.17	0.18	0.19	0.19	0.18	0.18	0.19	0.21	0.19	0.20			
1.2 Feature	0.32	0.32	0.28	0.28	0.31	0.28	0.34	0.29	0.28	0.29	0.28	0.32	0.30	0.31	0.33	0.30	0.29
LCP at 2	0.00	0.58	0.56	0.55	0.57	0.56		0.56	0.56	0.55	0.56	0.59	0.58	0.58	0.57	0.62	0.62
HCP at 2	0.60	0.56	0.56	0.56	0.56	0.56	0.70	0.56	0.56	0.56	0.56	0.57	0.57	0.57			

* These values denote the percentage pyroxene that has a high-calcium composition estimated to be in the material measured. This is estimated using the relative strengths of the LCP and HCP bands in both the 1 and 2 µm regions using the method outlined by Sunshine and Pieters (1993).

Table IV-4: Continuum-removed band 1 and band 2 centers, BARs, and MGM-derived band centers and strengths for the Vestoids.

	1929 Kollaa	2045 Peking	2511 Patterson	2566 Kirghizia	2579 Spartacus	2653 Principia	2763 Jeans	2795 Lepage	2851 Harbin	2912 Lapalma	3155 Lee	3782 Celle	3908 Nyx	4188 Kitezh	4215 Kamo
CONTINUUM REMOVED BAND CENTERS (µm):															
Band 1	0.94	0.94	0.93	0.93	0.94	0.93	0.94	0.93	0.92	0.93	0.92	0.93	0.92	0.93	0.92
Band 2	1.94	1.95	1.94	1.94	1.99	1.95	1.98	1.95	1.92	1.93	1.90	1.92	1.93	1.94	1.93
BAR	2.10	2.51	2.44	2.11	1.63	1.97	2.10	2.33	2.33	2.39	2.69	1.88	2.13	2.17	1.82
MGM BAND CENTERS (µm):															
1 µm M1											0.84	0.88			
LCP at 1	0.91	0.91	0.92	0.90	0.89	0.91	0.91	0.90	0.91	0.89	0.93	0.94	0.88	0.89	0.91
HCP at 1	0.99	0.99		0.98	1.00	1.00	0.99	0.99		0.97			0.99	0.98	
1.2 Feature	1.19	1.19	1.18	1.18	1.18	1.17	1.19	1.17	1.16	1.16	1.14	1.15	1.12	1.17	1.15
LCP at 2	1.90	1.91	1.94	1.90	1.93	1.91	1.93	1.89	1.91	1.91	1.90	1.94	1.85	1.90	1.94
HCP at 2	2.28	2.28		2.25	2.27	2.27	1.27	2.26		2.27			2.19	2.27	
MGM RELATIVE STRENGTHS (log reflectance):															
Extra M1											-0.27	-0.36			
LCP at 1	-0.81	-0.72	-0.88	-0.64	-0.64	-0.76	-0.60	-0.62	-0.97	-0.80	-0.36	-0.36	-0.81	-0.60	-0.63
HCP at 1	-0.16	-0.12		-0.19	-0.44	-0.12	-0.18	-0.21		-0.25			-0.40	-0.23	
1.2 Feature	-0.21	-0.19	-0.19	-0.19	-0.23	-0.21	-0.18	-0.19	-0.20	-0.19	-0.17	-0.14	-0.19	-0.19	-0.14
LCP at 2	-0.61	-0.57	-0.56	-0.61	-0.49	-0.58	-0.48	-0.56	-0.65	-0.65	-0.62	-0.50	-0.66	-0.52	-0.43
HCP at 2	-0.20	-0.15		-0.20	-0.18	-0.18	-0.17	-0.21		-0.08			-0.34	-0.17	
% HCP from 1*	20	19		28	59	18	29	32		30			46	37	
% HCP from 2*	33	27		33	36	31	35	37		17			48	32	
MGM BAND WIDTHS (µm):															
Extra M1											0.24	0.25			
LCP at 1	0.25	0.25	0.24	0.23	0.18	0.22	0.22	0.22	0.24	0.24	0.19	0.18	0.15	0.25	0.21
HCP at 1	0.20	0.20		0.19	0.18	0.20	0.20	0.20		0.19			0.28	0.19	0.31
1.2 Feature	0.29	0.29	0.29	0.28	0.27	0.29	0.29	0.28	0.30	0.27	0.31	0.32	0.59	0.28	
LCP at 2	0.59	0.59	0.62	0.60	0.55	0.59	0.59	0.60	0.63	0.58	0.61	0.60	0.58	0.60	0.61
HCP at 2	0.60	0.60		0.60	0.58	0.60	0.60	0.60		0.60				0.60	

* These values denote the percentage pyroxene that has a high-calcium composition estimated to be in the material measured. This is estimated using the relative strengths of the LCP and HCP bands in both the 1 and 2 µm regions using the method outlined by Sunshine and Pieters (1993).

Table IV-5: Modified Gaussian bands required in the MGM fits for the HEDs and Vestoids.

	Absorption	ALH A81001	BTN 00300	Chervony Kut	EET 87520	GRA 98098	Ibitira	MAC 02522	MET 01081	Moore County	PCA 91078	Serra de Mage	EET 87503	QUE 94200	Y-791573	EET A79002	LAP 91900	GRO 95555
		BE	BE	BE	BE	BE	BE	BE	BE	CE	BE	CE	H	H	H	D	D	D
Band 1	Charge Transfer	Y	Y	Y	Y	Y	Y	Y	Y	Y	Y	Y	Y	Y	Y	Y	Y	Y
Band 2	Charge Transfer	Y	Y	Y	Y	Y	Y	Y	Y	Y	Y	Y	Y	Y	Y	Y	Y	Y
Band 3	Cr^{3+}	Y	Y	Y	Y	Y	Y	Y	Y	Y	Y	Y	Y	Y	Y	Y	Y	Y
Band 4	1 µm M1	N	Y	Y	N	N	N	Y	N	N	N	N	N	N	N	N	N	N
Band 5	LCP 1 µm	N/A*	Y	Y	Y	Y	Y	N/A*	Y	Y	Y	Y	Y	Y	Y	N/A*	N/A*	N/A*
Band 6	HCP 1 µm	N/A*	Y	Y	Y	Y	Y	N/A*	Y	Y	Y	Y	Y	Y	Y	N/A*	N/A*	N/A*
Band 7	1.2 µm	Y	Y	Y	Y	Y	Y	Y	Y	Y	Y	Y	Y	Y	Y	Y	Y	Y
Band 8	LCP 2 µm	N/A*	Y	Y	Y	Y	Y	N/A*	Y	Y	Y	Y	Y	Y	Y	N/A*	N/A*	N/A*
Band 9	HCP 2 µm	N/A*	Y	Y	Y	Y	Y	N/A*	Y	Y	Y	Y	Y	Y	Y	N/A*	N/A*	N/A*
Band 10	Water band	Y	Y	Y	Y	Y	Y	Y	Y	Y	Y	Y	Y	Y	Y	Y	Y	Y

	Absorption	1929 Kollaa	2045 Peking	2511 Patterson	2566 Kirghizia	2579 Spartacus	2653 Principia	2763 Jeans	2795 Lepage	2851 Harbin	2912 Lapalma	3155 Lee	3782 Celle	3908 Nyx	4188 Kitezh	4215 Kamo
Band 1	Charge Transfer															
Band 2	Charge Transfer	Y	Y	Y	Y	Y	Y	Y	Y	Y	Y	Y	Y	Y	Y	Y
Band 3	Cr^{3+}	Y	Y	Y	Y	Y	Y	Y	Y	Y	Y	Y	Y	Y	Y	Y
Band 4	1 µm M1	N	N	N	N	N	N	N	N	N	N	Y	Y	N	N	N
Band 5	LCP 1 µm	Y	Y	N/A*	Y	Y	Y	Y	Y	N/A*	Y	N/A*	N/A*	Y	Y	N/A*
Band 6	HCP 1 µm	Y	Y	N/A*	Y	Y	Y	Y	Y	N/A*	Y	N/A*	N/A*	Y	Y	N/A*
Band 7	1.2 µm	Y	Y	Y	Y	Y	Y	Y	Y	Y	Y	Y	Y	Y	Y	Y
Band 8	LCP 2 µm	Y	Y	N/A*	Y	Y	Y	Y	Y	N/A*	Y	N/A*	N/A*	Y	Y	N/A*
Band 9	HCP 2 µm	Y	Y	N/A*	Y	Y	Y	Y	Y	N/A*	Y	N/A*	N/A*	Y	Y	N/A*
Band 10	Water band	Y	Y	Y	Y	Y	Y	Y	Y	Y	Y	Y	Y	Y	Y	Y

N/A* for band numbers 5, 6 and 8,9 denotes eucrites that only needed one pyroxene in the model and, therefore, instead of separate LCP and HCP bands only one pyroxene band was needed in both the 1 and 2µm regions.
BE = basaltic eucrite, CE = cumulate eucrite, H = howardite, D = diogenite

Table IV-6: Size and suggested mineralogy for the Vestoids.

Vestoids	1.2 μm feature present	MGM Model # of pyroxenes	Diameter in km	Suggested mineralogy
3155 Lee	N	1	6.3	Diogenite
2851 Harbin	N	1	7.2	Diogenite
3908 Nyx	N	2	0.7	Mixture
4215 Kamo	N	1	6.9	Diogenite
2912 Lapalma	N	2	6.0	Mixture
3782 Celle	N	1	6.6	Diogenite
2511 Patterson	N	1	6.6	Diogenite
2566 Kirghizia	Y	2	6.3	Mixture
2795 Lepage	Y	2	4.8	Mixture
2653 Principia	Y	2	7.9	Mixture
4188 Kitezh	N	2	6.0	Mixture
1929 Kollaa	Y	2	7.5	Mixture
2045 Peking	Y	2	7.5	Mixture
2763 Jeans	Y	2	6.3	Eucrite
2579 Spartacus	Y	2	5.2	Eucrite

Vestoids are in order of band 1 center values, starting with the shortest.
Diameter was calculated using the formula from Bowell et al. (1989) where $D \sim 10^{((6.258-0.4H-\log_{\pi})/2))}$ where H=absolute magnitude, ρ=visual albedo, taken to be 0.42 (Vesta's Infrared Astronomic Satellite albedo). Values of H were taken from the JPL small-body database.

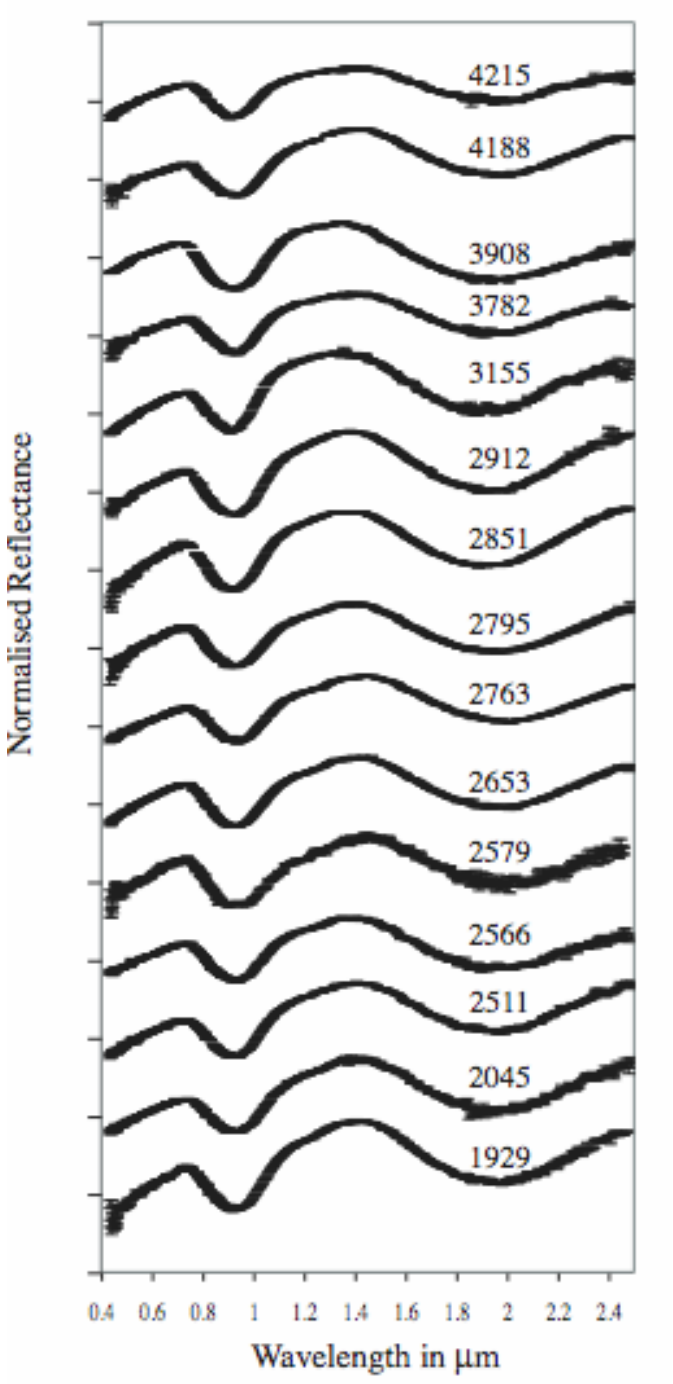

Figure IV-1: The VIS-NIR reflectance spectra of all 15 Vestoids studied in this paper. The spacing between two tick marks on the y-axis is equal to a ΔR (reflectance) value of 1. Spectra are offset by a value of 1 for clarity. Error bars are shown on spectra.

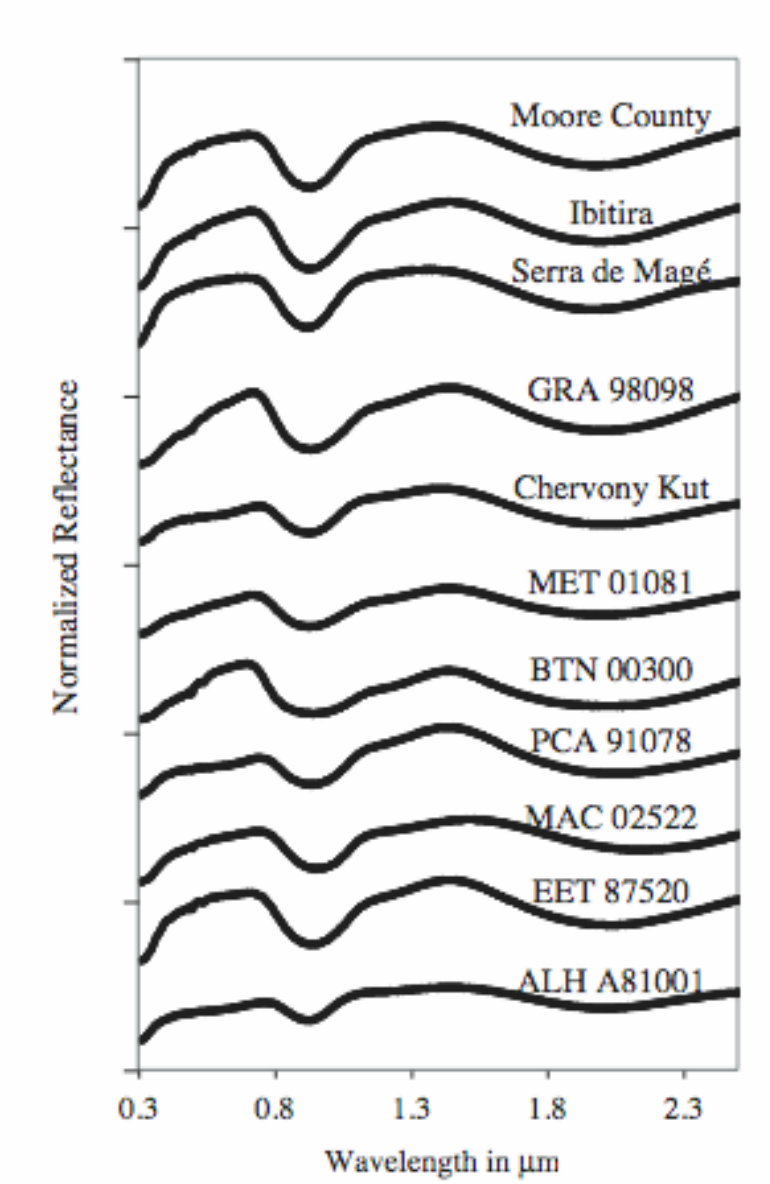

Figure IV-2: The VIS-NIR reflectance spectra of the unbrecciated eucrites. . The spacing between two tick marks on the y-axis is equal to a ΔR (reflectance) value of 1. Spectra are offset by a value of 1 for clarity. Spectra are taken from Mayne et al. (2008 – Part III of this dissertation).

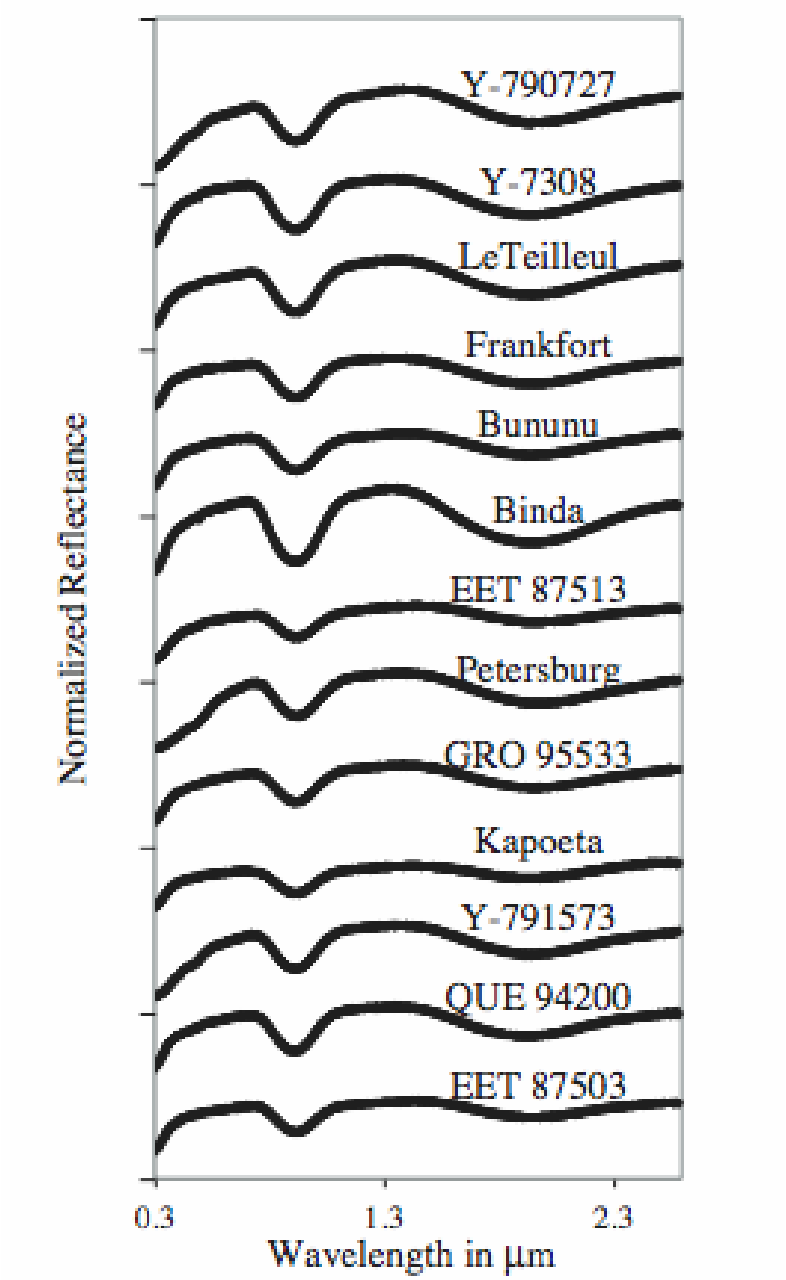

Figure IV-3: The VIS-NIR reflectance spectra of all the howardites used in this study. . The spacing between two tick marks on the y-axis is equal to a ΔR (reflectance) value of 1. Spectra are offset for clarity by a value of 1. These spectra were avaialble for download from the RELAB database.

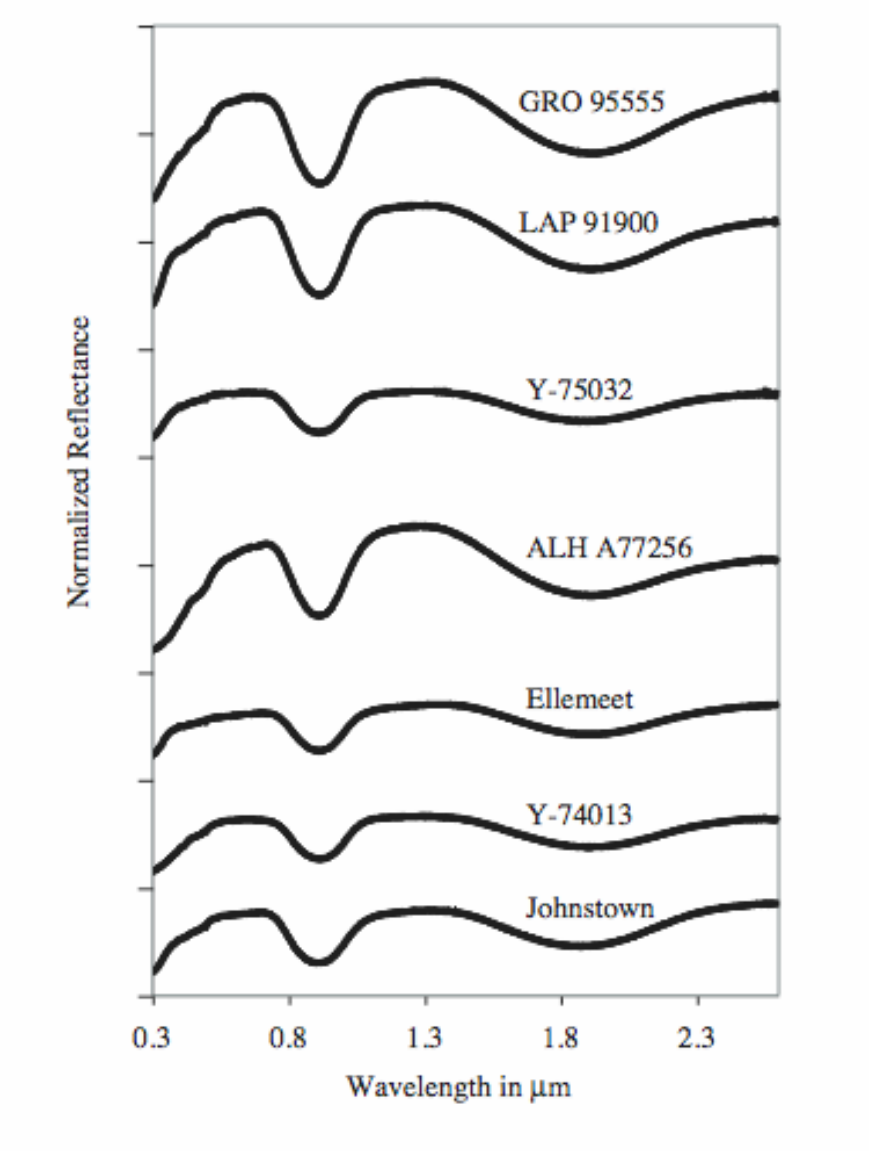

Figure IV-4: The VIS-NIR reflectance of the diogenites used in this study. . The spacing between two tick marks on the y-axis is equal to a ΔR (reflectance) value of 0.5. Spectra are offset by a value of 1 for clarity. All spectra were available for download from the RELAB database.

Figure IV-5: Continuum-removed band centers for Vestoids and HED spectra. (a) Continuum-removed band centers for the HEDs. (b) Continuum-removed band centers for the Vestoids, superimposed upon the ranges seen within the HEDs. The Vestoid band centers predominantly overlap the howardite filed, with a few spectra also in the eucrite and diogenite fields. (c) The Vestoid continuum-removed band center data compared to data collected for pyroxenes of known composition by Adams (1974; 1975), Cloutis and Gaffey (1991), and Hazen (1978). The open symbols represent HCP (Wo>11%, Cloutis and Gaffey, 1991), and the closed symbols LCP. The Vestoid spectra can be observed to plot between the LCP and HCP compositions.

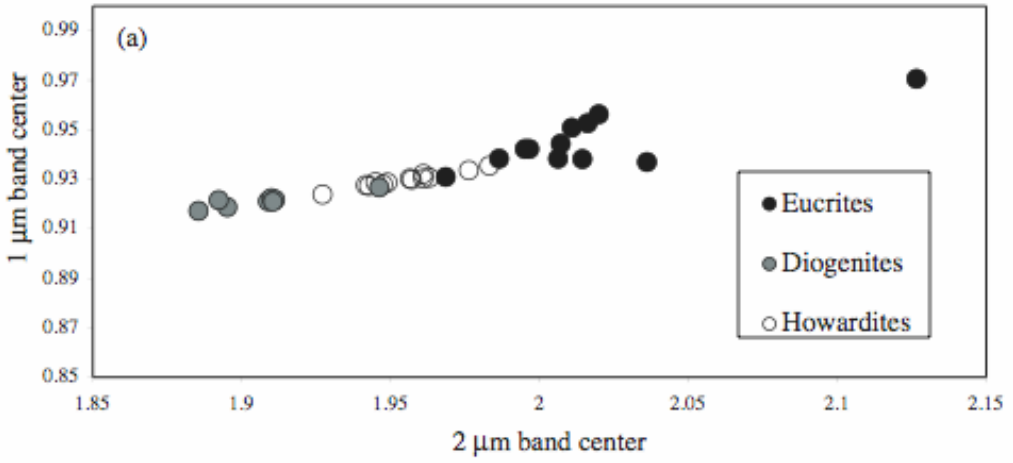
(a)
1 µm band center
2 µm band center
0.99
0.97
0.95
0.93
0.91
0.89
0.87
0.85
1.85
1.9
1.95
2
2.05
2.1
2.15
Eucrites
Diogenites
Howardites

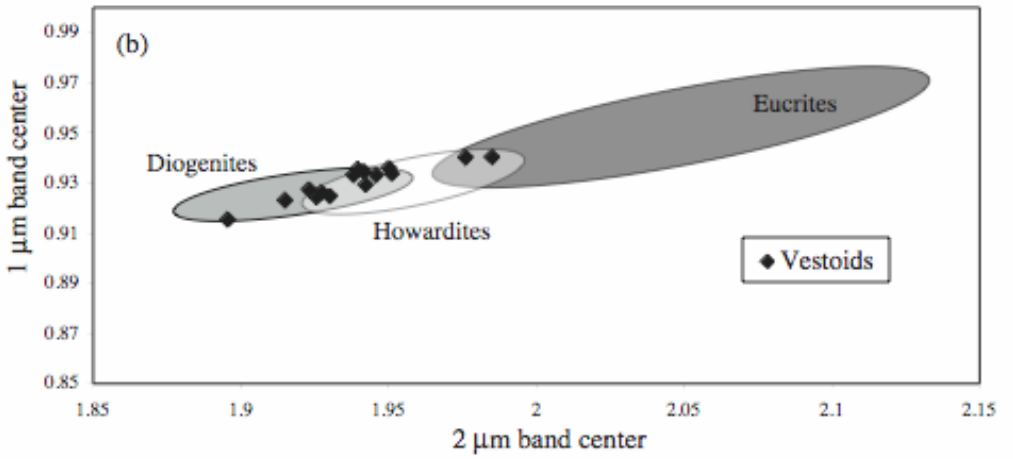
(b)
1 µm band center
2 µm band center
Eucrites
Diogenites
Howardites
Vestoids

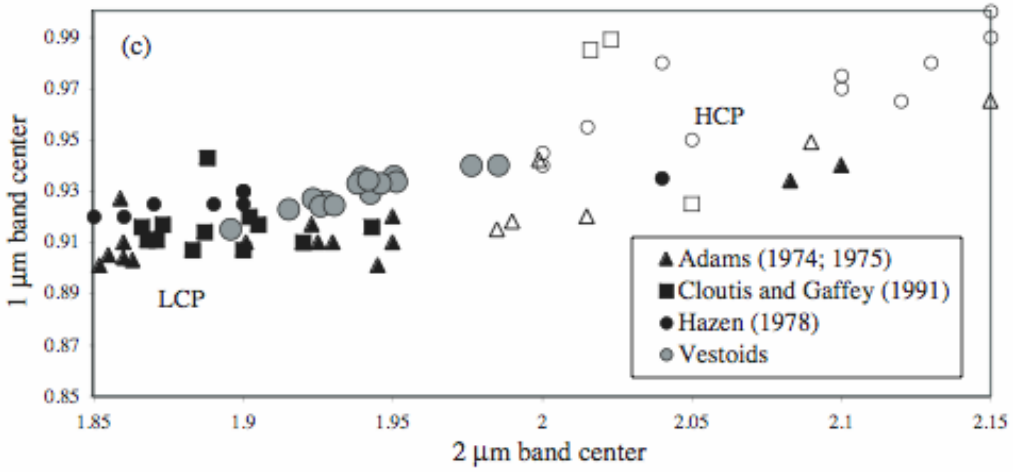
(c)
1 µm band center
2 µm band center
HCP
LCP
Adams (1974; 1975)
Cloutis and Gaffey (1991)
Hazen (1978)
Vestoids

Figure IV-6: MGM fits for the howardites, diogenites, and three selected eucrites from Mayne et al. (2008 – Part III of this dissertation). The eucrite spectra chosen show the range of spectral features seen within the group. The individual absorption bands modeled by modified Gaussians are shown in dark grey. The upper black line represents the residual error of the model; the lower black line represents the continuum. The measured spectrum is plotted with grey +'s, and the black is the modeled value. A large arrow is used to denote the LCP band in the 1 and 2-μm region, and a small arrow for HCP in the howardites. All diogenites are fit well with a one-pyroxene model and, therefore, only have one LCP band in both the 1 and 2-μm region, whereas both the howardites and eucrites have two-pyroxenes. It can be seen that all spectra have a 1.2-μm band in the model fit.

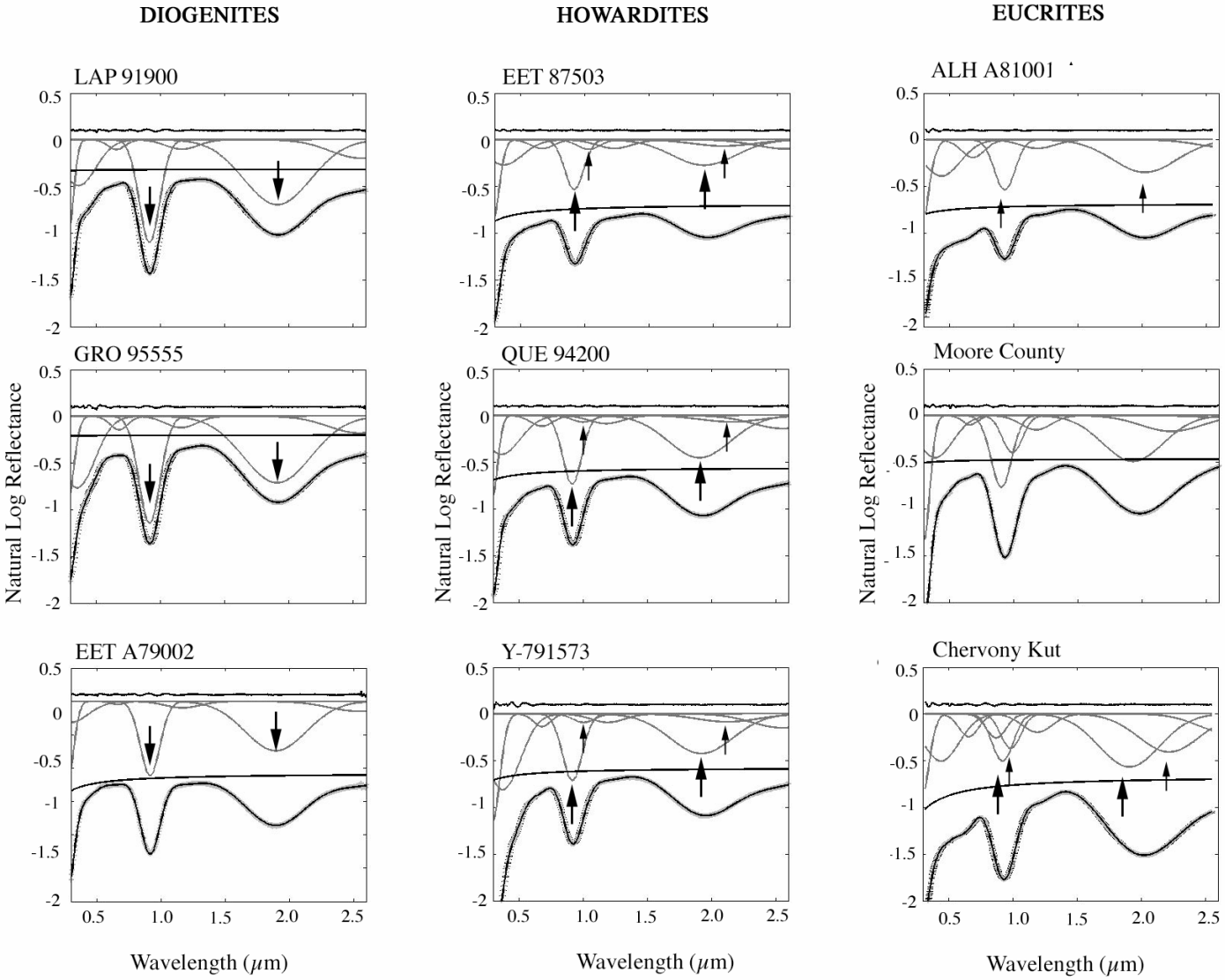
DIOGENITES
HOWARDITES
EUCRITES
LAP 91900
EET 87503
ALH A81001
GRO 95555
QUE 94200
Moore County
EET A79002
Y-791573
Chervony Kut
Natural Log Reflectance
Wavelength (μm)

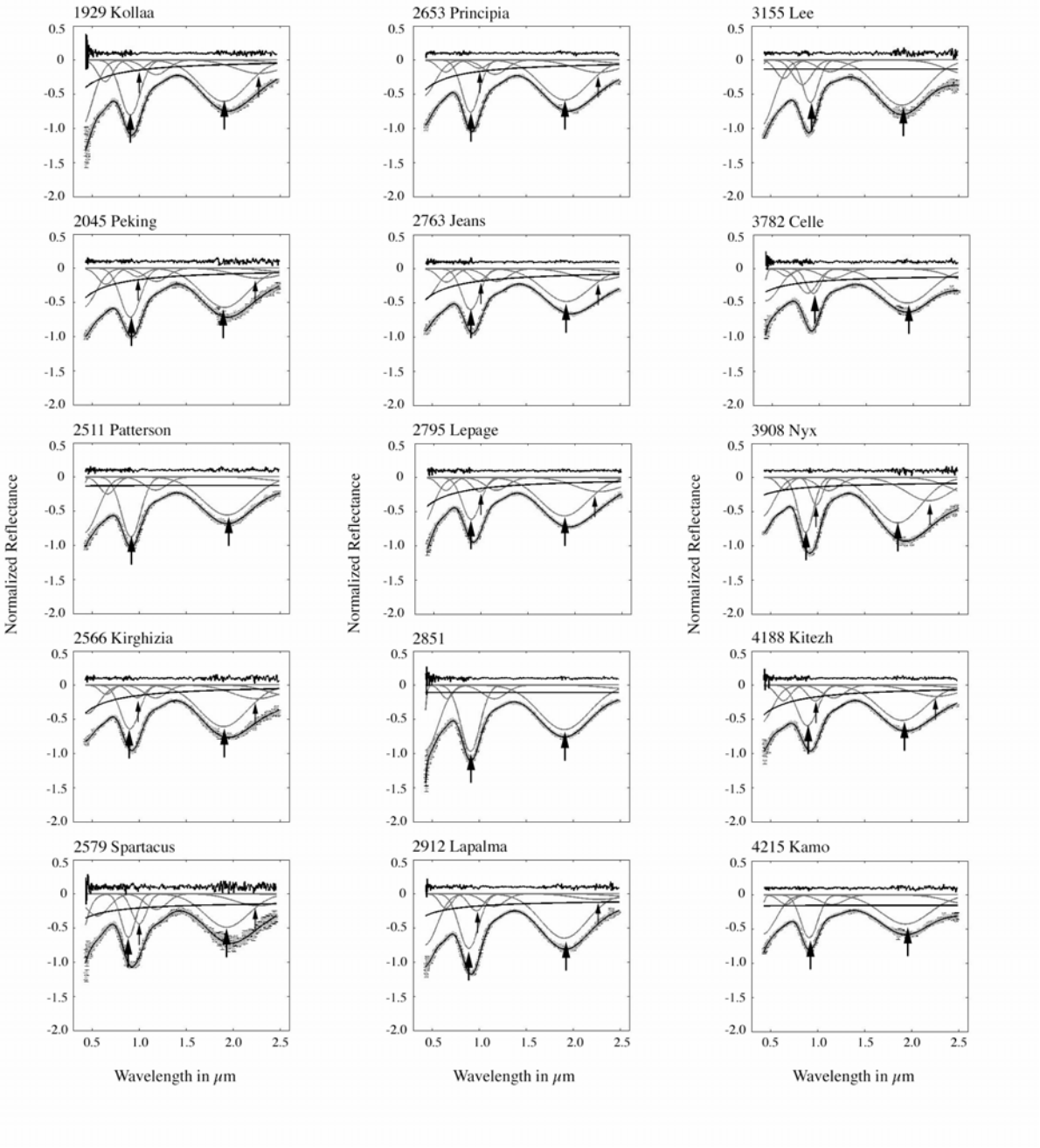

Figure IV-7: MGM model fits of the Vestoids. The individual absorption bands modeled by modified Gaussians are shown in dark grey. The upper black line represents the residual error of the model; the lower black line represents the continuum. The measured spectrum is plotted with grey +'s, and the black is the modeled value. A large arrow is used to denote the LCP band in the 1 and 2-μm region, and a small arrow for HCP.

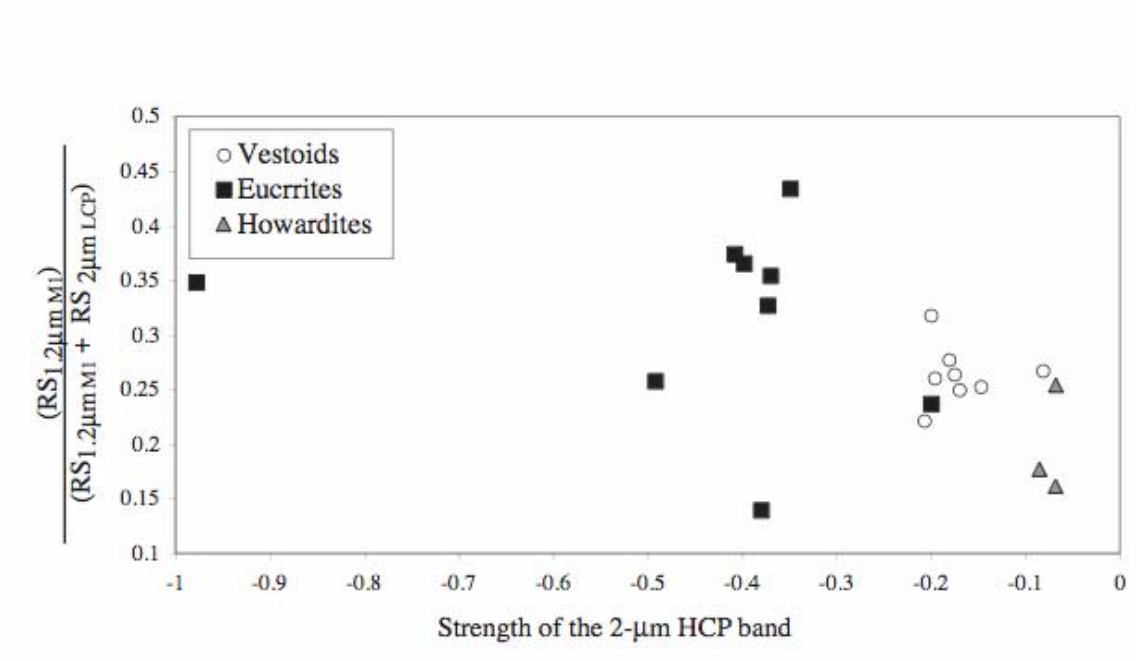

Figure IV-8: Change in the relative strength of the 1.2-µm band with respect to the strength of the 2-µm HCP MGM-derived band center. The 'relative strength 'of the 1.2-µm band refers to its absolute strength normalized to that of the 2-µm LCP band strength. The relative strength of the 1.2-µm absorption increases with increasing HCP content. The eucrites, which have the highest modal percentage of HCP (and the strongest HCP 2-µm band), have the strongest 1.2-µm feature and the howardites have a lower value, with the Vestoid lying in-between. The diogenites and some of the Vestoids do not have separate LCP and HCP pyroxene bands in their MGM fits and are, therefore, not included.

Figure IV-9: Simplified model of the crust of Vesta. Here we invoke the serial magmatism model for the formation of the crust, which is supported by evidence from the petrology of the unbrecciated eucrites (Mayne et al., 2008a – Part II of this dissertation). The Vestoids show that both large and small-scale units exist on and within Vesta's crust. Red boxes outline areas of the same scale that consist of one lithology (eucrite or diogenite) alone or a mixture of lithologies (eucrite and diogenite).

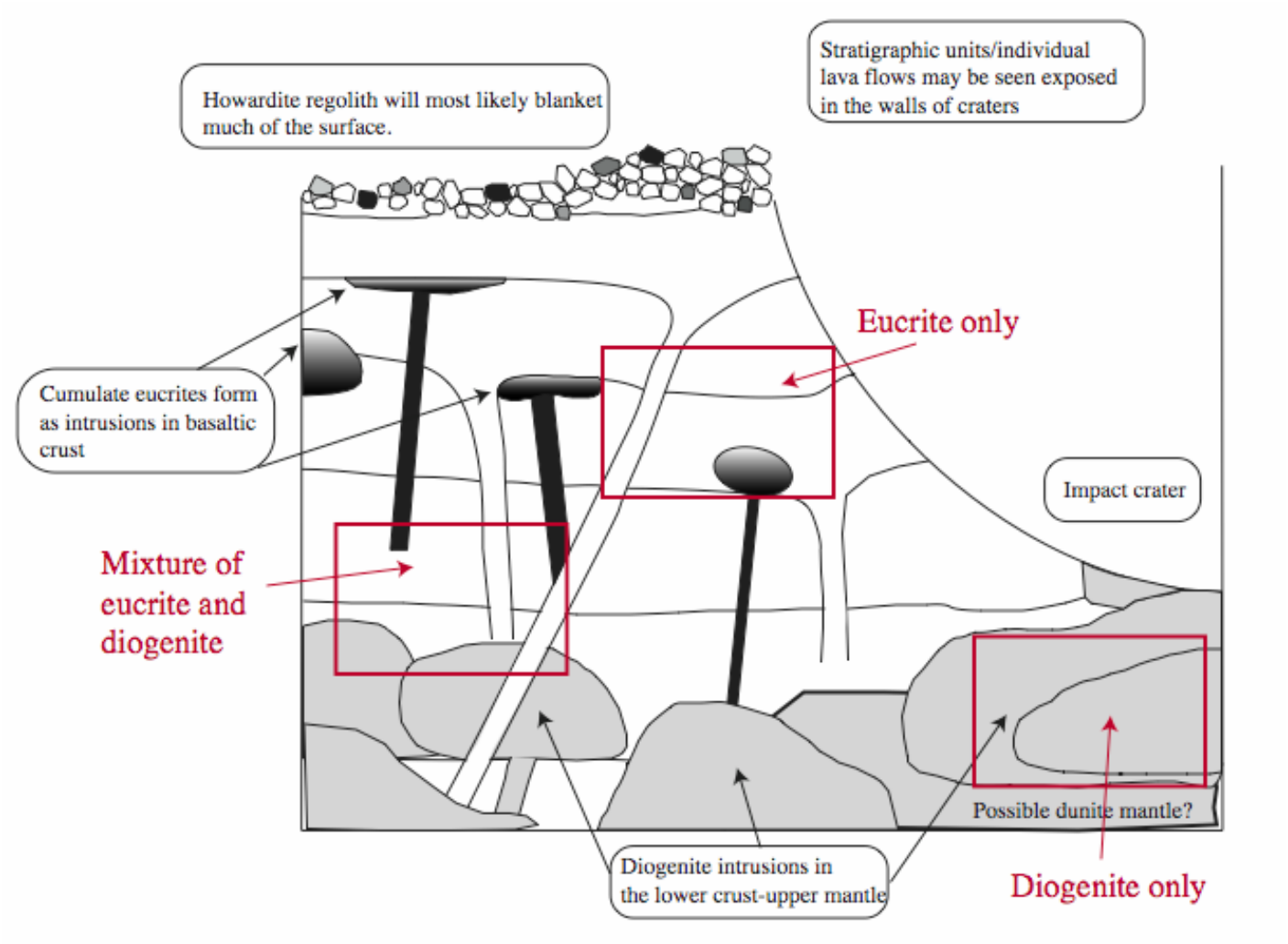
Howardite regolith will most likely blanket much of the surface.
Stratigraphic units/individual lava flows may be seen exposed in the walls of craters
Eucrite only
Cumulate eucrites form as intrusions in basaltic crust
Impact crater
Mixture of eucrite and diogenite
Possible dunite mantle?
Diogenite intrusions in the lower crust-upper mantle
Diogenite only

Vita

Rhiannon Gwenllian Mayne was born on March 26th, 1980 in Shrewsbury, England, to parents Peter Llewelyn and Linda Ann Mayne. She spent six months between 1982 and 1983 living in Zimbabwe, where she cultivated a lovely head of white-blonde hair that she has never seen since. She then returned to the UK and attended Shrewsbury High School until the family moved to Northamptonshire in 1988. It was during her time as a pupil at Northampton High School that Rhiannon's interest in the Planetary Sciences really flourished. She attended Space Camp at Brunel University in 1997 and, consequently, told her Careers Advisor that she wanted to pursue a degree in Astrophysics. Astrophysics, and the Planetary Sciences, she was told were far too specialized and would get her nowhere.

Rhiannon graduated from Northampton High School in July 1998 and shortly thereafter went to the University of Edinburgh to study towards a degree in Geophysics. This subject choice was inspired by the Geophysicists in the British archaeological television show 'Time Team'. They never seemed to get the right answer and yet remained employed. This seemed like the perfect career. In the first year of her degree, however, she discovered her love for Geology and, as a result, changed her major. In 2001, Dr Rhian Jones from the University of New Mexico came to Edinburgh as a Mineralogical Society of America Distinguished Lecturer, and gave a talk entitled "From Stardust to Asteroids: Meteorites and their Record of Solar System Formation."

Rhiannon suddenly realized that her love for rocks and space could be combined and a new career path was born.

Rhiannon graduated with a 2:1 BSc. Hons. in Geology in the summer of 2002.and, shortly after graduation, moved to Knoxville, Tennessee to begin her doctoral studies in the Earth and Planetary Sciences Department (formerly Geology) at the University of Tennessee. There she cultivated her southern twang and rebelled against taking the 'u' out of colour. She successfully graduated with her Doctor of Philosophy degree in Geology on the 8th May 2008.

Rhiannon will be moving to Washington, DC to begin a postdoctoral position at the Smithsonian National Museum of Natural History. She will be found playing amongst the meteorite collection like a kid in a candy store.